The systematic consideration of the large-scale fed-batch fermentation inhomogeneities using a genetically modified *C. glutamicum* strain as a model organism

Williams Chidozie Olughu

A Thesis submitted to Loughborough University
For the degree of

DOCTOR OF PHILOSOPHY

School of Aeronautical, Automotive, Chemical and Materials Engineering
Department of Chemical Engineering
Loughborough University
LE11 3TU
United Kingdom
February 2018

Abstract

The loss of efficiency and performance of bioprocesses on scale-up is well known, but not fully understood. This work addresses this problem, by studying the effect of some fermentation gradients (pH, glucose and oxygen) at a larger scale in a bench-scale two compartment reactor (PFR + STR) using the cadaverine-producing recombinant bacterium, *Corynebacterium glutamicum* DM1945 Δact3 Ptuf-ldcC_OPT.

The initial scale down strategy increased the magnitude of these gradients by only increasing the mean cell residence time in the plug flow reactor (τ_{PFR}). The cell growth and product related rate constants were compared as the τ_{PFR} was increased; differences were significant in some cases, but only up to 2 min residence time. For example, losses in cadaverine productivity when compared to the control fed-batch fermentation on average for the τ_{PFR} of 1 min, 2 min and 5 min were 25 %, 42 % and 46 % respectively. This indicated that the increasing the τ_{PFR} alone does not necessarily increase the magnitude of fermentation gradients.

The new scale-down strategy developed here, increased the magnitude of fermentation gradients by not only increasing the τ_{PFR}, but also considering the mean frequency at which the bacterial cells entered the PFR section (f_m). The f_m was kept constant by reducing the broth volume in the STR. Hence, the bacterial cells also spent shorter times in the well mixed STR, as the τ_{PFR} was increased (hypothesised as giving the bacterial cells less time to recover the non-ideal PFR section of the SDR). On adoption of this strategy cadaverine productivity decreases for the τ_{PFR} of 1 min, 2 min and 5 min were 25 %, 32 % and 53 % respectively. Thus, highlighting that loss in performance is most likely to occur as the magnitude of heterogeneity within the fermentation environment increases. However, *Corynebacterium glutamicum* DM1945 Δact3 Ptuf-ldcC_OPT did show some resilience in its biomass productivity. It was only marginally affected in the harshest of conditions simulated here.

Nomenclature

a - interfacial area
C^* - concentration of oxygen at the gas-liquid interface
C_L - concentration of oxygen in the liquid phase
F_0- feeding flow rate
P_f - impeller pumping number
P_0 - unaerated power input
Q – volumetric air flow rates
Q_r - volumetric recirculation liquid flow rate
$Y_{p/x}$ - product yield per dry cell weight
$Y_{x/s}$ - yield of dry cell weight on glucose
c_p - specific heat
$\frac{dC_L}{dt}$ - rate of change in oxygen accumulated in the liquid phase
$\frac{d\theta}{dt}$ - rate of change in temperature
f_m – mean frequency at which the cells entered the PFR
k_La - Volumetric mass transfer coefficient
k_L - mass transfer coefficient
q_{CAD} - metabolic quotient for cadaverine
q_{CFU} – colony forming unit productivity
$q_{glucose}$ - specific metabolic quotients for glucose
q_p - specific metabolic quotients for product
t_d - doubling time
t_m - mixing time
μ_{max} - maximum cell growth rate
τ_{PFR} – mean cell residence time in the plug flow reactor
τ_{STR} - mean cell residence time in the plug flow reactor
ADC - analogue to digital converter
ATP - adenosine triphosphate
CFD – computational fluid dynamics
CFU - colony forming unit
CRISPR - Clustered Regularly Interspaced Short Palindromic Repeats
CT - Circulation Time
CTD - Circulation Time Distribution
DCW - dry cell weight
DO – dissolved oxygen
DOT – dissolved oxygen tension
FSC - forward scatter
GMO - genetically modified organisms
HPLC – high performance liquid chromatography
IPTG - Isopropyl β-D-1-thiogalactopyranoside
mRNA - messenger ribonucleic acid

OTR - oxygen transfer rate
oxonol - DiBAC4(3) (Bis-(1,3-Dibutylbarbituric Acid) Trimethine Oxonol
P - aerated power input
PFR – plug flow reactor
PI - propidium iodide
PMT - photomultiplier tubes
QBD - Quality by Design
QBT - Quality by Testing
rhGH – recombinant human growth hormone
RQ - respiratory quotient
RTD - residence time distribution
SDR – scaled-down reactor
SSC - side scatter
STR – stirred tank reactor
TCA – Tricarboxylic acid
TSA - tryptone soya agar
TSB - tryptone soya broth
Da - Damköhler number
N - stirrer speed
OUR - oxygen uptake rate
S - feed glucose concentration
T - impeller diameter
V - the medium volume
t – time
μ - cell growth rate

Acknowledgements

I would like to acknowledge the following people that have helped made my PhD come to fulfilment.

I thank my parents, for their continued support and believe in me over the years. My wife, for seeing me through all times, making the trying times bearable and being my compass. My brother and sister for listening and encouraging me to be better.

My friend, James Wright for being my sounding board and letting me see that it is not all about work. Dr Gilbert Shama for his kindness and support. Mr Tony Eyre, for whom without his help and dedication my plug flow reactor would not exist. A special thank you to Mr David Smith for introducing me to the world of microbes.

Finally, I am grateful to my supervisors, Professor Chris Rielly and Professor Chris Hewitt for their continual advice, feedback and ultimately making this thesis possible.

The dust is unsettled,
From distant cries of bang! Bang!!
Our bodies attest to the lung-filled cordite air,
Our mothers, wives, sisters adorn raffia palm-belts,
Tight across their bellies to stave off the fangs of hunger,
As they flee miles away from the lung-filled cordite air,
In tow with three or four children,
Teary eyes and swollen bellies,
Balanced precariously on legs thin and brittle as dry sticks,
Ravaged from the loss of nutrients,
Their fathers, husbands, brothers vaporised to a higher state of entropy,
Whose molecules we inhale.

Dedication

To Saiva, Adaeze and Chinyere Olughu

Table of contents

Contents

List of tables

List of figures

CHAPTER 1

1 Introduction

The need for scaling up of processes arises from the economics of scale, and for the most part, as the size increases the cost of production per unit declines. This makes the cost of products to the consumer cheaper. However, scaling up brings challenges that come with handling large volumes (overpressure, high-temperature risk and health hazards). In developing biological systems from the laboratory to the marketplace, a certain amount of process knowledge is required if such a venture is to be successful. This process knowledge is usually gained by experimenting at a small-scale. In these experiments, process variables are screened, and the critical ones are identified. The proceeding step is then to optimise and design an operational space suitable for the biological system/organism. The data collated from these small vessels are then used to predict what might happen when the scale of the bioreactor is increased.

In the scale-up of most microbial processes, the predictions made from data collected from small-scale experimentations typically fall short, even when cultivation variables are similar (Noorman, 2011). This would indicate that simply increasing the reactor size and medium volume changes the hydrodynamics, which consequently affects a microbe’s productivity as the magnitude of environmental heterogeneities increase. Thus, the assumption that the reactor size is irrelevant if the process variables are kept constant across scale cannot be upheld. The lack of consideration of the differences (performance losses in most cases) that might occur on scaling up a bioprocess can amount to failure.

1.1 Project overview

The current understanding of how a bioreactor scale affects a microbe is limited, hence the gap in knowledge that this work will try to fill. Since it is known that bioprocess performance tends to depreciate with increasing scale, then it is safe to assume that large-scale bioreactors (> 10 m^3) environment are fundamentally different from the small-scale. The most straightforward method to obtain information on how an organism responds to varying scales is to carry out experiments in the different bioreactor sizes available. However, the cost of doing so is prohibitive, and for investors looking to develop a new bioprocess, it would be foolhardy to fabricate a commercial size bioreactor first and collate experimental data from it afterwards. Thus, cheaper/reliable ways of how to mimic the final commercial bioreactor must be sought and used to generate process knowledge. This work proposes the use of a small-scale two-compartment reactor to simulate a large-scale aerobic fed-batch bioprocess. This is done by identifying the likely zones of gradients (areas around the feed, acid/base addition pipes and the air sparger) within the large-scale vessel. Once identified, these zones are simulated in one section of the small-scale two-compartment reactor while the other typically larger section models the bulk region. Thus, the fermenting cells circulating within these two distinct sections may experience a similar environment as in the large-scale reactor which, would result in an approximately similar cell physiological response by the organism. Past studies have indicated that the mixing inefficiencies seen at the large-scale, due to energy and mass transfer limitations, result in the performance differences seen on scale-up (Lara *et al.,* 2006a; Takors, 2012). Hence, the large-scale environment is an inhomogeneous one, where temporal and spatial dead zones (chemical/physical gradients) may occur (Enfors *et al.,* 2001; Vrabel *et al.,* 2000).

The two-compartment reactor design approach used here tries to identify and compartmentalise these regions of interest. The ability to regulate and simulate the large-scale environment on the small-scale grants an economical means to understanding how a commercially important organism (such as *Corynebacterium glutamicum*) will respond to some fermentation gradients (pH, glucose and dissolved oxygen) on scale-up.

The genetically modified cadaverine-producing strain of *Corynebacterium glutamicum* was selected because it is not a human pathogen, has a long history as an industrial microorganism and its relatively well-understood metabolic pathways. The biorefinery concept has driven the search for biologically produced compounds that can be easily used as precursors to make important commercial product(s) as an alternative to the petrochemical refinery. The primary product of interest here is cadaverine (1,5 – diaminopentane), a platform chemical of the future which can be used in the production of various materials and polyamides, such as polyamide 5.4 which has a high fatigue resistance, high melting point and low density (Thielen, 2010). The ability to develop inexpensive and environmentally benign bioprocesses is key for achieving a sustainable future. Thus, understanding how the large-scale inhomogenous environment and genetic modifications affect bacterial cells is important to creating viable bioprocesses.

1.2 Objectives

Some of the questions which this work will try to address are, how does genetic modification affect a bacterial cell? Do fermentation gradients lead to losses of productivity? If they do, how do changes in the cell result in these losses? Is the magnitude of the cells physiological response related to the type of fermentation gradient(s) simulated? How does poor mixing affect cell population homogeneity and viability?

The objectives of this work are as follows.

- Evaluate the growth kinetics of the *Corynebacterium glutamicum* strains and the effect of gene modification on productivity.
- Scale-down simulator bioreactor studies for small-scale analysis of the large-scale bioreactor inhomogeneities to improve the prediction of large-scale fermentation performance on scale-up of microbial systems.
- Develop a suitable multi-parameter flow cytometry assay for *Corynebacterium glutamicum* to study the different physiological states that may exist during fermentation in relation to large-scale inhomogeneities in the environment.
- Develop a method for quantifying lysine and cadaverine production as an output for monitoring fermentation performance.

The bulk and single cell assays used here give insight not only into the physiological changes in the cell that occur but on the magnitude of changes that might happen on scale-up. The understanding of how the inhomogeneites in large-scale bioreactors interact with a dynamic microbial population will help create better predictive tools.

This work was part of a larger European Research Area Industrial Biotechnology project (EIB.12.057), which consisted of the following partners.

- Institute of Bio- and Geosciences, IBG-1: Biotechnology, Julich, Germany
- Technische Universität Berlin, Germany; Sequip S & E GmbH, Düsseldorf, Germany

- Asociación de Investigación (INBIOTEC) Instituto de Biotecnología de León, Spain
- Vitalys I/S, Esbjerg N, Denmark
- SINTEF Materials and Chemistry, Department of Biotechnology, Trondheim, Norway.

The overall aim of this collaboration was to highlight the effects of increasing inhomogeneities, which occur in large-scale bioreactors, with respect to microbial physiology and production performance of a cadaverine-producing *C. glutamicum* strain. The cellular and process understanding was achieved by integrating the scale-down simulator bioreactor technology, innovative process analytical technology, multi-omics analysis and genetic engineering.

This objectives here are to develop a relevant scaled-down model and strategy that mimics the large-scale fermentation environment and to study how the strain of *C. glutamicum* used responds to such inhomogeneous surroundings.

1.3 Thesis outline

This report consists of seven chapters; the next chapter of this work highlights a brief history of fermentation and its development. The challenges of scale-up will be introduced, and some of the most important criteria for scaling up of aerobic bioprocesses discussed. The latter part reviews the different approaches to studying the large-scale fermentation environment using various scale-down models. The importance of *Corynebacterium glutamicum* as an industrial microorganism is also discussed in the last section of Chapter 2.

Chapter 3 highlights the composition of the media used for the cultivation of *Corynebacterium glutamicum* parent and modified strains, bioreactor designs and growth conditions. The assay development of both bulk and single cell analyses were also reviewed.

In Chapter 4, the growth kinetics of the *Corynebacterium glutamicum* parent strain and modified strain are compared. The collated parameters were used to characterise the cells and evaluate the feeding profile for the fed-batch process.

In Chapter 5 and 6, the results of various large-scale scenarios simulated in the two-compartment reactor are discussed. A comparison was then made to a well-mixed situation and the magnitude of the fermenting cells physiological differences were highlighted.

Chapter 7 presents overall conclusions and suggests further work that should be undertaken to answer some of the questions raised by this study.

CHAPTER 2

2 Literature review

The origin of fermentation cannot be ascertained with accuracy, but it is most likely that its discovery was a fortuitous accident. Archaeological evidence shows that over 6000 years ago ancient Egyptians were actively producing bread, beer and wine (Reisman, 1993). However, it was not until the early 1700s that real large-scale fermenters for beer and wine production were established (Corran, 1975). Since the inception of industrial biological processes, it has been plagued by associated scale-up issues. These problems arise from the need to maintain product quality, productivity, stability, purity, safety, process reproducibility and cost reduction as the scale of production is increased. One of the first solutions to process optimisation in some of these early commercial breweries was the implementation of temperature control. This development led to the fabrication of the first rudimentary heat exchangers of the 1800s (Stanbury *et al.,* 1999). Since then, process control has become more advanced and refined, from temperature control to sophisticated biosensors which can control a bioprocess to a narrow operational space. The aim of controlling the bioreactor environment is to ensure that every part within is suitable for the microbe and the synthesis of wasteful by-products is minimised. Thus, by manipulating certain process conditions, the production of certain compounds can be optimised. This is best seen in the penicillin and inclusion body processes, where step changes in pH, temperature and dissolved oxygen (DO) lead to changes in the cell physiology. Hence, if a fermentation environment is homogeneous, the cell physiological response in any part of the bioreactor is expected to be approximately identical. This is probably true for small vessels, but for the large-scale bioreactor, it can not be said to be homogeneous, because of mixing inefficiencies. This is because as the bioreactor volume increases both the energy and cost required to create a well-mixed environment becomes prohibitive. Ultimately, compromises (suboptimal are made in the engineering of large bioreactors, which leads to both spatial and temporal physical and chemical heterogeneity. A good example is the control of DO concentration in a stirred vessel $\geq$ 100 m^3, where mixing times can reach 4 to 5 min. The DO concentration is typically maintained by either the stirrer speed, sparging of air or gas blending. However, the DO probes are fixed within the bioreactor and only give an indication of the condition around where they are positioned (which may not be an accurate reflection of the whole). This consequently results in the DO controller compensating for misrepresented DO concentrations, which may lead to dead zones and changing DO conditions within a large vessel. The now-defunct company SmartINST in France tried to quantify the DO profile in large-scale bioreactors by designing spherical sensors which could float freely within the vessel and transmit data wirelessly. Thereby, giving the DO controller a better picture of the whole system. However, SmartINST's idea was met with problems of the transmission range (due to the thick walls and thermal insulation of large-scale vessels), damage to sensors on impact with impellers, trapped sensors in crevices within the reactor and defining the optimal amount of sensors needed without changing the natural flow pattern of the system to mention but a few. Thus, the difficulties in gaining information on the inhomogeneity of the large-scale vessel still exist regardless of the current state-of-the-art sensors and control strategies.

2.1 Challenges of bioprocess scale-up

There is no doubt that the technological strides made in the field of biotechnology have improved the quality of life and health; the impact of penicillin and recombinant proteins cannot be overemphasised. However, there remain fundamental scale-up problems, which are still not well understood to date. Some of the challenges associated with scaling up are, sterilisation, handling large volumes of material, microbial lag phases, holding time, cleaning, effluent inactivation, inhomogeneities, mass & energy transfer and the material of construction (Reisman, 1993). This list is not comprehensive by any means, but it gives an insight into the vast number of variables that must be factored in for the successful scale-up of a biological process. The history of biotechnology indicates that technology, as opposed to scientific understanding, has been the primary force behind the development of commercial bioprocesses. This scenario remains valid today; most industrial bioprocesses are not well understood, and the bioreactor has been rightly described in some quarters as a ‘‘black box’’ (Takors, 2012). In the short to medium term, companies may manufacture useful novel products via biological means, albeit in a suboptimal and wasteful manner (Palomares & Ramirez, 2009). However, with the salient issues of today such as climate change, sustainability and population growth, a better understanding of biological systems will become a prerequisite for any thriving biotech industry of the future. This is why the regulatory bodies such as the Food and Drug Administration, European Medicines and Drug Agency and the Medicines and Healthcare Products Regulatory Agency are encouraging the shift from mainstream Quality by Testing (QBT) to Quality by Design (QBD) approach in manufacture (Yu, 2008). Also, as consumers become more knowledgeable and regulations stricter, only manufacturers with the scientific understanding of their process and embedded quality in the design of their system will be granted access to the marketplace.

The scaling up of bioprocesses as it is practised today is a synergy of art and science (Noorman, 2011). There is no universal template for scaling up, thus every bioprocess to be commercialised starts uniquely (Schmidt, 2005). A complete characterisation and resolution of the primary input variables or operating conditions that affect quality, yield and stability must first be carried out. This makes bioprocess development time consuming and expensive, with no guarantee of success. In the past decade, advancement in high throughput technology, such as parallel bioreactors (ambr® 250, BioLector®) and robotics have been developed to reduce both time and cost of process development (Marques *et al.,* 2010). However, there is the need to adapt this technology to generate data for understanding how cells respond to large-scale inhomogeneous surroundings.

More recent is the advent of disposable bioreactors. This invention is particularly advantageous for small start-up companies, granting them an economical route to developing innovative products (Palomares & Ramirez, 2009). Its other advantages are it requires no sterilisation protocol or cleaning (as it comes sterile and ready to use), turnover time from batch to batch is quick, it is flexible and modular, but its application is limited to small and medium scale bioprocesses. These disposable bioreactors are especially prevalent in mammalian cell cultivations. However, for bulk bio-products manufacture and most microbial fermentations the traditional stainless steel large-scale stirred bioreactor still predominates (Palomares & Ramirez, 2009). Thus, there is the need to study the cells' physiological response in the large-scale stirred tank bioreactor.

Although for every biological process, the path to commercialisation is unique in many ways, there are still some common fundamental principles. The variables which affect biochemical dynamics and transport phenomena relate to bulk mixing, mass and energy transfer, foaming, gas-liquid interfacial area, and shear amongst others are universal (Marques *et al.,* 2010; Noorman, 2011). On scale-up, they are ranked and selected based on how they affect the yield, quality, cost and purity of the intended process. Thus moving up in scale, the most important of these variables are kept close to optimum to ensure productivity, reproducibility and predictability.

In most commercial bioprocesses, the following factor(s) is/are the most likely parameters to be constant on scaling up - volumetric mass transfer coefficient (k_La), volumetric power input and mixing time (Garcia & Gomez, 2009; Oldshue, 1966). This list highlights bioprocesses scale-up overdependence on the physical environment of the bioreactor, which has been implicated as one of the reasons why there is no universal model. Takors, (2012) suggested that a shift to using parameters strongly linked to biological properties might bring about a scale-up template. Such models should include the cell generation number, morphology and population heterogeneity.

The interdependence of these standard bioprocess variables makes it impossible to replicate a small-scale bioprocess at the large-scale fully. For example, in the scale-up from an 80 L to 10,000 L bioreactor, Lara *et al.,* (2006a) showed that if the volumetric power input were held constant, the energy input requirement would be 125-fold more and the circulation time will triple. In practice, this might not be sustainable, so engineering adjustments are typical. These make commercial bioprocesses an amalgamation of compromises, which may result in a suboptimal large-scale production environment. Thus, to future-proof success on scale-up, scaled-down models are necessary for studying how the conditions of the industrial fermenters affect an organism.

This work is limited to an aerobic fed-batch process. Hence, the capacity to transport oxygen to the growing cells will be emphasised in the following sub-sections, while the two other conventional scale-up variables will be briefly highlighted.

2.1.1 Volumetric mass transfer coefficient (k_La) based scale-up

Oxygen is an essential element in aerobic bioprocesses; it is typically introduced to the bioreactor by sparging air at the bottom of the bioreactor. All aerobic microorganisms need oxygen for growth, metabolism and maintenance, but the magnitude of demand is organism-specific (Büchs, 2001). The quicker a microbe utilises oxygen, the more difficult it is to replenish at an optimal rate, in a large aqueous environment. This is mainly because of oxygen's poor solubility in water, which is approximately 7 mgL^{-1} at 35 °C and 1 bar. Thus, if an organism's oxygen uptake rate (OUR) is not properly considered on scale-up, a substantial part of the bioreactor may become oxygen limited as metabolic activity increases. Sandoval et al., (2005) work showed that the introduction of an oxygen-limited section in the fermentation using a recombinant strain of *E. coli* resulted in a specific growth rate reduction by 30 %, this example confirms the importance of oxygen in aerobic processes. Since the cultivation of aerobic microorganisms continually requires oxygen, information on the optimal oxygen transfer rate (OTR) is crucial for engineering design. The OTR is affected by a wide range of factors, some of which change in the course of any fermentation. These factors include – the physical properties of the fermenting medium, Oxygen mole fraction, power input, total pressure and biomass concentration (Garcia & Gomez, 2009). In order to avoid a limiting oxygen environment, the OTR should be equivalent to or greater than OUR. A modified Damköhler number (Da) can be used to determine if oxygen availability is the limiting step in a bioprocess (Calik *et al.,* 2004); this relationship is highlighted in Equation 2.1.

$$Da = \frac{OUR_{max}}{OTR_{max}} \tag{2.1}$$

If $Da > 1$, such a system can be said to oxygen limited, in a dynamic system. The ideal bioreactor condition would have a $Da \leq 1$ for aerobic processes, before it can be assumed that the cells are able to utilise oxygen at their maximum potential. Regardless of the scale-up criterion selected it is still necessary to know the value of $k_L a,$ as this gives an indication of the system's efficiency in transferring oxygen from the gas to the liquid phase. Equation 2.2 shows both the relationship between the OTR and OUR and the dissolved oxygen mass balance of a well-mixed batch bioprocess (Garcia *et al.,* 2010a).

$$\frac{dC_L}{dt} = OTR - OUR \tag{2.2}$$

where, $\frac{dC_L}{dt}$ is the rate of change in oxygen accumulated in the liquid phase, all terms in Equation 2.2 have the same unit – (mol m $^{-3}$ s^{-1}).

However,

$$OTR = k_{\mathrm{L}} a(C^* - C_L) \tag{2.3}$$

C^* is the saturated oxygen concentration at the gas-liquid interface and C_L the concentration of oxygen in the liquid phase. The Equation 2.4 is derived by substituting Equation 2.3 into 2.2,

$$\frac{dC_L}{dt} = k_L a(C^* - C_L) - OUR \qquad 2.4$$

For bioprocesses, the magnitude of the OUR depends on the organism and its growth phase, for example, *Pseudomonas putida* has a high OUR, while *Xanthomonas campestris* has a low OUR (García *et al.,* 2000). The other well-known organisms, such as *E. coli* and *C. glutamicum* fall between these two extremes in their OUR values (Stanbury *et al.,* 1999)

From Equations 2.3 and 2.4 the $k_L a$ is linked to the OTR, which is closely related to the bioreactor's physical properties. The magnitude of the $k_L a$ is dependent on the total pressure in the bioreactor, the bubble size and the viscosity of the broth. To a lesser extent, temperature also plays a secondary but important role. When $k_L a$ is used as a scaling-up criterion, there is an implicit assumption that it can be held constant. In practice, this is not possible due to the dynamic conditions which predominate in the bioreactor environment, as steady state is rarely achieved. The $k_L a$ is a combination of two variables, k_L (mass transfer coefficient) and a (specific interfacial area). The $k_L a$ signifies the degree of resistance to transporting oxygen from the gas to the liquid phase, which is arguably constant in the course of a fermentation process (Garcia *et al.,* 2010b). However, for a, it cannot be said to be constant, because it is a function of the gas hold-up time and bubble size, which varies all the time in the bioreactor. This is due to the changes in the medium (increasing viscosity) from the metabolic activities of growing cells. Hence, given this situation, the assumption that the bubble size distribution is uniform even in a small-scale well mixed bioreactor is unrealistic. Therefore, at the large-scale, a non-uniform bubble size distribution should be expected, due to the sometimes inefficient mixing situation in industrial fermenters (Lara *et al.,* 2006a). It is also important to note the even if all the physical conditions within a bioreactor are tuned to achieve a certain $k_L a$, considerable system deviation may occur because of the biochemical reactions during fermentation. This is especially true in high cell density fermentations where a broth's viscosity could substantially differ from its start-up value. These issues pose challenges to scaling up based on the maintenance of a fixed $k_L a$.

So far, models and empirical correlations from the literature for evaluating $k_L a$ have not been universally successful because of the complexity of different fermentation systems. These inadequacies have been attributed to differences in growth medium composition, changing biological properties, different process conditions, dissimilar vessel geometry and measurement errors (Garcia & Gomez, 2009). Hence, the need to experimentally confirm the $k_L a$ for every individual fermenter.

The gassing-out method for deriving $k_L a$ was used in this work. It was chosen over methods such as the Gas Phase Analysis Technique (Van't Riet, 1979), Hydrazine Reaction Technique (Lara Márquez *et al.,* 1994) and Isotope Krypton-85 Technique (Pedersen *et al.,* 1994) because of its simplicity, rapidity and reliability.

The typical DO profile for the gassing-out method is illustrated in Figure 2.1. This procedure can be broadly divided into three stages. This first step is to aerate the medium until the DO reaches saturation with the air bubbles at C^*.

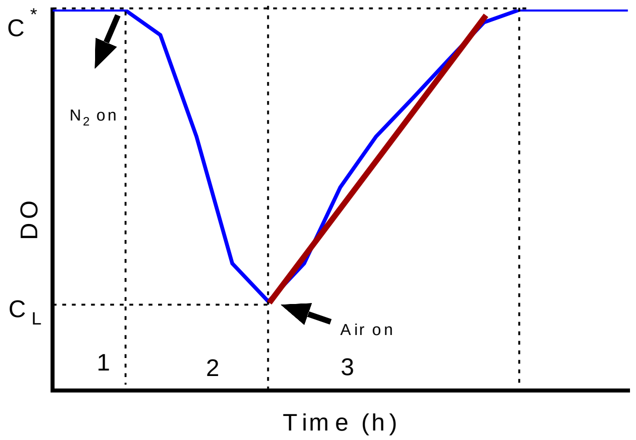

Figure 2.1 A typical plot of the dissolved oxygen concentration vs. time of the gassing-out method in the experimental determination of $k_L a$.

In the next stage, the air is turned off, and N_2 is turned on along with the agitation speed reduced to hasten the stripping out of the DO in the bioreactor, after that the air is turned back on until equilibrium is achieved. The last stage where the DO rises again is the region of interest and the slope of the red line in Figure 2.1 is estimated as the $k_L a$. If there are no cells in the medium used for the gassing-out experiment, the Equation 2.5 satisfies the mass balance around oxygen transfer in the bioreactor at stage 3.

$$\frac{dC_L}{dt} = k_L a(C^* - C_L) \qquad 2.5$$

Equation 2.5 can be rewritten in such a way that only measured C_L is needed to calculate $k_L a$ as shown in Equation 2.6.

$$C_L = -\frac{1}{k_L a}\left(\frac{dC_L}{dt}\right) + C^* \qquad 2.6$$

From a linear regression analysis of the straight-line Equation 2.6, $k_L a$ can be easily evaluated.

In situations where one DO probe is deemed sufficient to describe the DO concentration within the bioreactor, measurements are internally consistent.

However, in large vessels, more than one DO probe is typically used to track the DO profile. These probe locations are fixed within a bioreactor so in a sense the $k_L a$ estimate is truly based on a localised DO value. For smaller vessels, it is reasonable to assume a homogeneous environment, thus the $k_L a$ should be similar at any point within the bioreactor. However, for the large-scale bioreactor where more than one is used and mixing may not be efficient; it is important to bear in mind that the $k_L a$ estimate becomes more of a range or an average value, which may not reflect the true condition within the vessel. The success of the gassing-out method also depends on the oxygen probe response time, for if it is greater than $1/k_L a$, this method becomes unreliable (Van't Riet, 1979).

2.1.2 Other scale-up factors

The following factors are sometimes considered in the scale-up of biological processes.

Aerated power input (P)

This an important factor to consider in the design of any bioreactor and as a scale-up variable. The energy as a result of the P causes the circulation of the fluid held within a vessel, usually by mechanical agitation (Ascanio *et al.* 2004). Michel & Miller, (1962) indicated that empirical correlation of Equation 2.7 was suitable of Newtonian fluids.

$$P = \alpha * \left(\frac{P_0^2 * N * T^3}{Q^{0.56}}\right)^{\beta} \qquad 2.7$$

Where P_0 = unaerated power input, N = stirrer speed, T = reactor diameter and Q = volumetric gas flow rate. The constants α and β depend on the stirrer type and configuration; for a single Ruston impeller α and β equals 0.783 and 0.459

respectively (Gogate *et al.,* 2000). However, Equation 2.7 is not valid as Q approaches zero or at extremely high values (Michel & Miller, 1962)

Since the P causes turbulence and movement of the medium, it also influences the heat and mass transfer, mixing and circulation times. In large bioreactors, the cost of mixing can be considerable; it is, therefore, imperative to design a reactor that incorporates mixing efficiency with as small a power input as possible. Scaling up with a constant P has been mostly favourable for processes which require little energy input, such as in commercial yeast fermentations (Marques *et al.,* 2010).

Mixing time (t_m)

Ideally, in the mixing of different components held within a bioreactor, one of the main aims is to ensure that uniformity is achieved quickly. It can be defined by Equation 2.8.

$$t_m = \frac{V}{P_f N T^3} \qquad 2.8$$

where V = the medium volume, P_f = the impeller pumping number, N = stirrer speed and T = impeller diameter.

Therefore, if a bioreactor is well mixed, a sample drawn from any part of the reactor at any time, should be an accurate representation of the whole system. This makes the information about the time taken to homogenise the contents in a bioreactor a very useful design variable; longer mixing times may result in physical and chemical gradients (Chavan *et al.,* 1975).

One of the biggest challenges facing bioprocesses at the large-scale is in understanding how the industrial environment influences viable cells. The scale-down models can be useful in proffering answers at a reduced cost. Also, since the scaling up of every bioprocess is unique, the quest for a universal template can only be achieved if biological factors are actively included in future predictive models.

2.2 Scaled-down studies of the large-scale environment

The scale-up of a bioprocess usually happens towards the latter part of product development; it indicates an intention to commercialise. However, further upstream process development, small-scale bioreactors are predominantly used for characterisation. The data accumulated from this exercise is then used to predict performance on scale-up. The accuracy of this prediction depends on how close the small-scale experimental environment is to that of the large-scale.

In most cases these estimates fall short; hence the decrease in performance on the scale-up of fed-batch fermentation processes remains a major issue facing the bioprocess industry. This problem emanates from the inherent weakness of conventional scale-up methods, which do not take into account the often inhomogeneous chemical and physical environment that cells are likely to experience in a large scale industrial process (George *et al.,* 1993; Takors, 2012). In contrast, process optimisation, strain screening, and predictions on productivity are often based on data collected from small-scale well-mixed fermentations, where such inhomogeneities do not exist. It is, therefore, no surprise that initial productivity based on small-scale experiments fall short when applied to larger scales. The interaction of inefficient mixing, large hydrostatic pressure changes, and low gas solubility result in a situation, where temporal and spatial gradients predominate (Lara *et al.,* 2006a). The bacterial cell's response to the presence of dissolved gas (oxygen and carbon dioxide), nutrients, metabolites and pH concentration gradients are some of the primary reasons for losses in productivity seen at the large-scale (Amanullah *et al.,* 2001; Gray *et al.,* 1996; Xu *et al.,* 1999).

Toma et al., (1991) implicated shear stress damage, related to the introduction of turbines for mixing, as a detrimental factor in fermentation productivity. These studies could have been misinterpreted because counter studies have shown that as long as cell dimensions are less than the Kolmogorov microscale of turbulence, (typically for industrial fermentations > 20 μm) shear damage is unlikely (Boswell *et al.,* 2003; Chamsartra *et al.,* 2005; Hewitt *et al.,* 1998; Oh *et al.,* 1989).

Over the years, the quest to understand the large-scale fed-batch environment and how a bacterium responds within has fuelled the development of powerful experimental and analytical tools. One such tool is the scale-down reactor (SDR), which stems from the compartmentalisation of the large-scale environment into sections of interest (George *et al.,* 1993). Logically, any feed of a substrate should be added in the relatively well-mixed region of the impeller (area of highest energy dissipation rate), to reduce the magnitude of chemical gradients in large stirred tank reactors (George *et al.,* 1993; Hewitt & Nienow, 2007). However, this is not so in most industrial practice; the surface fed-batch process still predominates because of its ease of operation, ability to prove cleaning, the high cost of retrofitting longer dip pipes and the industry’s aversion to change. For a large-scale aerobic process, with a gas sparger located at the base of the vessel and a surface feed of a highly concentrated growth medium, the region around the impeller and sparger is considered to be well mixed and aerated but with low levels of nutrients (such as glucose). This results in an area where the cell metabolic rate is also low. Whereas, the zone where the growth medium is fed, is poorly mixed with a limited DO and a high carbon concentration. If there is rapid cell growth here (the formation of organic acids and stabilising proteins is increased), the DO concentration is even reduced further. In processes where the medium pH is controlled, the addition of a pH controlling agent (as the cell's response to a high nutrient/low oxygen concentration) leads to a localised region of high/low pH. Further away from these areas, towards the walls of the vessel, mixing is less efficient, creating a zone where both oxygen and nutrients are limited (Enfors *et al.,* 2001). The bulk region where cells spend most of their time has an environment somewhere in between the feed addition zone and the well-mixed area of the impeller, so growth rates adjust accordingly. For a circulating cell to adapt to this constantly changing environment at the large-scale, it typically responds by redirecting its carbon flux to maintain homoeostasis and/or switch to alternative metabolic pathways expending resource that could have been directed towards the desired end product(s) (Enfors *et al.,* 2001).

As already highlighted, one of the most economical ways of studying the large-scale environment is by experimenting with scaled-down reactors. These models are believed to be, to an extent, an approximation of the large-scale environment. Thus, a cell’s response during cultivation in these experimental models may mimic its response in an industrial fermenter. Here, the different types of models will be discussed and categorised based on the number of compartments. Previous studies from these SDRs will also be reviewed.

2.2.1 One-compartment SDR

Some of the earliest studies on mimicking large-scale reactors were done in a single small-scale reactor, usually the STR. If no thought is given to the final commercial scale environment, it is implicitly assumed that the small-scale well-mixed reactor is a good model of the large-scale reactor. As this is not true, researchers over the years have looked at ways of making SDRs a better approximation of the large-scale, e.g. by forcing time-varying operating or feed conditions in a single compartment STR.

Lin & Neubauer, (2000) studied the effect of glucose oscillations during a fed-batch fermentation of a recombinant strain of *Escherichia coli* K-12 in a single STR. They simulated short-term glucose starvation by equally turning off/on the glucose pump intermittently at periods of 30 s and 2 min - no explanation was given for the selection of these time scales, although they may have been chosen because the majority of *E. coli* proteins are influenced within 1 – 3 min of a change in cultivation condition (Neubauer *et al.,* 1995a). The product stability, cell death rate and the growth rate of plasmid-free cells of these simulations were then compared to a continuous glucose fed-batch control experiment. The α – glucosidase yield declined by 80 % as the pump on/off period was increased from 30 s to 2 min, at termination (20 h after induction with Isopropyl β-D-1-thiogalactopyranoside (IPTG)). Although both simulations had the same concentration of α – glucosidase (≈ 300 mgL^{-1}) 3 h after induction, only the 2 min glucose on/off cycle showed a substantial decline untill (≈ 80 mgL^{-1}) termination. They suggested that this large decrease in total α – glucosidase concentration was due to the elevation of the alarmone ppGpp (a stress response), which may have links to known proteolytic enzymes such as C1pP. However, the lowest number of plasmid-free cells (cells poorly adapted to fermentation conditions) was seen at the shorter 30 s glucose on/off cycle. They suggested that the higher transient levels of ppGpp resulted in the better adapted cells from the fermentation of the 30 s glucose on/off simulation. Furthermore, the dry cell weight (DCW) of the SDR with a glucose on/off period of 30 s experiments was 50 % less than that of 2 min which confirmed that the cell stress response was higher at the 30 s feeding interval.

Neubauer *et al.,* (1995a) used a similar SDR to investigate the profile of guanosine tetraphosphate ppGpp as a response to glucose oscillations in the fed-batch cultivations of *E. coli* K-12 W3110. The results showed that glucose starvation for ≥ 30 s led to an elevated ppGpp concentration reaching 10-fold the level recorded in their control fermentation, but no DCW loss was observed (maximum DCW attained was ≈ 9.2 gL^{-1}). However, Hewitt *et al.,* (2007) later highlighted that the effect of glucose starvation in this strain did not occur until after a DCW of 18 gL^{-1} had been achieved.

Schilling *et al.,* (1999) investigated the mixing time effect on a lysine fermentation fed-batch process using a leucine-auxotrophic strain of *Corynebacterium glutamicum*. Their scaled-down model (mimicking a 10,000 L STR) was a 42 L STR with six Rushton stirrers and five cylindrical disks retrofitted to increase the mixing time (a 13-fold increase compared to a standard 42 L STR). The fermentation results from this scaled-down model indicated a 7 % and 12 % decrease in dry cell weight and lysine concentration respectively when compared to the control 42 L STR. A productivity decline, which was attributed to the reduced citrate synthase, aspartate kinase and phosphoenolpyruvate carboxylase enzymes activities, from the cells response to the presence of DO, substrate and pH gradients.

Suarez-Mendez et al., (2014) studied the short-term response of *Saccharomyces cerevisiae* CEN PK 113-7D to a glucose on/off cycle in a chemostat fermentation. Their experiment was based on a 20 s glucose on and 380-s glucose off block-wise strategy in an STR of 3.9 L working volume. The report indicated a 5 % decrease in DCW and a 2-fold increase in specific acetate production (which indicates an elevated stress response), compared to the control chemostat fermentation. The pentose phosphate pathway, TCA cycle and the storage carbohydrate intermediates were also different, suggesting that the bacterial cells adapted to the glucose feed oscillations by modifying their metabolic pathway.

Thus, fluctuations in glucose concentration may result in changes in metabolic profile, improved robustness, reduced product quality and decreased DCW depending on the organism and type of fermentation.

The *S. cerevisiae* NCYC 1018 strain response to DO gradients was evaluated by Namdev et al. (1991). The following three different air supply strategies – continuous, fixed periodic and the Monte Carlo cycles were compared. They argued that the Monte Carlo-based cycle better represented the large-scale Circulation Time Distribution CTD compared to the fixed periodic oscillations. For the Monte Carlo simulation, the Circulation Time (CT) distribution curve was divided into 25 elements of equal probability, with each element representing a CT between 8 s and 44 s. This range of CT was chosen because they suggested that it was similar to that in a 100 m^3 STR. The total cycle time was selected at random from these 25 CTs, while the air was turned on for 5 s during each cycle. Their results showed that the continuous air supply fermentation achieved the highest DCW of all (14.8 gL^{-1} on average), while the Monte Carlo cycle saw a 16 % decrease in DCW and a slightly higher ethanol formation compared to the fixed periodic cycle. The increase in higher ethanol formation was attributed to DO limitation and fluctuation. They also highlighted that the difference seen between the Monte Carlo and fixed periodic cycle even with the same average CT indicated that the fermenting cells were also affected by the CTD. The response to oxygen fluctuations during the batch cultivations of a modified *E. coli* DH5α strain was investigated by Namdev et al.

(1993) using the Monte Carlo method as above. The Monte Carlo simulations showed a 50 % loss in plasmid copy number compared to the control batch fermentation (indicating an increased stress response), but neither loss in DCW nor yield of β-galactosidase was observed.

Cortés et al. (2005) compared the effect of DO oscillations of fixed on/off periods of 300 s, 600 s and 1200 s cycles in the batch fermentations of *Kluyveromyces marxianus* NRRL-Y1109 (no reason was given for the selection of these timeframes). These experiments were carried out in an STR of 1 L working volume. In comparing the 1200 s period of oscillating DO to the control (no DO oscillation), they reported no loss in DCW, but a 2.6-fold increase in ethanol and a 20 % decrease in the final β-galactosidase specific activity. This difference, they suggested was due to DO limitation which encouraged the cells' fermentative pathway. The report also showed that for the 300 s DO oscillating cycle the β-galactosidase specific activity increased by 12 % when compared to the control. They claimed that if the magnitude of DO fluctuation was low (< 300 s) it promoted better cell adaptation, which resulted in an increased β-galactosidase productivity.

The one compartment model is easy, quick and economical to set up. However, critics highlight that in these experiments all the cells are exposed to the same fluctuating values of DO and substrate concentrations, whereas in the large-scale fermenter different zones and CTD within the bulk flow are known to exist (Sweere *et al.,* 1988). Also, one of the limitations highlighted by the above investigators was the difficulty in simulating a cyclic environment at shorter periods. Namdev et al., (1993) attributed the lack of oscillation in the DO within the 20 s cycle to the slow response of the probe. In studies conducted by Neubauer, Åhman, et al., (1995); Lin &

Neubauer, (2000) and Suarez-Mendez et al., (2014) where nutrients were periodically dosed, no cyclic trend was observed, but a linear profile was recorded.

2.2.2 Two-compartment SDR

This is currently the most widely-used setup for studying the inhomogeneous conditions at the large-scale. The two forms of this model will be discussed below.

STR/PFR configuration

This setup consists of an STR in series with a PFR and the cell growth medium circulated through both reactors; Figure 2.2 shows a simplified schematic of this setup. The STR environment is usually well mixed and uniform, while the PFR is the poorly mixed section where potential chemical and physical gradients may exist.

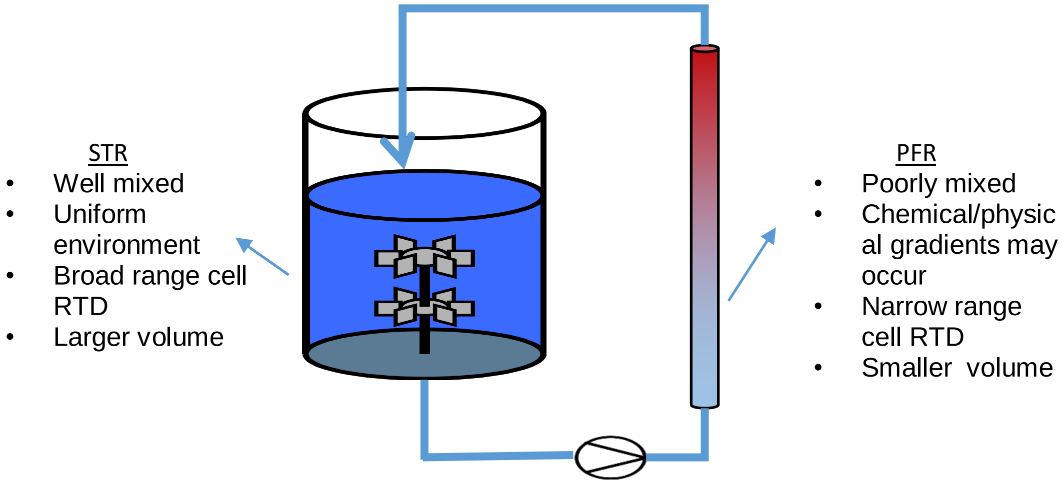

Figure 2.2 A simplified diagram of an STR/PFR two compartment SDR. Residence Time Distribution (RTD)

The cultivation conditions in the STR was different from that of the PFR (Figure 2.2). The STR working volume is usually the larger of the two reactors; it is where the cell spends the most time, hence the larger range in RTD. The ability to tightly control the cell mean residence time in the PFR, the relative ease of observing a cell physiological change with respect to the distance travelled along the PFR and its flexibility, are some of the STR/PFR advantages.

A two-compartment SDR was used to impose carbon (substrate - molasses) concentration oscillations during fed-batch fermentations of *S. cerevisiae*, which enabled George et al., (1993) to investigate the cells' metabolic response to the oscillations. They combined an aerated STR with an oxygen-enriched PFR, to remove any effect of DO limitation from the study. The concentrated feed (molasses of 29.5 % w/w) was added either to the PFR or the STR in separate experiments. The PFR had a volume of 850 mL, while the STR volume was 15 L (no reason was given for the selection of these particular scales). Their simulation when the feed was added to the PFR showed a 6 % loss in the final DCW compared to a control fed-batch fermentation in just the STR. However, the claim of a higher ethanol yield (due to a higher rate of glycolysis) during their SDR simulation is debatable, because, in all experiments, its final concentration returned to zero. This disappearance of ethanol at the end of the process was attributed to evaporation, which is not possible as ethanol cannot only evaporate leaving behind an aqueous broth. George et al., (1998) went on to use the same SDR to further study the effect of molasses gradients on a Baker's yeast fermentation and compared its performance to that in a 215 m^3 bubble column reactor. The τ_{PFR} set at 60 s for their scaled-down reactor was claimed to match the mean circulation time of the large-scale bubble column reactor. The investigators reported a 6 to 7 % loss in DCW when the SDR and the large-scale fermentations were compared to the well-mixed bench scale cultivation. They showed that ethanol production was higher in the SDR, especially during the exponential growth phase when it was ≈ 1.7 times that of the control. The study also highlighted that the gassing power of this yeast cell improved when it was cultivated in a heterogeneous environment. This increased gassing power was recorded in both the SDR and the large-scale bubble column fermentation but not in the homogeneous small-scale STR.

Lorantfy et al., (2013) investigated the effect of limited oxygen conditions on a *Pichia pastoris* Mut+ SMD 1168 strain in batch fermentations. The PFR section was 10 % of the 1 L STR compartment, and they tested the τ_{PFR} range from 1 min to 7 min. In this configuration, the STR was aerated, but the air entrained in the broth before entering the PFR was eliminated. They showed that the cells' maximum specific growth rate was much more affected (≈ 12 % loss in DCW at τ_{PFR} of 7 min) compared to the control batch process. They also linked the increase in acetate concentration to the increase in τ_{PFR} in the oxygen limited PFR.

Neubauer, et al., (1995) studied the response of an *E. coli* W3110 strain to oscillations of glucose and DO concentrations during fed-batch fermentations. The setup had a 10 L STR in series with a PFR of 860 mL, which had a constant τ_{PFR} of 113 s (no justification was given for the selection of these values). Their paper indicated that when the concentrated glucose feed was added to the oxygen restricted PFR, a 24 % decrease in DCW and a 10-fold increase in acetate concentration were observed. This response was attributed to the localised high glucose concentration and DO limitation. The feeding profile used was constant, resulting in an ever-decreasing specific growth rate as the cell mass increased. This makes it difficult to compare performance across experiments, because the growth rate changes as the amount of glucose available decreases. Schweder et al. (1999) argued that the expression of stress genes can be used to monitor performance in large-scale bioprocesses. They showed this by comparing a SDR to a 30 m^3 industrial scale fermenter. The SDR consisted of an aerated 15 L STR (τ_{STR} of ≈ 9 min) connected to an unaerated 0.695 L PFR (τ_{PFR} of 54 s). The SDR was used to simulate both glucose gradients and glucose/DO gradients. A key finding from this work highlighted how quickly the *E. coli* W3110 strain responded to process stress such as localised high/low glucose concentrations and concomitant DO limitation. For example, they showed that these cells responded to a 7 °C increase in temperature from 35 °C to 42 °C within 13 s to 15 s. In their SDR experiments, they induced the synthesis of some of these stress mRNAs by circulating the broth through the PFR zone, which was high in glucose and low in oxygen. They then linked the *ackA* mRNA to the cell's overflow metabolism (induced by high rates glycolysis), *proU* mRNA to the osmotic condition of the medium and *frd* mRNA to oxygen availability. Interestingly in all variations of their SDRs, the stress mRNA profiles were different to the 30 m^3 fermenter. Although the difference in mRNA profiles indicated that their SDR was not a complete representation of the 30 m^3 STR, their work however showed that these mRNA profiles could be used to monitor and evaluate the physiological state of the bacterial cells. Hewitt et al. (2000) investigated *E. coli* W3110 response to glucose and dissolved oxygen gradients during fed-batch fermentations. The STR working volume started at 2.5 L rising to 4 L upon termination, while the PFR volume was held at 0.54 L. Four scenarios were simulated by varying the entry points of both air and glucose. These simulations led to different degrees of cell physiological response. In one of the simulations where the glucose and base were introduced into the unaerated PFR with a τ_{PFR} of 50 s. They reported a 35 % decrease in DCW yield and a 15 % increase in viability, results which were similar to that in a 20 m^3 fermentation. Based on this, the investigators concluded that this configuration best mimicked the large-scale. Nevertheless, this conclusion might be over simplistic, as there was neither data on the profile of other metabolites or transcriptional enzymes to support such a conclusion, which would give better evidence on the similarity of the cells response in both systems. From the additional flow cytometry results, they were able to show the *E. coli* cell membrane integrity and potential was related to its growth phase and the cultivation environment. For example, they observed that in the 20 m^3 fermentation, the population of healthy cells continually improved untill the end of the process, which was contrary to the well mixed small-scale situation. The authors inferred that process gradients somehow lead to better adapted cells, which improved viability as seen in the large-scale. They also showed that throughout the course of fermentation, healthy, depolarised and dead cells coexisted regardless of scale. This highlighted that the prevailing idea of a homogenous cell population even in a well-mixed system is questionable. Bylund *et al.,* (2000) studied the effect of glucose and DO gradients on protein quality during the fed-batch fermentations of a modified strain of *E. coli* W3110 in a two-compartment SDR. The SDR had a 7 L STR working volume, which increased to 9 L at the end, connected to a PFR of 0.44 mL with a constant τ_{PFR} of 24 s. Their results showed that after induction, formate rapidly accumulated in all reactors regardless of scale, but in the SDR it was twice that of either the 300 L pilot-scale reactor or the 7 L control. The DCW decreases in the SDR simulations ranged from 6 % to 10 %, which were attributed to the added stress of glucose and oxygen fluctuations. Oddly, the quality of the product (recombinant human growth hormone, rhGH) was highest in the SDRs, increasing on average by 10 %. In their own words, they explained this by stating that the SDR conditions made the bacteria cell ‘imagined’ that it was constantly in a glucose rich environment due to the oscillations. However, if it is supposed that the SDR was correctly modelling those conditions in the 300 L STR as proposed by the authors, then the quality of the product from these reactors should have been similar, which was not the case. Finally, they concluded that oxygen limitation triggered by glucose overflow was the critical parameter to *rhGH* productivity and quality. Junne et al., (2011) reported on the effect of glucose and oxygen oscillations on a non-sporulating *Bacillus subtilis* AS3 strain. The setup consisted of a 10 L STR connected to an unaerated 1.2 L PFR with a constant τ_{PFR} of 60 s. They observed a 6-fold and a 2-fold increase in ethanol and arginine concentration respectively during the SDR fermentations. This effect was attributed to some unknown re-assimilation mechanism. In all experiments, the final DCWs were similar (≈14 g/L) and no decreases were recorded.

Amanullah et al., (2001) argued that if the addition of base/acid was introduced at the liquid surface of the large-scale reactor (controlled by pH probe(s) at different fixed locations) pH gradients could occur if the mixing time was long and metabolic activity high. They then went on to simulate pH gradients during the batch fermentations of *B. subtilis* AJ1992 strain by adding the base at the 50 mL PFR section of the SDR (τ_{PFR} ranged from 30 – 240 s), while the 2 L STR had a working volume of 1 L. The bacterial cell response to the pH variations resulted in a 27 % decrease of the final product concentration (Acetoin and 2,3 – Butanediol) and a 0.75 gL^{-1} accumulation of acetic acid from zero compared to the control. This response was attributed to the bacterial cells' exposure to the PFR's limited DO and fluctuating pH values. They reported no loss in DCW productivity, this may be because the final values attained were low ≤ 4.61 gL^{-1} and any effect too small to be observed via the drying out method as suggested by Hewitt et al., (2000)

Onyeaka et al., (2003) simulated three chemical gradients (pH, glucose & dissolved oxygen) during fed-batch fermentations using the same *E. coli* W3110 strain and the experimental setup of Hewitt et al., (2000). In one of the simulations where the glucose and base were added to the unaerated PFR section (τ_{PFR} = 110 s) a 71 % decrease in the final DCW was observed, but the cell viability remained high (≥ 94 %). The substantial DCW loss was attributed to the high glucose, low DO concentrations and pH fluctuations of the PFR, which led to a predominant non-proliferating dormant cell population. The effect of these same gradients were later investigated on a recombinant *E. coli* BL21 MSD3735 protein (AP50)-producing strain during fed-batch cultivations (Hewitt et al., 2007). The SDR was the same as used by Hewitt et al., (2000). The result indicated that the formation of the AP50 protein exerted considerable stress on the cells, which led to a 70 % DCW decrease compared to the control where the formation of this protein was not induced. They also showed that when the cells were induced later on in the process, the growth rate was twice as high (a 9 h IPTG induction was compared to a 14 h), which meant the effect of AP50 expression was attenuated in the 14 h induction. This attenuation was claimed to be due to a reduction of IPTG concentration per cell. However, they did not quantify the actual AP50 protein levels, so could not show if the SDR simulations had any effect on productivity.

STR/STR configuration

The argument for this setup suggests that since chaotic mixing predominates in the large-scale vessel, it might best be mimicked by a system which has a similar CTD. Thus, proponents see the STR/STR configuration as a better choice, because in both compartments a broad range of RTD (residence time distribution) can be simulated under different uniform conditions (see Figure 2.3) (Limberg et al., 2016a).

The current influx of commercial parallel STR modules (such as the DasGip©) is set to make this configuration popular in future.

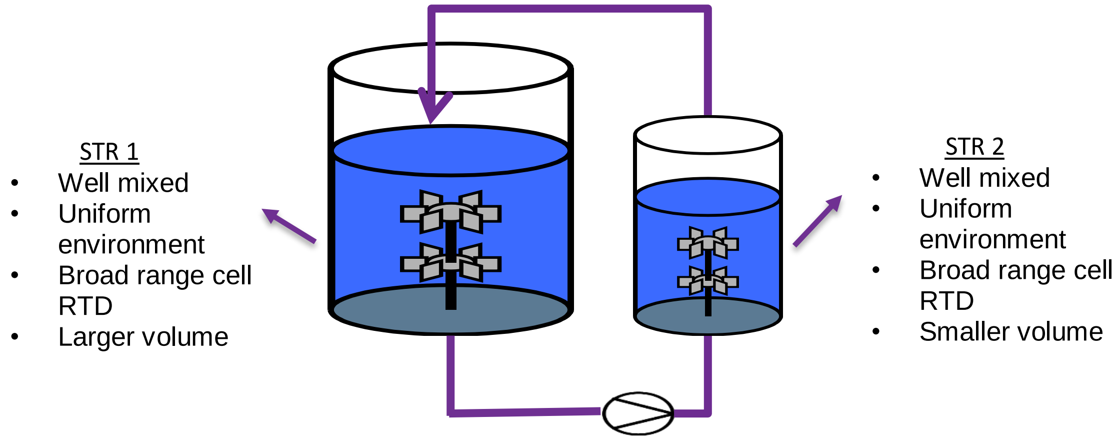

Figure 2.3 A simplified diagram of an STR/STR two compartment SDR

Oosterhuis *et al.,* (1984) studied the impact of DO fluctuation on the fermentation of *Gluconobacter oxydans* to produce gluconic acid; the two connecting STRs used had working volumes which varied from 0.25 L to 1.6 L. Their results indicated that decreasing the τ_{STR} in the aerated STR from 17 s to 6 s reduced the gluconic acid productivity by 60 %. They also noted irreversible cell damage when DO values exceeded 0.6 mmol L^{-1} in the simulations where pure oxygen was used to achieve high DOT values (> 80 %).

The metabolic profile of a cadaverine-producing *C. glutamicum* DM1945 strain was investigated by Limberg et al., (2016b) under fluctuating conditions of oxygen and glucose gradients during fed-batch fermentations. Their setup consisted of an aerated STR of working volume 0.78 L connected to an unaerated STR of 0.2 L which had a τ_{STR} of 3 min. There were two slightly different conditions simulated in the smaller STR. In one scenario, the DO was actively stripped with a N_2/CO_2 mix (anaerobic conditions), while in the other case (no gas stripping was done) the smaller STR was oxygen limited as its DO supply was from the trapped air bubbles coming from the larger STR. They reported no decrease in DCW and cadaverine productivity in all simulations investigated (for all cases, the final DCW reached was ≈ 12 gL^{-1} and cadaverine productivity was ≈ 0.22 mmol g^{-1} h^{-1}). Their work highlighted a significant alteration in the expression of 38 genes and 28 protein levels during the SDR experiments. They reported that the mRNA levels of L-lactate dehydrogenase (*ldh*) and malate dehydrogenase (*mdh*) increased on average 3.5-fold and 2.8-fold respectively compared to the control. This suggests the cells were responding to the oxygen limited conditions in the smaller STR. However, this increase in *ldh* and *mdh* were only significant only when the trapped O_2 in the smaller STR was actively stripped out with a N_2/CO_2 mix. There was no justification for actively stripping DO except for the need to elicit a stronger cell physiological response but doing so changes the dissolution rates of gas in the medium, which moves the SDR further away from the large-scale environment. They also argued that lactate produced in the smaller non-aerated STR was re-assimilated in the larger aerated STR. This argument is questionable because there was no mention of the glucose consumption rate. However, if the glucose feeding profile was exponential as they claimed, then at no point during the process was the glucose concentration too low in the larger STR, hence negating the bacterial cells need to re-assimilate lactate.

Lara et al., (2006) reported on the transcriptional and metabolic levels of a modified *E. coli* W3110 (ATCC 27325) strain response to spatial dissolved oxygen gradients using an STR-STR configuration. The larger STR (0.8 L, τ_{STR} = 33 s) was maintained under anaerobic conditions while the smaller STR (0.4 L, τ_{STR} = 17 s) was maintained at a DOT of 10 %. In their batch cultivations, they observed a 30 % decrease in the specific growth rate but, a 2.4-fold increase in specific glucose uptake, which indicates an increased cell maintenance requirement. The maximum concentration of lactate and succinate increased by 53-fold and 21-fold respectively in the SDR experiments. Their analysis of the various gene transcription profiles suggested that under oscillating DOT conditions the TCA cycle splits into two biosynthetic pathways. These consisted of a reductive branch producing succinyl-CoA and an oxidative branch producing 2-ketoglutarate. This indicated that *E. coli* adapted to DOT gradients by repressing the cytochrome O oxidase gene, thereby leaving the cells to utilise the less energy efficient, but high oxygen affinity, cytochrome D oxidase for respiration.

Sandoval et al., (2005) studied the effect of increasing the CT on a recombinant *E. coli* W3110 strain encoded for human proinsulin. Its response was quantified in term of DCW, productivity and by-products. Their experimental setup was made up of two STRs, an aerobic and an anaerobic compartment of 0.35 L and 0.7 L respectively. The CTs were varied from 7 – 180 s, to mimic a worsening mixing scenario. They noted a 30 % and 94 % decrease in specific growth rate and maximum proinsulin concentration as the CT was increased to 180 s.

The two-compartment model is currently the most popular setup amongst researchers for studying fermentation gradients at the large scale. This is due to its low cost, flexibility, ease of use and simplicity to mention a few. For example, top surface additions may be better represented in an STR/PFR setup, while for subsurface additions near the impeller, the STR/STR configuration.

2.2.3 Three-compartment SDR

Recently, researchers have started using three compartment SDR models to represent different gradients within a large-scale fermenter. A variant of this setup was used by Buchholz et al., (2014), see Figure 2.4.

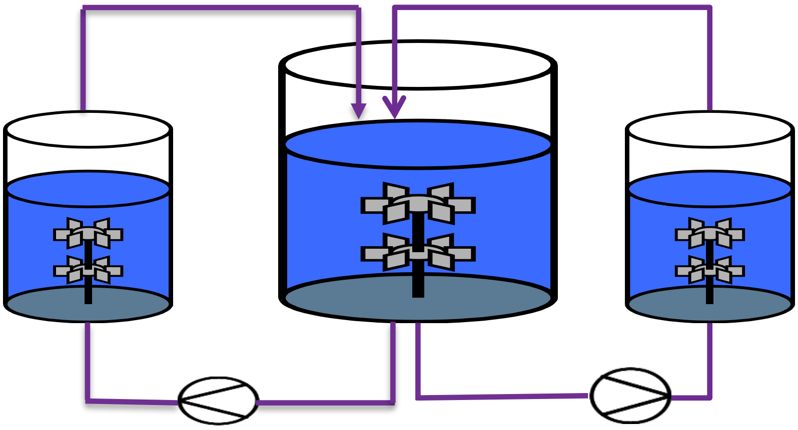

Figure 2.4 A simplified diagram of an STR/STR/STR three-compartment SDR.

In carrying out batch fermentations, Buchholz et al., (2014) went on to simulate CO_2/HCO^{3-} gradients of the large-scale in this SDR which comprised of three STRs as shown in Figure 2.4. The transcriptional response of these oscillations on a *C. glutamicum* ATCC13032 strain was then studied. The setup was made up of a 25 L working volume STR and two 1 L STRs connected in series. These 1 L vessels were slightly pressurised to increase the dissolved CO_2/HCO^{3-} in the medium. This was done to mimic the increased dissolution rate of CO_2/HCO^{3-} due to the high hydrostatic pressure observed in some large-scale fermenters of high aspect ratio. They recorded no decrease in the specific growth rate and DCW yield, but 29 gene transcripts were altered. The most affected were cg0992 (a putative sulfate permease), cg0993 (a putative transcriptional regulator) and cg2810 (a symporter), which saw a 3.58-fold, 3.34-fold and 3.53-fold increase respectively.

Lemoine et al., (2015) compared the effect of dissolved oxygen and glucose oscillations on a different *C. glutamicum* (DM 1800) strain in a two and three-compartment SDR, which consisted of an STR/PFR and an STR/PFR/PFR configuration respectively, see Figure 2.5 for this variant of the three-compartment reactor.

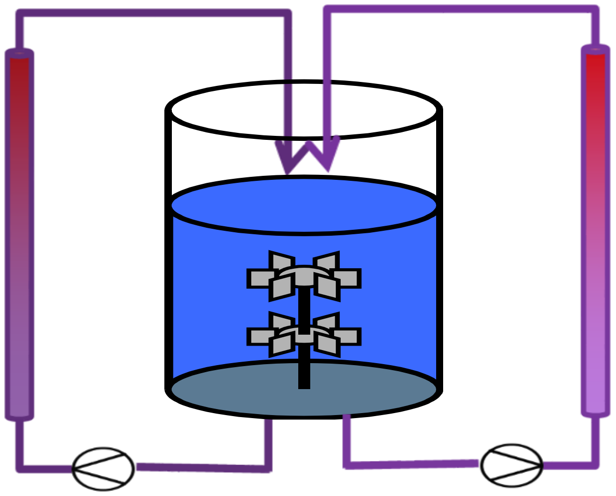

Figure 2.5 A simplified diagram of an STR/PFR/PFR three-compartment SDR.

In the three-compartment reactor, glucose was added to only one of the PFR, and both PFRs were unaerated. For the two-compartment reactor, the PFR (1.2 L) was unaerated, while the glucose was added to the aerated STR (10 L) section. All volumes remain the same as above, and the air was introduced at the STR. The feeding profile was constant at 0.0017 h^{-1} in all simulations. Their results showed no difference in both DCW and lysine productivity when both SDRs were compared. Some of the metabolites, such as fumarate, aspartate, acetate, and malate, showed no difference in their concentrations. Others such as glutamine, glycine, succinate and pyruvate showed slight differences, although experimental errors cannot be ruled out in this case, due to the low values involved (0 – 0.9 mmol). Also, the magnitude of experimental error was not indicated in their results to resolve this matter.

From the SDRs discussed thus far, it can be inferred that SDR/PFR setup is most popular amongst researchers. Not necessarily because it is the best, but it offers sampling flexibility which can be correlated to different residence times along the PFR and a tighter control on the cells' residence time. This allows the nature of the fermenting cell physiology to be studied quickly. Making SDRs more complicated (such as the three-compartment models) does not add much value to the understanding of how growing cells respond to bioprocess heterogeneity, and increases the cost of experimentation. This is because similar information can be easily obtained from two-compartment models, which was inadvertently illustrated by Lemoine et al., (2015). However, what is important to note is that none of the SDRs highlighted here are representative of the environment at the large-scale, but at best are crude approximations. Our understanding of the large-scale STR is limited, especially in large vessels > 50 m^3, where the relationship between growing cells and their environment is probably far from what is perceived currently. The interaction of factors such as gas dissolution rates (due to large hydrostatic pressures, where the solubility of gases could change by a factor of 2), gas stripping rates, metabolites production, changing viscosity (due to cell growth and product increase) are just a few issues which make the large-scale environment complicated. Also, the relationship between compartment volumes and mean residence times remains unresolved, as estimating the area of interest in relation to the vessel is difficult to measure directly. Thus, most researchers rely on CFD models (as done here) to infer this relationship. Even if these dead zones and gradient regions were measured directly, the dynamic environment of the large-scale STR makes it arduous to accurately monitor this relationship because it changes all the time during a process. Hence, simulating accurate models to mimic the hydrodynamics of the large-scale is hard. However, this does not mean that the present range of SDRs configurations available cannot be used, but expectations should be realistic. Also, current SDRs can be used to select robust strains, design operational space, highlight stress indicators and document cell stress response to the bioprocess gradients discussed thus far.

2.3 Enhancing *Corynebacterium glutamicum* productivity and achieving sustainability

With the two biggest issues of the 21st century, global warming and rising human population, developing innovative manufacturing strategies is crucial. The switch from high to low carbon footprint processes can be both economical and benign to the environment. The rapid development of metabolic engineering, systems and synthetic biology is set to bring novel products to the market. This will be aided by creating genetically modified organisms (GMO) which will increase bioprocesses yields and reduce cost. Thus, making the biotech route a much more compelling alternative to current conventional means of energy, drug and material manufacture.

Since the isolation of *C. glutamicum* in the 1950s, it has become an important industrial microorganism finding traditional use in the production of amino acids (Kinoshita et al., 1957). *C. glutamicum* is a Gram-positive, rod-shaped vegetative bacterium. Each year an increasing amount of research to manufacture essential novel products from exotic microorganisms is conducted. However, only a few of these products make it to market, and an even smaller number of microbes are used in commercial production. This makes industrial microorganisms a unique subset: they must be robust, malleable to modification and have a sustainable level of productivity. In order to increase the competitiveness of bioprocesses, it is necessary to engineer microbes which can utilise cheap feedstocks to produce useful products. One of the many advantages of *C. glutamicum* is its ability to use a broad range of carbon sources. Naturally, it can use glucose, fructose and sucrose, but with gene modifications, this ability can be broadened. The recycling of agricultural, industrial and human waste as feedstock for bioprocesses would allay the public fears on the diversion of human food for producing products. Figure 2.6 indicates the current carbon sources utilised by *C. glutamicum* and its many metabolic pathways.

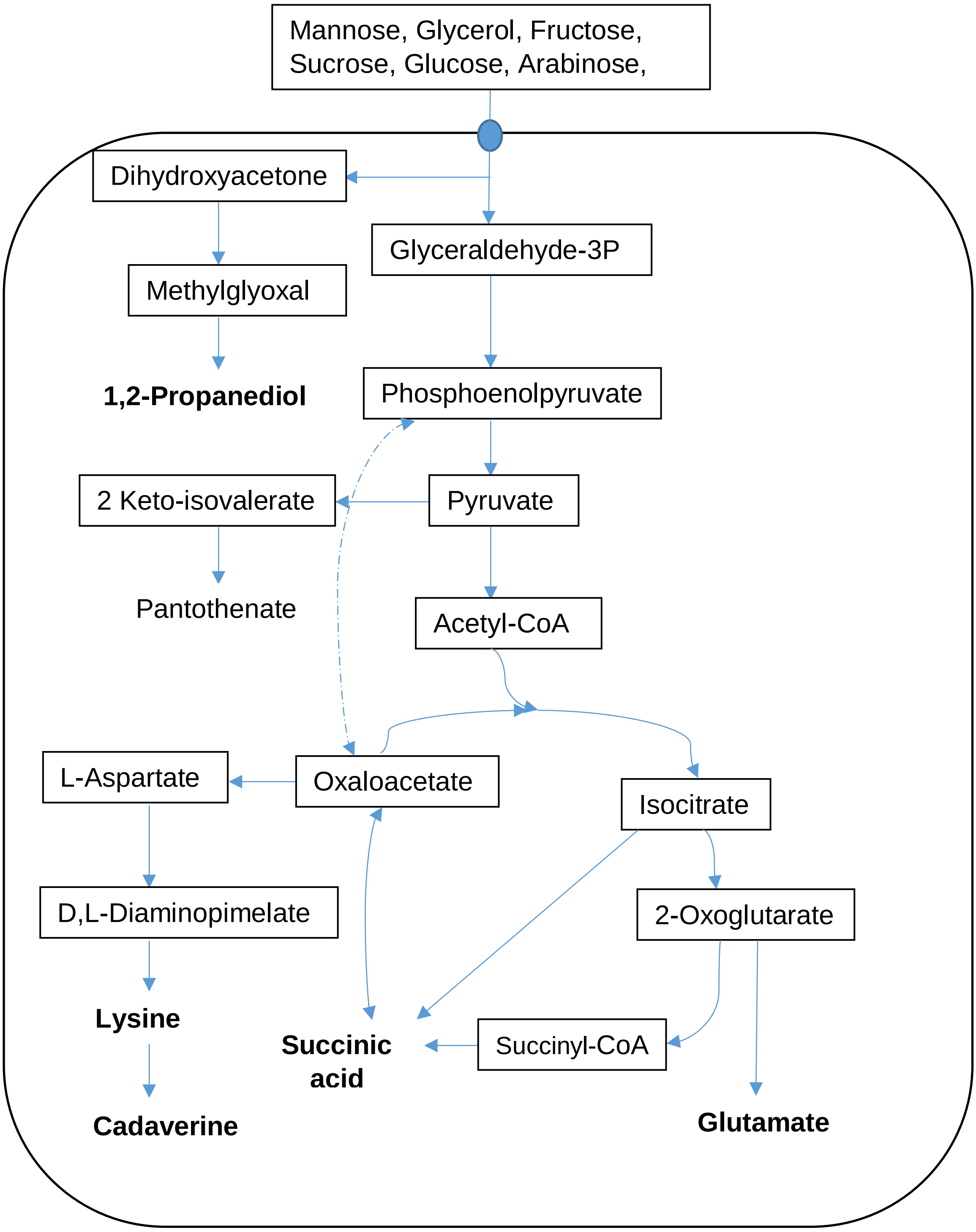

Figure 2.6 A simplified C. glutamicum metabolic pathway adapted from Dominguez *et al.* (1998) and Kind & Wittmann (2011)

Figure 2.6 shows the range of carbon sources that can be metabolised into useful compounds. Some of the studies highlighted below will illustrate the potential of modifying *C. glutamicum* to convert low-value feedstocks to high-value products. As the genome-editing technology improves (especially in the wake of the Clustered Regularly Interspaced Short Palindromic Repeats (CRISPR) technique), current unmetabolisable carbon sources are set to be made usable, thereby increasing bioproduct portfolio.

Adachi et al., (2013) constructed a beta-glucosidase (BGL), which gave *C. glutamicum* the ability to degrade cellobiose to produce L-lysine. After four days of fermentation, the final titre value of L-lysine reached was 1.08 gL^{-1} from 20 g of cellobiose. Kawaguchi et al., (2006) showed that under oxygen-limiting conditions the modified *C. glutamicum* CRX2 produced predominantly lactic and succinic acid from xylose. This strain carrying both the xylose isomerase and xylulo-kinase gene from *E. coli* could also utilise any combination of glucose and xylose without exhibiting a diauxic effect. Rittmann et al., (2008) engineered a *C. glutamicum* strain that grew on glycerol to produce lysine. This was done by inserting glycerol kinase, glycerol 3-phosphate dehydrogenase and aquaglyceroporin genes from *E. coli*.

These studies show *C. glutamicum* has the potential to metabolise a broad range of carbon sources. Presently, product yields from these alternative sources of carbon are low, but future work should be able to address this issue. The compounds in bold in Figure 2.6 will be discussed here in some detail, because of their significant current/future roles in the bioprocess industry.

2.3.1 L-glutamate

The salt form (monosodium glutamate) of this amino acid is a flavour enhancer used extensively in the food processing industry. The world annual market size was estimated to be over 2.9 million tonnes in 2014, and it is expected to grow annually at 7.5 % up till 2023 (Laura, 2014a). The pioneering work of Kinoshita et al.,

(1957) showed that the *C. glutamicum* wild-type strain was a natural overproducer of L-glutamate. Their study isolated various bacteria, fungi and yeast to compare L-glutamate production ability. *C. glutamicum* (formerly Micrococcus glutamicus) indicated the highest yield of 0.25 mole of L-glutamate per mole of glucose.

Since Kinoshita and his co-workers study, different methods have been developed to modify and improve the productivity of *C. glutamicum* fermentations. The following discussion illustrates the long history of processes involving *C. glutamicum*, its malleability to process and genetic manipulations. These are the factors which have contributed to it being used here as a model organism.

Nunheimer et al., (1970) showed that the addition of penicillin to fermenting *C. glutamicum* MB-1645 led to a 2-fold increase in L-glutamate productivity within the first hour of its introduction. However, by the 6th-hour productivity was down by 45 %, rapidly decreasing after that. They also showed that the accumulation of L-glutamate concentration from 10 gL^{-1} was sufficient to result in a 25 % decline in final titre. Marquet *et al.,* (1986) studied the effect of the surfactant (lauryl amine) on an industrial strain of *C. glutamicum* during fed-batch fermentations. They noted that the addition of lauryl amine during the cells' exponential growth phase led to a 13-fold increase in L-glutamate (final titre 100 gL^{-1} after 30 h) compared to fermentations of either biotin limitation or penicillin addition. They then suggested that the addition of lauryl amine resulted in a leaky cell membrane, hence the increase in productivity. Delaunay *et al.,* (1999) argued that although the addition of surfactants led to higher L-glutamate titre, problems of sterilisation, foaming and purification were major drawbacks. Thus, a temperature-sensitive *C. glutamicum* 2262 strain was then constructed which when induced by a temperature increase from 33 °C to 39 °C in the stationary phase of its growth cycle, a final L-glutamate concentration of 85 gL^{-1}

after 24 h was achieved. This straightforward and cheap method compared favourably to other studies which utilise surfactant to increase productivity without the associated disadvantages. Hoischen & Kramer, (1990) suggested all methods used in improving L-glutamate productivity altered *C. glutamicum*'s surface structure, which resulted in a leaky cell membrane. However, Nakamura *et al.,* (2007) later showed that the reason behind these improved yields was due to the alteration of the NCgl1221 gene which encodes an L-glutamic acid transporter and not due to a leaky cell membrane

2.3.2 L-lysine

This essential amino acid is mainly used in the agricultural industry, as a feed additive in swine and poultry farming. Lysine is a cheaper/better alternative to soybean, blood and bone meal for animal nutrition. The global market for lysine was projected to be over 1.9 million tonnes in 2014, and at an estimated annual growth of 6 %, it is expected to reach 3 million tonnes in 2023 (Laura, 2014b). Most of the world's production of L-lysine is via the L-aspartate branch of the *C. glutamicum* metabolic pathway, as shown in Figure 2.6.

Georgi et al., (2005) demonstrated that the overexpression of the fructose-1,6 bisphosphatase gene in a *C. glutamicum* DM1730 mutant doubled lysine yield on sucrose. During the batch fermentation of the *C. glutamicum* JVO1 strain, Van Ooyen *et al.,* (2013) showed that the addition of proline improved glucose uptake rate and lysine productivity by 14 and 29 % respectively. Eggeling *et al.,* (1998) highlighted that upregulating the dihydrodipicolinate synthase enzymes helped redirect the carbon flux. This improved lysine formation by 23 %, but the specific growth rate of *C. glutamicum* ATCC13032 was concurrently reduced by half.

Blombach et al., (2009) suggested that the deletion of the ilvB gene, which is responsible for the activation of acetohydroxy acid synthase (AHAS), leads to increased lysine production. On introducing the modified AHAS to two lysine producing strains *C. glutamicum* DM1729 and DM1933, final concentration rose by 43 % and 36 % respectively. Becker *et al.,* (2011) completely re-engineered a *C. glutamicum* ATCC 13032 strain to achieve one of the highest lysine titres ever published (120 gL^{-1}) during fed-batch fermentations. This was done by adopting 12 genome-based changes to the genes encoding important enzymes, which optimised the redirection of the carbon flux to lysine formation.

2.3.3 Succinic acid

Succinic acid is an important compound that has a broad range of applications in the chemical, food, pharma and the cosmetics sectors, to mention just a few. Currently, it is predominantly produced via a petrochemical synthesis route. In 2013, the global demand for bio-succinic acid was 51,000 tonnes; this is projected to rise to 593,400 tonnes in 2020 (SpecialChem, 2014). Okino et al., (2008) constructed a *C. glutamicum* strain which upregulated the gene encoding pyruvate dehydrogenase and downregulated the production of L-lactate dehydrogenase. This modified strain achieved high succinic acid titres (83 – 146 gL^{-1}) comparable to high performers such as *A. succiniciproducens* (50 – 84 gL^{-1}). They also showed that the succinate yield was dependent on the concentration of bicarbonate in the medium, rather than the available glucose. Litsanov et al., (2012a) highlighted that side product formation (acetate and lactate) during the anaerobic batch fermentation of *C. glutamicum* could be reduced if genes responsible for acetate and lactate synthetase were knocked out. This led to a final modified strain *C. glutamicum* BOL-3, which improved succinate yield by 20 %, but kept side product yields ≤ 0.1 mol per mol of glucose. Litsanov *et al.,* (2012b) argued that if succinate was produced in all stages of the cell's growth cycle aerobically, productivity was sure to improve. The final constructed *C. glutamicum* recombinant had deleted succinate dehydrogenase, acetate and lactate synthase genes. It also overexpressed the pyruvate carboxylase and phosphoenolpyruvate carboxylase enzymes which resulted in an 80 % increase in succinate final titre and an 82 % decrease in final acetate concentration compared to *C. glutamicum Δsdh*. Zhu *et al.,* (2013) improved succinate aerobic productivity by engineering a strain which had the acetyl-CoA synthetase from *Bacillus subtilis* and an upregulated citrate synthase enzyme. This modified *C. glutamicum* ZX1 (*pEacsAgltA*) showed a 2.6-fold specific succinate productivity increase and no acetate production compared to *C. glutamicum Δsdh*CAB.

2.3.4 1,2-Propanediol

This compound otherwise known as propylene glycol has applications in the pharmaceutical, plastic, food, chemical, and the cosmetics industry. Its annual demand surpasses 1.2 million tonnes, with most of it used in the chemical industry for the production of unsaturated polyester resins (Saxena *et al.,* 2010). Niimi *et al.,* (2011) showed that 1,2-propanediol could be produced from *C. glutamicum* RP3 by expressing the methylglyoxal synthase and glycerol dehydrogenase genes taken from *E. coli*. It also overexpressed some of the aldo-keto reductase activating genes, which resulted in 25 mM of 1,2-propanediol. Siebert & Wendisch, (2015) further engineered this *C. glutamicum* RP3 strain by including the alcohol dehydrogenase gene from *E. coli* and deleting the endogenous genes dihydroxyacetone phosphate phosphatase and lactate dehydrogenase. This improved strain showed a further 1.5-fold increase in final 1,2-propanediol titre.

2.3.5 Cadaverine

This short-chained aliphatic amine, also known as diaminopentane, is used in both the chemical and polymer industry. Its annual production exceeds 1.6 million tonnes (Lee *et al.,* 2011). One use of cadaverine is in the bio-based polyamide PA 5.10, which is both less dense and hygroscopic compared to the petrochemical-based PA 6. This makes it superior in applications where low weight and structural stability are of importance (Thielen, 2010).

Mimitsuka *et al.,* (2007) first reported the production of cadaverine from *C. glutamicum*. They engineered a recombinant strain by substituting the L-homoserine dehydrogenase gene for the L-lysine decarboxylase gene from *E. coli* to achieve a yield from glucose of 0.09 mol/mol. Kind *et al.,* (2010) amplified the pyruvate carboxylase encoding gene, and deleted the phosphoenol pyruvate carboxykinase gene; by also overexpressing most of the genes that converted L-aspartate to cadaverine, a yield of 0.2 mol/mol on glucose was achieved. However, when they cultivated this microorganism in the presence of pyridoxal (a lysine decarboxylase cofactor), this yield increased by 50 %. The concurrent accumulation of N-acetyldiaminopentane was rectified by deleting the diaminopentane acetyltransferase gene in their final recombinant, *C. glutamicum* DAP-4 strain. This strain then showed a further 11 % increase in cadaverine yield on glucose. Li et al., (2014) highlighted one other obstacle to improving cadaverine productivity in *C. glutamicum* as the transport from the cytoplasm to its exterior. They constructed a strain, *C. glutamicum* CDV-2, which had the lysine-cadaverine antiporter encoding gene - CadB from *E. coli*. After that the cadaverine secretion rate improved significantly, resulting in a 30 % yield increase. These compounds mentioned so far are just of few examples of *C. glutamicum*’s potential and importance to the biotech industry. In time, more novel compounds will be discovered, and *C. glutamicum* will share in the role of bringing these products from laboratories to the marketplace.

2.4 Conclusion

In the preceeding sections, the most important challenges of scaling up bioprocesses have been discussed. For aerobic processes the efficient transport of oxygen from the medium to the cell is crucial, hence the importance of knowing a bioreactor's k_La (other scale-up factors were also highlighted above). The compromises made in the engineering of large-scale fermenters (due to cost implications) creates a non-uniform environment where dead zones and physical/chemical gradients could exist. The understanding of how a bacterial cell will respond to the environment of typical industrial bioreactors is necessary if scale-up is to be successful. Thus, there is need to replicate the large-scale environment economically; the SDRs highlighted here grants the ability to do this. Albeit a crude approximation, it is still useful for prying information on how a cell responds to some known fermentation gradients, which may occur in large bioreactors. *C. glutamicum* was chosen as a model organism for this work because of its long history as a successful industrial microorganism and its safety upon genetic modification. A few commercial products derived from the fermentation of *C. glutamicum* were discussed to illustrate this organism's potential. It also shows that the fate of the future biotechnological industry is intertwined with the success of deciphering the physiology of these important industrial microorganisms.

The following Chapters will try to characterise and illustrate how a bacterial cell (*C. glutamicum*) reacts to some of these large-scale gradients using the STR/PFR compartment reactor. Hopefully, this approach can be used as a template for developing new bioprocesses.

CHAPTER 3

3 Materials and methods

On receipt of the cell lines to be studied from the Institute of Bio- and Geosciences, IBG-1: Biotechnology, Julich, Germany (Prof. Marco Oldiges Laboratory), preliminary shake flask experiments were carried out to confirm growth and product titres. Once this proved positive for our product of interest (lysine & cadaverine), a set of controlled batch experiments were scheduled to understand the bacterial cell growth and product kinetics. The relevant growth parameters were then used to evaluate an exponential feeding profile. This feeding profile was then employed in fed-batch processes to cultivate the cells to high densities; this was done to increase productivity, reduce energy footprint and to find a reference from which a two-compartment reactor system could be compared to. After this control fermentation was established, fermentation gradients were then simulated in the two-compartment reactor system, and the magnitude of the cell's response quantified. In quantifying the physiological response of both strains, a toolbox of conventional microbiological assays was employed. In some cases, new ones had to be developed, such as the HPLC assay.

3.1 Organism strain

The two bacteria used for this study were *Corynebacterium glutamicum* DM1945 and *Corynebacterium glutamicum* DM1945 Δact3 Ptuf-ldcC_OPT (abbreviated, *C. glutamicum* DM1945x3). The latter strain (based on the lysine producing parent strain *C. glutamicum* DM1945) was genetically modified by insertion of the lysine decarboxylase ldcC gene from *Escherichia coli.* This is a gene responsible for the decarboxylation of intracellular lysine to extracellular cadaverine.

These strains of *C. glutamicum* were received from the Institute of Bio- and Geosciences, IBG-1: Biotechnology, Julich, Germany (Prof. Marco Oldiges Laboratory).

3.2 Medium composition

The inoculum medium (for shake flask cultivations) contained 30 g/L of Oxoid Tryptone Soya Broth (TSB) (Oxoid, UK) in deionised water. The TSB complex medium is well known to support the growth of many fastidious microbes. Table 3.1 highlights the composition of the TSB medium.

Compound	Concentration	Diluent
Casein peptone	17 gL^{-1}	Deionised water
Soya peptone	3 gL^{-1}	Deionised water
Sodium chloride	5 gL^{-1}	Deionised water
Dipotassium hydrogen phosphate	2.5 gL^{-1}	Deionised water
Glucose	2.5 gL^{-1}	Deionised water

Table 3.1 TSB medium composition

The TSB medium was used for cultivating the seed, which inoculated the STR in all investigations. However, the medium used for the small-scale bioreactor batch fermentations was the CGXII synthetic medium (Table 3.2).

Compound	Concentration	Diluent
Glucose	10 gL^{-1}	Deionised water
$(NH_4)_2SO_4$	20 gL^{-1}	Deionised water
Urea	5 gL^{-1}	Deionised water
$MgSO_4$ • 7 H_2O	0.125 gL^{-1}	Deionised water
KH_2PO_4	1 gL^{-1}	Deionised water
K_2HPO_4	1 gL^{-1}	Deionised water
*Protocatechuic acid	1 mL L^{-1}	CGXII medium
*$CaCl_2$ • $2H_2O$	1 mL L^{-1}	CGXII medium
*Biotin	1 mL L^{-1}	CGXII medium
*Trace elements (see composition in Table 3.3)	1 mL L^{-1}	CGXII medium

*Table 3.2 CGXII medium composition, * indicates that stock solutions of these components were made before addition to the medium.*

Both the TSB and some of the CGXII medium components were sterilised by autoclaving at 121 °C for 15 min; however, the glucose was heat sterilised separately to avoid the Maillard reaction. * Highlights additional components that complemented the CGXII medium (Table 3.2), these supplements were made up in separate stock solutions (Table 3.3). They were filter sterilised via a 0.22 µm syringe filter before being aseptically added to the CGXII medium matrix done in the BioMAT II biological safety cabinet (C.A.S, UK).

Compound	Concentration	Diluent
Protocatechuic acid	30 gL^{-1}	1 M NaOH
$CaCl_2 \cdot 2H_2O$	13.25 gL^{-1}	Deionised water
Biotin	0.2 gL^{-1}	1 M NaOH
Trace elements		
$FeSO_4 \cdot 7H_2O$	10 gL^{-1}	1M HCl
$MnSO_4 \cdot H_2O$	10 gL^{-1}	1M HCl
$ZnSO_4 \cdot 7H_2O$	1 gL^{-1}	1M HCl
$CuSO_4 \cdot 5H_2O$	0.313 gL^{-1}	1M HCl
$NiCl_2 \cdot 6H_2O$	0.02 gL^{-1}	1M HCl

Table 3.3 Stock solutions of supplements added to the CGXII medium

The diluent of either 1 M NaOH or 1 M HCl was used when deionised water could not sufficiently dissolve the component. For the fed-batch fermentations, the medium components as stipulated in Table 3.2 & 3.3 were used on start-up of the process. However, the feed addition medium utilised in the latter part of these fermentations was different (Table 3.4).

Compound	Concentration	Diluent
Glucose	620 gL^{-1}	Deionised water
$(NH_4)_2SO_4$	40 gL^{-1}	Deionised water
Urea	10 gL^{-1}	Deionised water
$MgSO_4 \cdot 7\ H_2O$	0.25 gL^{-1}	Deionised water
KH_2PO_4	2 gL^{-1}	Deionised water
K_2HPO_4	2 gL^{-1}	Deionised water
*Protocatechuic acid	2 mL L^{-1}	Addition medium
*$CaCl_2 \cdot 2H_2O$	2 mL L^{-1}	Addition medium
*Biotin	2 mL L^{-1}	Addition medium
*Trace elements	2 mL L^{-1}	Addition medium

*Table 3.4 Feed addition medium composition, * indicates that stock solutions of these components were made before being added to the medium.*

The same aseptic technique was also used when the supplement was being added to the feed addition medium. All the chemicals used here for all medium preparations were of reagent grade.

3.3 Inoculation preparation

On receipt, the cells were stored at – 80 °C in the Microbanks^{TM} preservation phials (Pro-Lab Diagnostics, UK). The inoculum was prepared by streaking a bead from a cell bank onto a Tryptone Soya Agar (TSA) filled plate (Oxoid, UK), and incubated for 48 h at 30 °C. After that, a viable colony was picked and transferred to an unbaffled Erlenmeyer flask containing 150 ml of sterile TSB medium. The TSB containing flask was then cultivated for 13 h in an Innova® incubator shaker (Eppendorf, USA) at 170 rpm, and 30 °C. On termination and transfer to the small-scale bioreactor, the DCW was approximately 1 gL^{-1}. This indicated that the microbial culture in the shake flask was somewhere between late exponential to early stationary growth phase before transfer.

3.4 Stirred tank reactor setup

The stirred tank reactors (STR) used for the batch and fed-batch fermentations were both the 1 L and 5 L double jacketed Biostat B plus vessels (Sartorius, Germany), see Appendix 1 for a detailed overview. These reactors were made of glass, equipped with pH EasyFerm Bio (Hamilton, Switzerland), VisiFerm DO (Hamilton, Switzerland) and antifoam (Sartorius, Germany) probes. The double jacketed 1 L STR was fitted with two Rushton turbines and three baffles. It had a height of 20 cm, internal diameter 11 cm, the distance from the vessel base to the lower impeller 2.6 cm, the diameter of the impeller 4.5 cm, and height of impeller 1.0 cm (Figure 3.1). While the double jacketed 5 L STR also had two Rushton turbines and baffles, its height was 34.5 cm, internal diameter 16 cm, clearance distance between the reactor's bottom and the lower impeller 7.6 cm; the diameter of the impeller 6.4 cm with a height of 1.4 cm (Figure 3.2).

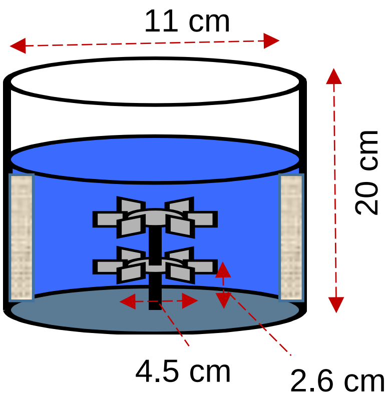

Figure 3.1 A simple overview of the external dimensions of the 1 L STR

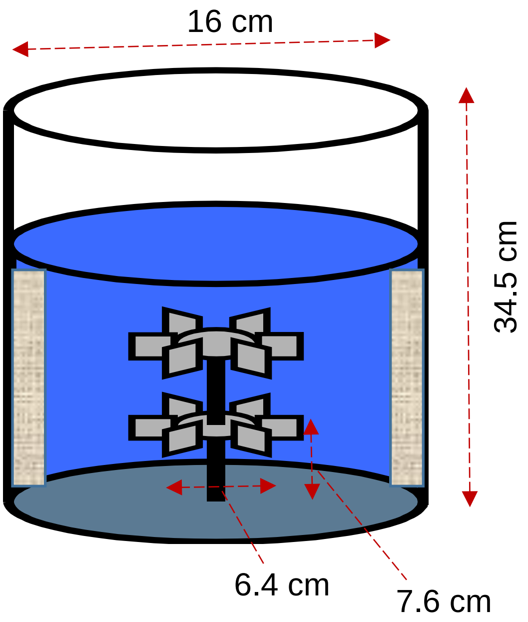

Figure 3.2 A simple overview of the outer aspects of the 5 L STR

The fermentation working volumes for both the 1 L and 5 L vessels were 0.6 and 3 litres respectively. The $k_L a$ in both STRs was calculated as the slope of the linear Equation 3.1 (a modified version of Equation 2.5), using the gassing-out method (Enfors 2011).

$$\ln(DOT' - DOT) = -K_L a(t - t_0) + \ln(DOT' - DOT_0) \qquad 3.1$$

In Equation 3.1, DOT represents the dissolved oxygen tension at any time - t, DOT' the equilibrium value at maximum rate of air aeration and DOT_0 the value after stripping the vessel's dissolved oxygen with nitrogen at the start of experiment time - $t_{0.}$ The $k_L a$ for the 5 L and 1 L STRs were 170 /h and 100 /h respectively.

3.5 Two-compartment reactor setup

This study used a two Compartment Scaled-Down Reactor (SDR) set up, comprising a plug flow reactor (PFR) connected in series to a STR. Figures 3.3 & 3.4 show the schematic and pictorial representations of the SDR setup used in all scale-down experiments done here. The PFR was fabricated in-house (see Appendix 2 for detailed engineering design); it was made of stainless steel and had a length and an internal diameter of 165 cm and 1.5 cm, respectively. At the PFR inlet, mid-point and outlet, pH and DO probes were positioned to monitor the fermenting conditions along the length of the PFR (Figure 3.3). There were 96 mixing elements along its length to aid radial mixing and to enhance plug flow (Figure 3.4).

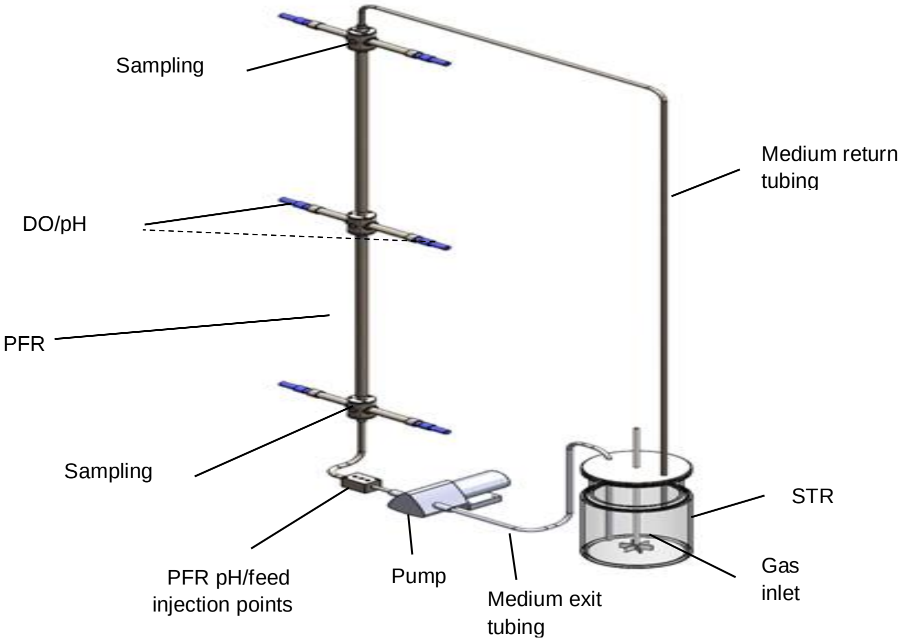

Figure 3.3 A schematic representation of the SDR experimental rig

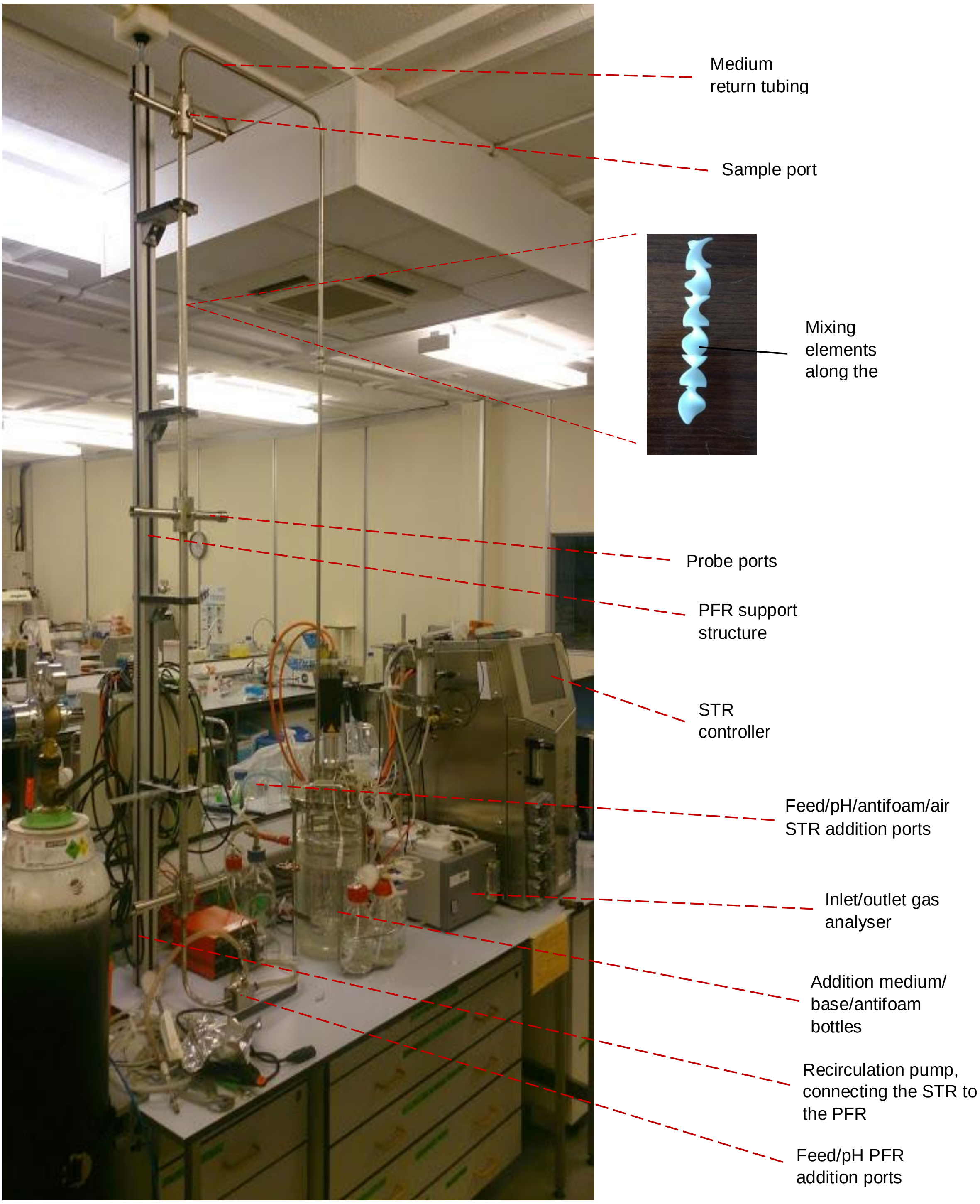

Figure 3.4 A pictorial representation of the SDR experimental rig

The PFR had a total volume of 300 mL; this ranged from 10 % - 50 % the total working volume of the STR depending on the simulation investigated. The medium was recirculated at volumetric flow rates (Q_r) of 5.33 mL/s, 2.67 mL/s and 1.07 mL/s by a 100-series peristaltic pump (Watson-Marlow, UK) to achieve a cell mean residence time in the PFR (τ_{PFR}) of 1, 2, and 5 min respectively. The controller in all experiments was located in the STR section. The pH and DOT were controlled and monitored in the STR, but only monitored in the PFR. The active aeration of the SDR occured only at the STR in all experiments.Tthe PFR was insulated in polystyrene to minimise heat losses to the surroundings (Figure 3.5), while the STR temperature was regulated by heating coils and a cooling water system.

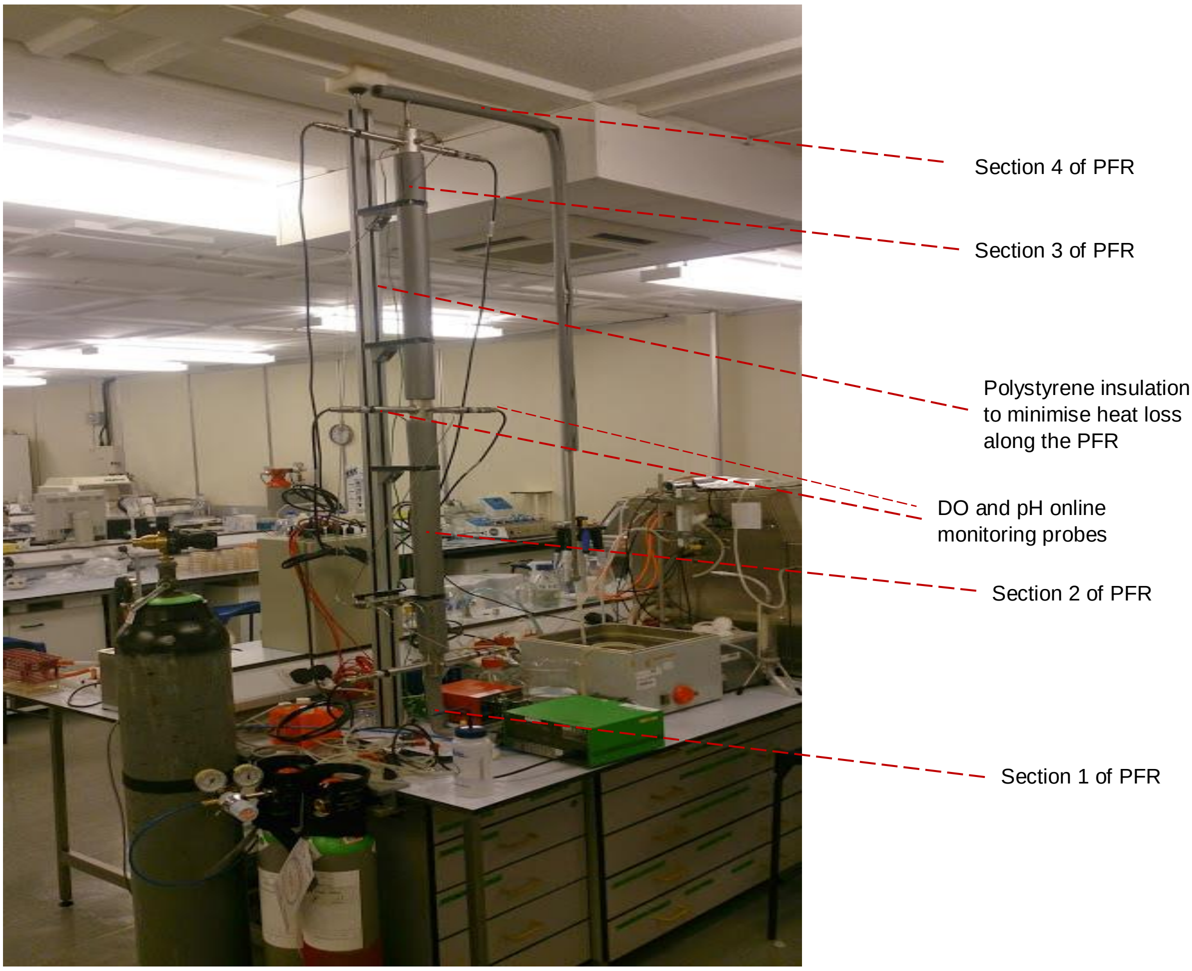

Figure 3.5 A pictorial representation of the PFR

pH probes were located along the length of the PFR and in the STR. However, the broth's pH value was controlled from the STR by the addition of 4 M NH_4OH (base) via its inlet point. In investigations where high pH gradients were to be induced, this base was instead added at the PFR inlet point. There was only one air inlet port, which was located at the STR. The DO was controlled by sparging the medium with compressed air and air blended with pure oxygen when the growing cells' demand for oxygen increased.

The sterilisation of the STR was straightforward; it was autoclaved at 121 °C for 20 min. On cooling, all loose tubing and valves were coupled aseptically. However, for the PFR because the length was longer than the autoclave, it had to be taken apart before sterilisation. It was split into four sections (Figure 3.5), this was demarcated by the sampling ports (Figure 3.4). The exposed ends of these sections were pached with cotton wool, and aluminium foil, which was secured with autoclave tape to avoid any cross contamination when recoupling the sections. It was autoclaved at 121 °C and held for 15 min due to its smaller volume. On completion of every fermentation, the discard cycle was 122 °C for 25 min before the spent broth was poured down the drain with a copious amount of water.

3.6 Bioreactor cultivation conditions

The two fermentation processes carried out in the bioreactors were batch and fed-batch. For the comparative/growth kinetics study of *C. glutamicum* DM1945 and the modified *C. glutamicum* DM1945x3, the batch process was used. These batch fermentations took place in the 5 L STR, and lasted for 24 hours. The pH was controlled at 7 by the addition of 4M NH_4OH. The DOT was maintained ≥ 40 %; this was achieved by varying the agitation rate (100 rpm – 800 rpm) since the air sparging rate was held constant at 1.5 vvm. The temperature of 30 °C was kept constant by cooling water held within the double-walled STR.

However, for the STR only and SDR experiments, the cultivation conditions were slightly different. The fed-batch process occurred in both the one-compartment STR and the two-compartment reactor. These fermentations all began as batch processes in the STR. The feeding (for both the STR only and SDR experiments) and recirculation (for the SDR experiments) between the STR and PFR commenced at 8 h, when the DCW concentration had reached ~ 1 g/L. The fermentations were carried out at a temperature of 30 °C, and the impeller speed was set at 800 rpm. The air was constantly sparged at a rate of 1.5 vvm to maintain a DOT of ≥ 40 %. However, during the latter part of the process, gas blending with pure oxygen was initiated when the cells reached high densities (DCW > 25 g/L). The pH of 7 was held by the controlled addition of 4 M NH_4OH. To quantify the amount of feed needed to sustain a cell growth rate of 0.1 /h during a fed-batch process, Equation 3.2 was used.

$$F_0 = \frac{\mu}{S * Y_{x/s}} * (X_0 V_0) * e^{\mu t} \qquad 3.2$$

Where F_0 = feeding flow rate at t, (L h^{-1}), μ = intended cell growth rate (/h), S = feed glucose concentration (gL^{-1}), X_0 = DCW at t (g L^{-1}), V_0 = volume at t (L), t = time (h), $Y_{x/s}$ = yield of biomass on glucose (gg^{-1}), data derived from past batch studies.

This exponential feeding flow rate profile was adhered to, until the termination of all fed-batch fermentations, thereby inducing a μ of 0.1 h^{-1}. This low μ was adopted to minimise side products attributed to a high rate of glycolysis. George et al., (1993) had highlighted that a high μ (due to high glucose concentration) would reduce the yield of yeast cells to achieve high cell density in a fed-batch fermentation and Onyeaka, Nienow, and Hewitt, (2003) also showed this to be the case for *E. coli.*

3.7 Bulk cell measurements methods

The following analytical methods below, categorised as bulk cell measurement techniques were used in quantifying *C. glutamicum* DM1945 and *C. glutamicum* DM1945x3 physiological response to the various simulations investigated. The response derived from these measurements are average values, which gives an overview of the cell performance. Hence, if there are deviating cell responses from a sub-population, this can be easily lost by averaging out. This is why it is best practice to complement the bulk cell measurements with single-cell measurements (as employed here). The combination of these techniques improves the chance of identifying a deviating cell sub-population. The majority of the bulk cell measurement techniques are relatively accurate, easy and economical, hence their popularity. The techniques used here to quantify fermentation performance are discussed as follows.

Dry cell weight

The growth of cells was monitored by quantifying the concentration of the dry cell weight per litre. These values were derived by centrifuging a 5 mL sample at 4000 G and 4 °C for 10 min; the resulting precipitate was then washed and re-centrifuged under similar conditions, after that it was allowed to dry at 80 °C for 48 h before weighing.

Glucose and lactate concentrations

A 1:10 dilution of the cell sample in a filtered (via a 0.22 µm syringe filter) phosphate buffered saline solution was injected into the 2300 STAT Plus^{TM} (YSI, USA) to analyse glucose consumption and lactate production. This analyser was fitted with a glucose and a lactate membrane housed in an injection chamber. When the analytes from the fermentation sample pass through these membranes, they come in contact with an immobilised oxidase enzyme. The oxidation reaction from this contact results in the production of hydrogen peroxide (H_2O_2). Equation 3.3 illustrates an example in which glucose is the analyte and GO_x the oxidase enzyme.

$$\beta\text{-D-glucose} + O_2 \xrightarrow{GO_x} \text{glucono-}\delta\text{-lactone} + H_2O_2 \qquad 3.3$$

This hydrogen peroxide is then oxidised at the platinum anode (which is stacked next to the membrane) to produce electrons (see Equation 3.4). There is a steady-state response when a dynamic equilibrium is reached; at this point the rate of H_2O_2 production and the rate at which it leaves the immobilised glucose enzyme is constant. The electron flow (current) is linearly proportional to the steady-state concentration of H_2O_2, and, therefore is correlated to the analyte concentration.

$$H_2O_2 \xrightarrow{Pt} 2H^+ + O_2 + 2e^- \qquad 3.4$$

The calibration of 2300 STAT Plus^{TM} was carried out by using a known dual standard, 2.5 g/L of glucose and 0.5 g/L of lactate supplied by the manufacturer (YSI, USA). The procedure for measurement was to run the manufacturers supplied standard calibration solutions before the samples.

Cadaverine and lysine quantification

A high-performance liquid chromatography (HPLC) series 200 (Perkin Elmer, USA) fitted with a 265, 4.8 nm UV/Vis detector was used to determine both cadaverine and lysine concentrations. A pre-column Raptor™ARC-18 (Restek Corporation, USA) derivatisation reaction was needed for cadaverine and lysine quantification. 150 µL of 30 mM 9-fluorenylmethoxycarbonyl chloride (FMOC) in 150 µL acetonitrile and 150 µL of 0.2 M borate buffer were reacted with a 150 µL filtered (0.22 µm filter) fermentation sample. A reaction time of 5 min (stipulated by the column manufacturer – Restek Corporation, USA) was deemed sufficient to allow the complete conversion of lysine and cadaverine into their respective 9-fluorenylmethyl-chloroformate derivatives, which are detectable by the HPLC. Two mobile phases were used, the first was a mixture of 0.1 % formic acid and 20 mM ammonium formate in water (A) and the second was 0.1 % formic acid and 10 mM ammonium formate in 90:10 acetonitrile:water (B). Table 3.5 shows the gradient flow of these mobile phases which was adapted from Restek, (2016).

Time (min)	Flow (mL/min)	% A	% B
0.00	0.8	80	20
6.00	0.8	60	40
9.00	0.8	40	60

Table 3.5 The two mobile phases A & B flow gradient, adapted from (Restek, 2016)

The column and sample chamber temperatures were maintained at 30 °C and 40 °C respectively. The peak elution times for cadaverine and lysine were approximately 7.3 min and 4.4 min respectively (Figure 3.6)

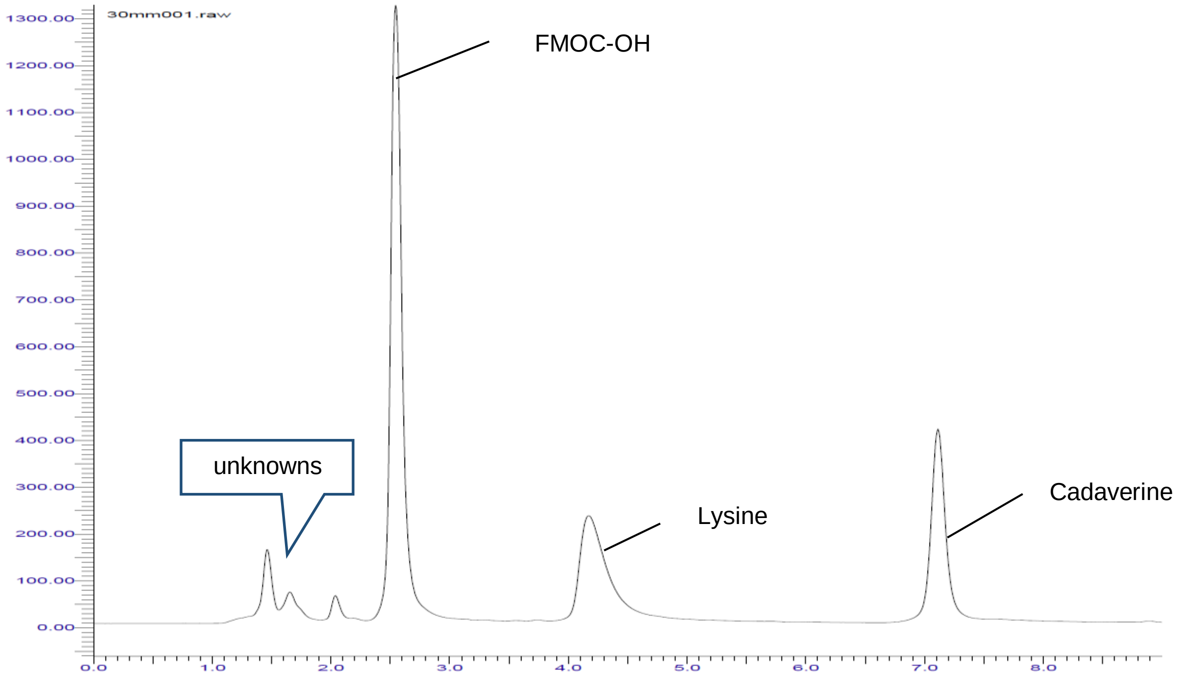

Figure 3.6 The HPLC chromatogram printout of a 100 ppm lysine and cadaverine standard

The peaks eluted between 1 and 2 min could not be identified; the 9-fluorene methanol (FMOC-OH) was produced alongside the FMOC reaction with either lysine or cadaverine. The FMOC-OH is a product of the reaction between FMOC and hydroxide ions present in the solution. A 10, 50, 100, 150 & 200 ppm standards of lysine and cadaverine were made up and ran along with the samples. Once the areas of the peaks were calculated, the standard curve was then used to evaluate the concentrations of these compounds in the samples.

Inlet and outlet air composition

A Tandem gas analyser (Magellan BioTech, UK) was used to measure the oxygen and carbon dioxide composition of the air going in and out of the fermenting vessel. A sample of air was filtered via a 0.22 µm filter and diverted to the analyser, which was fitted with oxygen and carbon dioxide sensors. The oxygen was measured by the rate of its diffusion through the enclosing Teflon membrane barrier, which was correlated with the amount of electrical current produced. The carbon dioxide was quantified by a solid state sensor equipped with an infrared source, which had a narrow bandpass filter unique to carbon dioxide. This device was calibrated using a cylinder of known oxygen/carbon dioxide composition, from which subsequent readouts were compared. Profiling the change in the inlet/outlet air composition was done to give information on the cells oxygen consumption and carbon dioxide production rates. These rates were necessary to track metabolic changes in the growing cell or the cell's response to the fermentation gradients simulated.

3.8 Single cell measurement method

The single cell measurement techniques have certain advantages over the bulk cell measurement technique. Such as, the ability to probe the individual cell to see how it performs in relation to other cells. Therefore, single cell techniques give more indepth information on how the individual bacterial cells respond to their environment. The examples of such techniques used here are as follows.

Flow cytometry protocol

A BD FACSJazz^{TM} cell sorter (BD Biosciences, USA) flow cytometer was used to evaluate the cell membrane potential and integrity of *C.glutamicum* DM1945 and *C. glutamicum* DM1945x3. All flow cytometers are made up of three elements, namely – optics, fluidics, and electronics. Figure 3.7 depicts the typical components of a flow cytometer. The optics consist of the laser light, filters, mirrors and the photomultiplier tubes (PMT).

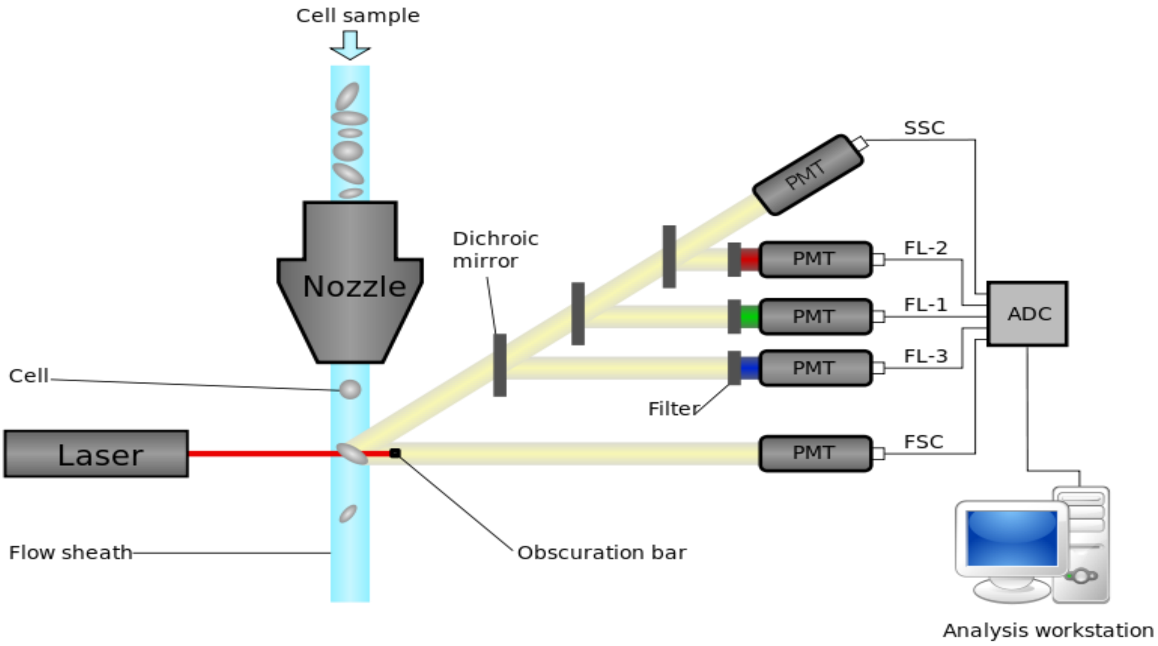

Figure 3.7 A schematic of the inner workings of a typical flow cytometer adapted from Alex, (2017)

The flow cytometer starts from the fluidics; the sheath fluid focuses the cell sample, and as they pass through the nozzle there is a slight vibration which breaks up the stream into droplets containing single cells. Each droplet that is formed encapsulates the cell to be exposed to the laser light source. As the laser light hits the encapsulated cell, there is a scatter of light which is collected by mirrors stacked within the cytometer which separates and magnify the signal according to its wavelength and intensity (Figure 3.7). The forward scatter (FSC) signal is related ‘loosely’ to the cell size while the side scatter (SSC) indicates the internal cell complexity. If the cell is tagged with a fluorochrome, then the dye is excited by the selected laser of suitable wavelength, and the subsequently emitted ray is filtered to allow in only the light with the stipulated wavelength to strike the PMT. Initially, this emitted light ray/signal is relatively weak, but the PMT magnifies this signal which is then digitised by the Analogue to Digital Converter (ADC).

The BD FACSJazz^{TM} Cell Sorter flow cytometer used here had three laser light sources, blue (488 nm at 80 mW), red (640 nm at 50 mW) and violet (405 nm at 50 mW). However, only the blue laser was used for this work, as it was sufficient to excite the fluorochromes utilised here. These fluorochromes were Propidium Iodide (PI) and DiBAC4(3) (Bis-(1,3-Dibutylbarbituric Acid) Trimethine Oxonol) (oxonol). Light signals were collected after the 670 Longpass, and 530/40 bandpass filters for PI and oxonol respectively. These fluorochromes are typically excluded from healthy cells with intact fully polarised cytoplasmic membranes (Hewitt et al., 1998;1999). The PI will bind to the DNA of any cell with a breached membrane barrier. The oxonol is a lipophilic, anionic dye, which will accumulate intracellularly if the cell is unable to transport oxonol out of its cytoplasm efficiently, hence making it depolarised (due to gain in charge (Nebe-Von-Caron *et al.,* 2000)). The combination of these dyes (PI & oxonol) indicates the state of the cell’s membrane and its charge. Stock solutions of 3 µM oxonol in dimethyl sulfoxide and 20 mM of PI in deionised water were made up for this analysis. From this, 0.2 µL oxonol and 0.1 µL PI were added to a diluted 1 mL solution ($\approx 10^6$ cells per mL) of cell suspension in filtered PBS. This solution was then mixed and incubated at room temperature in the dark for 10 minutes, before injection into the flow cytometer. The cells were discriminated and gated by their light scattering footprint on an SSC versus FSC dot plot (Figure 3.8). The laser alignments were optimised to allow for PI detection from a 670 long pass filter and oxonol from a 530/40 bandpass filter. During this assay development, the dead and live cell population were artificially made up. The dead cell population was made by heating a 10 mL sample of thriving cells in a water bath at 80 °C for 1 h. After which it was left to cool to room temperature before it was added to a 10 mL live cell sample. This mixture was then stained with PI and oxonol using the staining protocol as described above. The flow cytometry assay developed was successful as it discriminated between the dead and live cells in the sample (Figure 3.8).

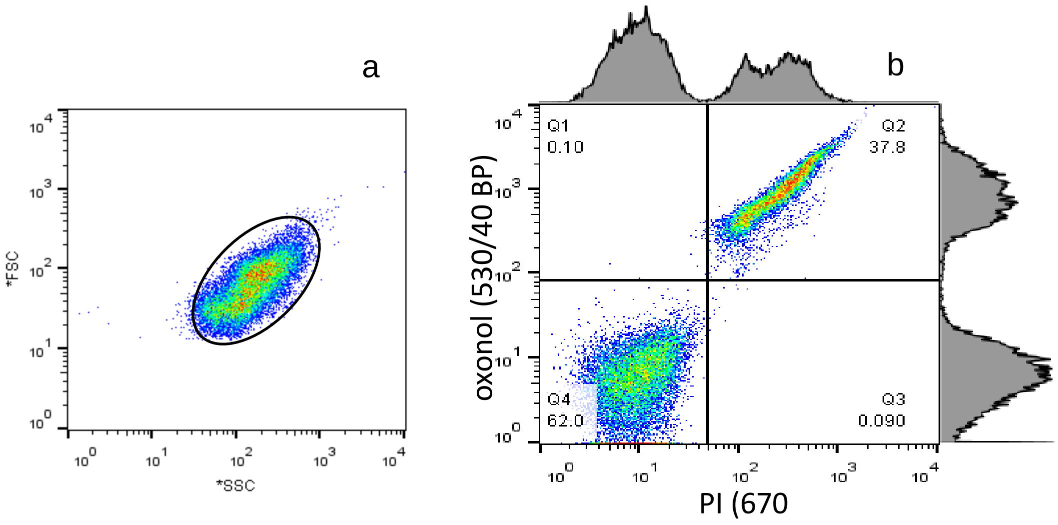

Figure 3.8 Flow cytometer analysis of an artificially simulated live/dead population of C. glutamicum DM1945

Figure 3.8 a shows the cluster of the cell population of *C. glutamicum*; this discrimination of cells from noise or debris is based on size and internal complexity. A gate is drawn around this population cluster and then plotted on the receiving channel, PI 670 LP against oxonol 530/40 BP. Here, the cells are separated based on the condition of their cytoplasmic membrane. Figure 3.8 b was demarcated into four quadrants, Q4 shows the cells with intact membrane (62 % of the total population deemed live), as they took up neither PI or oxonol. The Q2 quadrant indicates cells with a breached cytoplasmic membrane (37.8 % of the total population deemed live dead) because they took up both PI and oxonol. There were hardly any depolarised cells (noted in Q1), and Q3 represented debris/noise. The higher ratio of live to dead cells even when an equal proportion was made up, may suggest the heat treatment was not 100 % effective.

Viability determination by plating

The ability of a cell to form a culturable colony on an agar plate indicates that it is healthy and viable. However, this technique rules out some cells which are metabolically active but are not culturable on an agar plate (Davey & Kell, 1996; Oliver, 1993). With the aid of a flow cytometer Serpaggi et al., (2012) observed that the non-culturable cells of *Brettanomyces bruxellensis* LO2E2 population increased when they were exposed to SO_2. They suggested that the increase in non-culturable cells may be a typical stress response in non-spore forming bacteria/yeast cells. Hence, the colony forming ability on an agar plate should be seen as one of the properties of viability.

Here, the CFU was measured by pouring a sterile tryptone soya agar (Oxoid, UK) solution into Petri dishes, which held 100 µl aliquots of diluted cell suspensions ranging from 10^{-5} to 10^{-7}. This mixture was then gently stirred and incubated at 30 °C for 48 h before counting the visible colonies under a magnifying glass.

Not one measurement method discussed above is without limitation, but their combined results give a better understanding of how much a cell responds to its surroundings.

CHAPTER 4

4 Quantifying the effect of genetic modifications on the cadaverine-producing *C. glutamicum* DM1945x3

In the development of commercial bioprocesses, the interacting biological, physical and chemical systems are typically engineered to attain an optimal operating space. Biological engineering may lead to GMOs which are designed in the laboratory or by evolutionary pressures and as such selected based on their productivity. Other examples of altering the physical system in bioprocesses are in the selection of the bioreactor type; while the growth medium matrix choice may be chosen for specificity, to improve productivity. In this chapter, the emphasis will be based on studying the physiological response to a batch fermentation environment of the modified cadaverine-producing *C. glutamicum* DM1945x3 strain compared to its parent strain (*C. glutamicum* DM1945).

4.1 *C. glutamicum* physiological response in batch fermentations

To compare and quantify the physiological response of a batch fermentation environment of these strains, both bulk and single cell measurement techniques were used (highlighted in Chapter 3, Subsection 3.7 and 3.8). The parent strain (*C. glutamicum* DM1945) had two point mutations coding for pyruvate carboxylase (*pycP458S*) and aspartate kinase (*lysCT311I*) (Georgi *et al.,* 2005). These mutations release the feedback control of *LysC* and result in the overproduction of lysine. While the daughter strain, *C. glutamicum* DM1945x3 differed from its parent due to the added lysine decarboxylase gene *ldcC* integrated into its genome. The addition/modification of gene(s) to a bacterial cell in most cases affect internal chemical pressures, which tend to change the physiological properties from its parent (Ikeda, 2006). The batch fermentation experiments conducted here were used to create a reproducible environment where the growth performance and productivity of both strains could be measured. The information on how the growth and product kinetics of any organism is useful when characterising and scaling-up a process. Understanding the growth kinetics of *C.glutamicum* DM1945x3 batch fermentations was needed to evaluate relevant parameters for calculating the feeding profile for subsequent fed-batch studies.

Details on fermentation conditions and equipment specifications are given in Chapter 3 (Subsection 3.6). In these sets of experiments both the parent and the modified strains were grown under the same conditions and their physiological response compared.

4.1.1 Cell growth

The specific growth rates (µ) of *C. glutamicum* (parent and daughter strain) were quantified by observing the rate of change of the dry cell weight (DCW). The trend in the DCW concentration profiles of both strains (Figure 4.1) indicated a typical bacterial cell life cycle: the lag, exponential, deceleration and the stationary growth phase. In all cases, the fermentation process was terminated at 24 h, when all the glucose in the broth was depleted.

The DCW production rates during the lag phase did not show any difference when the daughter and parent strains were compared (from 0 to 2 h). The length of the lag phase is dependent on the organism, growth medium, state of the inoculum, growth inhibitors, spore germination and bioreactor condition (Pirt, 1975; Stanbury *et al.,* 1999). During the lag phase, the bacterial cells are adapting to their new environment, and metabolic rates are typically low. However, the amino acids uptake rates are usually highest in this phase (Pirt, 1975; Stanbury *et al.,* 1999). Here, the main contributing factor to the lag phase of Figure 4.1 may be due to the state of the inoculum. This is because at the time the inoculum was harvested it was somewhere around the deceleration and stationary growth phase. Also, the medium used in cultivating the inoculum was complex TSB, which was different from the synthetic medium (CGXII) of the STR (see Chapter 3, Section 3.2). Thus, when the inoculum was introduced to the STR, the time required for the bacterial cells to synthesise RNAs relevant to adapt to the new bioreactor environment correspond to the lag time (Stanbury *et al.,* 1999).

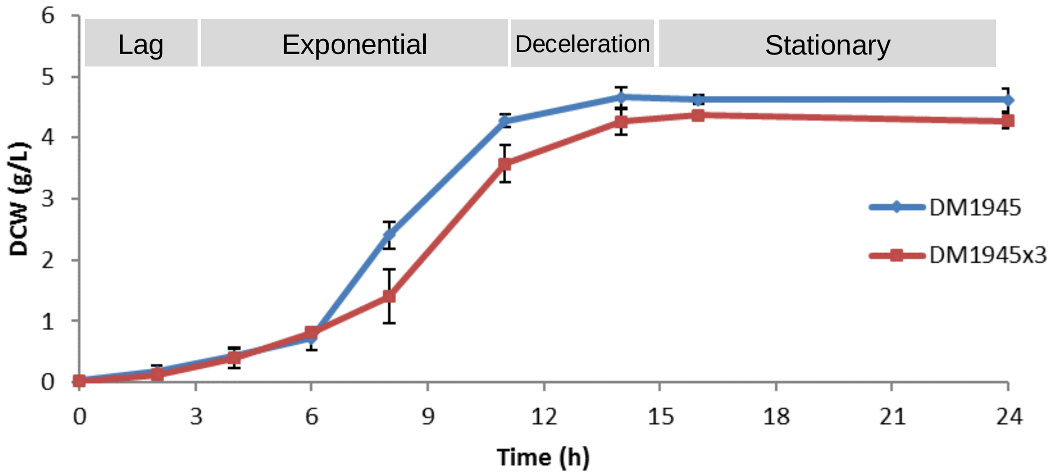

Figure 4.1 DCW production rates for the batch fermentation of C. glutamicum DM1945 and DM1945 x3, the data points represent the mean values from biological triplicates and the error bars equivalent to the standard deviations at these points.

After the lag phase, both bacterial cell strains had completely adapted to their new environment, and since no nutrient was lacking or inhibiting further growth, they replicated rapidly. This exponential growth phase started from 2 h and ended at 11 h for both strains (Figure 4.1); their specific growth rates were calculated by the growth model of Equation 4.1.

$$\frac{dX}{dt} = \mu X \qquad 4.1$$

Where μ = cell specific growth rate (h^{-1}), X = cell concentration (gL^{-1}) and t = time (h) Integrating equation 4.1 from start (X_0) of exponential growth to completion (X(t)) with respect to time results in the straight-line Equation 4.2.

$$\ln X(t) = \mu t + \ln X_0 \qquad 4.2$$

Thus, μ is the slope in a plot of lnX(t) against time t. Conventionally, μ is assumed to be constant for simplicity (especially in the exponential growth phase), which make it easier to compare growth rates amongst microorganisms. Also, during this period a microorganism's maximum specific growth rate (μ_{max}) is achieved (Pirt, 1975; Stanbury *et al.,* 1999). The μ for both *C. glutamicum* strains were calculated from Figure 4.2 a – b.

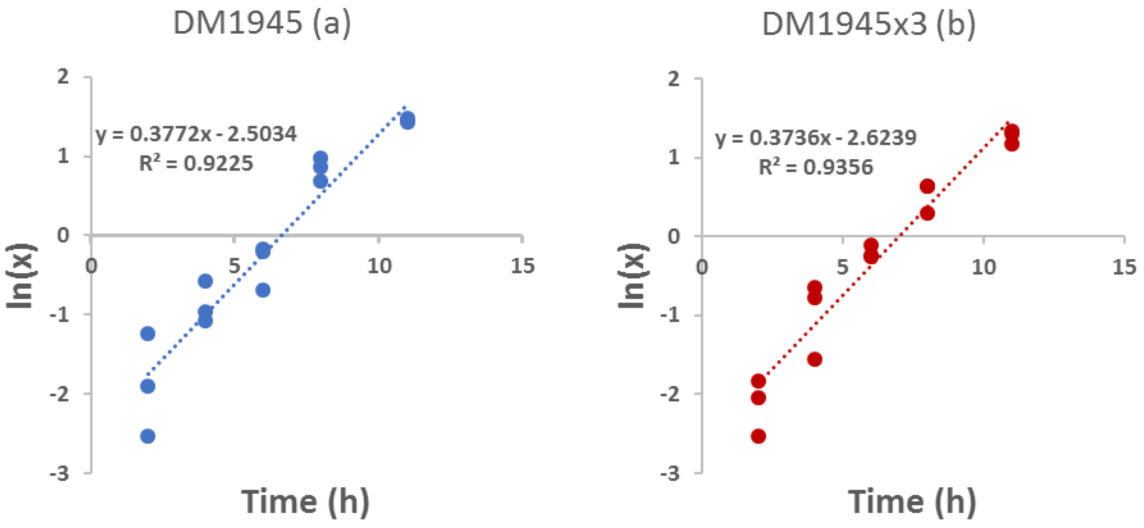

Figure 4. 2 a – b Plots of lnX(t) against fermentation times used in deriving the μ for C. glutamicum DM1945 and DM1945x3. The three data points at each sample time represent separate biological run.

Figure 4.1 indicated that the averaged DCW at the end of the exponential growth phase for *C. glutamicum* DM1945 and DM1945x3 was 4.3 gL^{-1} and 3.6 gL^{-1} respectively, a 16 % decrease when compared. However, Figure 4.2 a – b suggests that this difference was not significant, as the μ for *C. glutamicum* DM1945 and DM1945x3 was 0.38 h^{-1} and 0.37 h^{-1} respectively. Table 4.1 shows a summary of the μ statistical data analyses for both bacterial strains.

C. glutamicum strain	DM1945 μ	DM1945x3 μ
Mean	0.38	0.37
Standard Error	0.026	0.033
Standard Deviation	0.045	0.058
Sample Variance	0.0020	0.0033
Replicates	3	3
Confidence Interval (95.0%)	0.27 – 0.49	0.23 – 0.51
P value (two-tailed test)	0.94	

Table 4.1 DCW statistical analyses of μ values in the batch fermentation of C. glutamicum DM1945 and DM1945x3

The analyses in Table 4.1 also show that any difference seen in Figure 4.1 was not significant and within the system's measurement variability. This was confirmed by the overlapping 95 % confidence interval and a P value > 0.05 Thus, both parent and daughter strain showed no difference with respect to DCW productivity in the exponential growth phase.

Another index used to measure bacterial cell growth is the doubling time (t_d), which was evaluated from Equation 4.3.

$$t_d = \frac{\ln(2)}{\mu} \tag{4.3}$$

This estimated the t_d to be similar, 1.8 h for *C. glutamicum* DM1945 and 1.9 h for *C. glutamicum* DM1945x3.

Although the μ value depends on the microorganism and the bioreactor environment. The μ here still agreed with the work of Limberg et al., (2016), where they estimated the value of the closely related *C. glutamicum* DM1800 to be 0.41 h^{-1}. This agreement may be because the same CGXII medium and similar cultivation conditions were used. To confirm the best growth profile from 2 h to 11 h, the DCW trend was fitted to the models in Figure 4.3 (a – d) for both strains.

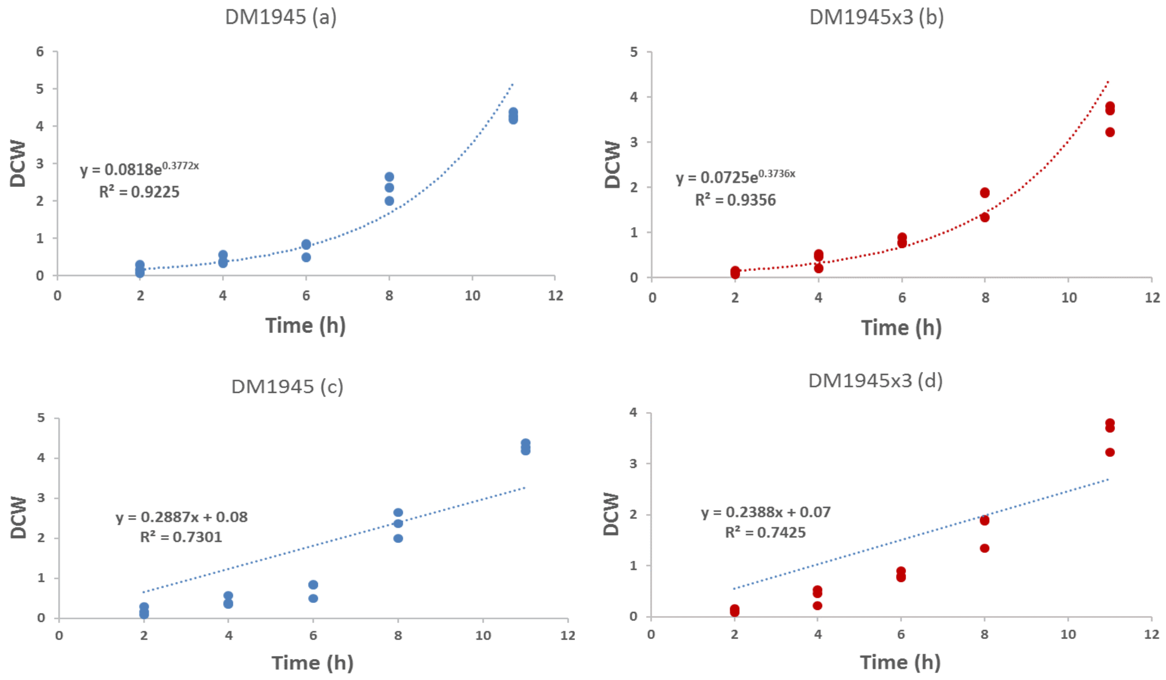

Figure 4.3 a – d A comparison between an exponential and linear best fit lines of the DCW profiles for C. glutamicum DM1945 and DM1945 x3 from 2 h – 11 h of batch fermentations. The three data points at each sample time represent separate biological run.

Figure 4.3 a and b fitted the data points to an exponential equation while Figure 4.3 c and d was to a linear equation. For the exponential model, the R-squared values for *C. glutamicum* DM1945 and *C. glutamicum* DM1945x3 were 0.92 and 0.94 respectively. However, for the linear models of Figure 4.3 c and d, the R-squared values for *C. glutamicum* DM1945 and *C. glutamicum* DM1945x3 were 0.73 and 0.74 respectively. This comparison shows that the cell growth (based on the DCW) between 2 h and 11 h was exponential. This is because the R-squared correlation coefficient values from the exponential models were higher than the linear models for both strains. Thus, indicating that the exponential equations of Figure 4.3 a and b reasonably represent the DCW profiles for *C. glutamicum* DM1945 and *C. glutamicum* DM1945x3 during this period. After 11 h, the cell growth decelerated as the glucose in the broth became limiting (Figure 4.4). The availability of a carbon source (glucose) in a broth is linked to the amount of Adenosine Triphosphate (ATP) generated (Bothun *et al.,* 2004; Suarez-Mendez *et al.,* 2014). Thus, when glucose becomes low, the amount of ATP reduces, and the energy generated by cells decreases. A condition which forces the bacterial cell to prioritise its energy utilisation, such as, reducing replication (DCW productivity declines) and diverting more energy to maintenance (Pirt, 1975; Stanbury *et al.,* 1999). This response led to the decline in DCW productivity during the deceleration phase between 11 h and 14 h (Figure 4.1). Also, as bacterial cells entered their stationery growth phase (14 h to 24 h), this trend in energy utilisation becomes the norm. During this period the bacterial cells use energy for ‘‘housekeeping duties’’ such as, consolidating their cell membrane and production of stress response enzymes rather than replicating (Follmann *et al.,* 2009b; Schweder *et al.,* 1999). Hence, the lack of increase in DCW observed between 14 h and 24 h in both *C. glutamicum* cell strains.

4.1.2 Glucose consumption

The CGXII medium was used in all fermentations carried out in the bioreactor; its composition is as highlighted in Chapter 3 (Section 3.2). The makeup of this medium indicates that glucose is the sole source of carbon. Thus, the consumption rate of glucose can be accurately evaluated, which is an advantage of using a synthetic medium, where mass balances are simpler and the controlling factors are more easily known to the experimenter. The glucose consumption rates of both strains are depicted in Figure 4.4. The general trend in the glucose profiles for *C. glutamicum* DM1945 and *C. glutamicum* DM1945x3 was similar. It starts off from the lag phase when the bacterial cells were adapting to the new environment and the DCW low, hence, the low glucose consumption from 0 to 2 h. The exponential growth phase saw the highest glucose consumption rate, which coincided with the rapid increase in DCW, as seen in Figure 4.1. Then the deceleration phase which saw the continual decrease in glucose concentration until it became scarce and finally, the stationary phase in which the low glucose concentration reduced cell growth.

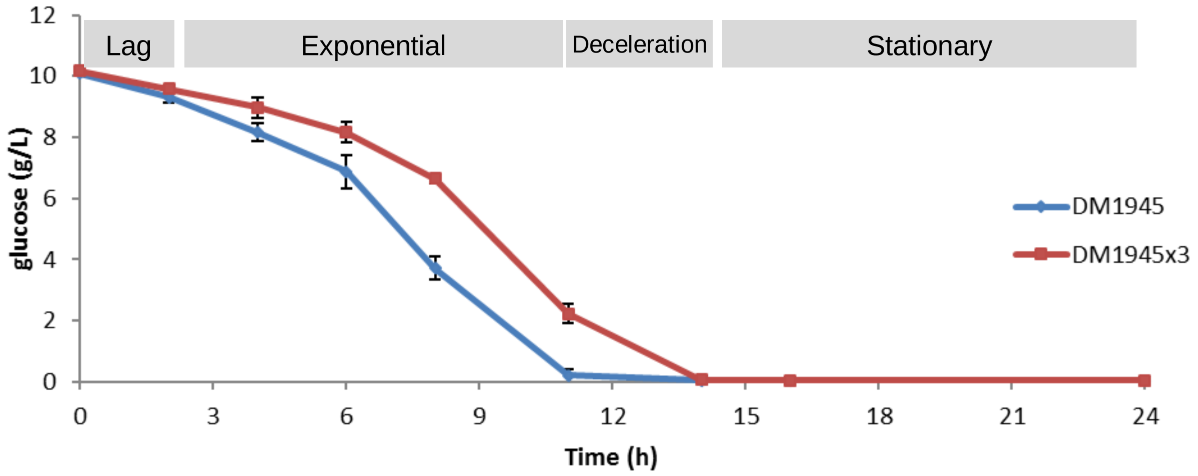

Figure 4.4 Glucose concentration during batch fermentations of C. glutamicum DM1945 and DM1945 x3; the data points represent the mean values from biological triplicates, and the error bars are equivalent to the standard deviations at these points.

Figure 4.4 indicates that all the batch fermentations started with a glucose concentration of 10 gL^{-1}, and by the end of the deceleration phase (14 h) it had been depleted in all cases. Figure 4.4 shows an apparent higher glucose consumption rate for *C. glutamicum* DM1945 compared to *C. glutamicum* DM1945x3. However, the information from the DCW yield on glucose ($Y_{x/s}$) and the specific metabolic quotients for glucose ($q_{glucose}$) give a better index for comparing glucose utilisation rates and performance. Since most of the glucose consumed was during the exponential growth phase, the estimation of $Y_{x/s}$ and $q_{glucose}$ were limited to the data points in this period. The $Y_{x/s}$ was calculated by Equation 4.4.

$$Y_{x/s} = \frac{x_m - x_0}{S_0 - S} \qquad 4.4$$

where x_m = DCW (gL^{-1}) at end of exponential phase, x_0 = DCW (gL^{-1}) at start of exponential phase, S_0 = initial glucose concentration at x_0 and S = glucose concentration at x_m.

The $Y_{x/s}$ for both strains were similar, on average 0.45 g of DCW/g of glucose for *C. glutamicum* DM1945 and 0.47 g of DCW/g of glucose for *C. glutamicum* DM1945x3. Table 4.2 shows the data analyses of the $Y_{x/s}$ values of *C. glutamicum* DM1945 and DM1945x3.

C. glutamicum strain	DM1945 $Y_{x/s}$	DM1945x3 $Y_{x/s}$
Mean	0.45	0.47
Standard Error	0.016	0.020
Standard Deviation	0.028	0.035
Sample Variance	0.00077	0.0012
Replicates	3	3
Confidence Interval (95 %)	0.38 – 0.52	0.38 – 0.56
P value (two-tailed test)	0.56	

Table 4. 2 Statistical analyses of $Y_{x/s}$ values in the batch fermentation of C. glutamicum DM1945 and DM1945x3

Table 4.2 also indicates that the $Y_{x/s}$ values of both strains were similar, as confirmed by the overlapping 95 % confidence intervals and a P value > 0.05. To obtain further information on the strains efficiency at producing DCW from consumed glucose per hour, the $q_{glucose}$ was evaluated using Equation 4.5.

$$q_{glucose} = \frac{\mu}{Y_{x/s}} \qquad 4.5$$

The average $q_{glucose}$ for both strains were similar, the values for *C. glutamicum* DM1945 and DM1945 were 0.83 and 0.80 g of glucose consumed / g of DCW produced / h respectively. The data analyses of these $q_{glucose}$ values are shown in Table 4.3.

C. glutamicum strain	DM1945 $q_{glucose}$	DM1945x3 $q_{glucose}$
Mean	0.83	0.80
Standard Error	0.042	0.052
Standard Deviation	0.073	0.091
Sample Variance	0.0053	0.0083
Replicates	3	3
Confidence Interval (95 %)	0.65 – 1.01	0.57 – 1.03
P value (two-tailed test)	0.62	

Table 4. 3 Statistical analyses of $q_{glucose}$*values in the batch fermentations of C. glutamicum DM1945 and DM1945x3*

Table 4.3 shows that the 95 % $q_{glucose}$ confidence intervals for both *C. glutamicum* strains overlap and a P value > 0.62. Hence, confirming that the apparent difference of Figure 4.4 was insignificant. The high $q_{glucose}$ values also suggest an inefficiency in converting glucose to DCW. Thus, for growth-related products such as lysine or cadaverine, productivity is expected to be low. Another contributing factor to these high $q_{glucose}$ values may be a high resting maintenance requirement. This is the case when a cell uses up a substantial amount of energy for consolidation (protein sythesis, cell membrane/wall development) at the expense of replication.

All analyses carried out thus far indicate that there was no significant difference in the growth dynamics and substrate consumption when both strains were compared during the exponential growth phase. This lack of effect may be because the lysine decarboxylase gene *ldcC* was integrated to the chromosome of *C. glutamicum* DM1945, which made the resulting *C. glutamicum* DM1945x3 structurally stable, a major advantage of the chromosomal gene integration method over gene modification via a plasmid-based overexpression. Also, the plasmid-based method is plagued with issues of plasmid instabilities, the need for selecting antibiotics and inducing agents such as Isopropyl β-D-1-thiogalactopyranoside (Friehs, 2004). These added complexities typically increase fermentation and environmental cost (Gu *et al.,* 2015).

4.1.3 Lysine/Cadaverine productivity

As already highlighted, *C. glutamicum* DM1945 is a lysine producer, while *C. glutamicum* DM1945x3 was modified to produce cadaverine. Figure 4.5 shows the product profiles for *C. glutamicum* DM1945 and DM1945x3. The blue data points represented the lysine concentrations for *C. glutamicum* DM1945, while the red data points represented the cadaverine values for *C. glutamicum* DM1945x3 at different sampling times.

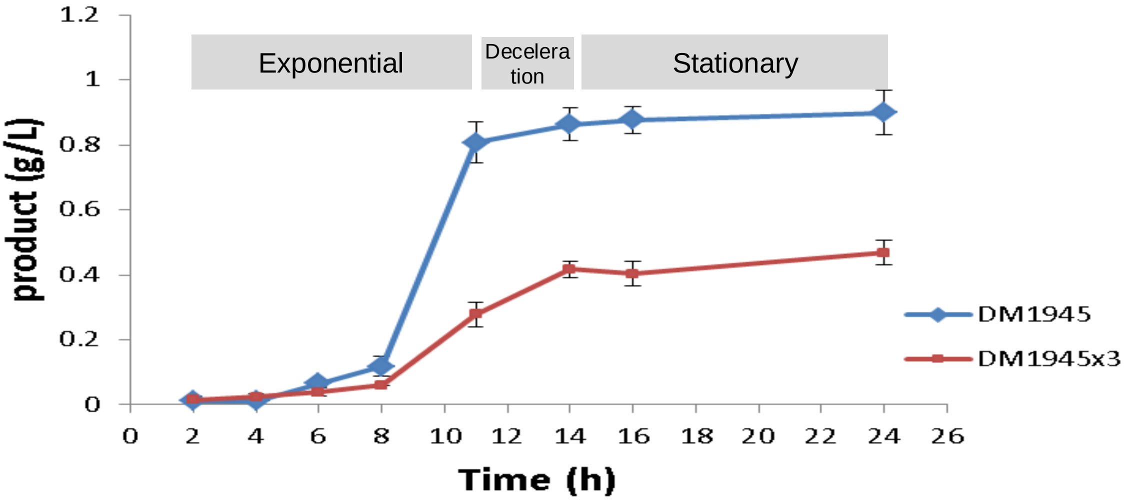

Figure 4.5 *Lysine production profiles for C. glutamicum DM1945 in blue, and cadaverine production profile for C. glutamicum DM1945x3 in red. The data points represent the mean values from biological triplicates, and the error bars are equivalent to the standard deviations at these points.*

C. glutamicum DM1945 is a lysine producer without the lysine decarboxylase gene *ldcC*. Hence, it cannot decarboxylate lysine, which was why no cadaverine was detected in all cases. For *C. glutamicum* DM1945x3 only cadaverine was quantifiable, if there was lysine produced, it was too low to be detected by the quantification method used here (see Chapter 3, section 3.7).

Figure 4.5 indicates that cadaverine and lysine were mainly formed during the exponential growth phase for *C. glutamicum* DM1945x3 and DM1945 (2 h – 11 h), However, more product formation was seen in the latter stages of the exponential growth phase (8 h – 11 h) and for *C. glutamicum* DM1945x3 cadaverine production continued into its deceleration phase (11 h – 14 h).

On average, the lysine and cadaverine concentrations produced between 2 h and 11 h were 0.80 g/L and 0.27 g/L respectively. These values represent 89 % and 57 % of the total lysine and cadaverine produced throughout these fermentations. Hence, both compounds are considered to be primary metabolites, because their production was growth-related. In confirmation, when the concentration of glucose declined from 14 h, productivity decreased rapidly. Also, in the stationary phase (14 h to 24 h) product formation stopped in both strains. So far, the growth and glucose uptake kinetics for both strains have shown to be similar (subsection 4.1.1 and 4.1.2). However, the results of Figure 4.5 highlight a difference between both strains concerning product formation. On average, in the deceleration phase, *C. glutamicum* DM1945 produced only 0.05 g/L of lysine (6 % of total lysine produced), while *C. glutamicum* DM1945x3 produced 0.14 gL^{-1} (30 % of total cadaverine produced). This shows that *C. glutamicum* DM1945x3 was still productive well into its deceleration phase. This disparity in product kinetics may be due to the different diffusion rates of lysine and cadaverine across the cytoplasmic membrane and/or the added decarboxylation step of converting intracellular lysine to cadaverine increasing the reaction time (Green & Mecsas, 2016; Kind & Wittmann, 2011). All quantification of metabolites made here relate to their extracellular concentrations, which are most likely different to their intracellular concentrations. This is because a cell semi-permeable barrier restricts the indiscriminate flow of material from a cell to the environment and vice-versa. Thus, material concentrations across a cell barrier tend to be different.

Products such as cadaverine and lysine which are produced within the cytoplasm have to pass through two main barriers to reach the extracellular environment. For *C.* glutamicum, the first hurdle in product transport is its cell membrane and to surmount this barrier the cells commonly recruit either the general secretion (Sec) or the twin-arginine translocation (tat) pathway to transport materials into the periplasmic space. From here, the product is then transported across the peptidoglycan layer either by passive diffusion or by means of the Type VII secretion system (Green & Mecsas, 2016). This rate-limiting step could explain the low production rates of cadaverine and lysine seen between 2 h and 4 h (Figure 4.5). Hence, an early exponential phase low in lysine and cadaverine productivity, with a weak correlation to the DCW profile (compare Figure 4.1 to 4.5 between 2 h and 4 h).

Figure 4.5 indicates that by the end of the deceleration phase 14 h, the lysine concentration measured was twice that of the cadaverine concentration. To confirm if this difference was significant, the product (lysine or cadaverine) yield per DCW ($Y_{p/x}$) and the specific metabolic quotients for these product (q_p) were compared during the exponential growth phase. This is because, it is assumed that during this period the bacterial cells were growing close to their maximum potential without limitations or inhibitions (Pirt, 1975; Stanbury *et al.,* 1999). Thus, a puesdo-steady state is assumed. The $Y_{p/x}$ for *C. glutamicum* DM1945 and DM1945x3 was estimated using Equation 4.6.

$$Y_{p/x} = \frac{p_m - p_0}{x_m - x_0} \qquad 4.6$$

Where p_m = concentration of product (g/L) at end of exponential phase, p_0 = concentration of product (g/L) at the start of the exponential phase, x_m = DCW (g/L) at the end of the exponential phase, x_0 = DCW (g/L) at the start of the exponential phase.

The average $Y_{p/x}$ in *C. glutamicum* DM1945 was 0.19 g of lysine / g of DCW, while the cadaverine yield in *C. glutamicum* DM1945x3 was 0.077 g of cadaverine / g of DCW. Table 4.4 shows the data analyses of $Y_{p/x}$ for both strains.

C. glutamicum strain	DM1945 $Y_{p/x}$ (Lysine)	DM1945x3 $Y_{p/x}$ (cadaverine)
Mean	0.19	0.077
Standard Error	0.0033	0.0076
Standard Deviation	0.0058	0.013
Sample Variance	3.36E-05	1.74E-04
Replicates	3	3
Confidence Interval (95 %)	0.18 – 0.20	0.044 – 0.11
P value (two-tail test)	0.00079	

Table 4.4 Statistical analyses of $Y_{p/s}$values in the batch fermentations of C. glutamicum DM1945 and DM1945x3

Table 4.4 indicates that this difference seen in yields for lysine and cadaverine for *C. glutamicum* DM1945 and DM1945x3 respectively was significant. The 95 % confidence intervals show no overlap, and the P value $\ll$ 0.05; hence the calculated yields are different. Since the products of interest are growth linked (primary products) in both strains, Equation 4.7 was used to evaluate q_p.

$$q_p = Y_{p/x}\,\mu \qquad 4.7$$

The average q_p for *C. glutamicum* DM1945 fermentations was 0.074 g of lysine produced / g of DCW produced / h, while for *C. glutamicum* DM1945x3 was 0.029 g of lysine produced / g of DCW produced / h. Table 4.5 shows the data analyses for both strains.

C. glutamicum strain	DM1945 q_p (Lysine)	DM1945x3 q_p (cadaverine)
Mean	0.074	0.029
Standard Error	0.0013	0.0028
Standard Deviation	0.0022	0.0049
Sample Variance	4.86E-06	2.39E-05
Replicates	3	3
Confidence Interval (95 %)	0.069 – 0.080	0.017 – 0.041
P value (two-tail test)	0.00070	

Table 4.5 Statistical analyses of q_p values in the batch fermentations of C. glutamicum DM1945 and DM1945x3

Table 4.5 confirms that the difference observed in the q_p values was significant; there was no overlap in the 95 % confidence intervals of both strains and the P value was $\ll$ 0.05. On average, a 61 % loss in q_p was highlighted in Table 4.5 when *C. glutamicum* DM1945x3 was compared to the parent strain. This suggests that the integration of the *ldcC* gene to *C. glutamicum* DM1945 genome affected q_p. Since the concentration of extracellular cadaverine is linked to the decarboxylation of intracellular lysine in *C. glutamicum* DM1945x3 (Becker & Wittmann, 2012; Kind & Wittmann, 2011). The low q_p in *C. glutamicum* DM1945x3 may be either due to a rate limiting decarboxylation step or/and the sub-optimal transport of intracellular cadaverine out of the cell. A rate limiting decarboxylation step would encourage competitive pathways, resulting in more carbon flux from aspartate (a cadaverine precursor) to asparagine and threonine to the detriment of cadaverine formation (Kind *et al.,* 2011). Likewise, a poor transport system would result in the considerable accumulation of cadaverine in the periplasmic region of the cells. These results indicate that more work is needed in developing a strain that will improve the cadaverine productivity of *C. glutamicum* DM1945x3.

4.1.4 Cell viability determination by plating

The CFU was used as a measure of the cells reproductive viability in all fermentations (refer to Subsection 3.8, where this method was discussed). However, as already highlighted, viability measurements via this technique excludes a certain class of metabolically active cells that do not form visible colonies on an agar plate (Nebe-Von-Caron *et al.,* 2000; Trevors, 2011). The ability of a cell to form a colony on an agar plate is a measure of both a cell's health and its robustness. Hence, when bacterial cells are rapidly dividing (exponential growth phase), the potential to form colonies is at a maximum (Nebe-Von-Caron *et al.,* 2000). Figure 4.6 shows the CFU profiles for both strains; it indicated that the maximum rate increase in CFU/mL occurred during the exponential growth phase.

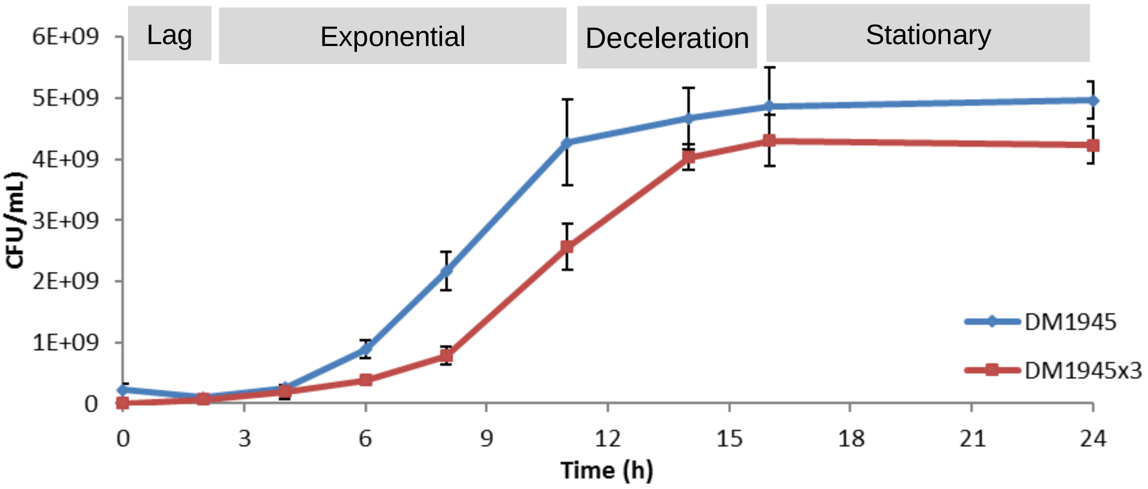

Figure 4.6 Colony forming cell counts during the batch fermentation of C. glutamicum DM1945 and DM1945 x3. Each data point represents the mean values from biological triplicates, and the error bars are equivalent to the standard deviations at these points

The lag phase saw little cell proliferation until the exponential growth phase where the bacterial cells had the most ability to proliferate. After this, the deceleration phase saw a decrease in the cells colony forming rates, which led to a stationary phase where these rates plateaued. From studying Figures 4.5 and 4.6 closer, it may be inferred that only healthy cells with high metabolic activities contribute to product formation. This is because as *C. glutamicum* DM1945 entered its decelerating phase (from 11 h), product formation decreased rapidly. However, for *C. glutamicum* DM1945x3 the increase in CFU rate did not decrease until after 14 h, which also coincided with the decrease in cadaverine production (see figures 4.5 and 4.6).

Figure 4.6 indicated a difference in the *C. glutamicum* strains CFU rates. In order to assess the significance of this difference, the CFU/mL yields of both strains in the exponential phase were calculated and compared using Equation 4.8.

$$Y_{c/x} = \frac{C_m - C_0}{x_m - x_0} \qquad 4.8$$

Where C_m = CFU/mL at the end of the exponential phase, C_0 = CFU/mL at the start of the exponential phase, x_m = DCW (gL^{-1}) at the end of the exponential phase, x_0 = DCW (gL^{-1}) at the start of the exponential phase.

The average $\mathrm{Y_{c/x}}$ values for *C. glutamicum* DM1945 and DM1945x3 were 1.02E+09 CFU/mL and 7.16E+08 CFU/mL respectively (Table 4.6).

C. glutamicum strain	DM1945 $\mathrm{Y_{c/x}}$	DM1945x3 $\mathrm{Y_{c/x}}$
Mean	1.02E+09	7.16E+08
Standard Error	6.39E+07	8.17E+07
Standard Deviation	1.11E+08	1.42E+08
Sample Variance	1.23E+16	2.00E+16
Replicate	3	3
Confidence Interval (95 %)	7.43E+08 – 1.29E+09	3.64E+08 – 1.07E+09
P value (two-tail test)	0.044	

Table 4.6 Statistical analyses of $Y_{c/x}$ values in the batch fermentations of C. glutamicum DM1945 and DM1945x3

Although, Table 4.6 showed that the 95 % confidence intervals of both strains had some overlap. The P value of < 0.05, however, suggests that the 30 % loss in the average $\mathrm{Y}_{\mathrm{c/x}}$ when the parent strain was compared to its modified strain was significant. The CFU productivities (q_{CFU}) for both strains were also evaluated from Equation 4.9 and compared.

$$q_{CFU} = Y_{c/x}\,\mu \qquad 4.9$$

The q_{CFU} for *C. glutamicum* DM1945x3 was 32 % less than of *C. glutamicum* DM1945. The data analyses that evaluated the significance of this loss is shown in Table 4.7.

C. glutamicum strain	DM1945 q_{CFU}	DM1945x3 q_{CFU}
Mean	3.87E+08	2.65E+08
Standard Error	2.43E+07	3.02E+07
Standard Deviation	4.21E+07	5.24E+07
Sample Variance	1.77E+15	2.74E+15
Replicate	3	3
Confidence Interval (95 %)	2.82E+08 – 4.92E+08	1.35E+08 – 3.95E+08
P value (two-tail test)	0.035	

Table 4.7 Statistical analyses of q_{CFU} values in the batch fermentations of C. glutamicum DM1945 and DM1945x3

Table 4.7 shows an overlapping 95 % confidence interval, but a P value < 0.05, which indicates that the difference seen in Figure 4.13 was significant. These statistical indicators above confirm that the parent strain had a higher capacity to form colonies on an agar plate. Thus, highlighting a subtle difference between both strains, even when they had identical μ. The higher CFU capability may suggest that *C. glutamicum* DM1945 was slighly more adaptable and robust of the two strains to the fermentation conditions and the semi-solid TSA medium used for the CFU count.

The process data logs for Subsection 4.1.1 to 4.1.4 for both *C. glutamicum* DM1945 and DM1945x3 batch fermentations can be seen in Appendix 3 and 4.

4.1.5 Oxygen utilisation

The oxygen utilisation profile was monitored online by evaluating the rate of change of Dissolved Oxygen Tension (DOT) in the bioreactor. In these batch fermentations, oxygen was supplied by sparging air at a constant rate of 1.5 vvm as described in Chapter 3, Subsection 3.1.6. The DOT in the bioreactor was set not to fall below 40 % irrespective of the bacterial cell growth phase; this control was achieved by increasing the impeller rate to improve the oxygen transfer rate as the bacterial cells metabolic activities increased. This ensured that at all times the bioreactor was well oxygenated (Figure 4.7 a). For both strains, the DOT gradually declined during the lag phase, due to low oxygen uptake rates of the slow-growing bacterial cells at this stage. However, as the cell metabolic activity and DCW increased, by the late exponential growth phase, the air supplied at 1.5 vvm and 100 rpm was no longer sufficient to hold the DOT $\geq$ 40 %. Hence, the resulting increase in the agitator speed seen in Figure 4.7 b to ensure that the DOT was maintained above the 40 % threshold.

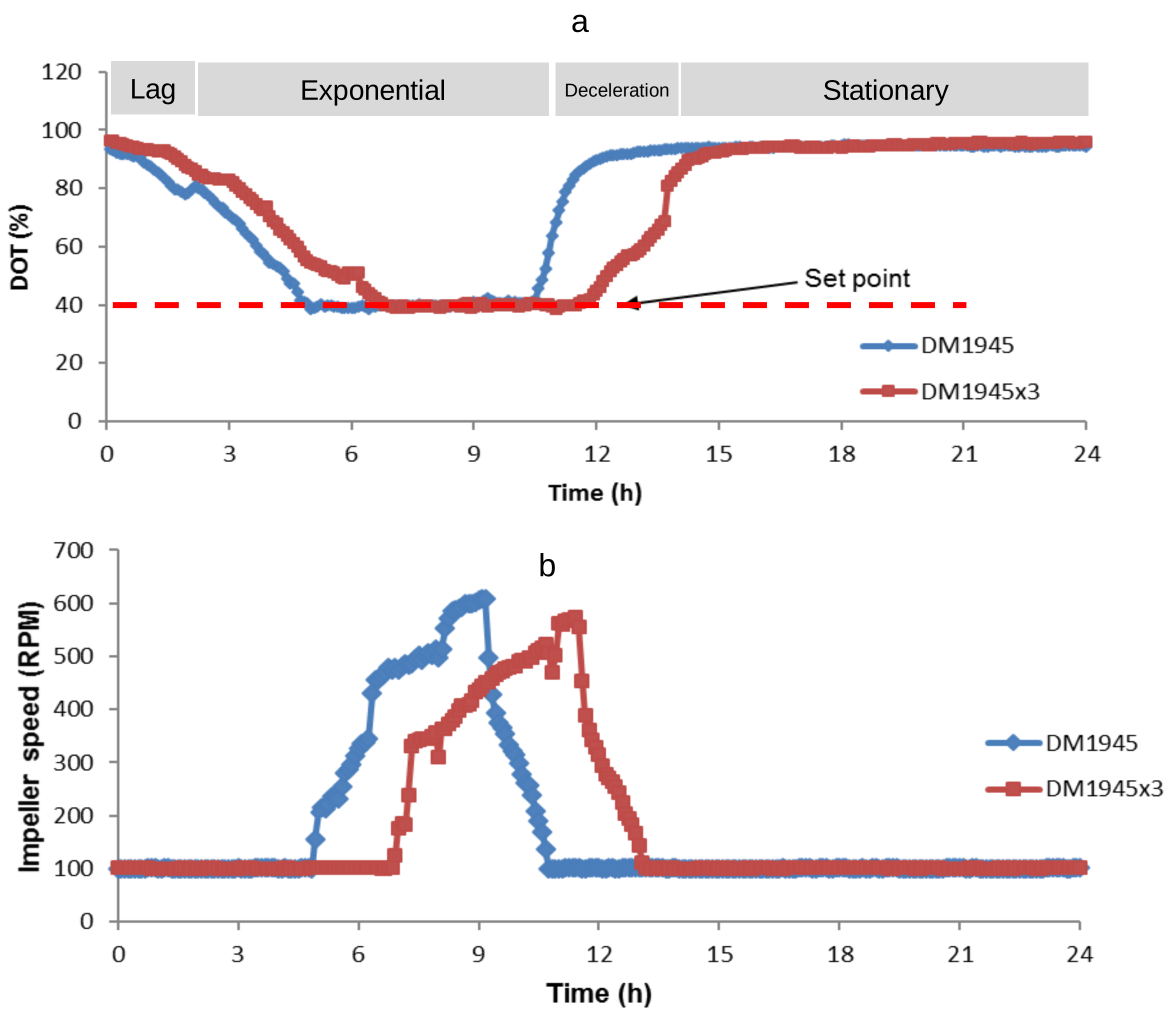

Figure 4.7 a – b Dissolved oxygen tension and a typical impeller speed profile during the batch fermentation of C. glutamicum DM1945 and DM1945 x3

The stirrer speed increased until the deceleration phase where bacterial cells metabolic rates slow down (due to glucose limitation (Figure 4.4)) saw the decrease in the impeller speed, as the demand for oxygen decreased. This period (11 h to 14 h) also saw a rise in DOT (Figure 4.14 a). In the stationary phase, the bacterial cells metabolic rates and DCW productivity remained low and unchanging. Hence, the constant impeller speed and DOT value throughout this phase.

The DOT profiles for *C. glutamicum* DM1945 and DM1945x3 showed a similar trend (Figure 4.14 a). The oxygen utilisation rates for both organisms could not be measured or compared, because of the imposition of DOT control. The changing impeller speeds to control DOT, particularly during the exponential growth phase meant that the OTR varied significantly. This can be seen between 4 h and 11 h where the DOT value was relatively constant but, the stirrer speed increases. The d(DOT)/dt equals zero at this point and the relationship to calculate the oxygen utilisation rate breaks down. In general, as the bacterial cells' metabolic activities increase the demand for oxygen also increases. Thus, the highest DOT utilisation rate occurred in the exponential growth phase for both strains.

4.1.6 Live/dead flow cytometry analyses

As already highlighted in subsection 4.2.4, estimating viability via a cells' ability to form colonies on an agar plate (CFU) only quantifies a subset of the healthy cell population. Hence, the need for the flow cytometer, which can better resolve a cell population of different metabolic states. Here, the flow cytometry was used to study the *C. glutamicum* strains viability in relation to their cytoplasmic membranes condition. Thus, significant changes in the cell population for both strains in the course of their fermentations were captured using the multiparameter flow cytometer technique discussed in Chapter 3, Section 3.8. Propidium iodide and Bis-(1,3-Dibutylbarbituric Acid) Trimethine Oxonol were the two fluorochromes used to assess the membrane integrity of *C. glutamicum* DM1945 and DM1945x3.

Propidium iodide is a typical dead/live fluorochrome; it will bind to a cell's DNA/RNA if its membrane integrity is breeched. Thus, a cell with a breached membrane cannot carry out normal metabolic functions and possesses no barrier to the external environment, so it is assumed to be not viable. Bis-(1,3-Dibutylbarbituric Acid)Trimethine Oxonol, on the other hand, enters a cell through its ionic channel.

This means that even healthy Gram-negative bacteria and some Gram-positive bacteria (*C. glutamicum* included) would take up this anionic dye. However, the healthy cell is differentiated from an unhealthy one by its ability to reisist the influx of this negative ion to maintain an optimal membrane potential (the resting membrane potential for *C. glutamicum* is ≈ – 170 mV at a pH of 7 (Follmann *et al.,* 2009a)). Unhealthy cells cannot resist the inflow of this fluorochrome as efficiently, resulting in a build-up of these negative ions intracellularly, and thus categorised as depolarised cells (Hewitt *et al.,* 1999). The spectral shift as a consequence of these ion accumulation/loss is used by flow cytometer to discriminate the different cell physiological states. The resulting flow cytometry dot plots during the batch fermentations of the *C. glutamicum* DM1945 and 1945x3 strains are shown in Figure 4.8 a – c and 4.9 a – c respectively.

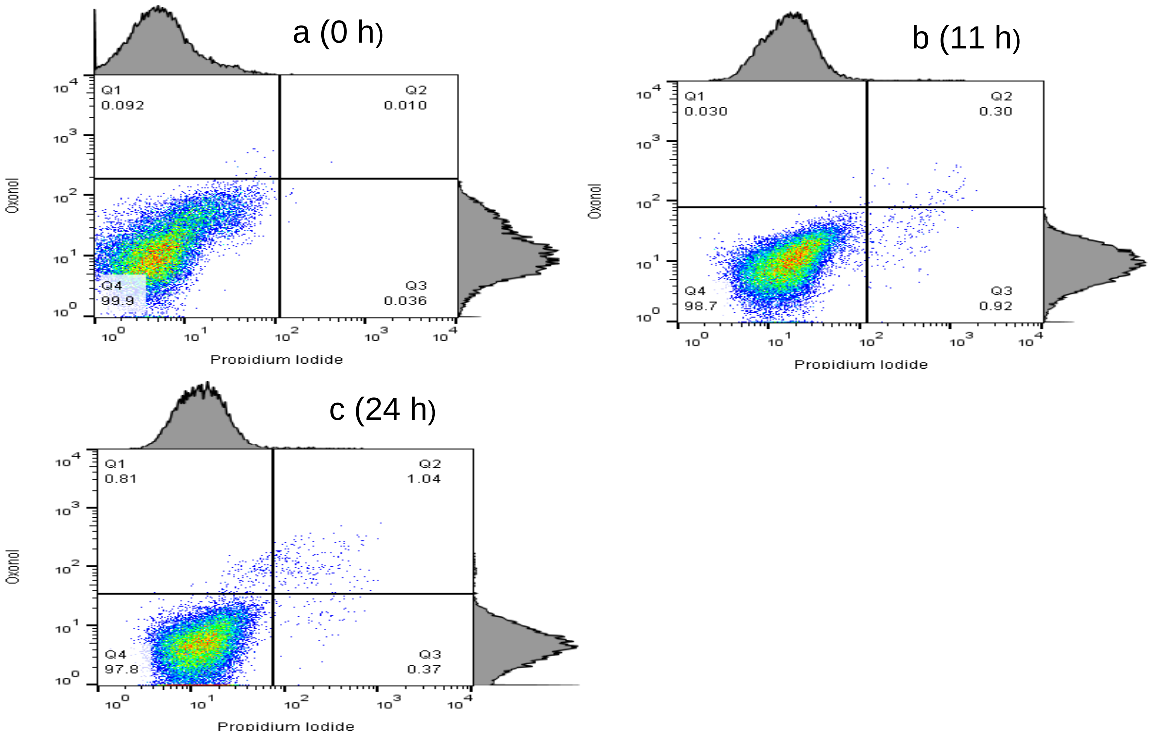

Figure 4.8 a – c Flow cytometry dot plots of C. glutamicum DM1945 physiological states based on membrane integrity during batch fermentations

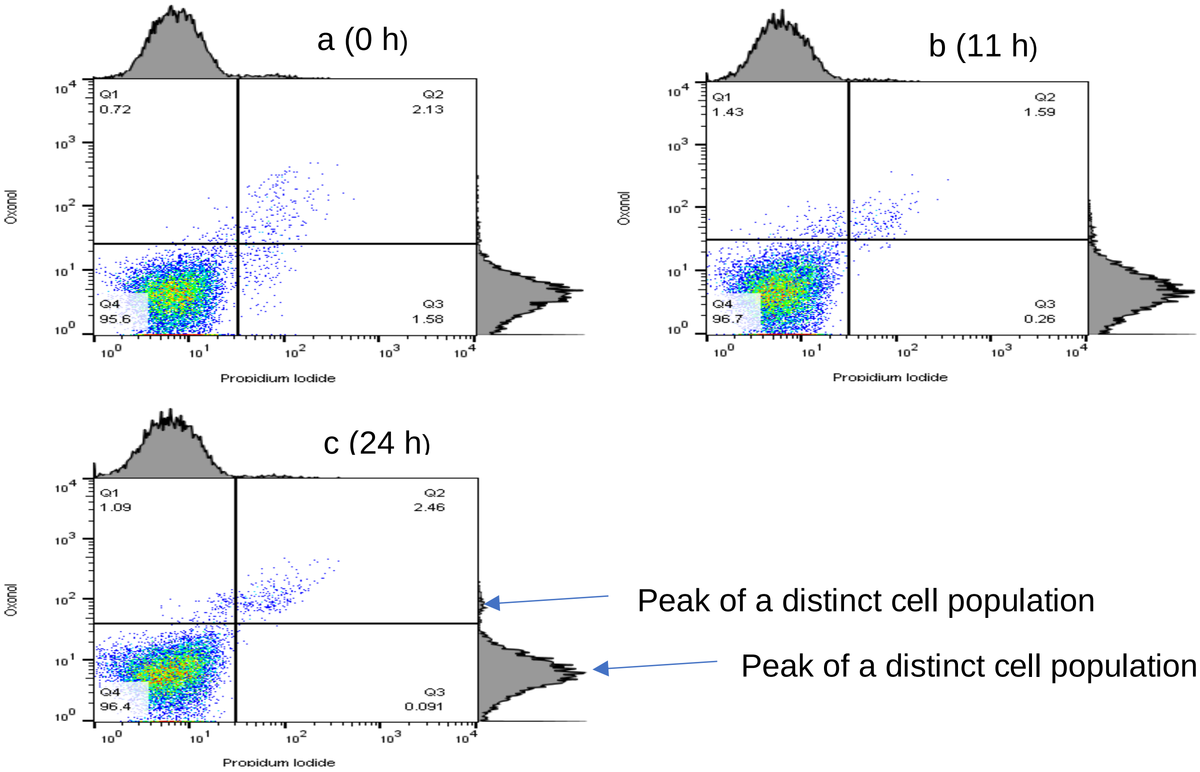

Peak of a distinct cell population

Peak of a distinct cell population

Figure 4.9 a – c Flow cytometry dot plots of C. glutamicum DM1945x3 physiological states based on membrane integrity during batch fermentations

The dots on each plot in Figure 4.8 and 4.9 represent data received from single cells, and their membrane conditions are categorised into Q1, Q2, Q3 and Q4 quadrants. The actual area of each quadrant occupied varied from graph to graph. This was due to the slight changing of laser alignment settings (done for calibration) and channel compensation from day to day operation, which resulted in a cell population projected on slightly variable axes points on the graph. However, the rationale behind the gating into quadrants for all experiments was based upon drawing lines intersecting at the trough of distinct population distribution curves (Figure 4.9 c). This meant that cells with the same light emission intensity shared similar properties and were grouped into a population subset. Each graph in Figure 4.8 and 4.9 has 10,000 dots with information on the membrane condition of 10,000 cells; the numbers seen on each of the quadrants represent the percentage of cells in relation to 10,000 cells interrogated. The cells gated in Q1 had a lower membrane potential than healthy cells (Q4) because they had accumulated oxonol ions and were considered unhealthy/depolarised. The cells in Q2 took up both propidium iodide and oxonol ions, confirming them as being non-viable. Quadrant Q3 most likely represents cell clusters of live and dead cells, as it is improbable that a cell will accumulate propidium iodide without oxonol ions since the accumulation of propidium iodide ions signifies a breached membrane. The cells in Q4 had neither taken up propidium iodide nor oxonol and consequently were deemed to be healthy due to their intact membrane.

There was no considerable difference in cell membrane state when both strains were compared. In the lag phase, the cells state was a function of the inoculum cell membrane integrity, details on the conditions of cultivation and harvest of the inoculum are given in Section 3.3. Figure 4.8 a and 4.9 a show that more than

95 % of the cells in the inoculum cells were healthy at the start of the fermentation for both *C. glutamicum* strains. By the end of the exponential phase (11 h), the percentage of healthy cells remained relatively constant i.e. > 95 % (Figure 4.8 b and 4.9 b). A trend, which did not change throughout the stationary phase (24 h), in both strains as the population was dominated by cells with intact membranes in all fermentations. If the CFU profiles at the stationary phase of Figure 4.6 are compared to the observation here, it can be inferred that from the deceleration phase onwards, there was a substantial decrease in the ability of many healthy cells to form colonies on an agar plate. Hence, the plateau in CFU counts seen in both strains, but no significant decrease in the healthy cell population from the flow cytometry analyse was revealed. This effect may be due to the rise in non-culturable metabolic active cells, a likely stress response to the low glucose concentration during this period (Nebe-Von-Caron *et al.,* 2000). The flow cytometer showed that majority of the cells were healthy and constituted over 95 % of the total number cells, but for the other subpopulations, none exceeded 3 % of the total number cells at any stage of the fermentation. There was not a significant difference between the strains as to how the state of their membranes varied in the course of the fermentation.

4.2 Conclusion

If the whole range of results presented in this chapter is considered, the gene modifications resulting in *C. glutamicum* DM1945x3 brought about a phenotype change. However, both strains still had similarities in their specific growth rates, glucose utilisation rates and cell membrane characteristics. *C. glutamicum* DM1945x3 showed a reduced ability to form colonies on an agar plate compared to *C. glutamicum* DM1945, but the main difference was seen in their product profile. *C.*

glutamicum DM1945x3 produced cadaverine and *C. glutamicum* 1945 lysine with different specific productivities.

Cadaverine productivity was low, which suggests that more work is needed to create a better producing strain if this process is to be commercialised. Finally, the growth parameters derived here will act as a baseline and used to calculate an exponential feed profile in the subsequent fed-batch process to be studied in the following chapters.

CHAPTER 5

5 Scale-down studies of *C. glutamicum* DM1945 Δact3 Ptuf-ldcC_OPT fed-batch fermentations in a constant STR volume.

These experiments were conducted to simulate some of the chemical gradients which are known to occur in an aerobic fed-batch large-scale environment, especially where a highly concentrated carbon source and pH controlling agents are introduced during such fermentations. The volumetric ratio between the STR and PFR used here was based on a large-scale study of a 30,000 L vessel (Enfors *et al.* 2001). This large-scale vessel, with a culture volume of 21,000 L to 22,000 L, was fitted with either four Ruston or four Scaba impellers. The feeding pipe was located at the top of the reactor, and the feed introduced just below the liquid surface. In this simulation of a surface feed fermentation, the computational fluid dynamics model indicated that the addition zone (the area around the point of substrate introduction) in the fed-batch process was ≈ 10 % of the total working volume in the vessel. This addition zone was typically high in substrate concentration, low in pH and low in DO. Thus, to mimic this large-scale environment on a small-scale, the PFR volume was set at 10 % of the STR volume.

5.1 Fermentation conditions across the two-compartment model

In this study, the PFR represented either the addition zone or the area close to the walls of a large-scale vessel during a fed-batch process, while the STR section represents the bulk and the well-mixed part of a large-scale reactor. In simulating these regions of interest using a two-compartment model, the magnitude of chemical gradients and the amount of time the cells spent in the two different vessels were controlled. This regulated setup enabled a better understanding of how the cells respond physiologically to the various simulations investigated. There were twelve different simulations studied (SDR 1 – 12), and the control was represented here as STR only, see Table 5.1 for an experimental overview.

	Glucose inlet	pH inlet	Air inlet	STR volume	PFR volume	τ_{PFR}	τ_{STR}
STR only	STR	STR	STR	3 L	N/A	N/A	N/A
SDR 1	STR	STR	STR	3 L	0.32 L	1 min	10 min
SDR 2	STR	STR	STR	3 L	0.32 L	2 min	20 min
SDR 3	STR	STR	STR	3 L	0.32 L	5 min	50 min
SDR 4	PFR	STR	STR	3 L	0.32 L	1 min	10 min
SDR 5	PFR	STR	STR	3 L	0.32 L	2 min	20 min
SDR 6	PFR	STR	STR	3 L	0.32 L	5 min	50 min
SDR 7	STR	PFR	STR	3 L	0.32 L	1 min	10 min
SDR 8	STR	PFR	STR	3 L	0.32 L	2 min	20 min
SDR 9	STR	PFR	STR	3 L	0.32 L	5 min	50 min
SDR 10	PFR	PFR	STR	3 L	0.32 L	1 min	10 min
SDR 11	PFR	PFR	STR	3 L	0.32 L	2 min	20 min
SDR 12	PFR	PFR	STR	3 L	0.32 L	5 min	50 min

Table 5.1 An experimental overview of the SDRs investigated

Table 5.1 shows that the volumetric ratio of the STR to the PFR was constant in SDR 1 – 12 and highlighted the various locations of the glucose, pH and air inlets with regards to the simulation studied. In all experiments, the air was sparged at the STR section of the SDR.

5.1.1 Effect of the PFR dissolved oxygen limitation in the PFR on fermentation conditions

In the SDR 1 – 3 simulations the cell broth mixtures were recirculated between the STR and PFR. The addition of feed (mainly containing glucose and trace elements), air and the pH controlling agent (NH_4OH) were introduced in the STR. This meant that the PFR section was lacking in both oxygen and glucose, while its pH value depended on the metabolic state of the cells. Figure 5.1 show two possible large-scale scenarios that can be mimicked by SDR 1 – 3. In one case, the PFR environment can be best described as the area in a large-scale STR furthest from the impeller, air sparger and feeding zone as depicted in Figure 5.1, i.e. the PFR matches the area closest to the walls of a large-scale vessel for surface feeding.

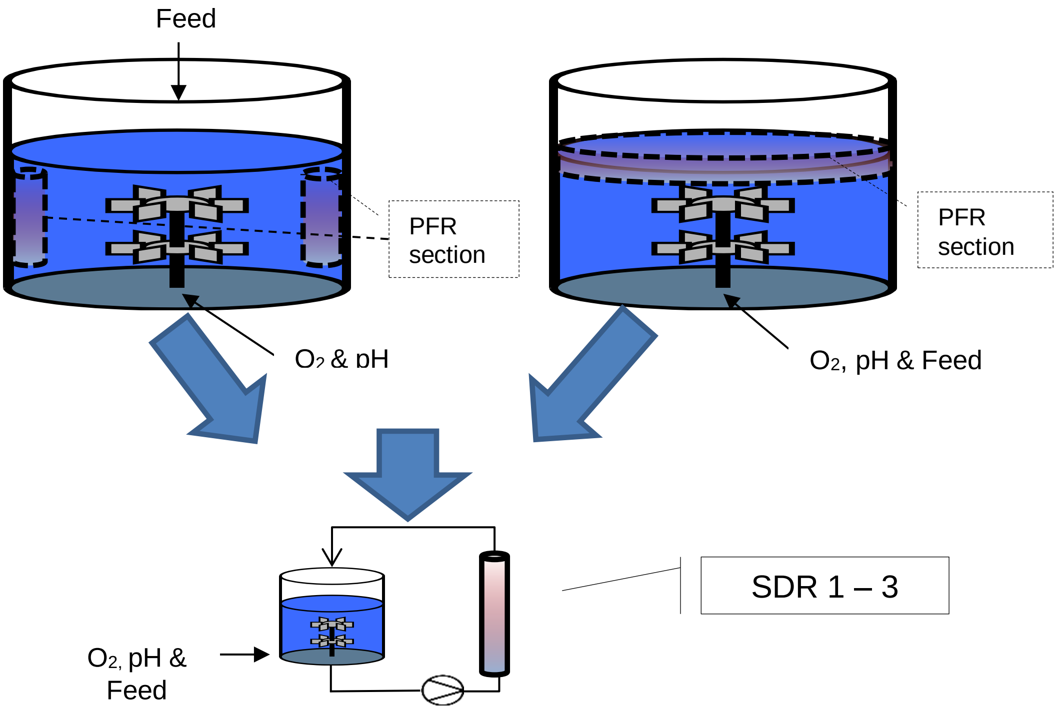

Figure 5.1 A simplified representation of the large-scale fermenter regions of interest mimicked by SDRs 1 – 3.

Alternatively, if the feed point is located at the bottom of the vessel close to the impeller; the PFR environment most likely represents the region around the medium’s surface. This zone in large-scale bioreactors, lacking both nutrient and oxygen is characterised by low cell metabolic rates, glucose and dissolved oxygen concentrations (Bylund *et al.,* 1998; George *et al.,* 1993; Hewitt *et al.,* 2000). The experimental setups of SDR 1, 2 and 3 were the same in all aspects but different in their τ_{PFR}, see Table 5.1.

All SDR experiments started out in the STR and circulation with the PFR commenced when feeding started, at 8 h, see Figure 5.2. The pH was also maintained at 7 in the STR throughout the process, by the addition, on demand of NH_4OH.

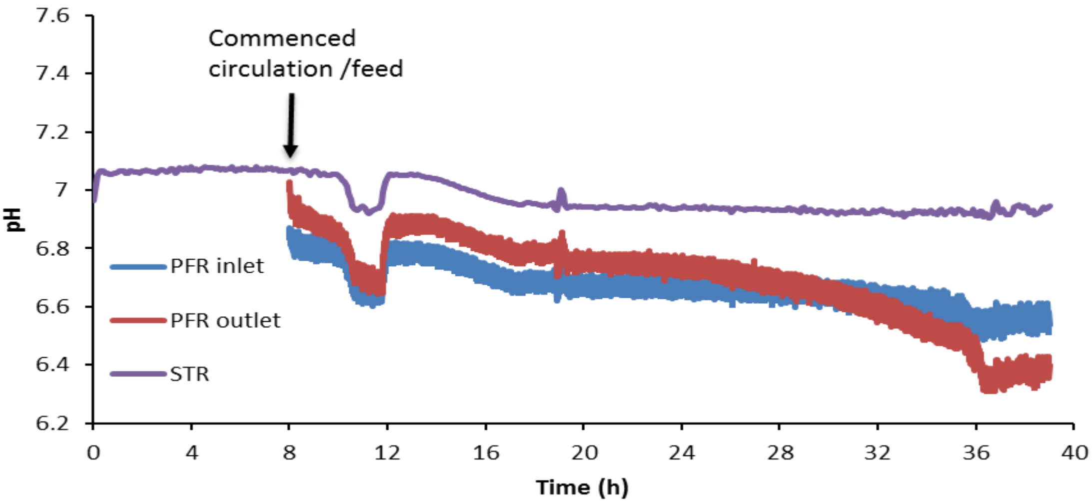

Figure 5.2 pH profiles at the PFR inlet/outlet and the STR for SDR 1

Figure 5.2 shows that there was an initial decrease in pH between 10 h and 12 h. This reduction in pH corresponded to the exponential growth in the batch phase when the cell metabolic rate was at its highest. For a cell to maintain a high growth rate, it must balance its redox potential, and in so doing, the production of organic acids is amplified, resulting in the pH decline seen here (Oktyabrskii & Smirnova, 2012). The increase in pH observed just after 12 h occurred because of the decline in the cell population’s metabolic rate (due to glucose depletion), as the cells were no longer producing significant amounts of organic acids to keep the pH value low. The second pH decrease after that was as a result of the cell growth rate and DCW increase due to exponential feeding. Interestingly, the pH value at the inlet up to 28 h was slightly higher than the outlet value. This might be simply due to the time lag between the PFR inlet and outlet because every reading taken at its outlet is approximately 1 min behind that at the inlet (due to the 1 min τ_{PFR}). The continual influx of fresh culture from the STR exacerbated this situation, especially at low DCW. However, as the culture reached high biomass densities (DCW > 20 gL^{-1} after 28 h), the cells' high metabolic rate led to the production of sufficient amounts of organic acids needed to reverse this scenario, as the cells travelled from the bottom to the top of the PFR.

The DOT profile in Figure 5.3 indicated that for most times during fermentation the PFR was limited in oxygen except during the batch to fed-batch transition period (12 to 18 h) when glucose had become severely depleted. During this transition period, the quantity of glucose added to the culture was insufficient to support any other metabolic activity apart from cell maintenance. Thus, the decline in the dissolved oxygen consumption and the rise seen in DOT between 12 and 18 h. Note that even after circulation between the STR and PFR commenced at 8 h, there was still enough glucose in the system. It was not until 12 h when most of the glucose in the culture was used up and the initial cell exponential growth phase was completed.

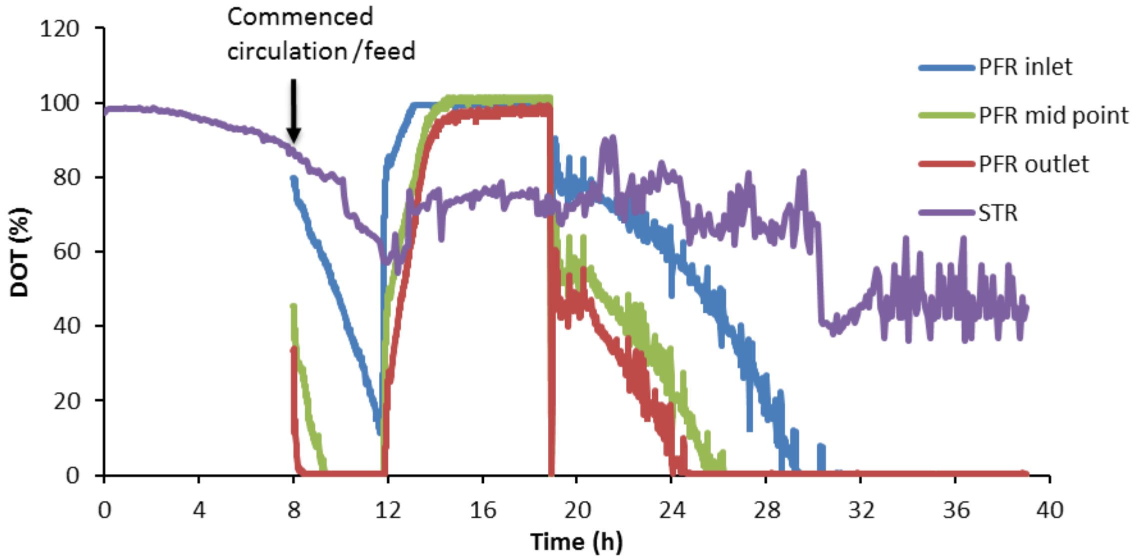

Figure 5.3 Dissolved oxygen tension profiles across SDR 1

However, well into the fed-batch stage (from 18 h), when the feeding rate had increased sufficiently to maintain a specific growth rate of 0.1 h^{-1} and other metabolic activities, the oxygen consumption rate rose again, and the DOT fell from then on towards 0 % saturation in the PFR. The DOT profile was different in the STR as gas blending with oxygen controlled the DOT, so it did not fall below 40 %. The DOT profile in the PFR also showed gradients across the reactor up until 28 h, when the number of cells was large enough to rapidly use up most of the dissolved oxygen from the STR before the PFR inlet.

Figure 5.4 shows the glucose profile across SDR 1, for the most of the fermentation, glucose was in short supply (14 h – 36 h). The start-up glucose concentration was 10 gL^{-1}, which was consumed in about 14 h. The addition of feed from 8 h to 14 h was insufficient to result in any accumulation of glucose and the rapidly growing cells easily utilised all the available glucose.

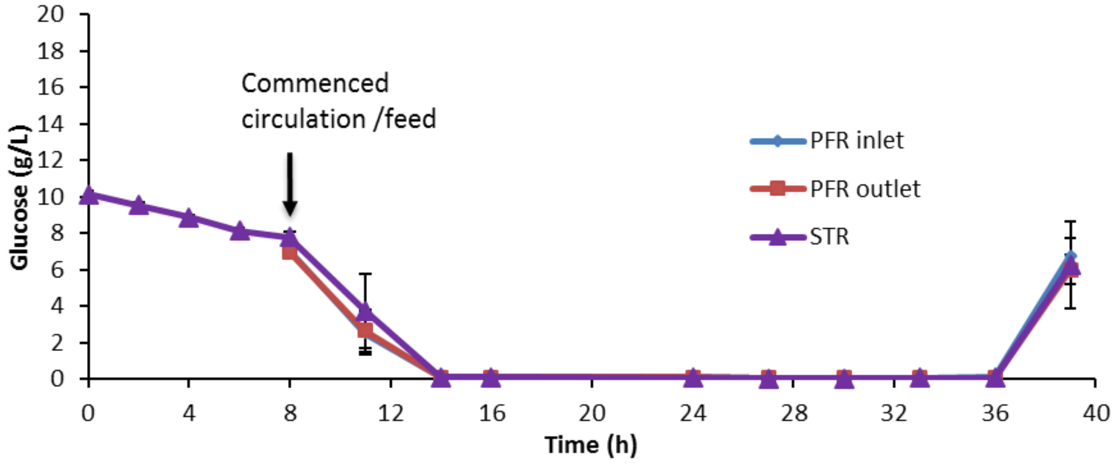

Figure 5.4 Glucose profiles across SDR 1, data points represent the mean values from two biological replicates, and the error bars depict standard deviations. The error bars between 14 h and 36 h are too small to be seen on this graph due to the high glucose concentrations at the start and end of fermentation.

From 14 h to 18 h, the glucose supplied was just enough for the maintenance of the cells as also confirmed as the transition phase in Figure 5.3. Low glucose concentrations persisted until 36 h. The feeding profile was set to achieve a specific growth rate of 0.1 h^{-1}. However, if at any point the cell growth rate is slightly reduced the accumulation of glucose will occur as seen from 36 h. Also, the chemical gradient effects at high cell densities (DCW ≈25 gL^{-1}) from 36 h could have contributed to a reduced glucose uptake which could result in the glucose accumulation observed (Lemoine *et al.,* 2015b). However, it is more likely that not one but the interaction of these factors led to the buildup of glucose at the end of the fermentation.

The data presented in Figures 5.2, 5.3 and 5.4 for the SDR 1 experiments were similar to that obtained for SDR 2 & 3, so the latter are not shown here. The results in Appendix 5 & 6 signify that the pH, DO, and glucose profiles for SDR 2 & 3 were similar in profile to SDR 1, but of a larger magnitude.

5.1.2 Effect of glucose addition in the limited oxygen PFR on fermentation conditions

In SDR 4 – 6 simulations, the pH-controlling agent and air were introduced to the well-mixed STR region, while the glucose feed was added at the inlet of the poorly-mixed unaerated PFR. This setup was carried out to study the effect of a localised high glucose concentration and its concomitant low dissolved oxygen region in a large-scale fermenter. Figure 5.5 signifies that the area of interest is around the feed inlet point, which was mimicked by the PFR, while the STR represented the relatively well aerated/low glucose region that comprises the bult of the medium in the large-scale vessel.

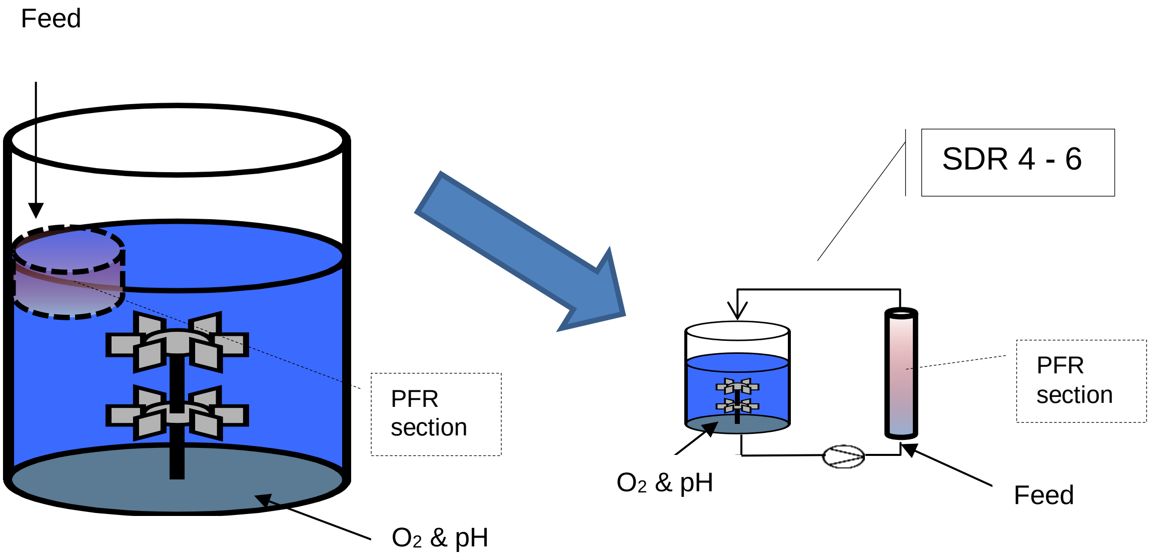

Figure 5. 5 A simplified representation of the large-scale fermenter regions of interest mimicked by SDRs 4 – 6.

SDR 4 – 6 creates a localised area of high glucose concentration at the glucose addition point in the unaerated PFR during the fed-batch stage of the process and a relatively optimal STR environment. The experimental setups for SDR 4, 5 and 6 were similar but different in their τ_{PFR}, see Table 5.1 above.

Figure 5.6 shows the pH profile across SDR 4. A larger pH gradient was noticed between the inlet and outlet of the PFR compared to SDR 1 (as seen in Figure 5.2), especially from the 28 h, when the culture was tending towards high cell densities (DCW > 15 gL^{-1}). This confirmed that the cells at the inlet exposed to the high glucose and low oxygen environment were metabolising glucose predominately via the fermentative pathway.

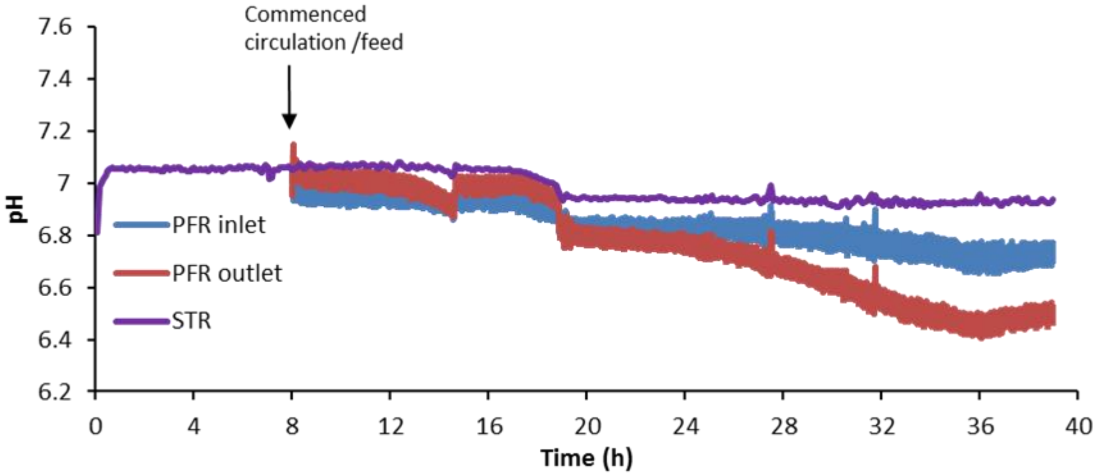

Figure 5.6 pH profiles across SDR 4 experiment

The increased production of organic acids seen in Figure 5.6 was essential to balance the cells' redox potential as they travelled towards the outlet of the PFR (Oktyabrskii & Smirnova, 2012). In the STR, the pH was relatively constant as the addition of the pH controlling agent was introduced there.

The DOT results of Figure 5.7 were like that of SDR 1, highlighted in Figure 5.3. On commencing circulation of broth from the STR to the PFR, the DOT gradients between 8 h – 14 h clearly indicate that as the cells flowed towards the PFR exit, dissolved oxygen become scarcer.

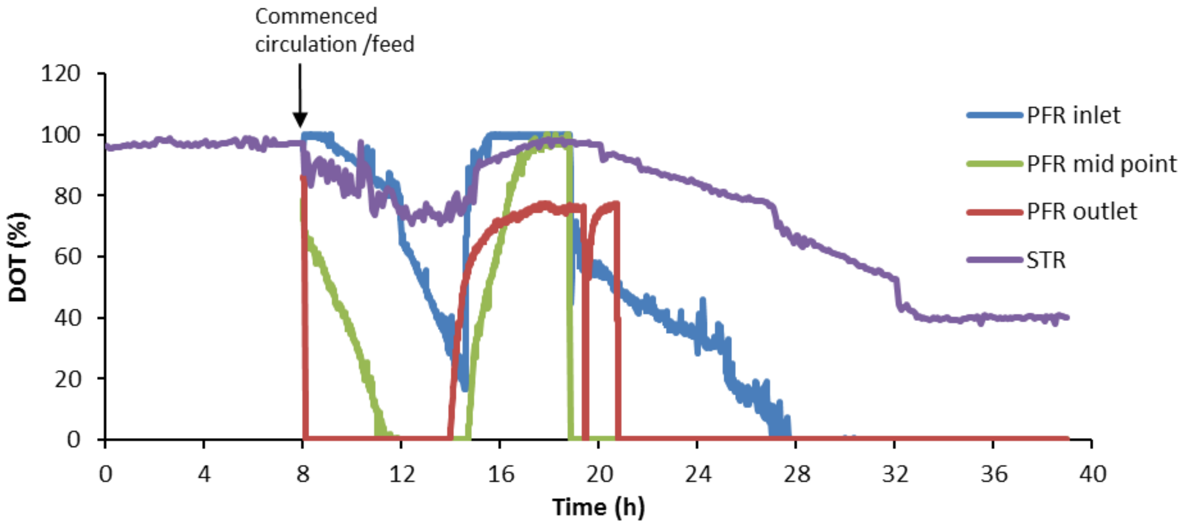

Figure 5.7 DOT profile for SDR 4 experiment

The transition phase of 14 h to 18 h saw an increase in DOT, which corresponded to the depletion of glucose and low metabolic activity. After 18 h, the inflow of feed became sufficient to promote growth, and from the 28 h, all parts of the PFR were limited in DO due to the high DCW > 15 gL^{-1}. The DOT in the STR was kept above 40 % by gas blending throughout the fermentation.

The glucose feed point and the sample points were at a different location within the PFR, see Chapter 3, Section 3.5 for details of the PFR design. This means that the glucose inlet sample value of the PFR, as noted in Figure 5.8, does not reflect the localised high glucose concentration at its point of entrance. Thus, by the time the cell broth mixture gets to the sampling point, its glucose concentration would have been diluted by the incoming fresh broth from the STR, with a proportion also having been metabolised by the cells. Figure 5.8 indicated a glucose concentration at the PFR inlet, which fails to capture the very high glucose concentration around the feed entrance. Hence, the effect of this localised high glucose concentration can only be inferred by the difference in the pH profile of SDR 4 compared to SDR 1.

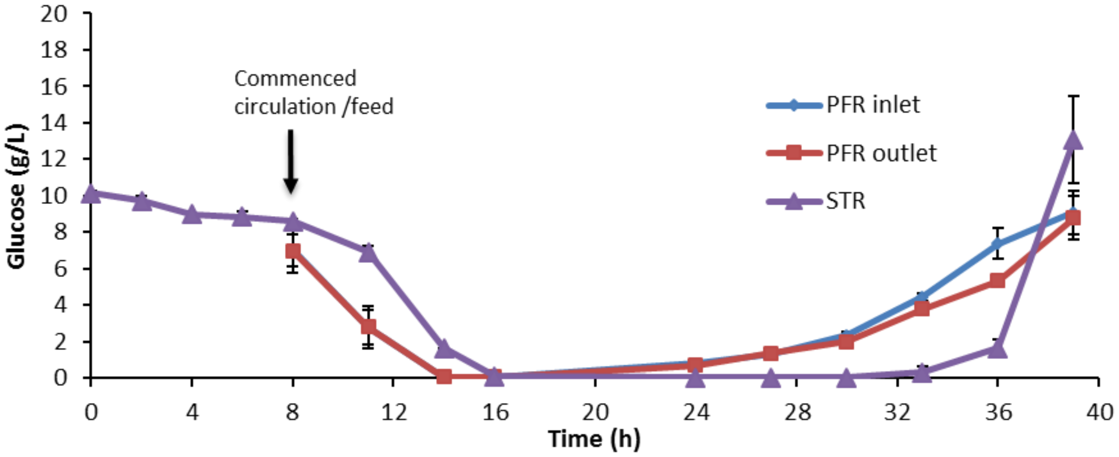

Figure 5.8 Glucose profiles across SDR 4 simulations, data points represent the mean values from two biological replicates, and the error bars are equivalent to their standard deviations. The error bars between 14 h and 36 h are too small to be seen on this graph due to the high glucose concentrations at the start and end of fermentation.

Schweder *et al.*, (1999) showed that bacteria cells could respond to fermentation stress within seconds, for example, *E. coli* cells responded to high glucose gradients in less than 13 s. *C. glutamicum* typical response in a carbon-rich environment is to increase metabolic rates and growth rate. However, in a limited dissolved oxygen environment, the increased metabolic rate is sustained via the fermentative pathway. The consequence of this leads to an increase in by-product formation such as organic acids and amino acids to mention but a few, and possibly accumulating some of these substances to a critical level, which can become detrimental to the cells. The effect of this was seen here in the reduced glucose uptake rate at the PFR starting much earlier (from 24 h) in Figure 5.8 compared to Figure 5.4 of the SDR. Thus, the accumulation of glucose in the PFR from 24 h, while for the aerated STR the build-up of glucose did not occur until 33 h.

Figures 5.6, 5,7 and 5.8 for SDR 4 were similar to those for SDR 5 & 6. The results in Appendix 7 and 8 show that the pH, DO and glucose profiles for SDR 5 & 6 were similar to SDR 4, but of a larger magnitude.

5.1.3 Effect of the pH controlling agent addition in the limited oxygen PFR on fermentation conditions

In SDR 7, 8 and 9 simulations, the glucose feed and air were introduced to the STR, while the pH controlling agent was introduced to the PFR. This simulation induces low glucose; low dissolved oxygen concentration and a zone of high pH periodically at the inlet of the PFR. The PFR environment in these simulations was designed to represent the area around the pH addition port of a large-scale reactor. Figure 5.9 shows that this area of interest is at the surface of the medium if the pH injection point is located at the top of the vessel.

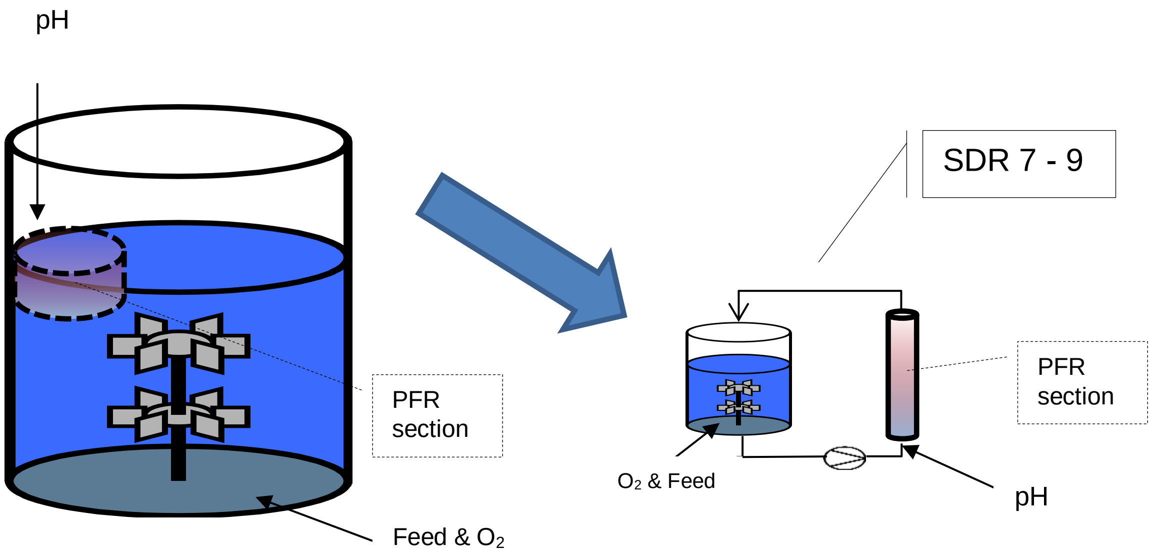

Figure 5.9 A simplified representation of the large-scale fermenter regions of interest mimicked by SDRs 7 – 9.

SDR 7 – 9 simulations were carried out to study what effect a periodically high pH has on the physiology of the cells.

Figure 5.10 shows the pH profile across SDR 7 setup; the pH in the STR was not as tightly controlled as that of SDR 4 (Figure 5.6). This was because the base needed to control the pH in the STR was injected into the PFR, and introduced a lag of approximately 1 min corresponding to the τ_{PFR} for SDR 7. Thus, the pH in the STR slightly mirrored that of the PFR, as noted in Figure 5.10. Since its change was partly related to the incoming pH value of the broth at the PFR outlet.

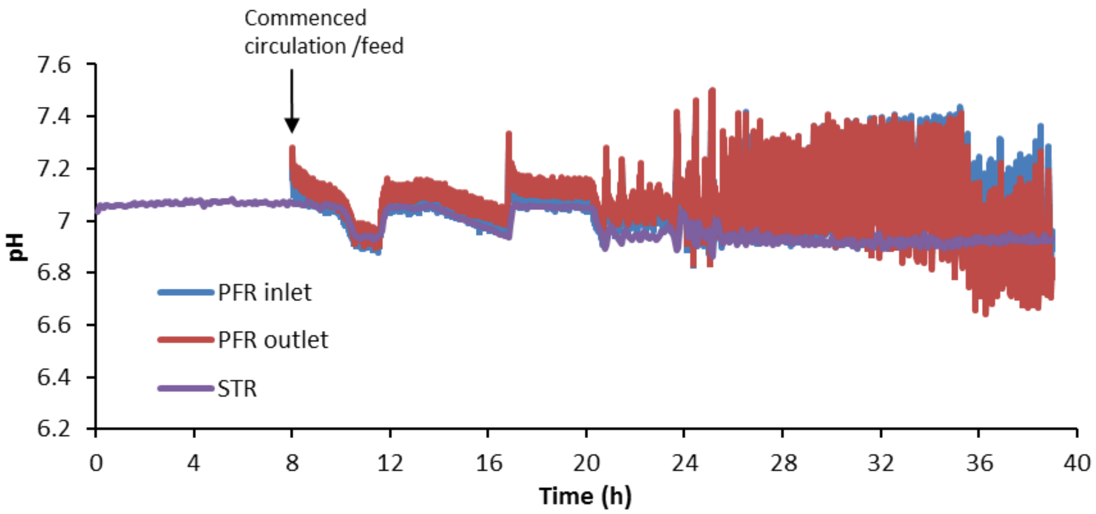

Figure 5.10 pH profiles across SDR 7 experiment

From 20 h, Figure 5.10 pH oscillations are observed; this corresponded to the increased cell metabolic activity, as the feeding was ramped in line with an exponential profile. The frequency and amplitude of these pH oscillations are closely related to the τ_{PFR}, cell growth rate and DCW concentration (see Appendix 9 & 10 for SDR 8 and 9 pH trends). The shorter the τ_{PFR} the higher the frequency of the pH oscillations, as it takes less time for a pulse of NH_4OH to travel from the PFR inlet to its outlet. Also, If the cell growth rate increases (as noted from 20 h, after the transition period, 12 h to 20 h), the rate of addition and quantity of base needed to neutralise the organic acids produced increases. This increased cell growth rate leads to a higher DCW concentration, which further raises the amount of the base needed and amplifies the pH oscillations as observed here from 20 h to 39 h.

The DOT profile as seen in Figure 5.11 is similar to the others illustrated in Figure 5.3 and 5.6. The characteristic uncontrolled exponential growth phase occurs between 8 h to 12 h, transition phase 12 h to 20 h and from then on, the controlled exponential growth, limited by glucose feeding.

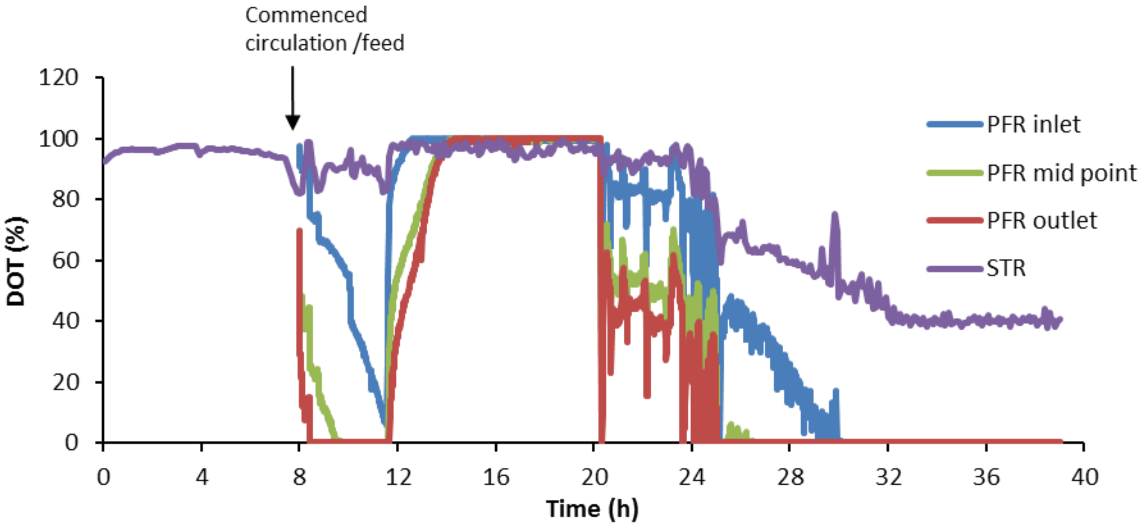

Figure 5.11 DOT profiles for SDR 7 experiment

The DOT in the STR was set not to fall below 40 % by gas blending. From 32 h, when the culture reached a high cell density (≅ 18 gL^{-1}), the set point was maintained by blending the air with oxygen. The DOT in the PFR was only monitored, so its concentration profile was a function of the cell growth cycle.

Figure 5.12 shows the glucose consumption profile, which was similar to Figure 5.4, a simulation where the feed was injected at the STR.

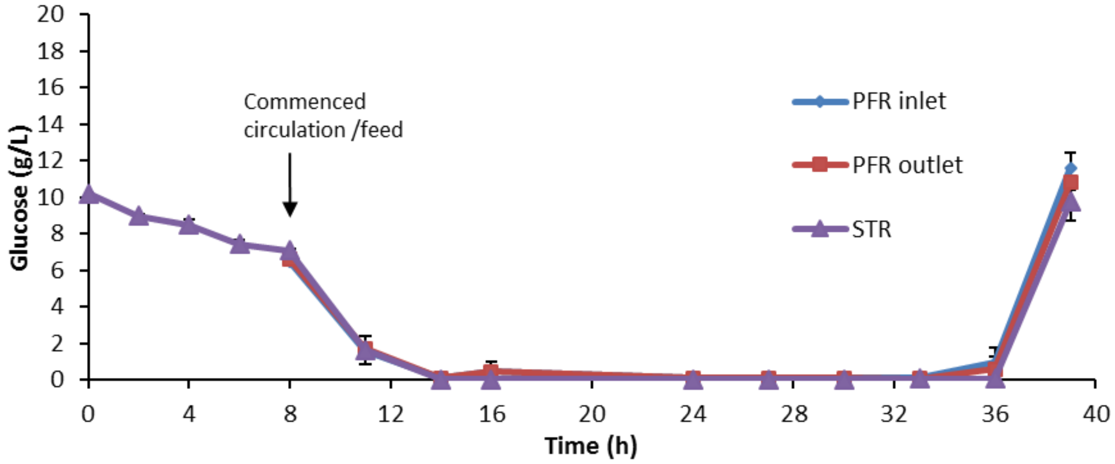

Figure 5.12 Glucose profiles across SDR 7 simulation, data points represent the mean values from two biological replicates, and the error bars are equivalent to their standard deviations. The error bars between 14 h and 36 h are too small to be seen on this graph due to the high glucose concentrations at the start and end of fermentation.

The different consumption rates also depended on cell metabolic activity. These results signify that for the most part, the concentration of glucose was relatively low, apart from the beginning 0 h to 14 h and the end, after 36 h.

Figures 5.10, 5.11 and 5.12 for SDR 7 experiments were similar to SDR 8 & 9. The results of which Appendix 9 & 10 signify that the pH, DO and glucose profiles for SDR 8 & 9 were similar to SDR 7, but of a larger magnitude.

5.1.4 Effect of glucose and pH controlling agent addition in the limited oxygen PFR on fermentation conditions

In SDR 10 – 12, both glucose feed and base were injected into PFR section, while air was sparged at the STR, see Figure 5.13. This most likely induced a high glucose concentration, especially around the injection area of the PFR.

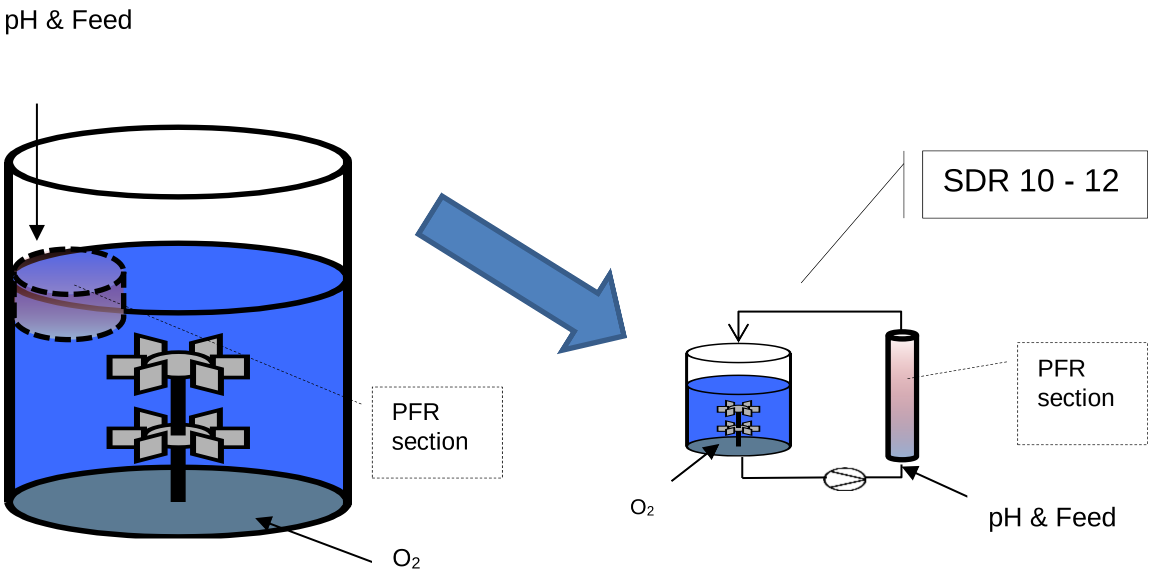

Figure 5.13 A simplified representation of the large-scale fermenter regions of interest, mimicked by SDRs 10 – 12.

Figure 5.13 shows that simulations SDR 10, 11 and 12 had a PFR environment set up to closely model the area around the addition zone of a large-scale reactor where the addition ports for the base and feed are in proximity and located at the top of the vessel. The STR section represented the rest of the bulk.

The pH change in time as illustrated in Figure 5.14 matches that of Figure 5.10, where the base was also introduced at the PFR section of the SDR. At low DCW (between 0 h – 20 h), the setpoint pH of 7 was easily controlled. During this period, the metabolic rate was relatively low, and the amount of organic acid produced was not significant, except for the initial exponential growth phase (between 13 h – 16 h), which saw the first decline in pH.

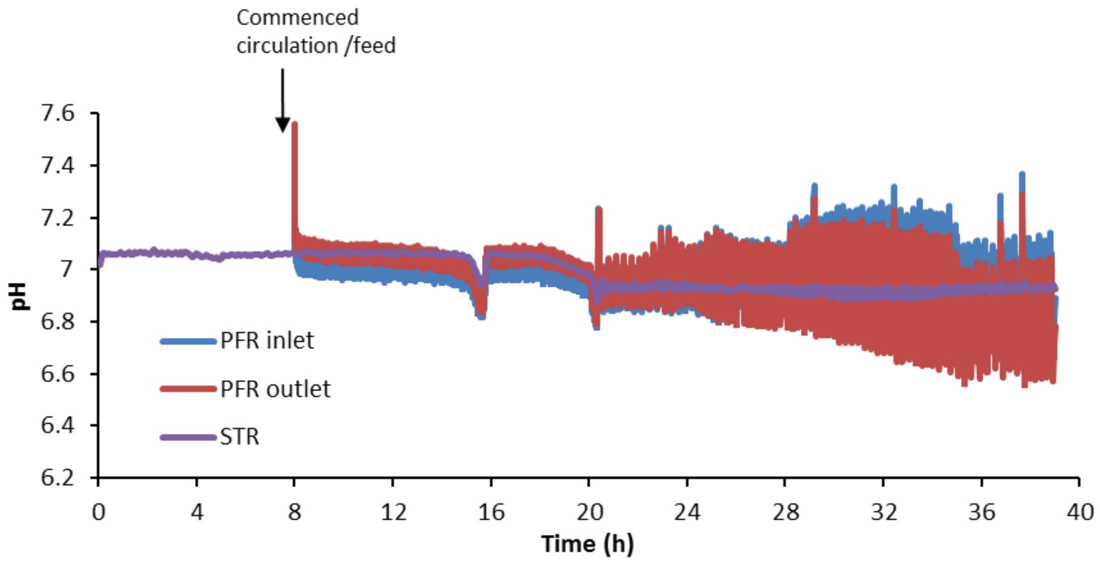

Figure 5.14 pH profiles across SDR 10 simulation

However, after 20 h, the DCW was rapidly on the rise and the metabolic activity was high. This resulted in the fluctuating pH values seen from then in the PFR; the reasons for the amplitude and frequency have already been highlighted in the discussion for SDR 7.

The DOT change in time is illustrated in Figure 5.15, a profile which remains similar to all the others discussed so far.

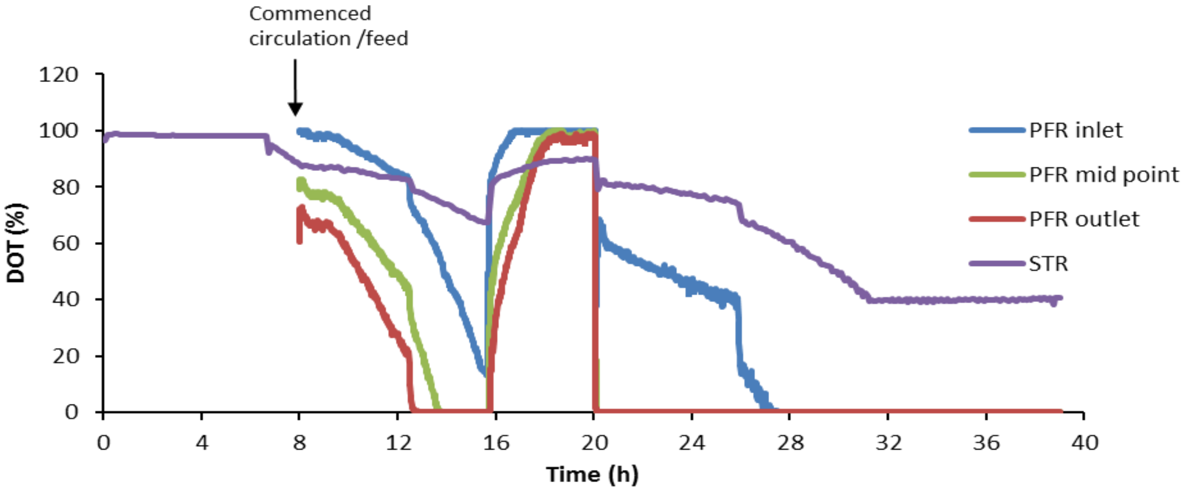

Figure 5. 15 DOT profiles across SDR 10 simulation

Figure 5.15 shows the complete cell cycle for this process, the batch phase, the transition phase and the fed-batch phase.

The graph of glucose versus time as shown in Figure 5.16 was observed to be similar to the SDR 4 glucose profile. Both had the feed injected in the PFR which led to an earlier accumulation of glucose from 20 h.

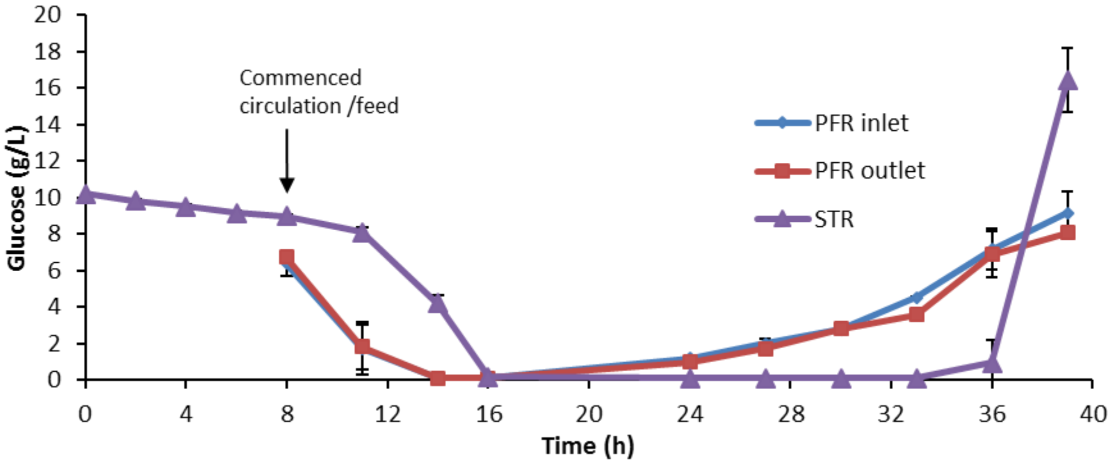

Figure 5.16 Glucose profiles across SDR 10 simulation, data points represent the mean values from two biological replicates, and the error bars are equivalent to their standard deviations. The error bars between 14 h and 36 h are too small to be seen in this graph due to the high glucose concentrations at the start and end of fermentation.

One observable trend in simulations where the glucose was introduced at the PFR, showed that glucose accumulation was greater in SDR 4 - 6 & 10 – 12 compared to SDR 1 – 3 & 7 – 9. This increase in accumulation may have been attributed to a reduced glucose uptake in SDR 4 - 6 & 10 – 12, as these simulations may have induced a stronger cell physiological response due to their high glucose and low dissolved oxygen PFR environment.

Figures 5.14, 5.15 and 5.16 for SDR 10 experiments were similar to those from SDR 11 & 12. The results of Appendix 11 & 12 show that the pH, DO and glucose profiles for SDR 11 & 12 were similar to SDR 10, but of a larger magnitude.

In all the above cases, the STR section of the two-compartment reactor represented the bulk region of the large-scale fermenter, assumed to be aerated and well-mixed.

5.2 Cell growth

For all fed-batch fermentations, the cell growth rate was controlled by limiting the glucose added to the medium via a Watson Marlow peristaltic pump. The pump feeding flow rate was automatically regulated by the Biostat B-Plus station such that it adhered to the feeding profile calculated using Equation (3.2) (see Chapter 3, Section 3.6). This feed pump flowrate was set to achieve a low μ of 0.1 h^{-1}, which was done to reduce the side product formation (Onyeaka *et al.* 2003).

The DCW concentration change quantified the cell growth. Figures 5.17 a – d indicated that, regardless of the SDR simulated, the DCW profile was similar in all cases investigated. The final DCW concentration ranged from 29.33 to 32.12 gL^{-1}, while μ was relatively constant at 0.09 h^{-1} to 0.10 h^{-1} (shown in Table 5.2).

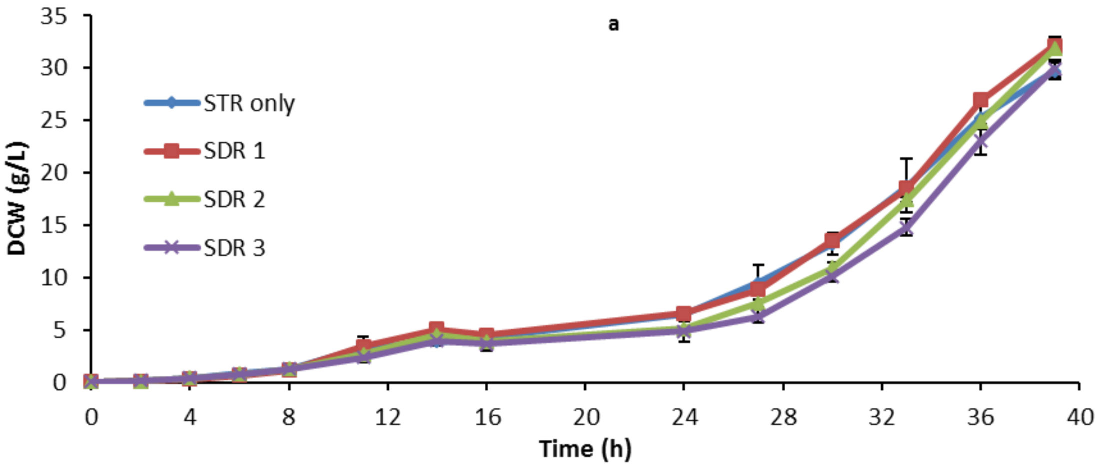

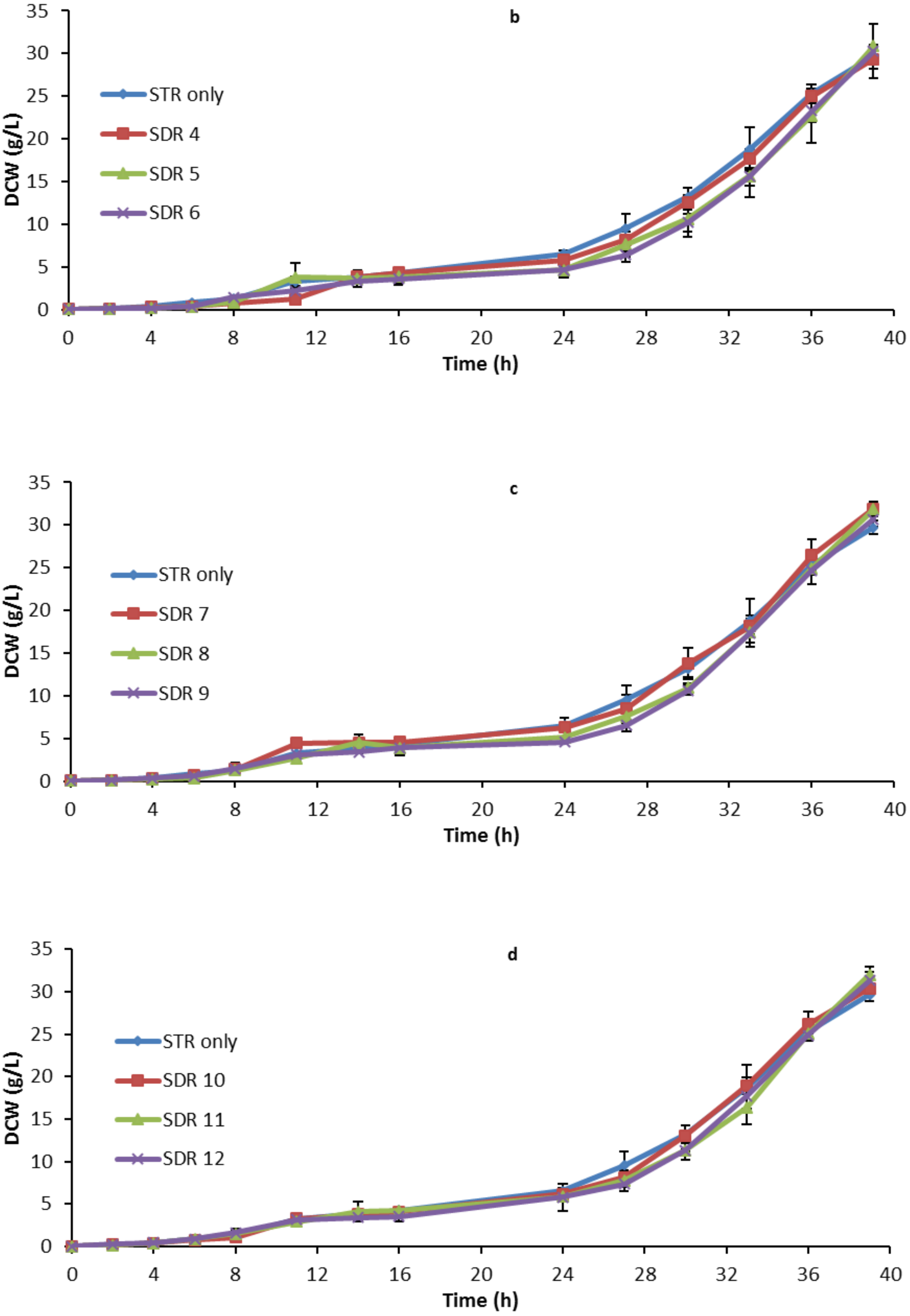

Figure 5.17 a – d Dry cell weight (DCW) profiles for simulations SDR 1 –12 compared to STR only. Legend STR only, signifies the control fed-batch fermentation in a well-mixed stirred tank reactor, data points represent the mean values from a set of biological replicates and the error bars equivalent to their standard deviations.

	Final DCW (g/L)	μ (/h)
STR only	29.68	0.09
SDR 1	32.12	0.09
SDR 2	31.85	0.10
SDR 3	29.95	0.10
SDR 4	29.33	0.09
SDR 5	30.84	0.10
SDR 6	30.28	0.10
SDR 7	31.90	0.09
SDR 8	31.85	0.10
SDR 9	30.68	0.10
SDR 10	30.37	0.10
SDR 11	31.97	0.09
SDR 12	31.30	0.10

Table 5.2 A summary of the final dry cell weight (DCW) attained at the end of fermentation 39 h

All fermentations started out as batch processes between 0 – 8 h; from 8 h, medium addition was introduced, albeit in very small quantities at the start. Also, at this same time, the recirculation of the broth from the STR to PFR commenced in the scaled-down models. The transition phase from the batch to a fed-batch process was observed between 13 and 22 h: (Figure 5.17 a – d). The cell growth rate here was very low due to the low concentration of glucose. The cell most probably survived by reducing replication to a minimum and any scavenged carbon available at this time was used for maintenance. This phase predominated until the cells became properly adapted to the nutrient-restricted environment from 21 h of the fermentation and the inflow of glucose increased sufficiently to maintain and support a specific growth rate of 0.1 h^{-1}. This resulted in 80 % of the biomass being produced in the last fifteen hours of fermentation.

That the DCW profile was unaffected tallied with the findings of Käß et al., (2014) who had concluded that *C. glutamicum* was relatively robust when subjected to glucose and dissolved oxygen restriction in their scaled-down experimental studies. They reported no drop in the DCW profile when the *C. glutamicum*

ATCC13032 strain was exposed to a non-aerated PFR section of their SDR for 45 to 87 s during their scaled-down experiments. They highlighted the increased production of lactate within the PFR, which they suggested was re-assimilated by the cells in the aerated STR. However, the relatively unchanged intracellular metabolites measured and compared in both the PFR and STR points more to a dilution effect, not the re-assimilation of lactate by the cells. Since the STR was approximately 4.6 times larger than the PFR volume, the relatively high lactate concentration in the PFR when recirculated back into the larger volume STR environment resulted in an observable decline in lactate concentration in the STR after mixing. This phenomenon can be easily misunderstood and described as lactate re-assimilation (Käß *et al.,* 2014). Käß *et al.,* (2014) did not give details of the glucose profile across the SDR, from which it would have been easy to see if the cells had indeed made the switch to an alternative carbon source while in the STR. A similar work (Lemoine *et al.,* 2015b) using a three-compartment model (PFR+STR+PFR) was claimed to be superior at mimicking such the large-scale environment as described here. Both PFRs were unaerated, but only one had a feed addition point, while the STR was aerated and was subject to pH control. On comparing their results to those of Käß *et al.*, (2014) (two-compartment model), they found that the DCW and lysine production profiles were similar. They also showed that the kanamycin-resistant *C. glutamicum* DM1800 pekeX2cadA cells when exposed to the two non-aerated PFRs for up to 4 min, recorded no loss in biomass productivity. These examples confirm what was observed here, that cultures of *C. glutamicum* exposed to a non-ideal PFR environment of τ_{PFR} ranging from 1 – 5 min showed no decrease in DCW productivity (see Figure 5.17 a – d).

5.3 CO_2 productivity

CO_2 is both a product of anabolic and catabolic metabolism within a cell; its production rate gives an indication of the physiological state of a cell. A change in a cell's metabolism could be indirectly observed by a change in its CO_2 production profile. Thus, a cell's response to changes in its environment can be partially quantified by measuring the evolved CO_2.

The respiratory quotient (RQ) was not computed because the small reactor volumes and the low sensitivity of the Tandem gas analyser made it difficult to record any difference between the inlet and exit O_2 values when the enrichment of air with oxygen was initiated to maintain a DOT $\geq$ 40 %.

The measurement of CO_2 produced was acquired in real time, which gave instant results as to how the cells responded to the changing fermentation conditions of the SDRs. The rate of change of in CO_2 production can be seen in Figures 5.18 a – d. The first CO_2 productivity peak is shown in Figure 5.18 a – d (reached $\approx$ 0.013 $g{\cdot}L^{-1}{\cdot}min^{-1}$ in all cases) between 10 – 14 h indicated the completion of the initial uncontrolled exponential cell growth phase. This then led on to the transition phase which saw the decline in the cell metabolic activities due to the limited glucose environment (seen in Figure 5.4, 5.8, 5.12 and 5.16).

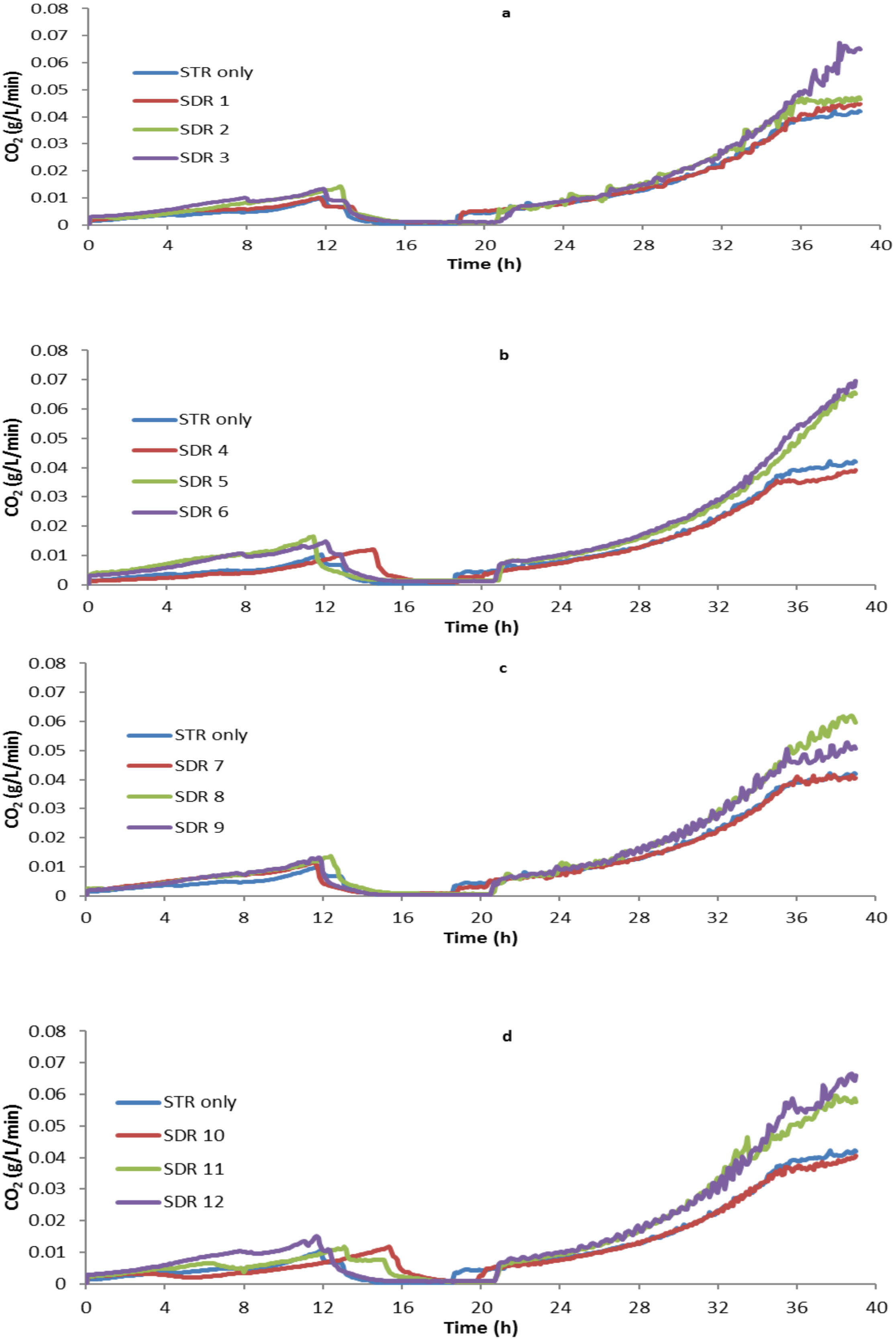

Figure 5.18 a – d CO_2 productivity for SDR 1 – 12, data points represent the mean values from a set biological replicate

This decrease is seen by the flat-lining CO_2 production (between 13 – 22 h), indicating that the cells adapted to this harsh regime by shutting down most cellular functions, apart from those necessary for survival. After the transition phase, the rate of glucose addition increased until it became sufficient for both maintenance and other cellular functions. Only then did the CO_2 evolution rate increase as the cells grew exponentially at a controlled rate of 0.1 h^{-1}. The growing cells ensured that the CO_2 productivity increased right until the end of the fermentation. However, in some cases the CO_2 production plateaued off as seen in SDR 1, 4, 7, 10 and the STR only fermentations, suggesting some other nutrient limitation apart from carbon or that product inhibition was occuring.

The 1 min simulations (SDR 1, 4, 7 & 10) were similar in their CO_2 production rate profiles to the STR only control; the final average value reached was $\approx$ 0.042 g/Lmin. Whereas the CO_2 production rate for 2 min (SDR 2, 5, 8, & 11) and 5 min (SDR 3, 6, 9 & 12) simulations was on average 0.058 and 0.063 $g{\cdot}L^{-1}{\cdot}min^{-1}$ respectively, representing a 38 % and 50 % increase. The biggest increases in CO_2 production rates were observed in simulations where the glucose was added at the PFR section of the SDR, particularly when the τ_{PFR} was highest (5 min). Thus, it can be inferred that inducing a region of high glucose concentration in a limited oxygen environment would result in more changes in the cells metabolic pathway. Also, differences seen in the CO_2 production rate profiles suggest a different product distribution. This may be the case for SDR 6 & 12 (showing the largest CO_2 profile deviation), when the cells spent the longest time in the PFR in a localised high glucose environment.

5.4 Cadaverine production

The cadaverine productivity of *C.glutamicum* DM1945 Δact3 Ptuf-ldcC_OPT was measured in a well-mixed STR only control and compared to simulations SDR 1 – 12. Figure 5.19 a – d showing the production of cadaverine from *C. glutamicum* DM1945 Δact3 Ptuf-ldcC_OPT was observed to be growth linked. The highest final cadaverine titre of 19.57 g/L was observed in the well-mixed STR only fermentation, see Table 5.3.

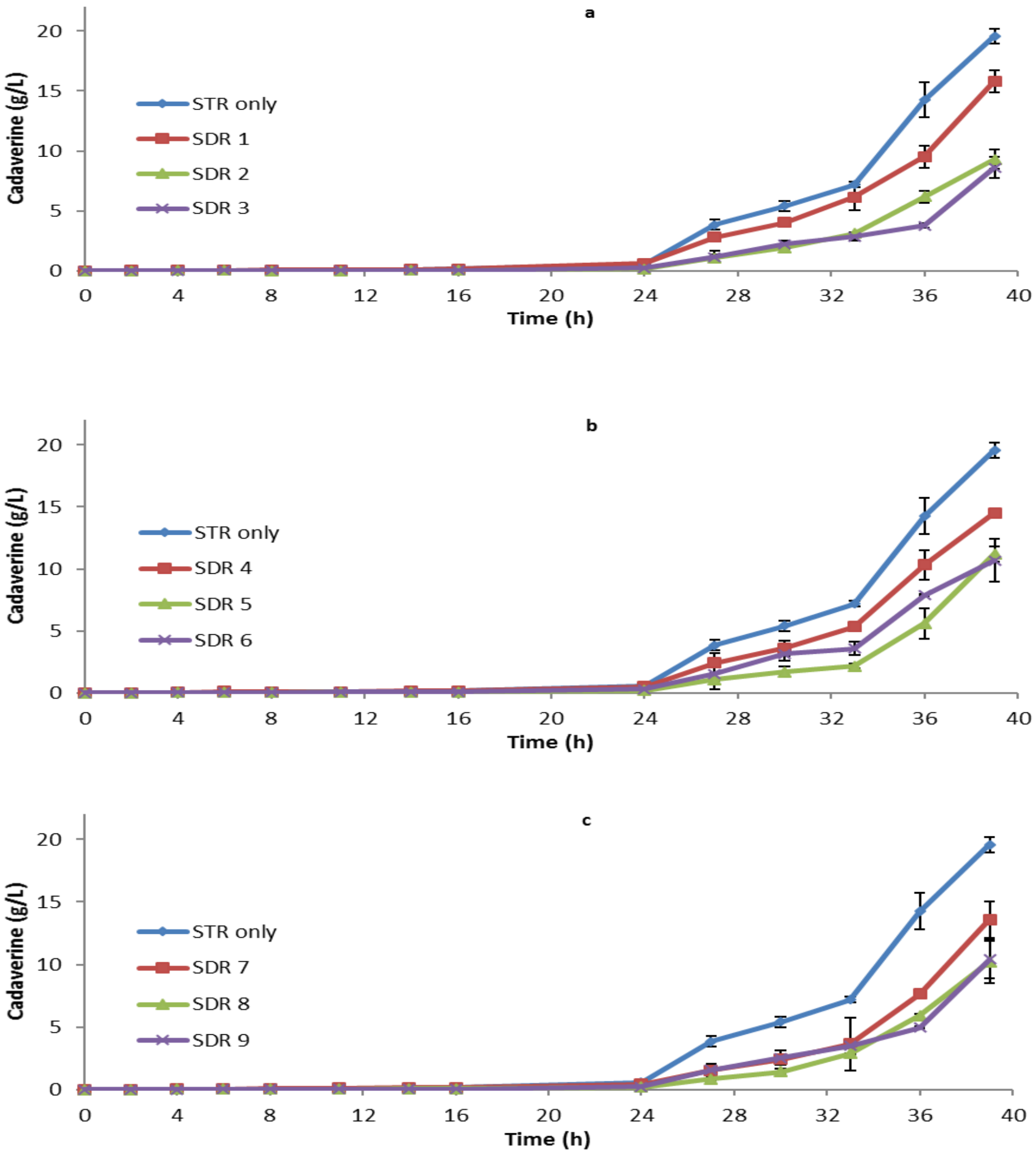

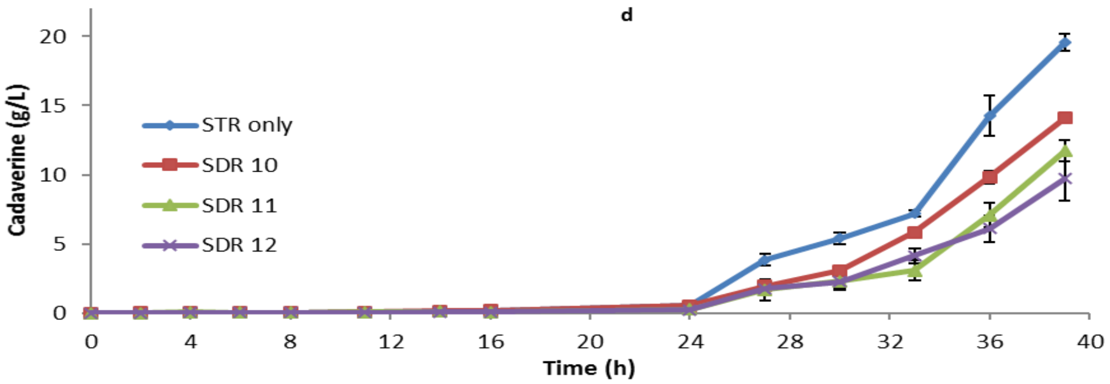

Figure 5. 19 a – d Cadaverine formation profiles for SDR 1 – 12, data points represent the mean values from biological replicates and the error bars equivalent to their standard deviations.

	Final cadaverine titre (gL^{-1})	Specific metabolic quotient for cadaverine (q_{CAD}) (g·L^{-1}·h^{-1}·g^{-1})
STR only	19.57	0.057
SDR 1 SDR 2 SDR 3	15.81 10.23 8.60	0.045 0.030 0.030
SDR 4 SDR 5 SDR 6	14.53 11.20 10.66	0.043 0.035 0.032
SDR 7 SDR 8 SDR 9	13.60 10.23 10.39	0.042 0.032 0.033
SDR 10 SDR 11 SDR 12	14.08 11.72 9.73	0.041 0.036 0.028

Table 5.3 A summary of C. glutamicum DM1945x3 cadaverine formation for STR only and SDR 1 – 12 simulations

For example, the SDR 1, 2 & 3 simulations showed a decrease in cadaverine concentration of 19, 48 and 56 % respectively compared to the STR only. This trend clearly highlighted a substantial decline in cadaverine production as the amount of time the cells spent in the unaerated PFR section increased up till after the τ_{PFR} of 2 min. This was true for the other simulations which all recorded similar decreases. The lack of resolution between the τ_{PFR} of 2 and 5 min was rather puzzling. This is further highlighted by the average q_{CAD} for the τ_{PFR} of 1, 2 and 5 min simulations evaluated as 0.043, 0.033 and 0.031 $g{\cdot}L^{-1}{\cdot}h^{-1}{\cdot}g^{-1}$ respectively. Thus, hinting that, increasing the τ_{PFR} alone does not necessarily increase the magnitude of inhomogeneity across the system. This is because if the volume in the STR is kept constant while increasing the τ_{PFR}, the cell mean residence time in the STR (τ_{STR}) also increases, which may attenuate the extent of the cell population response to the simulated pH, DOT and glucose gradients across the SDR. In other words, there is a better chance for recovery if the cells spend longer times in the well-mixed aerated STR even after their τ_{PFR} in the non-ideal PFR environment was increased. To quantify this phenomenon, the mean frequency at which the cells entered the PFR (f_m) was evaluated for each increase in τ_{PFR}, see Equation 5.1.

$$f_m = \frac{Q_r}{V_{STR}} \tag{5.1}$$

Where, Q_r = volumetric recirculation flow rate and V_{STR} = working volume of the STR and Q_r is related to τ_{PFR} by Equation 5.2.

$$Q_r = \frac{V_{PFR}}{\tau_{PFR}} \tag{5.2}$$

Where, V_{PFR} = the PFR volume, combining Equation 5.1 and 5.2 result in Equation 5.3.

$$f_m = \frac{V_{PFR}}{\tau_{PFR}} * \frac{1}{V_{STR}} \tag{5.3}$$

The f_m for the τ_{PFR} of 1, 2 and 5 min simulations derived from Equation 5.3 were calculated as 0.0018, 0.0009 and 0.0004 /s respectively. These values showed that at a constant V_{STR}, the f_m decreased considerably when the τ_{PFR} was increased. This confirmed that the cells were indeed spending more time in the STR every time the τ_{PFR} was increased.

The production of cadaverine from *C. glutamicum* is strongly linked to the operation of the TCA cycle. This is because one of its main precursor (oxaloacetate) is formed within this cycle (Becker *et al.* 2011). Thus, if there is a reduction of carbon flux into the TCA cycle, the amount of carbon available to produce oxaloacetate declines. When chemical and physical pressures are exerted on cells, they redirect the carbon flux to adapt to their environment (Larsson & Törnkvist, 1996). This encourages the production of metabolic products that help maintain intracellular homoeostasis at the expense of other non-essential products (such as cadaverine). A carbon balance analysis was used to quantify the difference in the carbon product profile to characterise how the cells responded to various SDRs. A typical unbalanced fermentation reaction as shown in Equation 5.4, which highlights the major components.

$$C_6H_{12}O_6 + (NH_4)_2SO_4 + NH_4OH + O_2 \rightarrow Biomass + C_3H_6O_3 + C_5H_{14}N_2 + CO_2 + H_2O\ +\ Z \qquad 5.4$$

Z represents the unidentified carbon containing products, which were not measured. If the carbon containing substances are only considered, Equation (5.4) can be simplified further to Equation 5.5.

$$C_6H_{12}O_6 \rightarrow Biomass + C_3H_6O_3 + C_5H_{14}N_2 + CO_2 +\ Z \qquad 5.5$$

C. glutamicum elemental biomass composition was analysed as $C_{3.97}H_{6.46}O_{1.94}N_{0.845}$ and 3.02 % ash (Vallino & Stephanopoulos, 1992). Hence, Equation 5.5 can be rewritten as seen in Equation 5.6.

$$C_6H_{12}O_6 \rightarrow C_{3.97}H_{6.46}O_{1.94}N_{0.845} + C_3H_6O_3 + C_5H_{14}N_2 + CO_2 +\ Z \qquad 5.6$$

Re-writing the above on basis of carbon, 1 mole of glucose yields Equation 5.7

$$CH_2O \rightarrow Y_{x/s}\, CH_{1.63}O_{0.49}N_{0.21} + Y_{LAC/s}\, CH_2O + \; Y_{CAD/s}\, CH_{2.8}N_{0.4} + Y_{C/s}CO_2 + Y_{z/s}Z \qquad 5.7$$

$Y_{x/s}$ = yield of C-mole biomass on glucose, $Y_{LAC/s}$ = yield of C-mole lactate on glucose, $Y_{CAD/s}$ = yield of C-mole cadaverine on glucose, $Y_{c/s}$ = yield of C-mole CO$_2$ on glucose, $Y_{z/s}$ = yield of C-mole unknown carbon containing compounds on glucose.

Thus, a carbon mole balance is represented in Equation 5.8.

$$1 = Y_{x/s} + Y_{LAC/s} + Y_{CAD/s} + Y_{c/s} + Y_{z/s} \qquad 5.8$$

All yield terms in Equation 5.8 apart from $Y_{z/s}$ were empirically derived. For illustrative purposes, $Y_{z/s}$ for the STR only experiment was used as an example and evaluated as follows.

Molar mass on a carbon mole basis of CH_2O (glucose) = 30 gmol^{-1}, $CH_{1.63}O_{0.49}N_{0.21}$ (biomass) = 24.41 gmol^{-1}, CH_2O (lactate) = 30 gmol^{-1}, $CH_{2.8}N_{0.4}$ (cadaverine) = 20.4 gmol^{-1}, CO_2 (carbon (IV) oxide) = 44 gmol^{-1}.

$$Y_{x/s} = \frac{29.68/24.41}{94/30} = 0.3881$$

$$Y_{LAC/s} = \frac{0.25/30}{94/30} = 0.0027$$

$$Y_{CAD/s} = \frac{19.57/20.4}{94/30} = 0.3062$$

$$Y_{c/s} = \frac{27.24/44}{94/30} = 0.1976$$

Substituting these yield values in Equation 5.8

$$1 = 0.3881 + 0.0027 + 0.3062 + 0.1976 + Y_{z/s}$$

Thus, $Y_{z/s}$ = 0.1054 which indicated that ≈ 10 % of the fermentation products were not quantified. To have an estimate on how many of these unmeasured products were present in the cultivation broth, a redox balance was carried out. The degrees of reduction for the elements C = +4, O = -2, H = +1 and N = -3.

Substituting these and the yield values in Equation (5.7) resulted in a redox balance as follows,

$$4 + (1 * 2) - 2 = 0.3881\big(4 + (1 * 1.63) + (-2 * 0.49) + (-3 * 0.21)\big) + 0.0027(4 + (1 * 2) - 2) + 0.3062\big(4 + (1 * 2.8) + (-3 * 0.4)\big) + 0.1976\big(4 + (-2 * 2)\big) + 0.1054Z$$

Hence,

$$4 = 1.5602 + 0.0108 + 1.7147 + 0 + 0.1054Z$$

$$Z = 6.8$$

From the value of Z, it can be inferred that the number of unquantified carbon containing product(s) (C – products) in the cultivation broth was most likely ≥ 2. Table 5.4 gives an overview of the percentage of unquantified products and equivalent degree of reduction for the various simulations investigated.

Simulation	% of unquantified C – products	Deficit degree of reduction
STR only	10.54	6.8
SDR 1	12.86	7.3
SDR 2	18.19	7.7
SDR 3	19.11	8.3
SDR 4	15.76	6.7
SDR 5	16.32	8.7
SDR 6	22.74	7.4
SDR 7	16.02	6.9
SDR 8	26.35	6.5
SDR 9	20.54	7.3
SDR 10	11.24	8.2
SDR 11	18.86	7.8
SDR 12	24.36	7.2

Table 5.4 A summary of the percentage composition of unmeasured carbon-based products derived from C. glutamicum DM1945x3 consumption of 1 mole of glucose

The general trend highlighted in Table 5.4 showed an increase in the percentage of unquantified C – products as the τ_{PFR} increased. However, the degree of reduction remained relatively unchanged. This suggests that the number of C – products with low degrees of reduction were predominant when the τ_{PFR} was increased from 1 min to 5 min. Hence, it is expected that more product diversity, with substantial short chained carbon containing compounds, will be present in simulations where the cells spent more time in the PFR.

5.5 Lactate formation

In *C. glutamicum* cultivation, lactate is mainly produced from the fermentative and the overflow metabolic pathway (Dominguez *et al.* 1998). Thus, it is a reasonable index for characterising the degree of *C. glutamicum* response to fermentation heterogeneity. However, since lactate can also be utilised by *C. glutamicum* as an alternative carbon source (Pirt 1975), its interpretation of results could be challenging in a limited glucose environment (such as a fed-batch process). Figures 5.20 a – d illustrate how the lactate concentration changes in the course of

STR only and SDR 1 – 12 fermentations. Figure 5.20 e also gives an overview of the lactate gradient across the reactor at the end of the process.

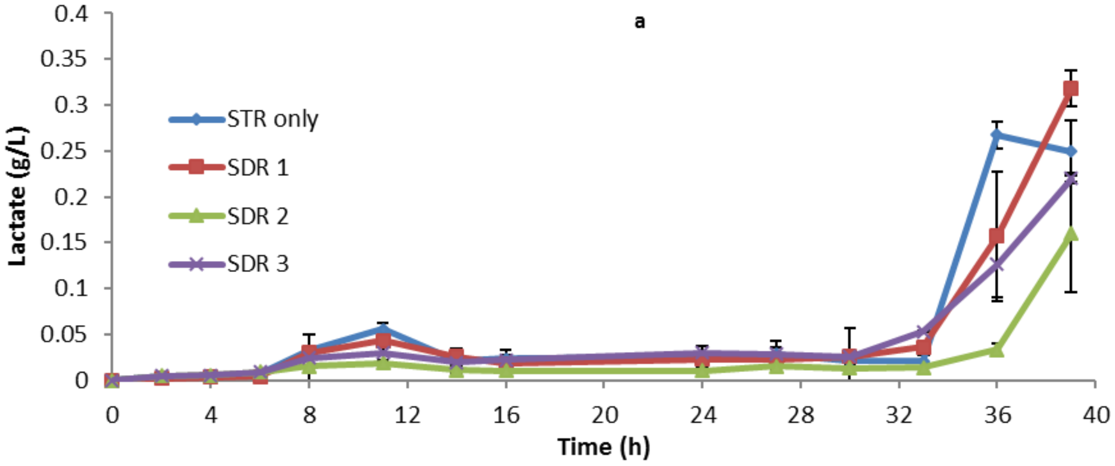

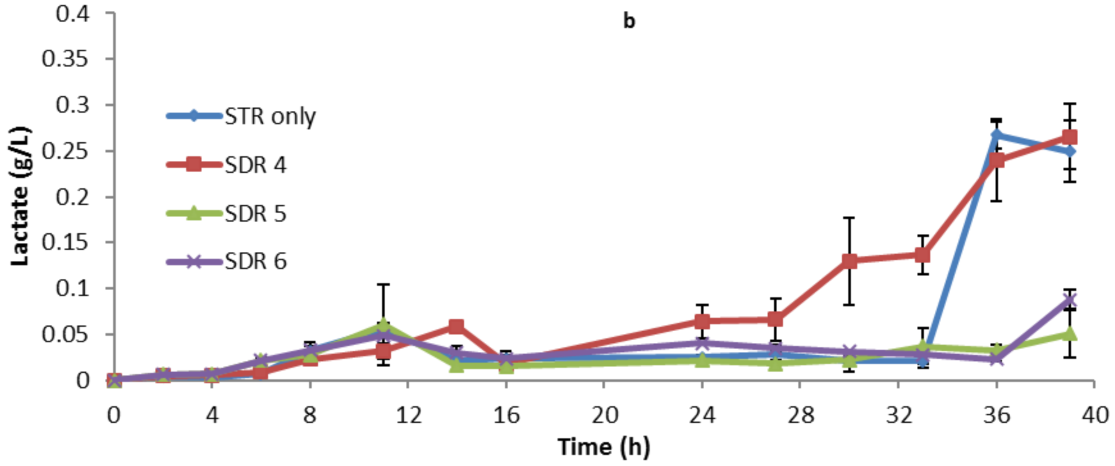

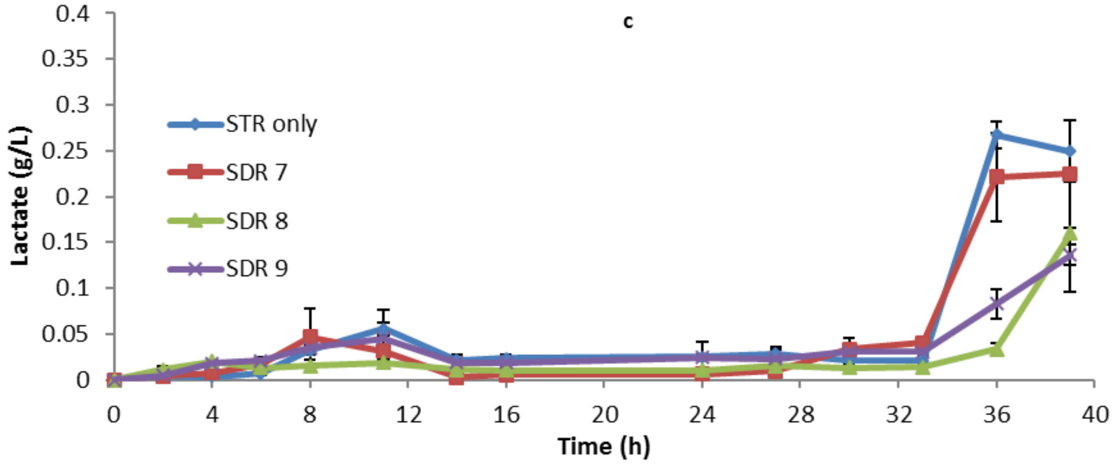

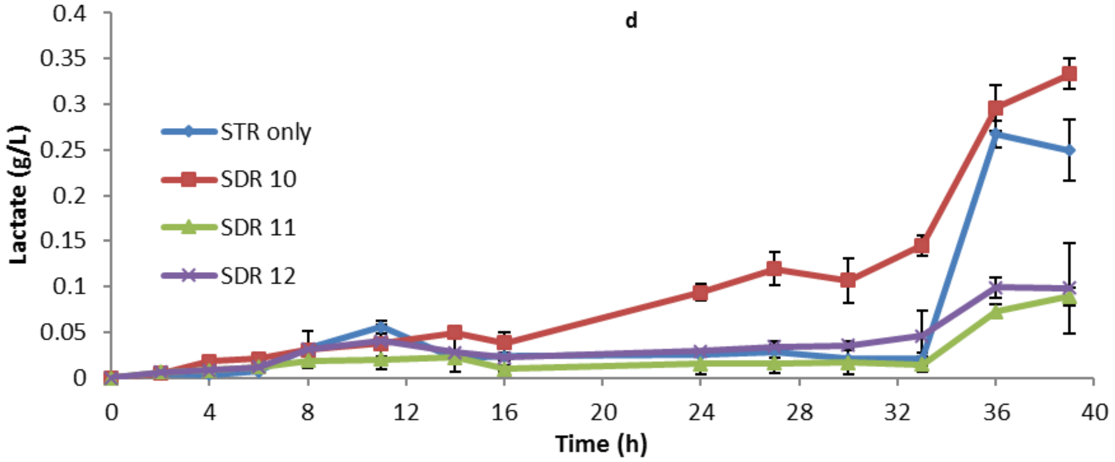

Figure 5.20 a – d Lactate accumulation profiles for SDR 1 – 12, data points represent the mean values from biological replicates and the error bars equivalent to their standard deviations.

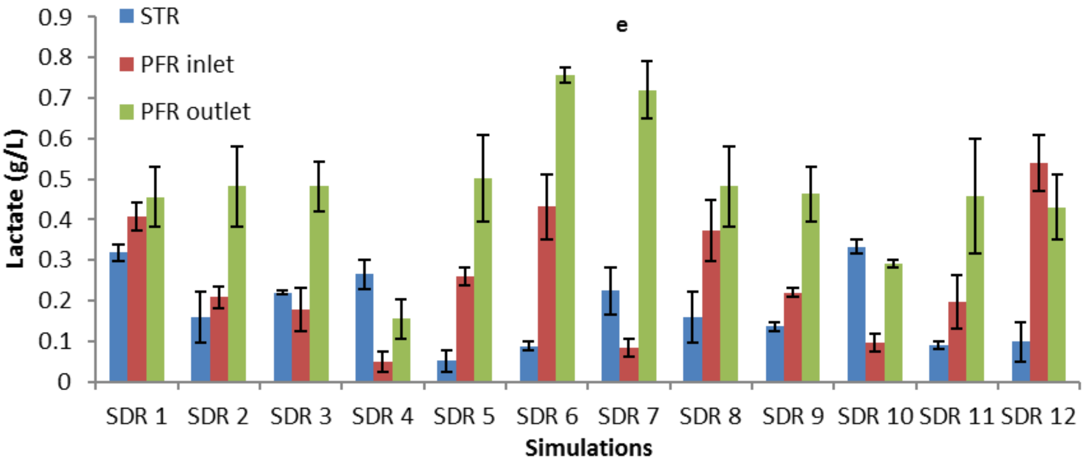

Figure 5.20 e Lactate gradient across the whole system for SDR 1 – 12 simulations, sampled at the end of fermentation (39 h), data points represent the mean of biological replicates and the error bars equivalent to their standard deviations.

The initial rise in lactate accumulation seen in Figure 5.20 a – d corresponded to the exponential growth period (6 – 11 h) of the batch phase. During this period the rate of glycolysis is at the highest as the cells have become well adapted to the bioreactor environment. The availability of nutrient brings about rapid growth; the increased carbon flux upstream activates an overflow metabolic pathway which results in an increased production of organic acids to balance its redox potential. Lactate being one of the major products of this pathway is excreted extracellularly and accumulates in the broth. This excretion of potential carbon sources, such as lactate, tends to find a secondary use when glucose becomes scarce. Thus, the cells will reuse some of the secreted organic acids as an alternative source of carbon, if glucose is unavailable. During the transition phase, when glucose became limited, the cells reverted to the organic acids present in the medium for energy, thus, the decline in lactate concentration between 13 – 22 h. After 24 h, the cells grew at a controlled specific growth rate of 0.1 h^{-1}, and as the DCW increased (> 15 gL^{-1}), the dissolved oxygen in the PFR plummeted (see Figures 5.3, 5.7, 5.11 & 5.15). This situation encouraged energy generation via the fermentative pathway within the PFR, observed by the increasing lactate concentration as the cells move through the PFR. This lactate gradient was especially predominant as τ_{PFR} increased. At the end of fermentation (39 h), the lactate concentration was typically highest at the exit point of the PFR (see Figure 5.20 e). Although, the broth recirculated back to the STR (exit broth from the PFR) typically had the highest lactate concentration, the average concentration in the STR did not rise significantly. This effect was more likely due to dilution within the STR (because of difference in volumes, STR $\approx$ 10 x PFR) rather than the re-assimilation of lactate by the cells.

5.6 Glucose accumulation

Glucose was the main carbon source in all the experiments, on start-up of the batch phase it was at 10 gL^{-1}, as shown in Figure 5.21 a – d. However, in the feed, glucose was more concentrated (600 gL^{-1}). Regardless of this high concentration, the inlet flow rate was low enough to ensure that for most of the fed-batch phase (14 h – 36 h), glucose was the limiting nutrient.

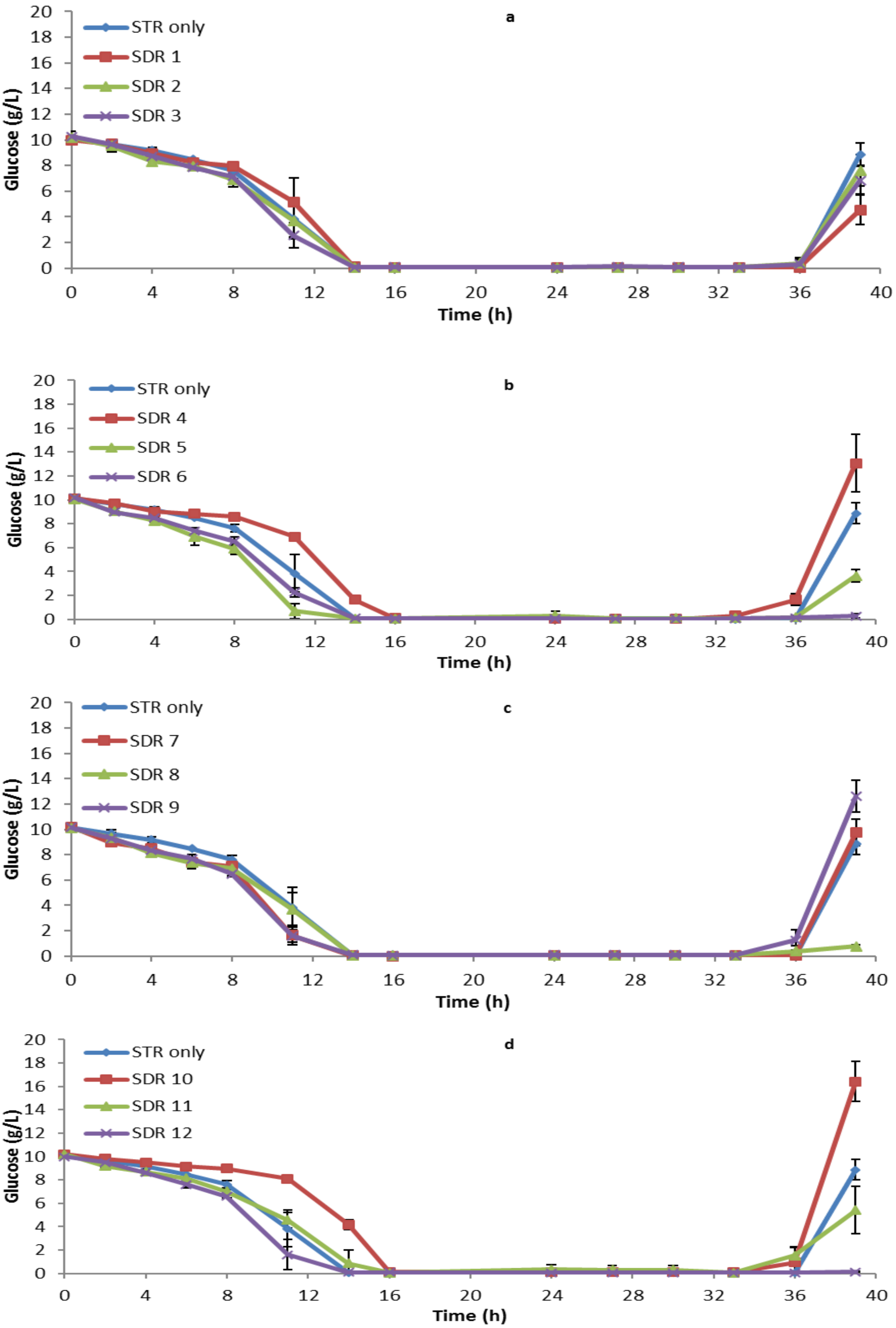

Figure 5.21 a – d Glucose utilisation profiles for SDR 1 – 12, data points represent the mean values from biological replicates and the error bars equivalent to their standard deviations. The error bars between 14 h and 36 h are too small to be seen in this graph due to the high glucose concentrations at the start and end of fermentation.

The glucose utilisation profile was similar in all the experiments carried out. The initial start-up glucose concentration during the batch phase was completely consumed between 14 and 16 h. The variations seen in the time taken to use up the initial glucose (10 gL^{-1}) can be attributed to the inoculum quality. The seed cultures were fermented in unbaffled shake flasks, with only a temperature and a shaking speed controller (see Chapter 3 for details of shake flask cultivation conditions). The other important factors such as pH, glucose and DO were neither monitored nor controlled, making it difficult to optimise the seed fermentation. This fermentation was carried out overnight for 13 hours and at the point of transfer could be anywhere between its early exponential and deceleration phase. The seed culture at this period was acidic, whilst limited in glucose and DO. The interaction of these factors probably contributed to the variability in growth rates seen in the batch phase. For example, if the seed culture were transferred after the exponential growth phase, a longer batch phase would be expected (as might have occurred in SDR 4 & 10). In general, the glucose profile shows that between 16 – 36 h, the fermenting environment was glucose limited, regardless of feeding. However, during the last 3 hours of fermentation, glucose started to accumulate, suggesting the effect of a reduced cell growth rate and a diminished glucose uptake, as already highlighted at the start of this chapter.

5.7 Flow cytometric analyses

The metabolic measurements using flow cytometry clearly distinguished three physiological states depicted in the quadrants of Figures 5.22 to 5.25. Q4, Q1 and Q2 quadrants represent healthy, depolarised and permeabilised (dead) cells respectively. Q3 most likely indicates cell clusters (doublets) or equipment noise. *C. glutamicum's* unique outer membrane structure made it challenging to develop a suitable multi-stain assay for characterising the aforementioned physiological states. Its outer layer is composed of mycolates with similar functions to that of a Gram -ve organism (Puech *et al.,* 2001). Hence, its uncharacteristic high resting membrane potential of ≈ 170 mV in a neutral medium (Follmann *et al.,* 2009b). The complexity of this outer layer also makes it incompatible with carbocyanine based fluorochromes, contrary to use with a typical Gram-positive bacterium, such as *B. subtilis*. Thus, the fluorochromes which were found suitable here are commonly used for the analysis of Gram-negative organisms.

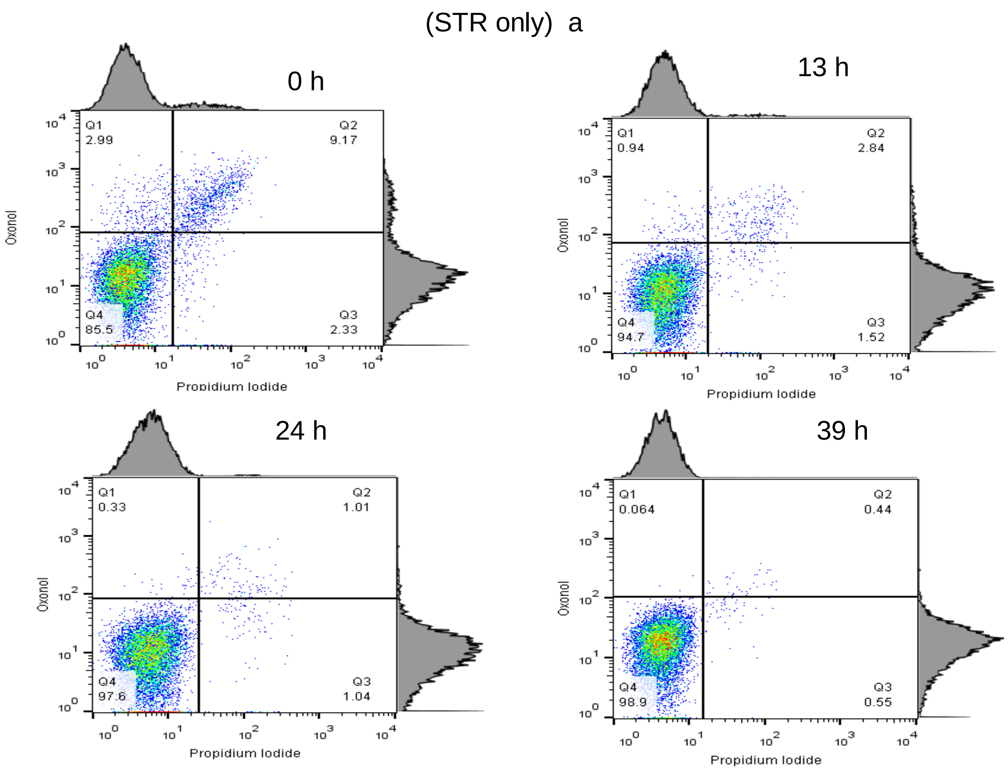

(SDR 1) b

Glucose and acid/base to STR, τ_{PFR} = 1 min

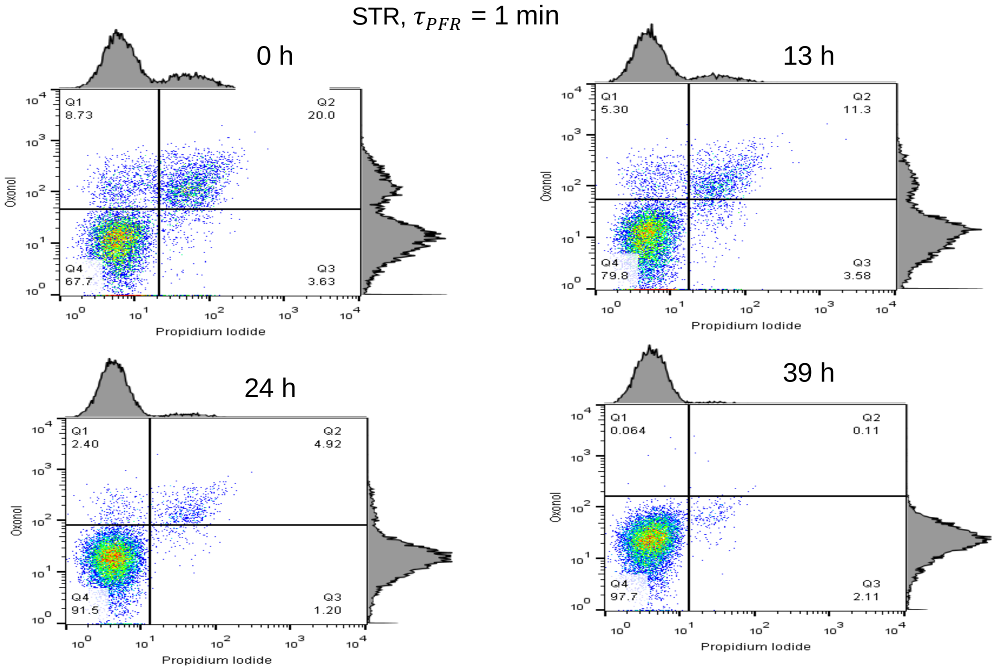

(SDR 2) c

Glucose and acid/base to STR, τ_{PFR} = 2 min

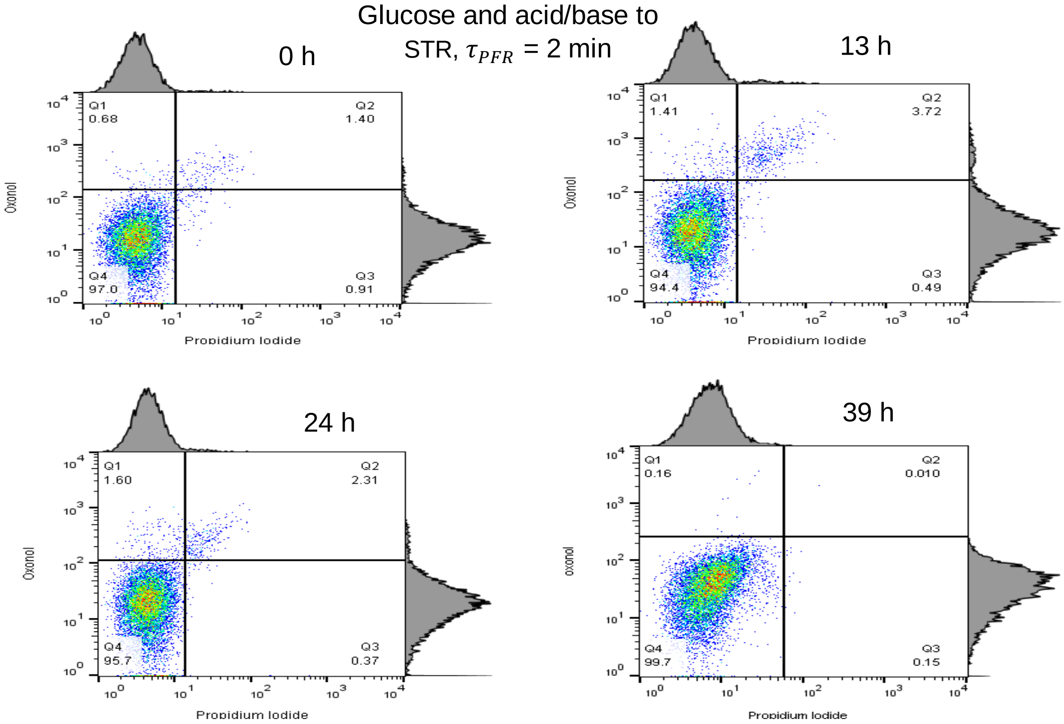

(SDR 3) d

Glucose and acid/base to STR, τ_{PFR} = 5 min

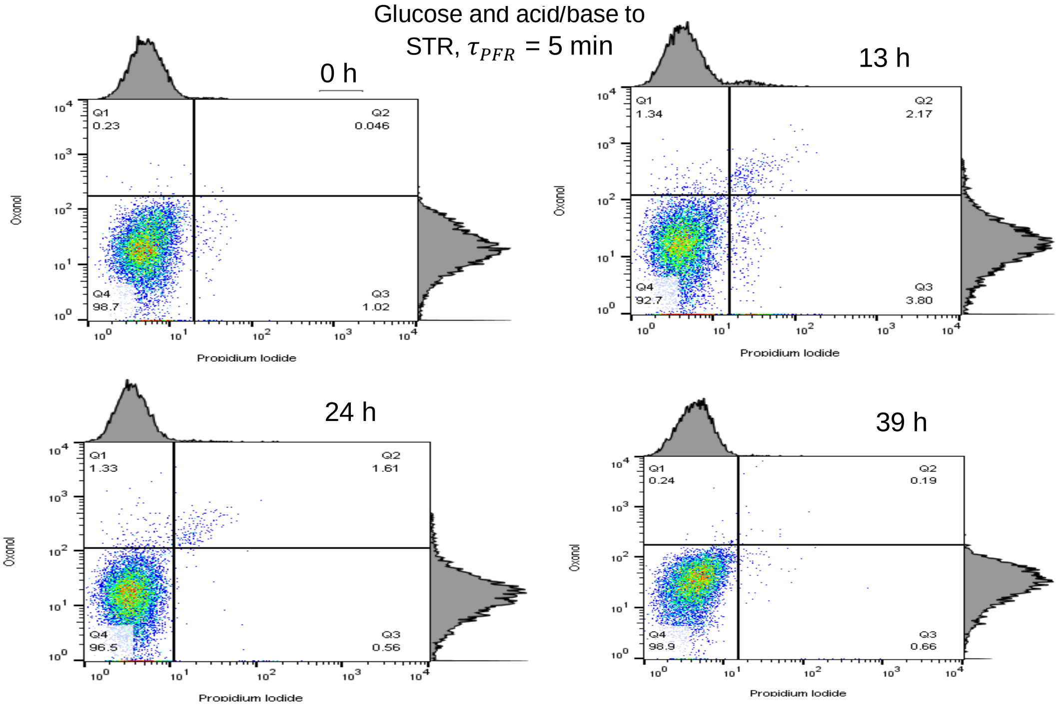

Figure 5.22 a - d Flow cytometer dot plots for STR only, SDR 1,2 & 3 indicating the condition of the cell membrane at different time points during fermentation using the above fluorochromes. Each dot on the plot represents a cell of the 10000 cells interrogated.

(SDR 4) a

Glucose to PFR; acid/base to STR, τ_{PFR} = 1 min

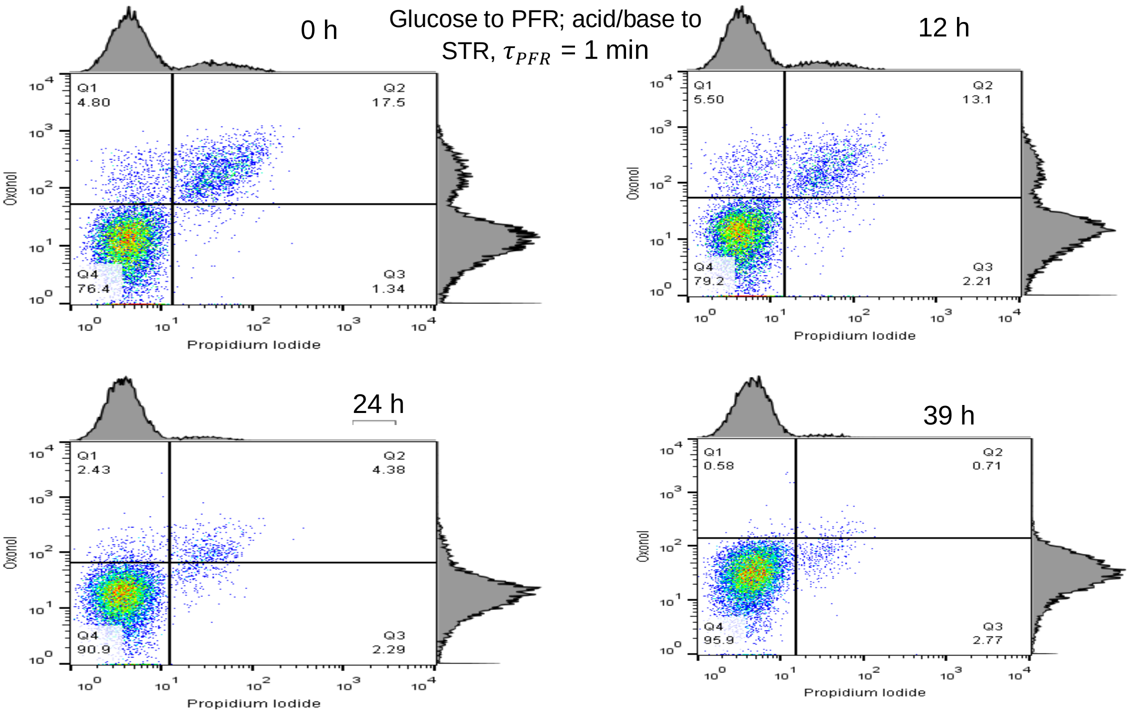

(SDR 5) b

Glucose to PFR; acid/base to STR, τ_{PFR} = 2 min

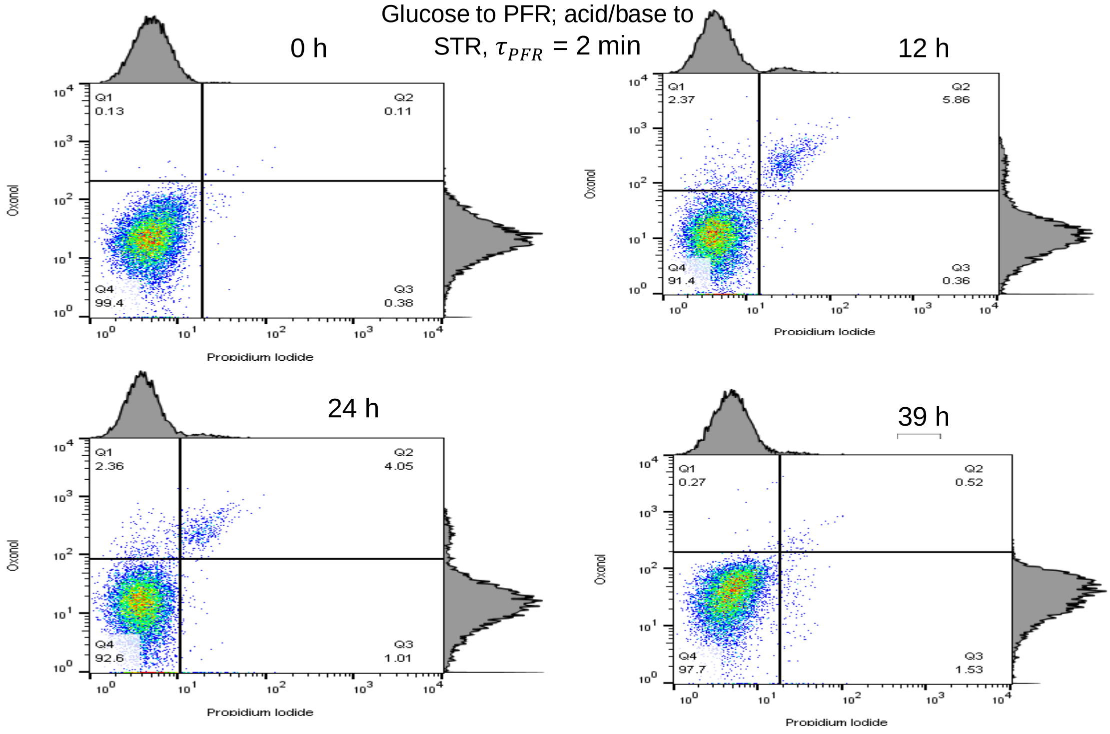

(SDR 6) c

Glucose to PFR; acid/base to STR, τ_{PFR} = 5 min

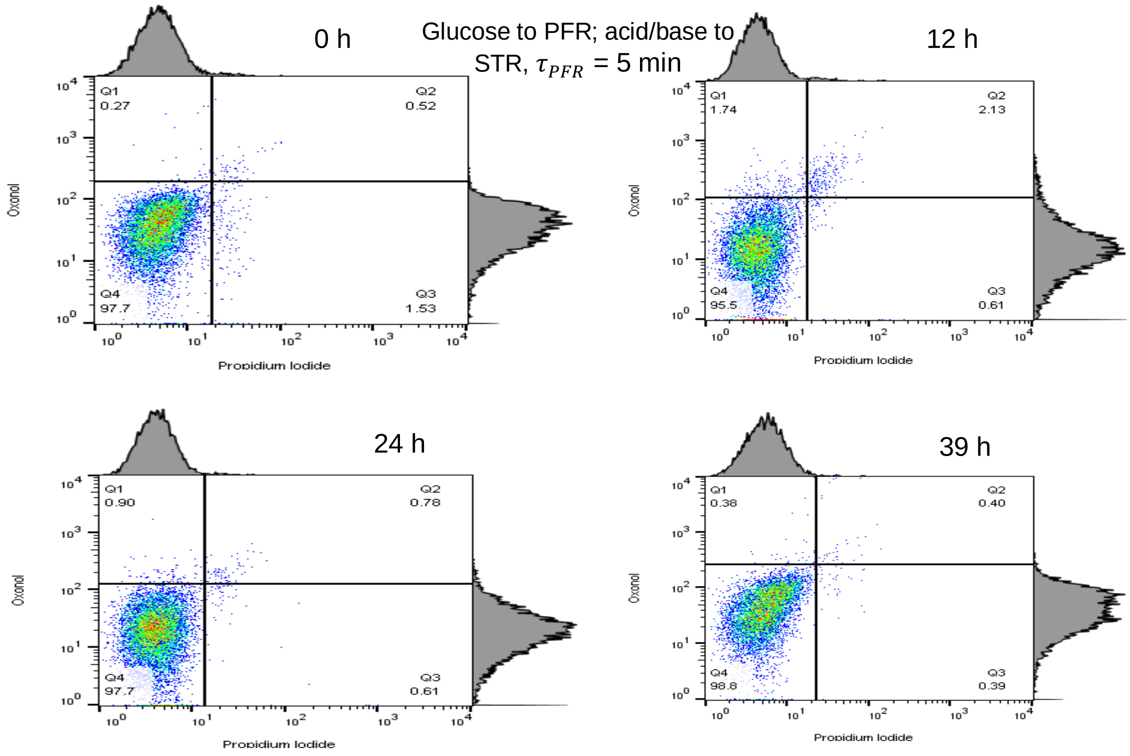

Figure 5.23 a – c Flow cytometer dot plots for SDR 4, 5 & 6 indicating the condition of the cell membrane at different time points during fermentation using the above fluorochromes. Each dot on the plot represents a cell of the 10000 cells interrogated.

(SDR 7) a

Glucose to STR; acid/base to PFR, τ_{PFR} = 1 min

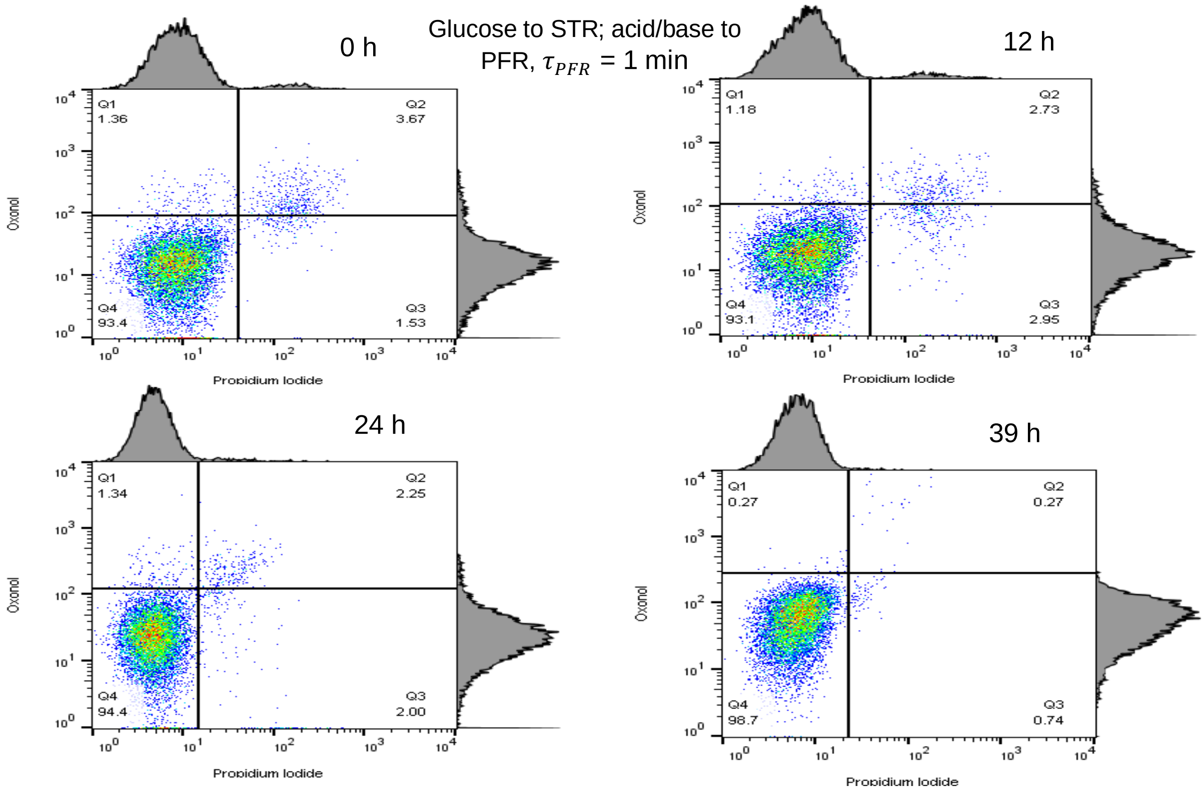

(SDR 8) b

Glucose to STR; acid/base to PFR, τ_{PFR} = 2 min

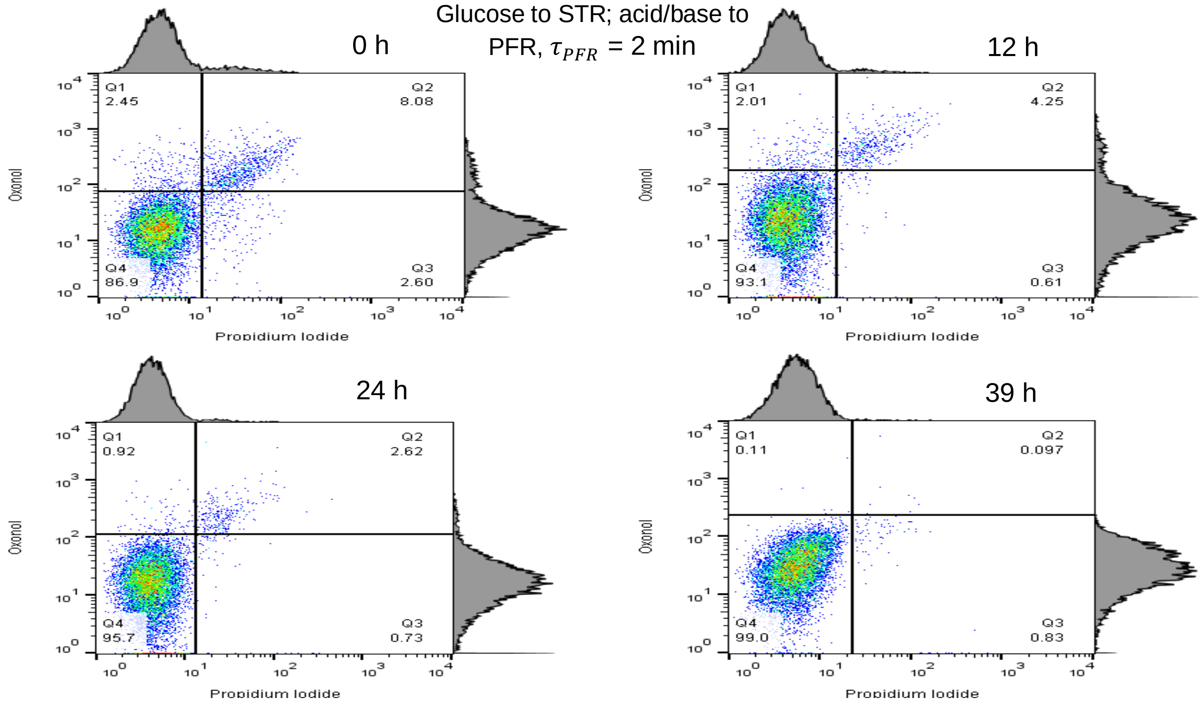

(SDR 9) c

Glucose to STR; acid/base to PFR, τ_{PFR} = 5 min

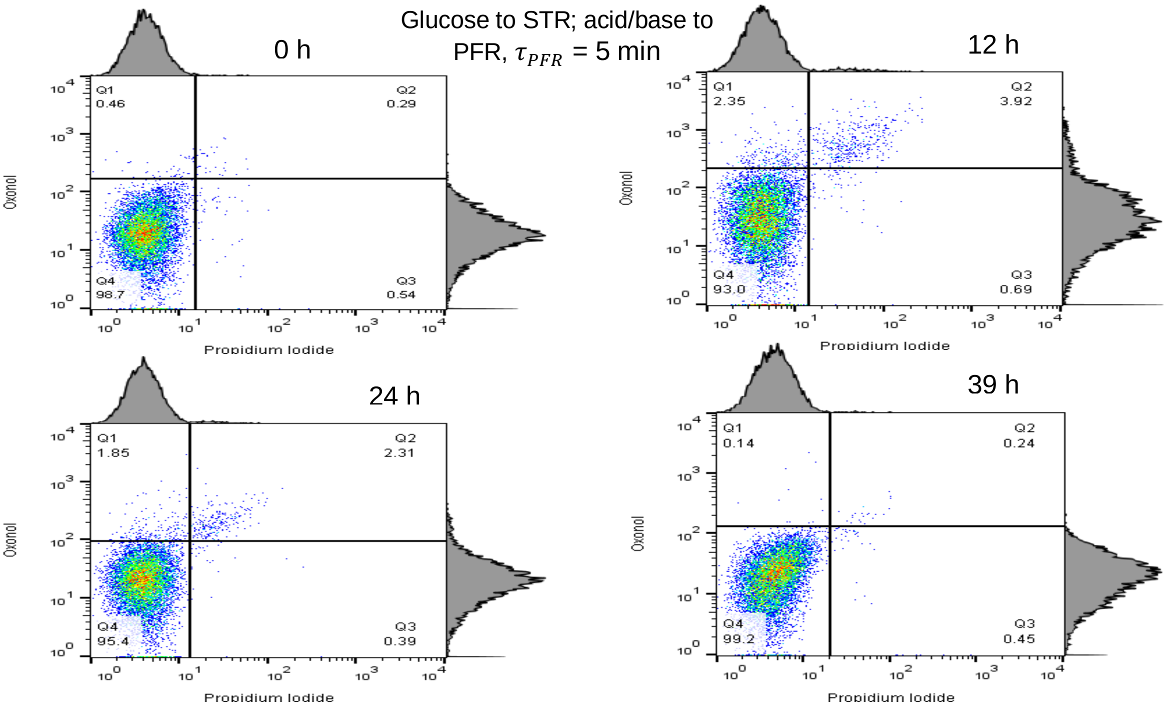

Figure 5.24 a – c Flow cytometer dot plots for SDR 7, 8 & 9 indicating the condition of the cell membrane at different time points during fermentation using the above fluorochromes. Each dot on the plot represents a cell of the 10000 cells interrogated.

(SDR 10) a

Glucose and acid/base to PFR

τ_{PFR} = 1 min

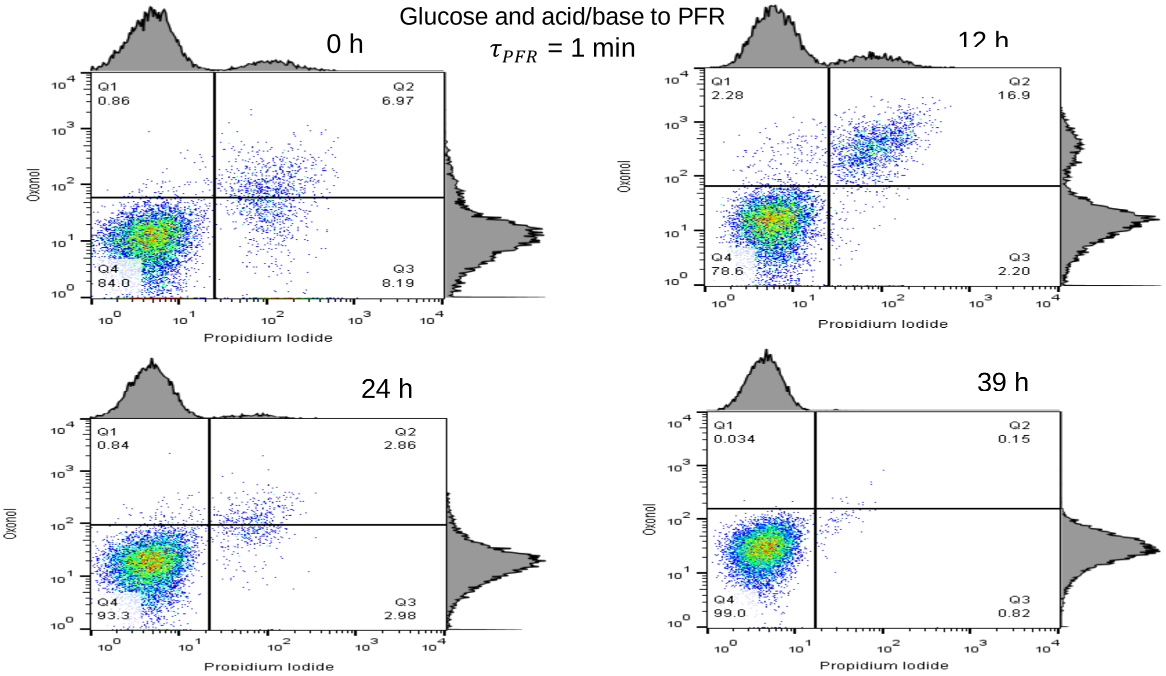

(SDR 11) b

Glucose and acid/base to PFR

τ_{PFR} = 2 min

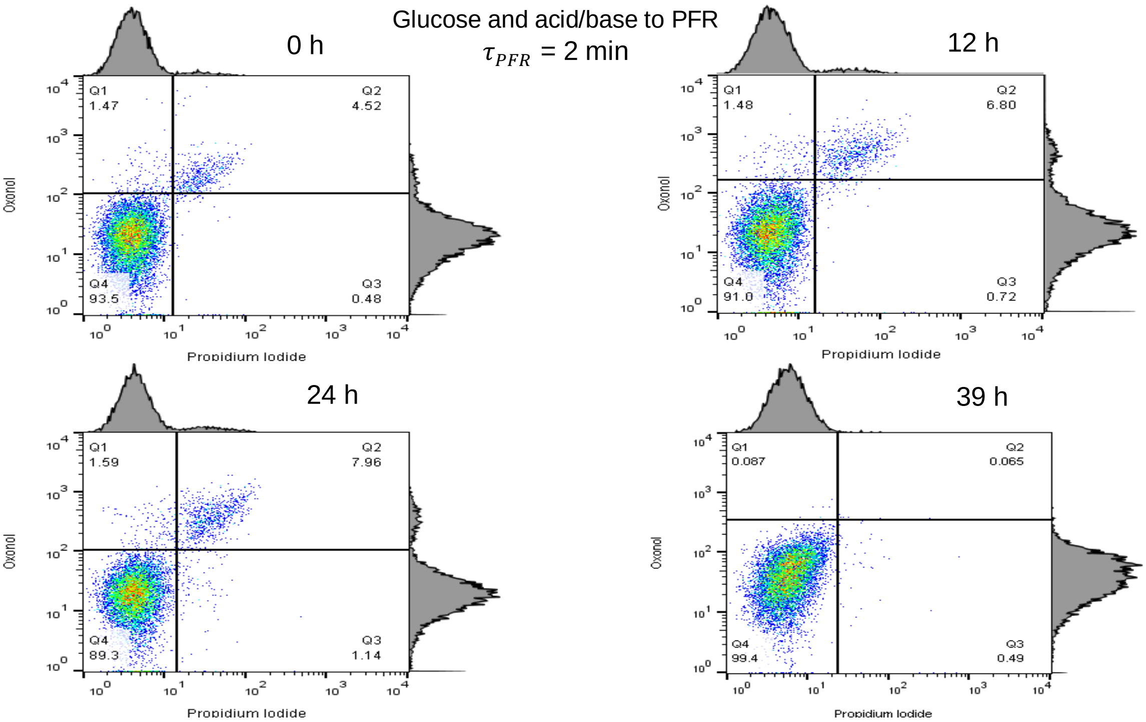

(SDR 12) c

Glucose and acid/base to PFR

τ_{PFR} = 5 min

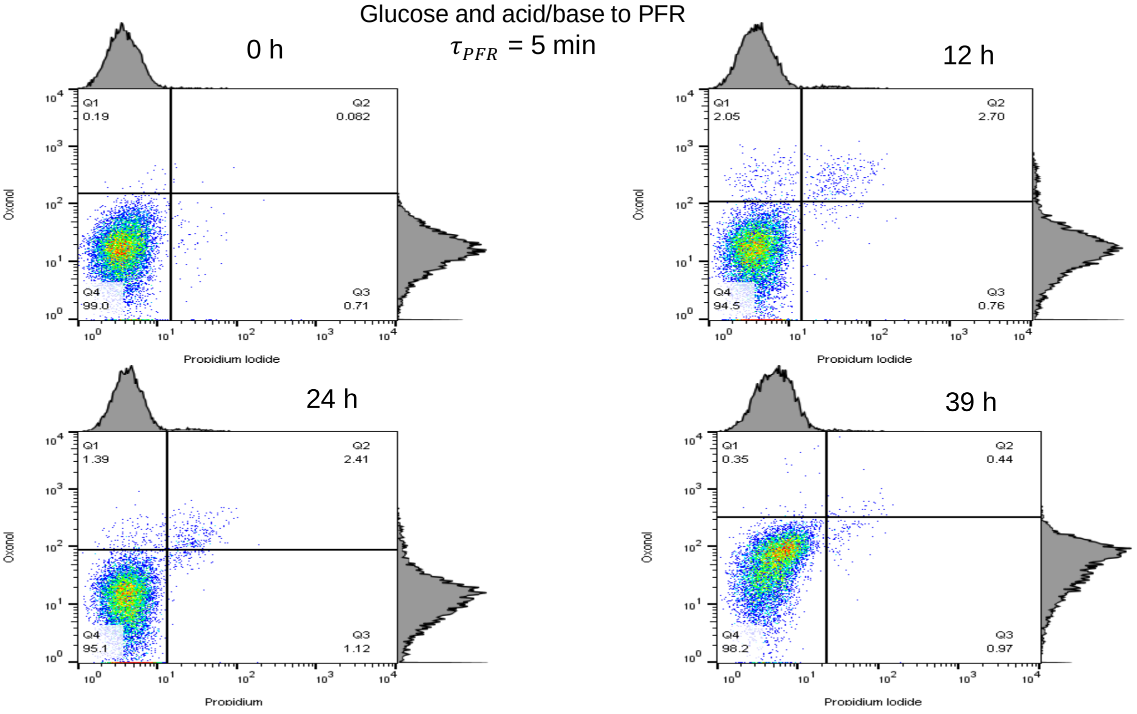

Figure 5.25 a – c Flow cytometer dot plots for SDR 10, 11 & 12 indicating the condition of the cell membrane at different time points during fermentation using the above fluorochromes. Each dot on the plot represents a cell of the 10000 cells interrogated.

The graphs in Figures 5.22 a & b, Figures 5.24 a & b and Figure 5.25 b (SDR 1, 4, 7, 8 & 11) all highlighted the carryover of depolarised (Q1) and permeabilised cells (Q2) as well as healthy cells (Q4) from the seed culture of the shake flask. The common trend of this subset is illustrated in Figure 5.22 a. The result shows that on start-up, 3 % and 9 % of the cells had depolarised and permeabilised membranes respectively. 12 hours later the number of cells with depolarised and permeabilised membranes was down at 1 % and 3 % respectively. Finally, at the time of termination (39 h), almost all the cells (≈ 99 %) were indicated to be healthy.

Although the graphs on Figures 5.22 c & d, Figures 5.23 b & c, Figure 5.24 c, Figures 5.25 a & c (SDR 2, 3, 5, 6, 9, 10 & 12) started out differently from those above, the general trend was similar. Here the results showed no significant amount of depolarised and dead cell population on start-up. This indicated that there were no carry-over of these cell subpopulations from the seed shake flask culture, which would have been reflected on the 0 h plots. For illustration purposes, Figure 5.22 c is used to explain this trend; the healthy cell population was at 97 % on start-up while the depolarised and permeabilised cell population was estimated at 0.68 % and 1.4 % respectively. After 13 hours, the healthy cell population decreased to 94.4 % with the depolarised and permeabilised cells increasing to 1.41 % and 3.72 % respectively. On completion, the healthy cell population had increased to 99.7 %. The slight decline in the healthy cell numbers coincided with the transition phase of growth, 13 – 22 h. This indicated that the severe glucose limitation during this phase was the major contributing factor, but as feeding increased exponentially with time, the cells adapted, and healthy cell numbers rebounded.

In summary, the cell viability trend remained the same regardless of the SDR simulated. The variability in the viability of the start-up cell population was more a manifestation of the quality of seed taken from its shake flask culture, especially if these cells were transferred after the exponential growth phase. The cells seem to adapt to the bioreactors conditions as the fermentation progressed and the time spent in the non-ideal PFR environment was not sufficient to result in a significant loss of membrane integrity.

5.8 Cell viability determination by plating

The ability of a cell to form a colony on an agar plate indicates that it is healthy and cultivable on a solid agar medium. Although this method is known to underestimate the viable cell count, due to issues of agar selectivity and the cell's physiology, it still gives some useful information on the condition/growth of the cells. Figures 5.26 a – d show the trends in the viable cell count, grown on TSA using the plating technique (see the Material & Methods section for conditions of cultivation).

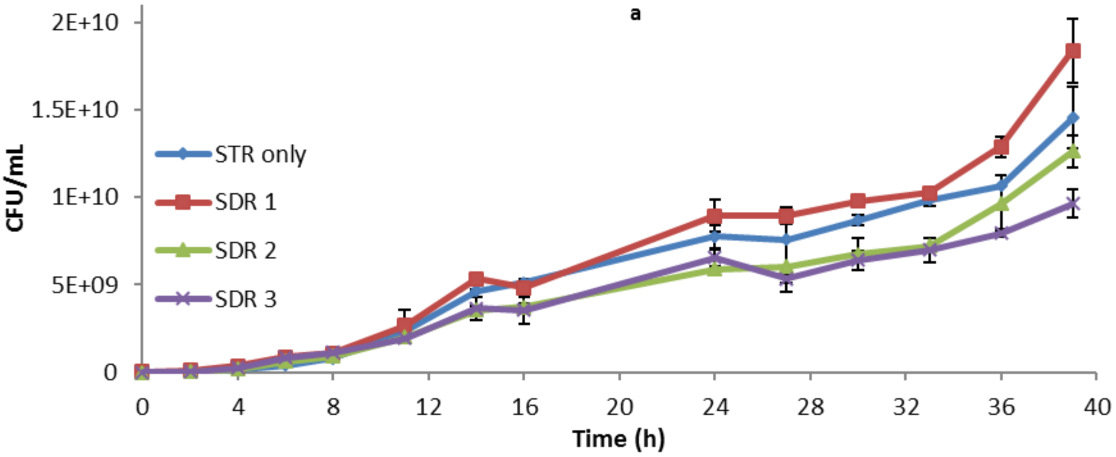

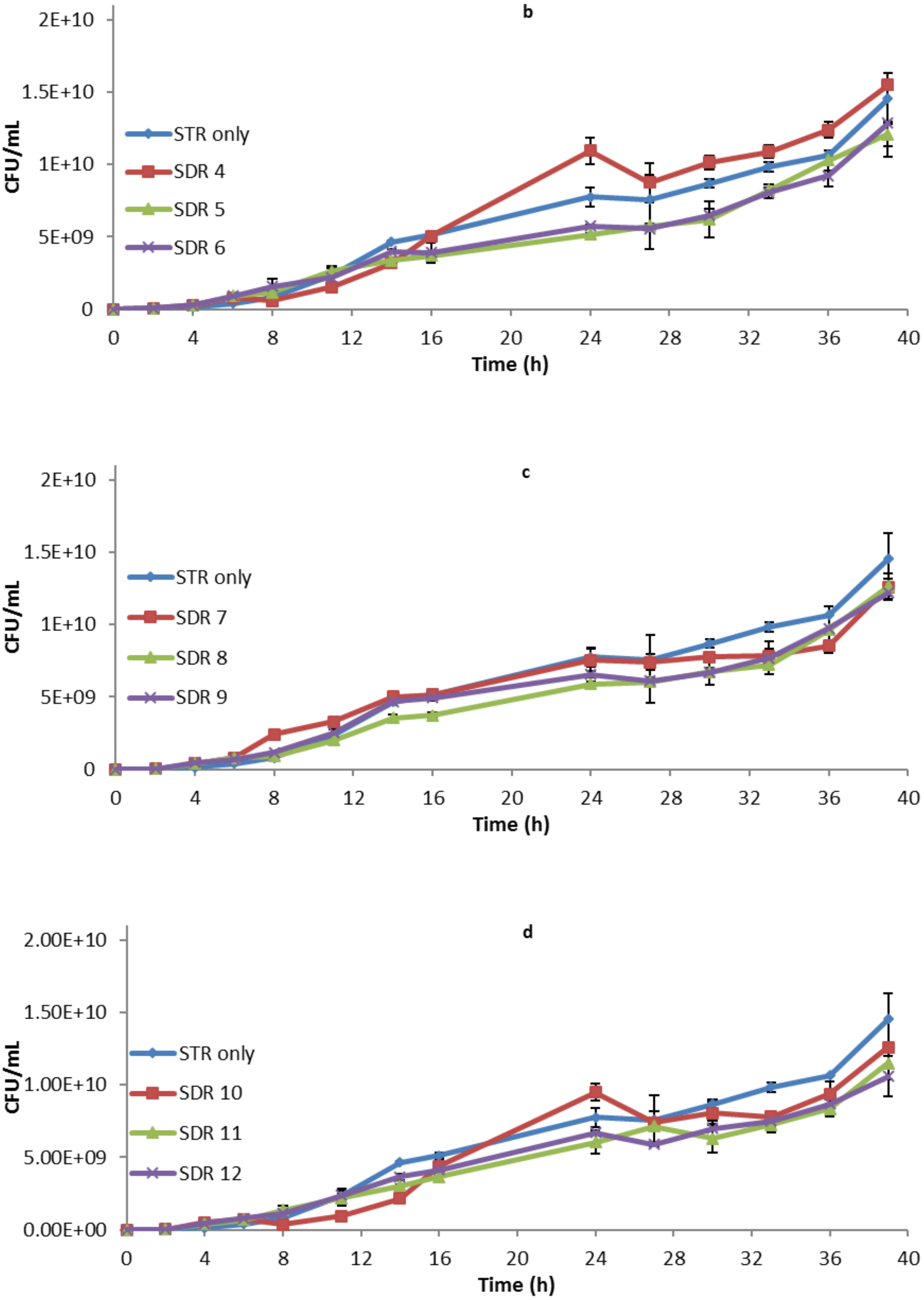

Figure 5.26 a – d Viable counts on a TSA medium for SDR 1 – 12, data points represent the mean values of biological replicates, and the error bars equivalent to their standard deviations.

The rate of viable colony increase can be broadly divided into two. From the start of the process, the CFU/ml was $\approx$ 3.5*10^6 cells$\cdot$mL^{-1}, but by the start of the transition phase (14 h), the average viable cell count was at about 4.7*10^9 cells$\cdot$mL^{-1}. This indicated just over a 1300-fold increase from the start cell concentration. However, for the next 25 hours (14 h – 39 h), the viable cell count only increased by 3-fold, $\approx$ 1.5*10^{10} cells$\cdot$mL^{-1} at 39 h. This shows that the main viable cell count increase occurred between 0 – 14 h, indicating that in the course of fermentation the ability of the cells to form colonies on an agar plate decreased. (Enfors *et al.,* 2001) had suggested that there might be a cell mechanism behind this decline in the CFU ability, especially as μ tends to 0.05 h^{-1}. However, it is more likely that this seemingly decline in the cell's colony count might be due to misinterpretation from increasing cell clustering as the DCW increased. Since cell clusters are known to predominate in nutrient limited fermentations (Käß *et al.,* 2014), it is likely that more clusters are being counted as one colony as the fermentation progresses. In high cell density fermentations in a nutrient limited environment, the frequency of cell clustering increases, resulting in a grossly understated viable cell count. Also, the practice of serial dilution before plating adds to counting error from inconsistent pipetting. If there are viable but non-culturable cells as reported by Nebe-Von-Caron *et al.*, (2000), the plating method will underestimate cell viable numbers.

The process data logs for sections 5.2 to 5.8 for *C. glutamicum* DM1945x3 fed-batch fermentations can be seen in Appendix 13 to 25.

5.9 Conclusion

The SDR simulations induced a different response compared to the well-mixed STR only control fermentation. Even though no loss in the cell's biomass productivity was recorded, differences were seen in cadaverine and CO_2 productivity. These differences also varied depending on the SDR simulation implemented. The simulations which saw a τ_{PFR} increase from 2 min to 5 min did not result in any significant change. As earlier highlighted, increasing the τ_{PFR} also changed the f_m, which was hypothesised to attenuate the cells response. Hence, the experiments presented in the next chapter were setup to investigate this issue.

CHAPTER 6

6 Scale-down studies of *C. glutamicum* DM1945 Δact3 Ptuf-ldcC_OPT fed-batch fermentations in varying STR volumes.

In Chapter 5, when the plug flow residence time τ_{PFR} was increased from 2 min to 5 min (by decreasing the exchange flow rate between the STR and PFR) whilst maintaining the STR volume fixed at 3 L, no significant difference in *C. glutamicum* DM1945x3 physiological response was observed. Although this lack of physiological difference did not happen when the τ_{PFR} was increased from 1 min to 2 min. The results presented in Chapter 5 strategy did show that after 2 min, the longer time spent in the STR most likely attenuated the effect of the cells spending more time in non-ideal PFR environment. Hence, for experiments with τ_{PFR} > 2 min, the cells that had experienced oxygen or glucose limiting conditions in the upper parts of the PFR might have had more time to recover in the near optimal growth conditions of the STR, as their residence time there also increased. For example, experiment SDR 1 had a τ_{STR} of 10 min, while SDR 3 had a τ_{STR} of 50 min (Table 5.1), which shows that the cells were spending on average 5 times longer in the STR when the τ_{PFR} was raised to 5 min. As highlighted in Chapter 5 Subsection 5.1.3, the mean frequency at which the cells entered the PFR, f_m of all experiments with a τ_{PFR} of 5 min was 80 % less than that when the τ_{PFR} was 1 min.

The idea of decreasing the STR volume, for fixed values of τ_{PFR} (i.e. changing the ratio of volumes of the PFR and STR) was done to mimic situations where a bioreactor's mean mixing time and dead zone is increased due to an increasing cell metabolic activity and reduced power input. Also, in certain high cell density fermentations, mixing performance can start out suitably sufficient, but towards the latter part of a fed-batch process may become insufficient due to increases in cell population, product formation (both can increase broth viscosity) and metabolic rate. Noorman, (2011) highlighted that in large-scale vessels, high cell density cultures, filamentous and polymer-type bioprocesses can easily reach dynamic broth viscosity >50 mPa.s within the period of fermentation. Hence, as the dynamic broth viscosity exceeds 50 mPa.s, the flow becomes transitional, the volumetric mass transfer and heat transfer coefficients declines and dead zones may appear (Noorman, 2011). This means that given a constant power input of a bioreactor, its mixing time could still vary due to the changing cell metabolic rate and broth viscosity. Thus, if mixing efficiency declines during a fermentation (depicted in STR + PFR models by increasing the τ_{PFR}) the dead zones within the bioreactor may become more prominent and their proportion in relation to the bioreactor volume increases. Figure 6.1 shows a simplified representation on the effect of mixing deterioration during a top-feed high cell density fermentation of a large-scale STR and how these situations can be simulated using the two-compartment model.

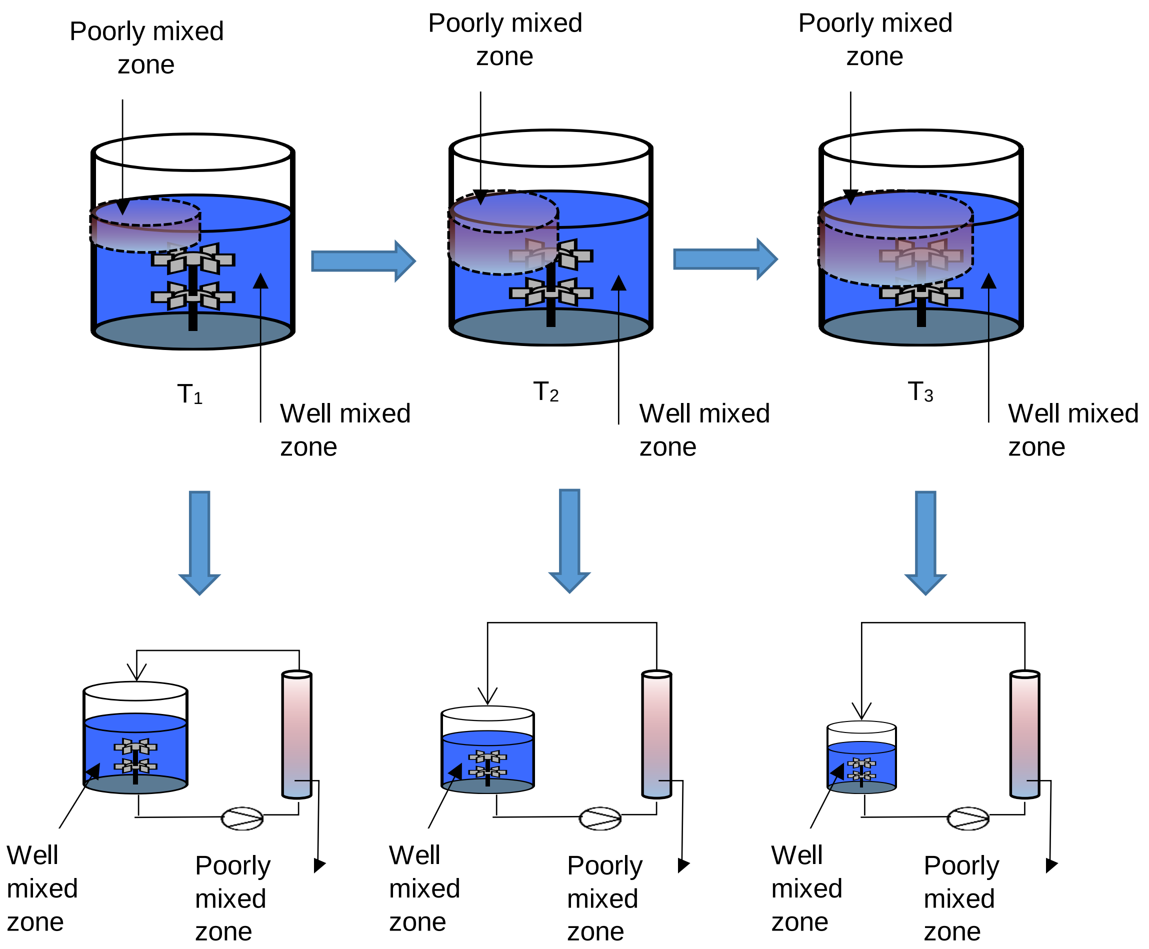

Figure 6.1 The two-compartment scale down models adapted to mimic changes in the dead zone proportions of a high cell density large-scale process due to declining mixing efficiency. T_1, T_2 and T_3 represent increasing timeframes during the fermentation process.

Figure 6.1 indicates that the proportion of the poorly mixed zone to the well-mixed zone increases as the mixing time decreases (note that time $T_1 < T_2 < T_3$). The strategy to mimic the effect of increasing the mixing time using the two-compartment model is also illustrated in Figure 6.1. The progression from T_1 to T_3 for the scale down study was mimicked by reducing the volume in the STR while the PFR volume stayed constant (Table 6.1). This changing ratio of the poorly mixed zone to the well-mixed zone is thought to be a closer reflection to increasing the magnitude of fermentation gradients when the τ_{PFR} is increased.

As in Chapter 5, the experiments presented here also compared *C. glutamicum's* physiological response to the τ_{PFR} (1 min, 2 min and 5 min), glucose and pH gradients. However, the volume in the STR was reduced as the τ_{PFR} was increased to keep the f_m constant at 0.0018 s^{-1} regardless of the simulation investigated (Table 6.1). Hence, for the τ_{PFR} of 1 min, 2 min and 5 min, the STR volume was kept at 3 L, 1.5 L and 0.6 L respectively. This was done to reflect an increase in mixing time in a fermenter and the constant f_{max} ensured that proper comparison could be made across the three values of τ_{PFR}.

6.1 Fermentation conditions across the two-compartment model

In the simulations investigated, the cultivation conditions in the SDR were different as shown in Table 6.1. The following results below were grouped based on the similarity of where the pH controlling agent and glucose feed were introduced to the SDR (Table 6.1). Hence, the simulations SDR 1, 13 & 14, SDR 4, 15, & 16, SDR 7, 17 & 18 and SDR 10, 19 & 20 are segregated and discussed below. Table 6.1 also introduces the experimental overview of this Chapter and highlights the decreasing STR volume as the τ_{PFR} increases.

Simulation	Glucose inlet	pH inlet	Air inlet	STR volume (L)	PFR volume (L)	τ_{PFR} (min)	τ_{STR} (min)	f_m (s)
SDR 1	STR	STR	STR	3	0.3	1	10	0.0018
SDR 13	STR	STR	STR	1.5	0.3	2	10	0.0018
SDR 14	STR	STR	STR	0.6	0.3	5	10	0.0018
SDR 4	PFR	STR	STR	3	0.3	1	10	0.0018
SDR 15	PFR	STR	STR	1.5	0.3	2	10	0.0018
SDR 16	PFR	STR	STR	0.6	0.3	5	10	0.0018
SDR 7	STR	PFR	STR	3	0.3	1	10	0.0018
SDR 17	STR	PFR	STR	1.5	0.3	2	10	0.0018
SDR 18	STR	PFR	STR	0.6	0.3	5	10	0.0018
SDR 10	PFR	PFR	STR	3	0.3	1	10	0.0018
SDR 19	PFR	PFR	STR	1.5	0.3	2	10	0.0018
SDR 20	PFR	PFR	STR	0.6	0.3	5	10	0.0018

Table 6.1 An experimental overview of the SDRs investigated

6.1.1 Effect of the PFR dissolved oxygen limitation in the PFR on fermentation conditions

SDR 1, 13 and 14 had both the glucose and pH controlling agent addition points located in the STR but differed slightly because their τ_{PFR} were 1 min, 2 min and 5 min respectively; the STR volumes were also varied, as stated in Table 6.1. The pH profiles across the two-compartment model for SDR 1, 13 and 14 are illustrated in Figure 6.2.

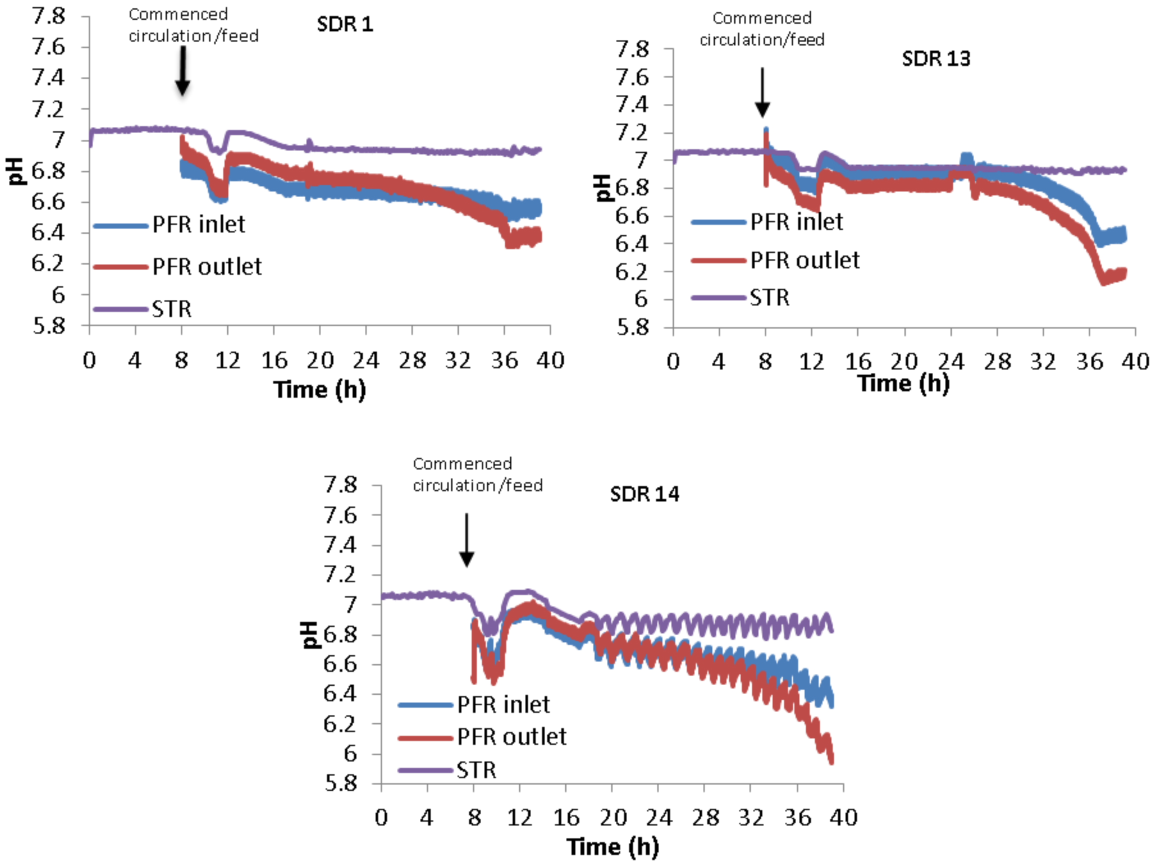

Figure 6.2 pH profiles across SDR 1, SDR 13 and SDR 14 simulations

The pH in the STR was tightly controlled (pH setpoint was 7) in SDR 1 & 13. However, for SDR 14 the pH was more challenging to control as its profile was oscillatory from 16 h onwards. This pH oscillation was as a result of the acidic broth exiting the PFR to the STR, due to the increased production of organic acids from a predominant fermentative pathway as the cells spent more time in the oxygen-limited

PFR environment (Hewitt *et al.,* 2000; Junne *et al.,* 2011; Neubauer *et al.,* 1995b; Pirt, 1975). The small amount of broth (0.6 L) in the STR for SDR 14 was not sufficient to act as a buffer for the incoming pH variations from the PFR. This was in contrast to SDR 1 and 13, which had higher STR volumes of 1.5 L and 3 L and lower rates of organic acid production hence the reduced pH oscillations recorded. Thus, for SDR 14, the acidic broth from the PFR (due to DOT limitations and the presence of mixed acid fermentation products) was able to reduce the pH in the STR. The pH controller compensated continuously for this by the addition of 4 M aqueous NH_4OH (in the STR), which resulted in the oscillations observed in SDR 14. For most of these fermentations, the pH in the PFR was lower than in the STR, indicating a higher formation rate of organic acids (for example, lactic and acetic acid) in the PFR section. The limited oxygen environment of the PFR encouraged *C. glutamicum* DM1945x3 growth via the fermentative pathway, which increased lactic acid production rates (Junne et al., 2011). As shown in Figure 6.2, the pH gradient (difference between inlet and outlet pH) in the PFR was more pronounced towards the end of the fermentation process. This was due to the high density of metabolically active cells generating ATP in the PFR oxygen-limited environment (increasing organic acid side products). The top section of the PFR recorded the lowest pH; confirming that an increasing τ_{PFR} in a low DOT environment favoured the production of organic acids (formic, lactic and acetic acids). The pH gradient in SDR 14 was the most pronounced of the graphs in Figure 6.2, which suggests its condition was probably the most non-uniform of the three SDRs and thus it should elicit the strongest response.

Figure 6.3 indicates that an increased cell metabolic rate results in an increased rate of dissolved oxygen concentration. In all cases, the DOT was set not to fall below 40 %. Hence when values were above 40 %, there was no control. The DOT trends in SDR 1, 13 & 14 were similar; the first decline in the DOT happened during the uncontrolled exponential growth (0 to 14 h) of the batch phase. After that was the pseudo-stationary growth (14 h to 21 h) of the batch to a fed-batch phase transition, which produced an increase in the DOT. Lastly, was the controlled exponential growth (21 h to end) of the fed-batch phase, which recorded another decrease in DOT, but as the STR was set not to fall below 40 %, the inlet air enrichment with pure oxygen to keep the DOT above the set point. Since the $k_L a$ was relatively constant throughout the process, enriching the air raised the composition of oxygen in the inlet air. This increased the oxygen concentration at the gas-liquid interface of the medium and consequently the oxygen transfer rate (Equation 2.3). The DOT in the PFR was not controlled; its profile depended on *C. glutamicum* DM1945x3 metabolic activity. For example, the burst in increased metabolic activity at the end of the pseudo-stationary growth phase led to the rapid DOT decline in the PFR.

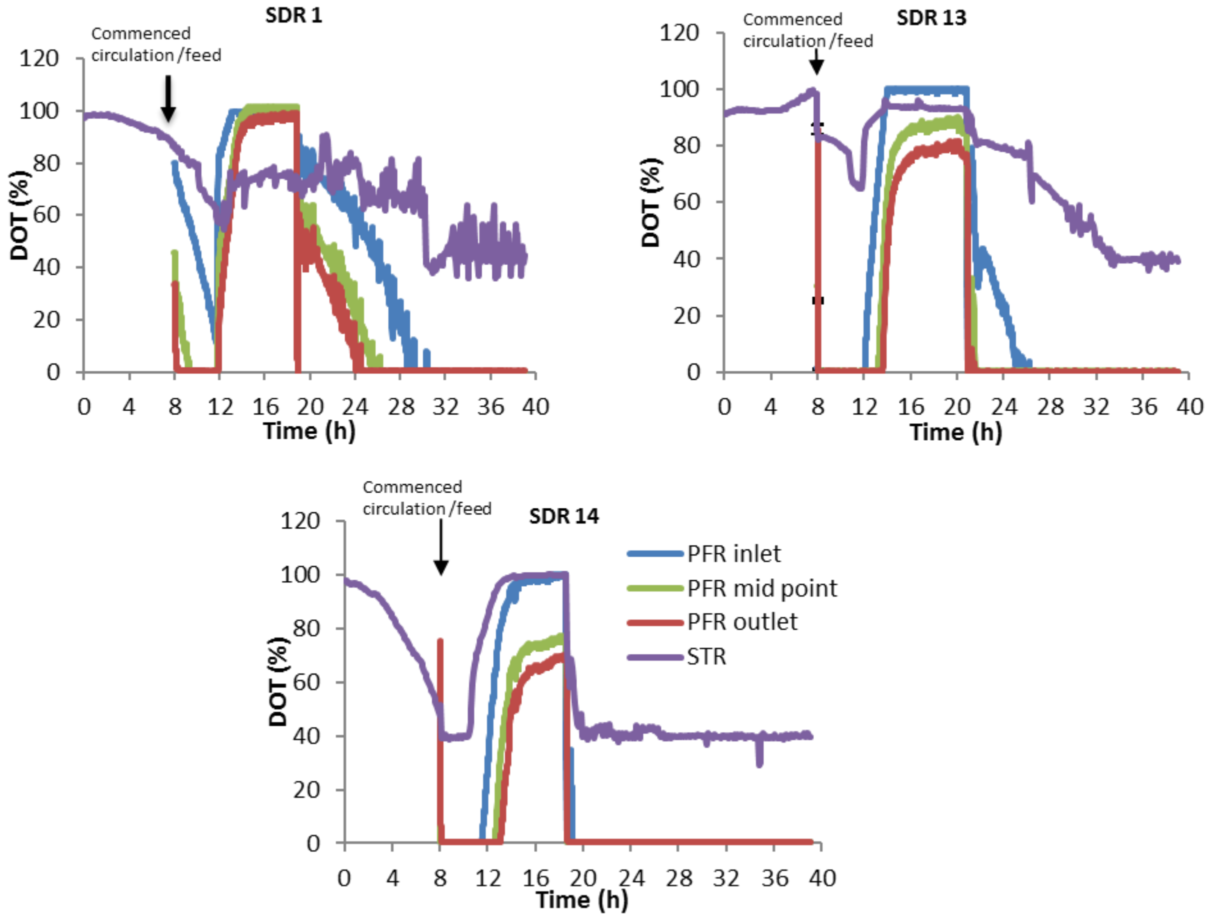

Figure 6.3 DOT profiles across SDR 1, SDR 13 and SDR 14 simulations

As a bacterial cell population increases, the rate of nutrient utilisation also increases. Thus, if an essential nutrient is limited, the cell growth rate will slow down. Here, glucose restriction was used to control *C. glutamicum* DM1945X3 growth rate during the fed-batch part of these fermentations. In all simulations, on attaining a DCW of 1 gL^{-1} after eight hours of a strict batch process, glucose was slowly introduced into the reactor. Thus, by limiting the amount of glucose available in the broth from then onwards, the cell growth rate was brought to a minimum after another six hours (from 14 h) and then controlled at 0.1 h^{-1}, corresponding to the exponential feed rate. The glucose concentration measurements for SDR 1, 13 and

14 are illustrated in Figure 6.4. These profiles were similar regardless of the sample location in the two-compartment model.

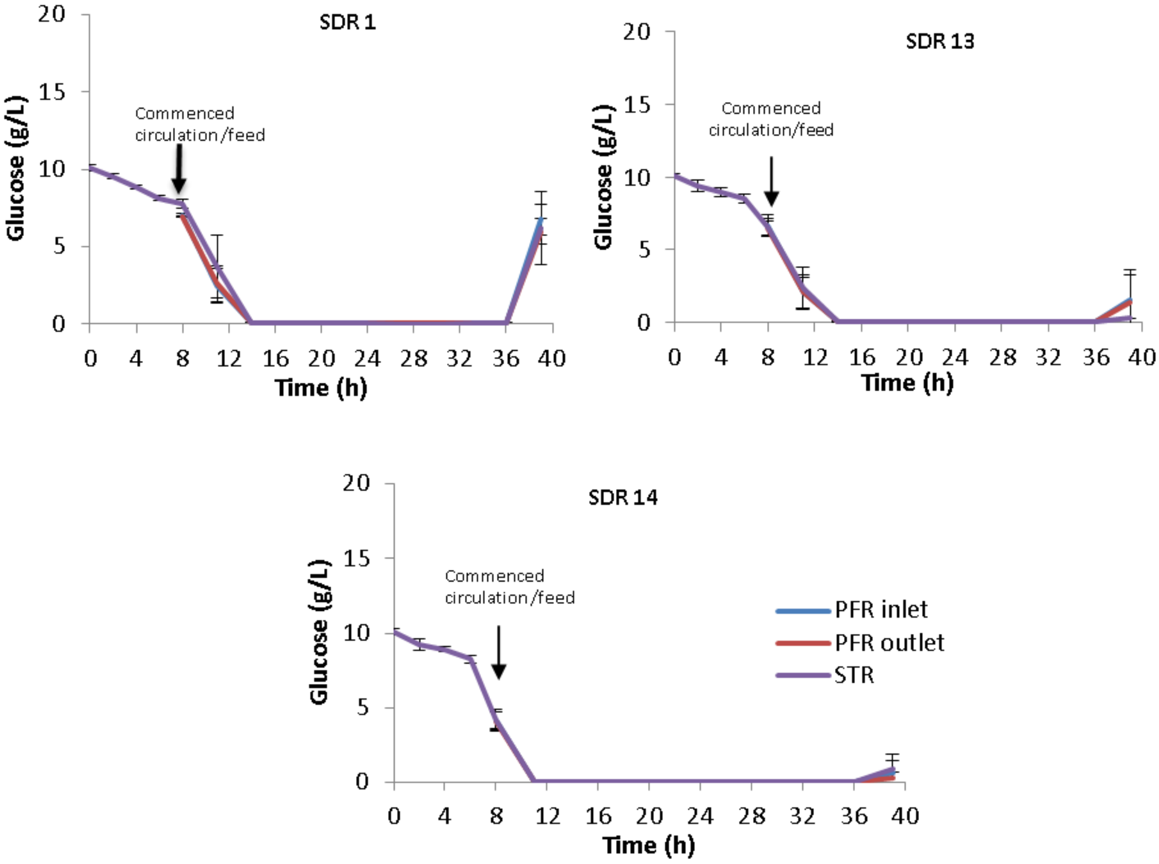

Figure 6.4 Glucose profiles across SDR 1, SDR 13 and SDR 14 simulations. The data points represent the mean values from biological duplicates, and the error bars are equivalent to their standard deviations.

The error bars between 14 h and 36 h are too small to be seen in Figure 6.4 due to the high glucose concentrations at the start and end of fermentation. Although feeding commenced at 8 h, between 8 h and 14 h the amount of glucose added (average glucose addition rate was ≈ 0.3 g·L^{-1}·h^{-1}) was not sufficient to sustain a μ_{max} which ranged from 0.7 h^{-1} to 1.0 h^{-1} (average glucose consumption rate ≈ 1.8 gh^{-1}) during this uncontrolled growth phase. This deficit eventually led to the situation where glucose became limiting after 14 h. From then onwards the feeding profile was such that it forced the bacterial cells to grow at a μ of 0.1 h^{-1} to adapt to this glucose limited environment (see Chapter 3, Subsection 3.6). The latter increase in glucose concentration from 36 h may be due to the feed pumping error at high speed, especially in SDR 1 simulation. The feed pump speed increased as the cell density increased to maintain a μ of 0.1 h^{-1} (Figure 6.5). Thus, if the feed pump was unstable at high RPMs, it could deviate from the calculated flowrate, thereby adding slightly more glucose than required, hence the accumulation observed in SDR 1.

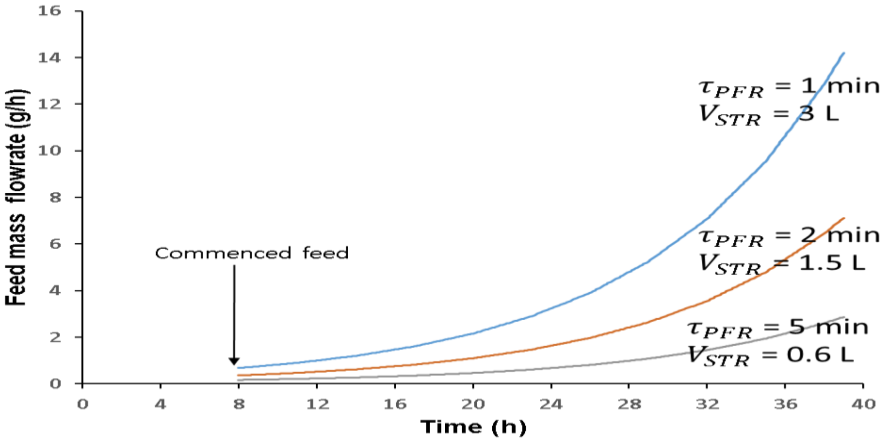

Figure 6.5 Feeding flow profiles for the τ_{PFR} of 1 min, 2 min and 5 min

Figure 6.5 indicates that as the STR volume was decreased to keep f_m equal, the feed pump flowrate was reduced. For example, the feed mass flowrate at the end of SDR 1 was five-fold higher than that of SDR 14. Hence, a smaller pump was used in SDR 14 to accommodate a lower feed flowrate range, which may have changed the flow characteristics.

6.1.2 Effect of glucose addition in the limited oxygen PFR on fermentation conditions

In SDR 4, 15 & 16 the glucose was added to the lower part of the PFR, while the pH controlling agent and air were introduced in the STR. The SDR 4, 15 & 16 differed in their τ_{PFR} and STR volumes (Table 6.1). Figure 6.6 shows the pH profile across both reactors in these simulations. The pH trends in Figure 6.6 were similar to Figure 6.2. However, the pH gradient across the PFR was more pronounced as the τ_{PFR} increased. This was because the localised glucose rich and low DO PFR environment encouraged more diversion of the carbon flux from the TCA cycle to the fermentative pathway.

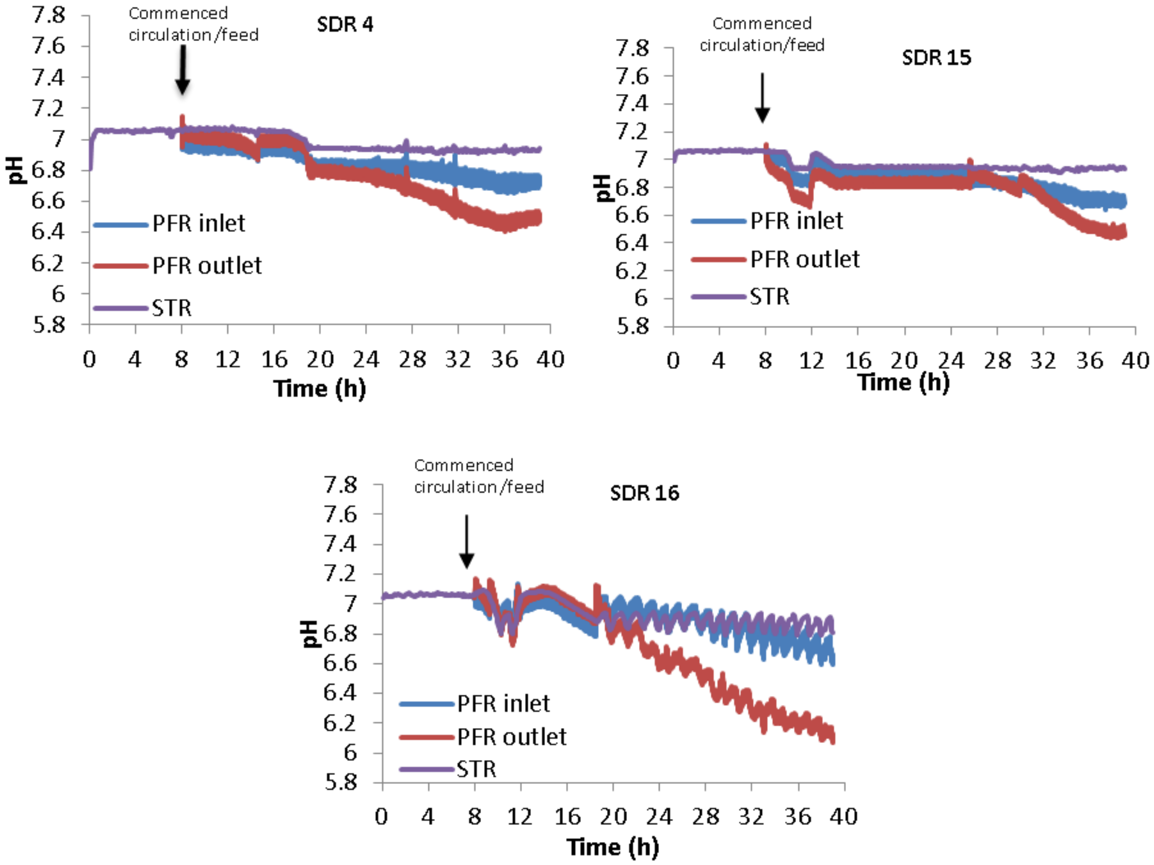

Figure 6.6 pH profiles across SDR 4, SDR 15 and SDR 16 simulations

The physiological response of *C. glutamicum*, which led to an increase in the production of organic acids (for example, lactic acid) made the broth more acidic as the cells spent more time in the PFR (Käß *et al.,* 2014). The largest pH difference between the top and bottom of the PFR was recorded in SDR 16, suggesting that its condition induced the strongest cell response of the three simulations, i.e. the cells producing more organic acids, because of the extended time in a DO limited environment. The pH oscillations became prominent as the τ_{PFR} increased, especially towards the end of fermentation (when the process reached high cell densities). This reason for this oscillation is as highlighted in Subsection 6.1.2, Figure 6.2 above.

The DOT profile in Figure 6.7 highlights the three main phases of growth, the batch, transition to fed-batch and fed-batch phase, as described earlier in Subsection 6.1.1.

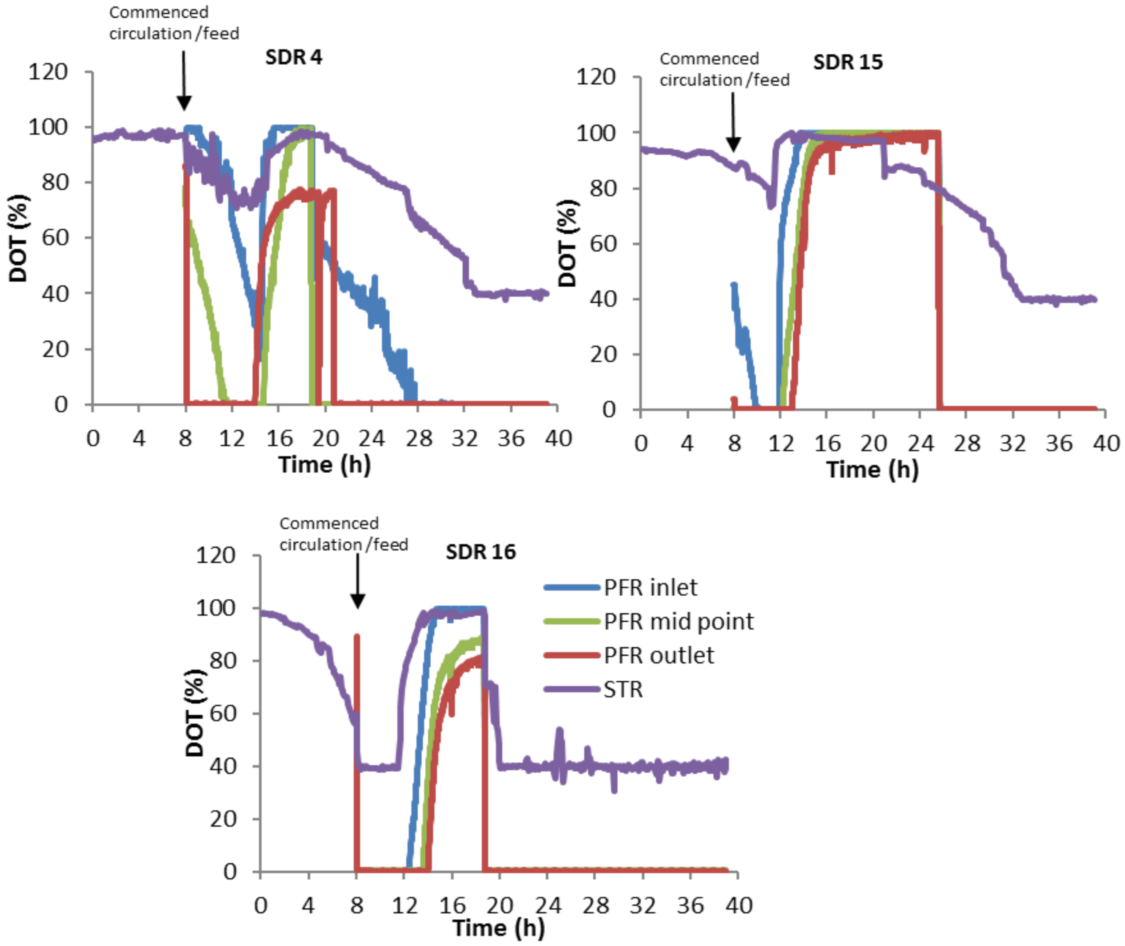

Figure 6.7 DOT profiles across SDR 4, SDR 15 and SDR 16 simulations

For the most part in the PFR, the DOT was limiting in all simulations. The SDR 16 showed the most prolonged period (27 h) of low DOT in the PFR, while SDR 4 recorded the least (17 h). This signified a 59 % increase in time the cells spent in an oxygen limited environment. Hence, confirming that SDR 16 should elicit the strongest cell response compared to STR only, SDR 4 & 15. The DOT profile in SDR 15 was different, although its τ_{PFR} was longer than SDR 4, it showed the longest duration at which the PFR was oxygenated. This is most likely due to the lower STR medium volume (SDR 15 - 1.5 L working volume in a 5 L STR; SDR 4 – 3 L working volume in a 5 L STR) of SDR 15, which held a higher concentration of dissolved oxygen due to the constant sparging rate of 1.5 vvm. Thus, allowing the

PFR to be oxygenated for longer, this made for the biomass concentration of higher metabolic activity from about 24 h before the PFR became oxygen limited in SDR 15.

The glucose profiles varied for SDR 4, 15 and 16 (Figure 6.8). The glucose accumulation in the PFR started after 24 h for SDR 4, but only a slight difference between the top and bottom of the PFR was recorded. The STR typically showed the lowest glucose concentration after 24 h.

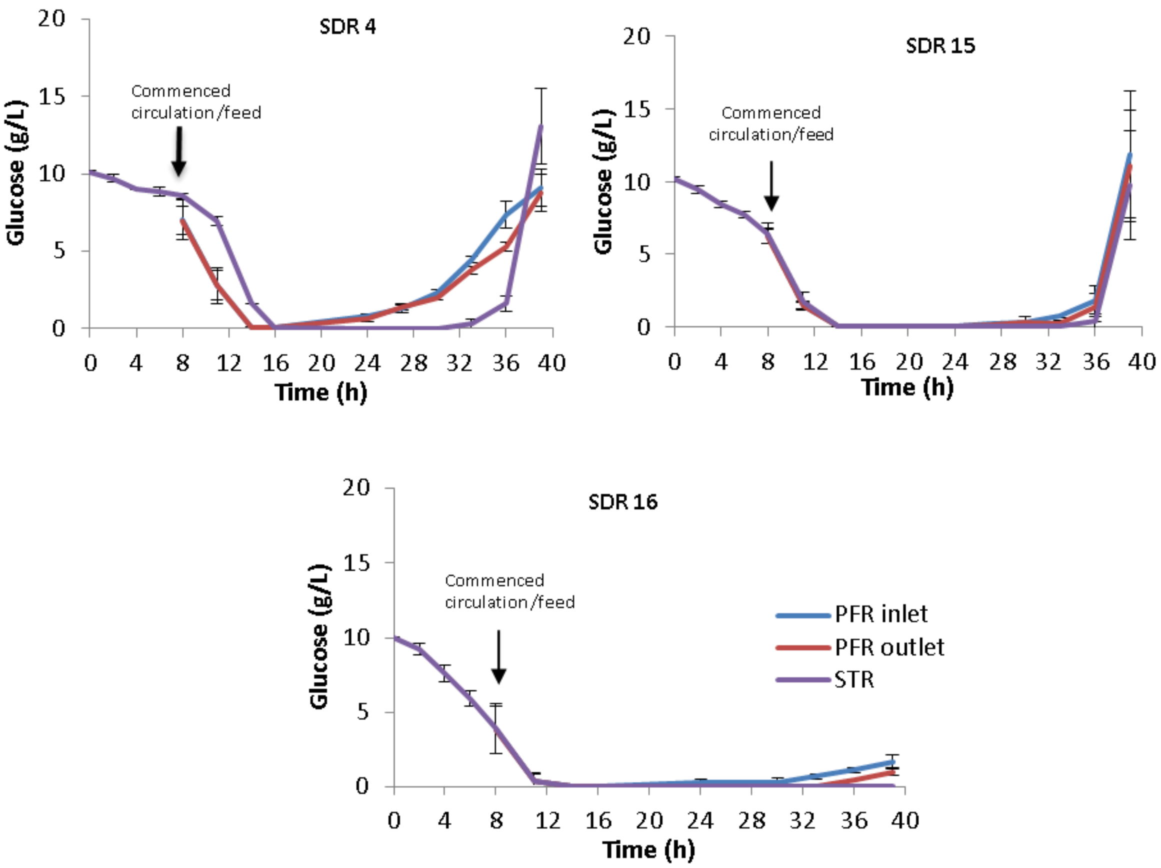

Figure 6.8 Glucose profiles across SDR 4, SDR 15 and SDR 16 simulations

SDR 4 had a shorter τ_{PFR} than SDR 15 and 16, due to the bacterial cells lower residence time from the bottom to the top of the PFR. Hence, the cells did not have sufficient time to completely utilise the incoming glucose before leaving the PFR section, which led to the build-up observed. This accumulation became noticeable from 24 h because at this point the feeding rate was relatively high and this increased rapidly throughout the process (feed mass flowrate at 8 h = 0.7 gh^{-1}, 24 h = 3.2 gh^{-1} and 39 h = 14 gh^{-1}). However, in the STR, glucose accumulation started at 32 h in all simulations, and the reasons for this have already been highlighted in the discussion of Subsection 6.1.1, Figure 6.4.

6.1.3 Effect of the pH controlling agent addition in the limited oxygen PFR on fermentation conditions

In SDR 7, 17 & 18 only the pH controlling agent was added to the PFR, while the controlling sensor was in the STR. The air and glucose were introduced in the STR section (Table 6.1). The pH profiles across these SDRs are illustrated in Figure 6.9. Across the PFR, for SDR 7 and 17 the majority (8 h to 32 h) of the fermentation was slightly alkaline. This was because during this period the number of cells producing organic acids was not sufficient to completely neutralise the NH_4OH that was added at the PFR as a response to the cell metabolic activity in the STR and pH value of the effluent broth from the PFR. However, after 32 h as the cell mass increased, the amount of organic acid produced in the PFR was in excess of the base added automatically as a function of the pH value in the STR. This resulted in the pH decrease seen towards the end of these fermentations.

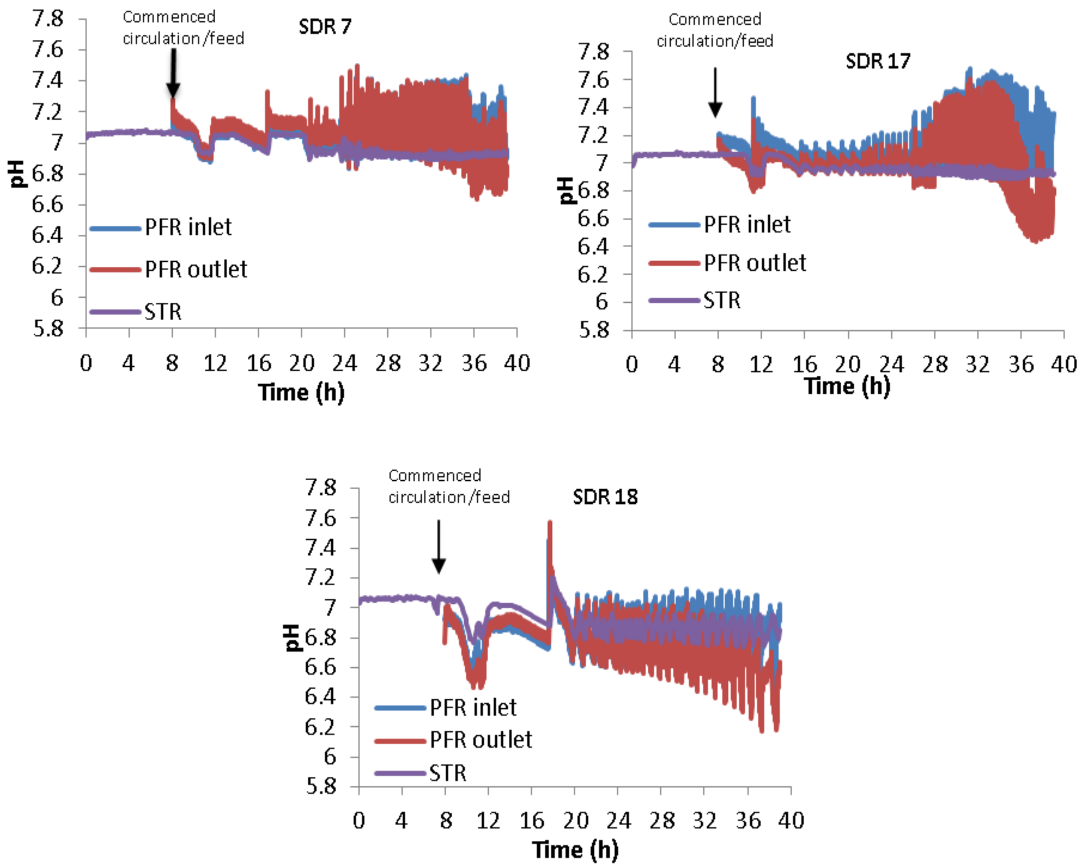

Figure 6.9 pH profiles across SDR 7, SDR 17 and SDR 18 simulations

Also, it should be noted that regardless of the pH values in the PFR for SDR 7and 17, the pH in the STR was relatively constant: the larger STR broth volumes of SDR 7 and 17 indirectly acted as a pH buffer; therefore, their STR pH values were much less affected by the fluctuating pH values of the PFR (Figure 6.9). The SDR 18 pH profile was different: after 20 h (as the cells metabolic activity increased) it recorded longer periods of pH oscillations due to its longer τ_{PFR} (more organic acid was produced in the limited DOT environment of the PFR). Hence, the pH at its PFR outlet became slightly acidic much earlier (from 20 h) when compared to SDR 7 and 17. Thus, the bacterial cells spent a longer time in the unaerated PFR, which led to a switching to its fermentative pathway and resulting in an increased production of organic acids (evaluated here by the pH profile). For all simulations, the period of the pH oscillations is related to the metabolic state of the growing *C. glutamicum* cells and the tuning of the controller. The controller increases the flowrate of the base addition, hence the oscillations observed in the poorly-mixed PFR section. This was made worse by the increased dead time between the base addition and the pH sensor done to accommodate an increased τ_{PFR}.

The DOT profiles for SDR 7, 17 and 18 (Figure 6.10) show no significant difference from SDR 4, 15 and 16 (Figure 6.7). The three main phases in these fermentations were also highlighted in Figure 6.10.

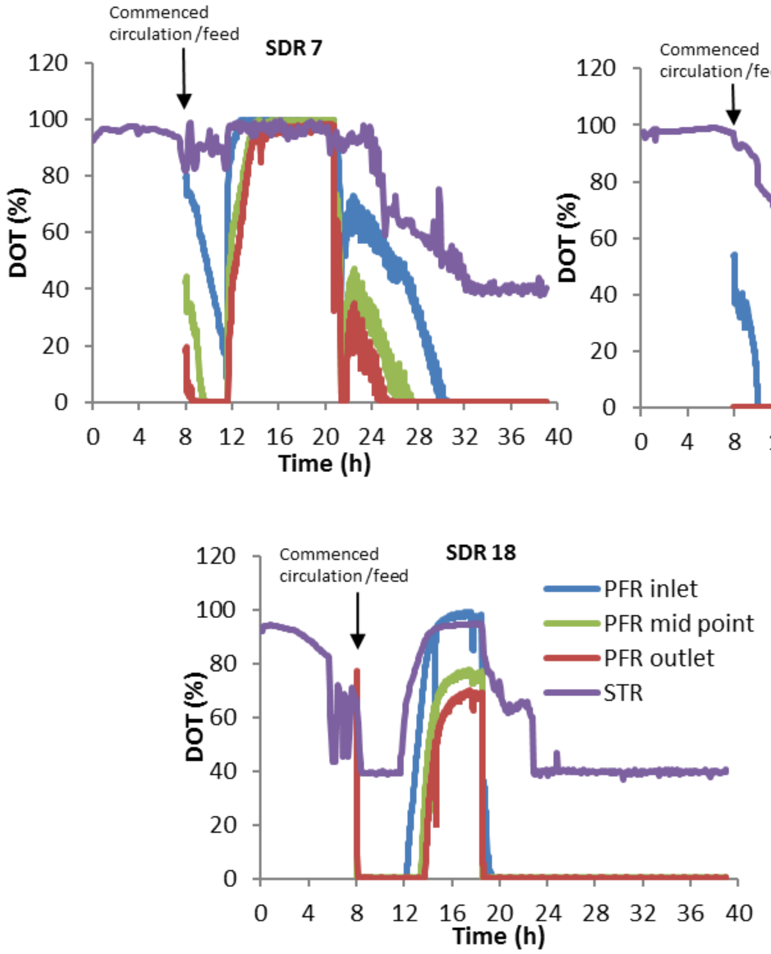

Figure 6.10 DOT profiles across SDR 7, SDR 17 and SDR 18 simulations

The exponential growth period of the batch phase which saw the first DOT decrease in the STR differed from run to run due to well-known variability which occurs in biological processes.

In the SDR 7, 17 and 18 simulations both the pH controlling agent and glucose were added to the PFR section of the SDR. The glucose concentration trends of Figure 6.11 show that these fermentations were predominantly glucose limited after the completion of the batch phase, up till 36 h.

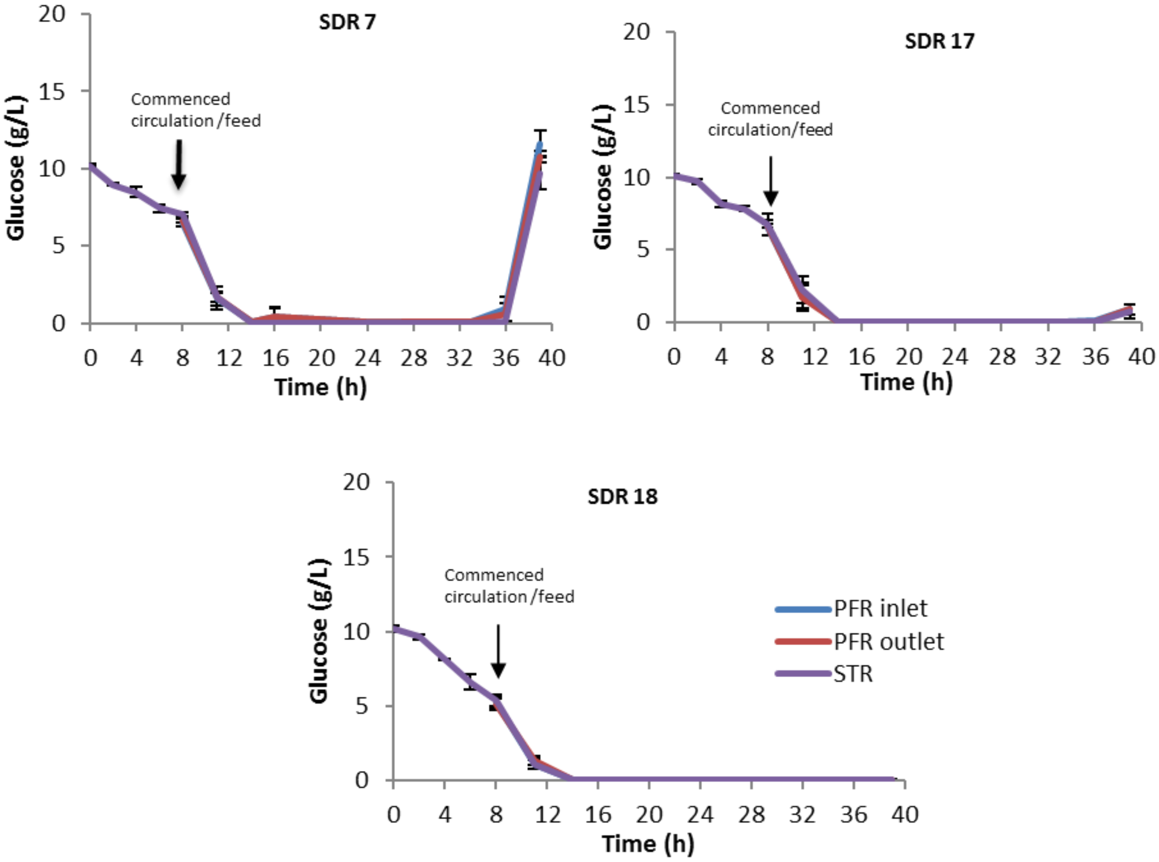

Figure 6.11 glucose profiles across SDR 7, SDR 17 and SDR 18 simulations

The rapid accumulation of glucose after 36 h was significant in SDR 7 when compared to SDR 17 and 18. This suggests that the feed pumping error at higher RPMs was the primary factor rather than a reduced glucose utilisation rate.

6.1.4 Effect of glucose and pH controlling agent addition in the limited oxygen PFR on fermentation conditions

In SDR 10, 19 and 20, the glucose and pH controlling agent was added to the PFR, while the controlling pH sensor was in the STR. The pH profiles for SDR 10, 19 and 20 (Figure 6.12) simulations were similar to SDR 7, 17 & 18 (Figure 6.9). The pH oscillations recorded in the graphs of Figure 6.12 show the same trend as in Figure 6.9. The reasons for these pH oscillations have already been discussed above.

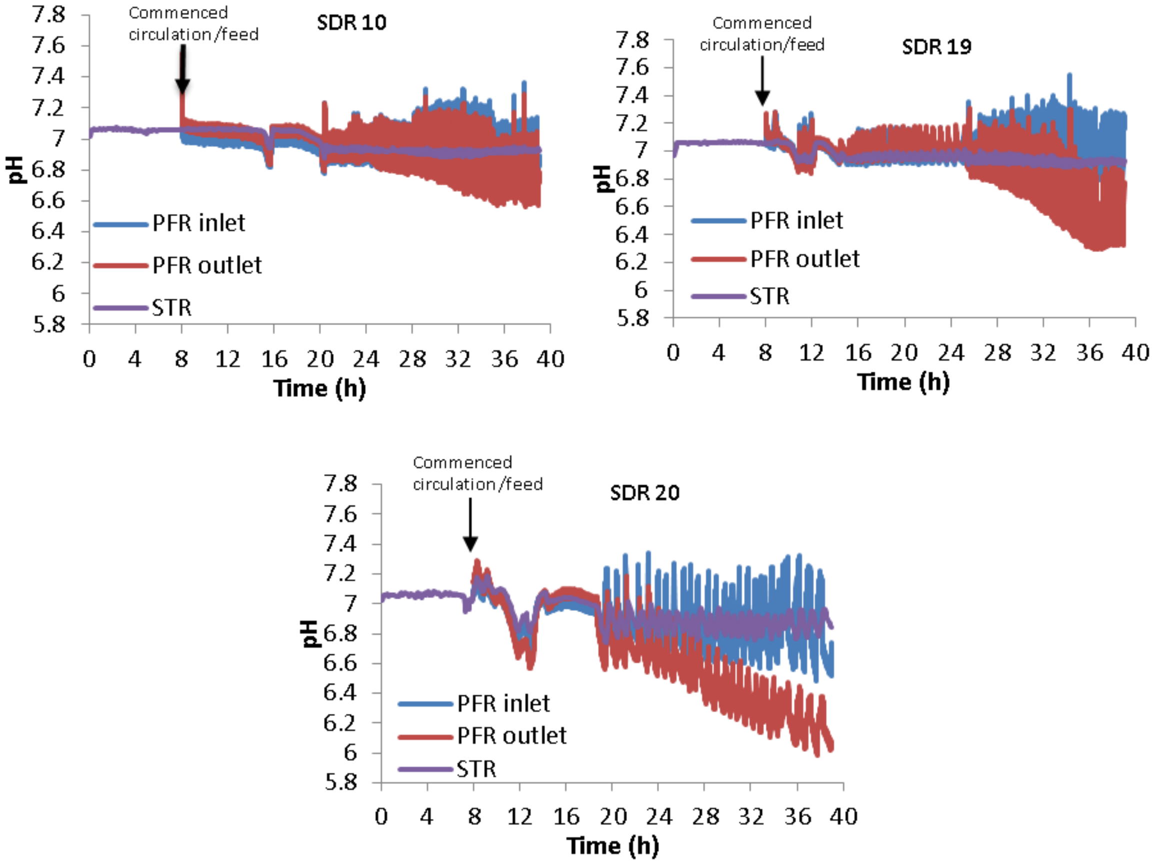

Figure 6.12 pH profiles across SDR 7, SDR 17 and SDR 18 simulations

However, metabolic activities via the fermentative pathway in the PFR was slightly higher (due to more organic acid produced, inferred from a lower pH value) in Figure 6.12 than those of Figure 6.9. For example, SDR 18 and 20 both show similar pH oscillations, but that of SDR 20 had a larger magnitude, and the pH value between the inlet and outlet was also greater. In SDR 20, the pH difference between the top and bottom of the PFR was more pronounced after 28 h. The addition of feed at the PFR inlet resulted in a high localised glucose concentration in the limited oxygen environment. Thus, encouraging the bacterial cells to generate ATP via the fermentative pathway and the consequence was increased organic acid production as shown in Figure 6.12.

The DOT profiles for SDR 10, 19 and 20 (Figure 6.13) were similar to the other simulations discussed thus far.

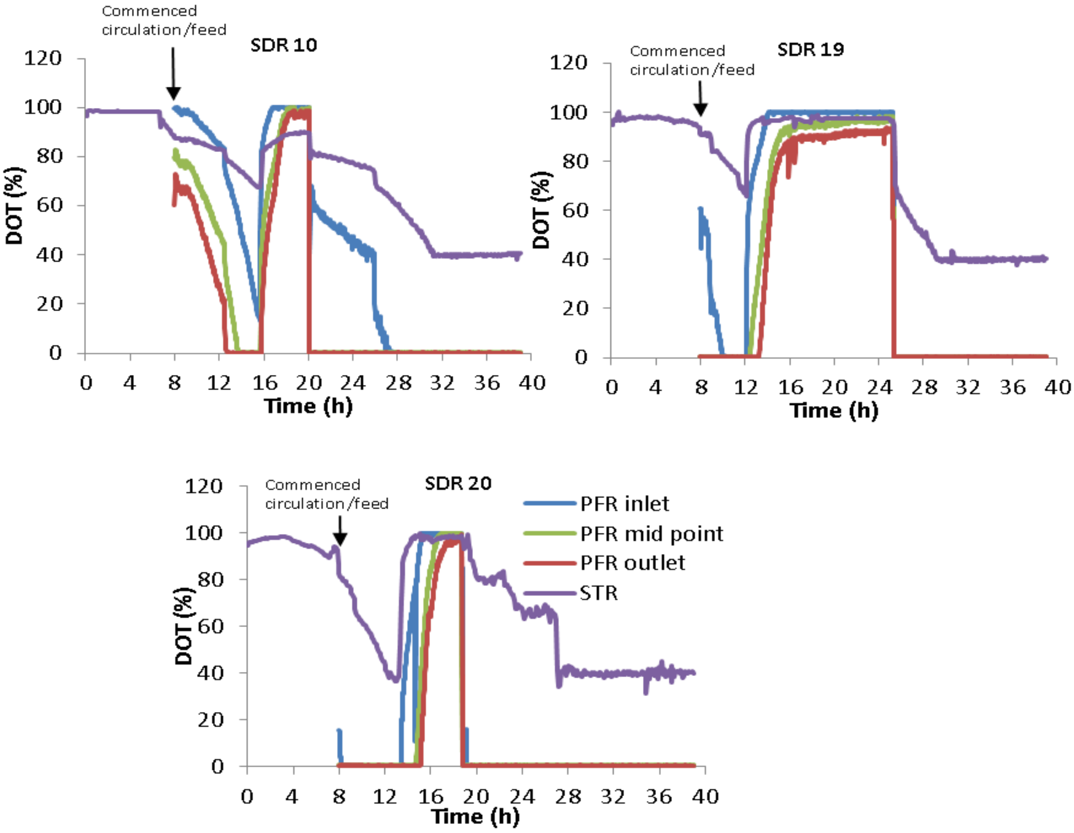

Figure 6.13 DOT profiles across SDR 10, SDR 19 and SDR 20 simulations

All the graphs in Figure 6.13 show the same initial uncontrolled growth of cells during the batch phase (0 – 14 h), which saw the first DOT decline. The transition phase (14 h – 20 h) and the fed-batch phase (20 h to 39 h).

The glucose concentration changes with time (Figure 6.14) for SDR 10, 19 and 20 simulations also follow the same trend as SDR 7, 17 and 18 (Figure 6.11).

The initial 10 gL^{-1} of glucose was depleted within the first fourteen hours, after which the SDRs were limited in glucose from 14 h to about 32 h except for the PFR section of SDR 10.

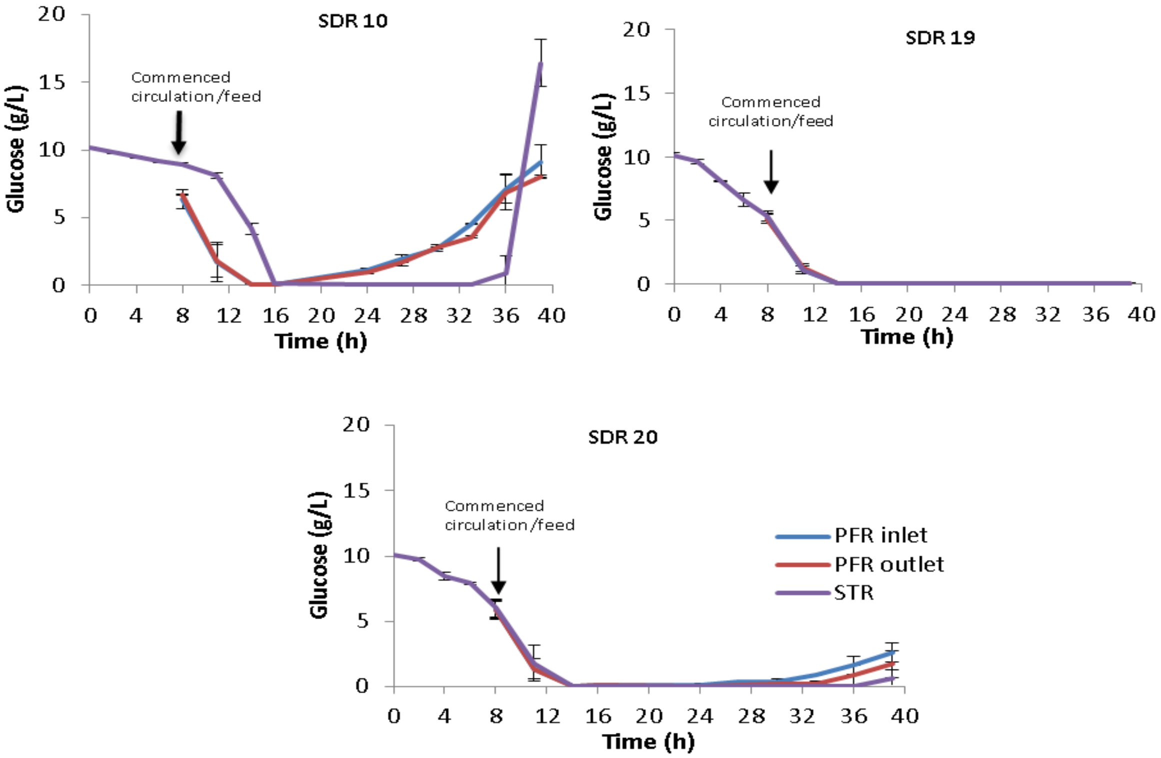

Figure 6.14 DOT profiles across SDR 10, SDR 19 and SDR 20 simulations

The reasons for the subsequent glucose accumulation seen in SDR 10 have been highlighted when SDR 4 of Figure 6.8 was discussed: the short PFR residence time does not the cells to deplete the glucose in the broth before they pass into the STR, during which the remaining glucose is consumed. Thus, in the STR, for most of the fermentation, the cell growth rate was controlled by the limited glucose environment.

The results from all four major simulations discussed thus far indicate that increasing the τ_{PFR} while decreasing the STR volume (to maintain a constant τ_{STR}) led to a harsher fermentation environment. The magnitude of the bacterial cells response increased, deviating more from the control fermentation, which was confirmed by the increased pH gradients and the overall longer time at which the PFR section remained oxygen limited. This is especially true for SDR 14, 16, 18 and 20, which had the longest τ_{PFR} investigated (5 min), a reasonable circulation time estimate in some large scale fermenters (Lara *et al.,* 2006a). The results so far suggest that the bacterial cells in these SDRs probably gave the strongest physiological response to the fermentation gradients simulated. The following sections look to quantify these physiological responses and compare variability across all simulations.

6.2 Cell growth

The cell growth was monitored by quantifying the DCW change in time; the feed rate controlled the cell growth during the fed-batch phase. The DCW gives the total cell mass concentration (viable and non-viable cells) in the bioreactor. Table 6.2 and Figures 6.15 a – d indicate the DCW profiles of all the simulations investigated in this chapter including the control fermentation (STR only).

Simulations	Final DCW (g/L)	μ (h^{-1})
STR only	30	0.09
SDR 1	32	0.09
SDR 13	31	0.08
SDR 14	28	0.08
SDR 4	29	0.09
SDR 15	31	0.08
SDR 16	29	0.08
SDR 7	32	0.09
SDR 17	31	0.08
SDR 18	28	0.08
SDR 10	30	0.10
SDR 19	32	0.09
SDR 20	29	0.08

Table 6.2 A summary *of C.glutamicum DM1945x3 growth kinetics indicating specific growth rates (µ) and the final dry cell weights (DCW) attained at the end of fermentation (39 h)*

The μ values above were estimated by fitting the DCW profile from 14 h to the exponential model described in Chapter 4, Subsection 4.1.1.

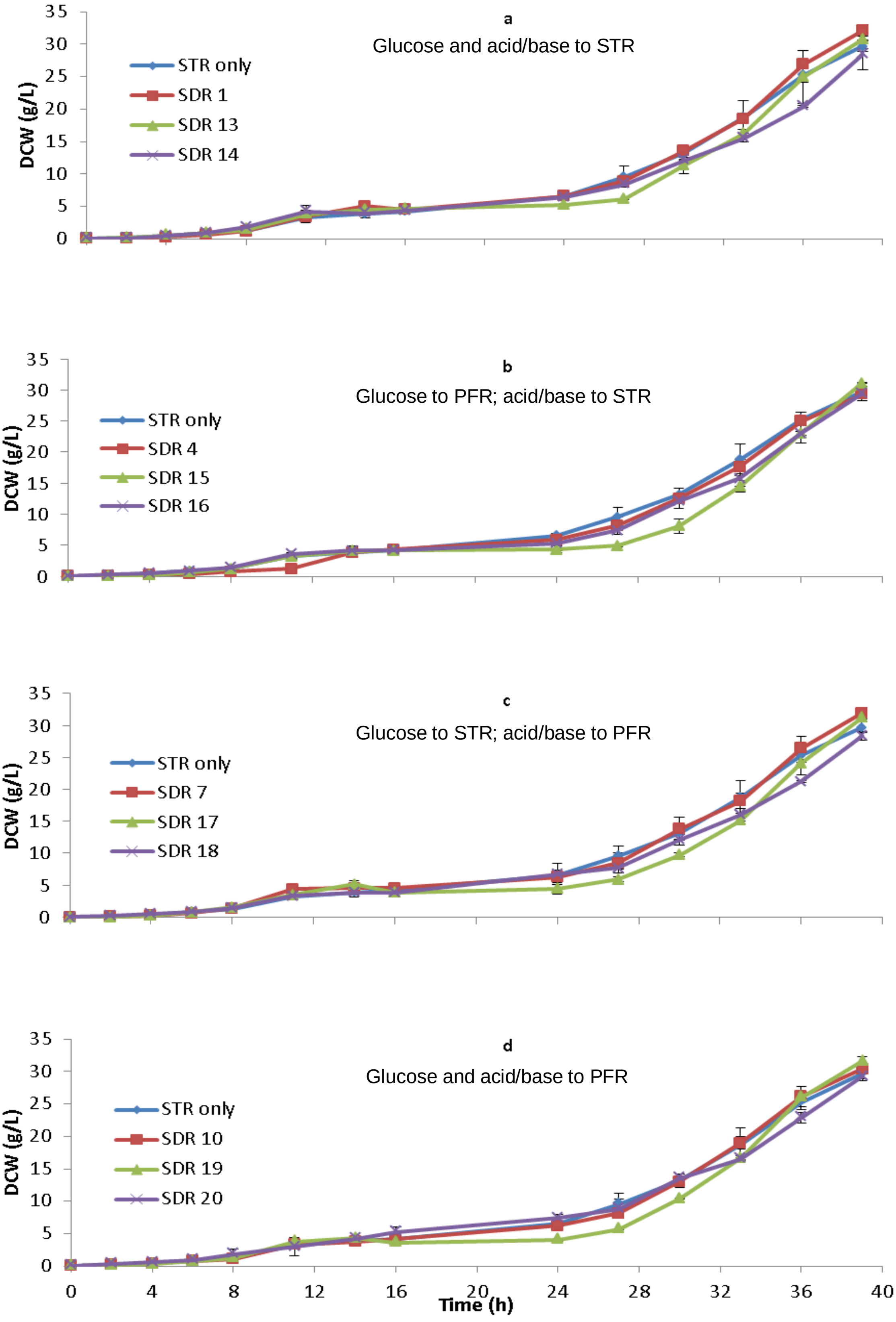

Figure 6.15 a – d Dry cell weight (DCW) profiles of various simulations compared to STR only. Legend STR only signifies the control fed-batch fermentation in a well-mixed stirred tank reactor; each data points represent the mean values from a set of biological duplicates, and the error bars represent their standard deviations.

Most of the cell growth occurred in the last fifteen hours of fermentation (from 24 h to 39 h); within this period, an 80 % increase of the total DCW occurred (Figure 6.15 a – d). The final DCW ranged from 28 gL^{-1} to 32 gL^{-1} (Table 6.2), with an average value of 30 gL^{-1}. The DCW profiles also illustrate the different cell growth rates at the various stages of these fermentations. The initial six-hour lag phase from the start was followed by the uncontrolled exponential growth phase (8 h – 12 h). This then led to the pseudo-stationary period (14 h – 24 h), due to the extremely limited glucose availability at this time. Finally, the controlled exponential growth period occurred between 24 h and 39 h.

The calculated values of μ from the simulations in Table 6.2 ranged from 0.1 to 0.08 h^{-1}, which indicates a 20 % difference. All the experiments which had the least STR volume of 0.6 L and the highest τ_{PFR} of 5 min (SDR 14, 16, 18 and 20) consistently had the lowest μ (0.08 h^{-1}). Additionally, these SDRs final DCW values were generally lower than the other simulations. This suggests that the DCW was negatively affected in these SDRs with the harshest environment.

The broad consensus from the findings of other works indicate that *C. glutamicum* is a resilient organism, which adapts easily to fermentation gradients without losses to DCW productivity (Käß *et al.,* 2014; Lemoine *et al.,* 2015a; Limberg *et al.,* 2016b). These observations correspond to that in the preceding Chapter 5 here. However, all these studies were based on experiments which had a decreasing mean frequency at which the cells entered the PFR as the τ_{PFR} increased. A setup which most likely attenuated the cell response to the fermentation gradients was simulated. To understand *C. glutamicum's* DCW resilience in the face of non-ideal growth conditions; the different metabolic pathways which provide the building blocks for biomass synthesis are illustrated in Figure 6.16

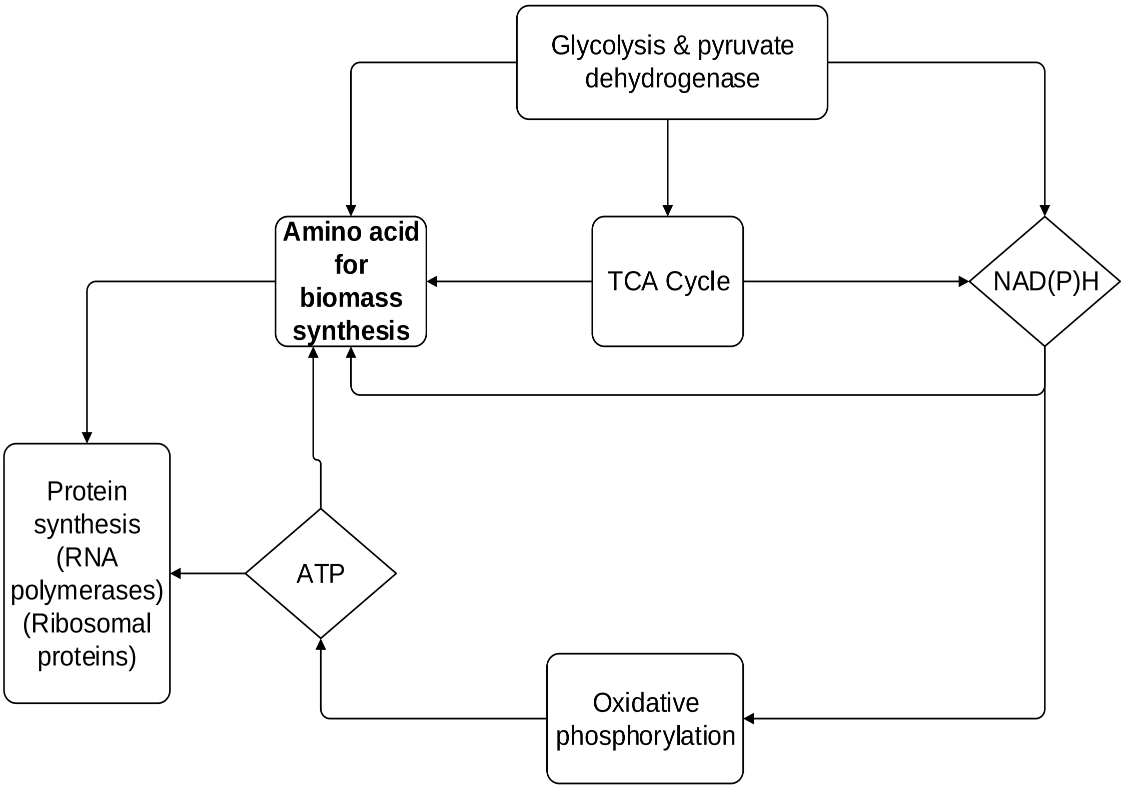

Figure 6.16 A simplified overview of a bacterial cell metabolic pathway resulting in the formation of biomass, adapted from (Li *et al.*, 2014b)

This robust biomass productivity of *C. glutamicum* may be attributed to its inherent ability to quickly switch pathways depending on the external pressures from the environment. For example, in a limited oxygen situation, *C. glutamicum* will favour the synthesis of biomass via lower glycolysis or/and oxidative phosphorylation to thrive, while energy generation from the TCA cycle is suppressed. Figure 6.16 thus shows that biomass formation and the energy required to drive the reaction can be derived from diverse pathways. The ability of *C. glutamicum* to easily tap into any one of this biomass forming pathways sets it apart from other organisms such as *E. coli* and gives it some level of resilience to fermentation gradients. The results here show that increasing the magnitude of fermentation gradients only slightly affected the *C. glutamicum* DM1945x3 DCW productivity.

6.3 CO_2 productivity

The production of CO_2 is dependent on the growth rate and metabolic pathway(s) of a bacterial cell. Hence, if two microorganisms with the same growth rate have different metabolic pathways to ATP production, their CO_2 production rate will vary. This is because the numbers of intermediate oxido-redox reactions are pathway-specific (Siebert & Wendisch, 2015). The graphs of Figure 6.17 a – d show the CO_2 production rate per working volume as it was related to the SDR investigated.

The peaks in CO_2 productivity which occurred between 10 h – 14 h in all fermentations indicate the uncontrolled exponential growth phase of the initial batch stage. The second increase in CO_2 production occurred during the fed-batch period from approximately 19 h. The graphs in Figure 6.17 a – d suggest that CO_2 profiles across all simulations can be divided into two categories:

1. Glucose feed to the STR: SDR 1, 7, 13, 14, 17 and 18 of Figure 6.17 a and c
2. Glucose feed to the PFR: SDR 4, 10, 15, 16, 19 and 20 of Figure 6.17 b and d)

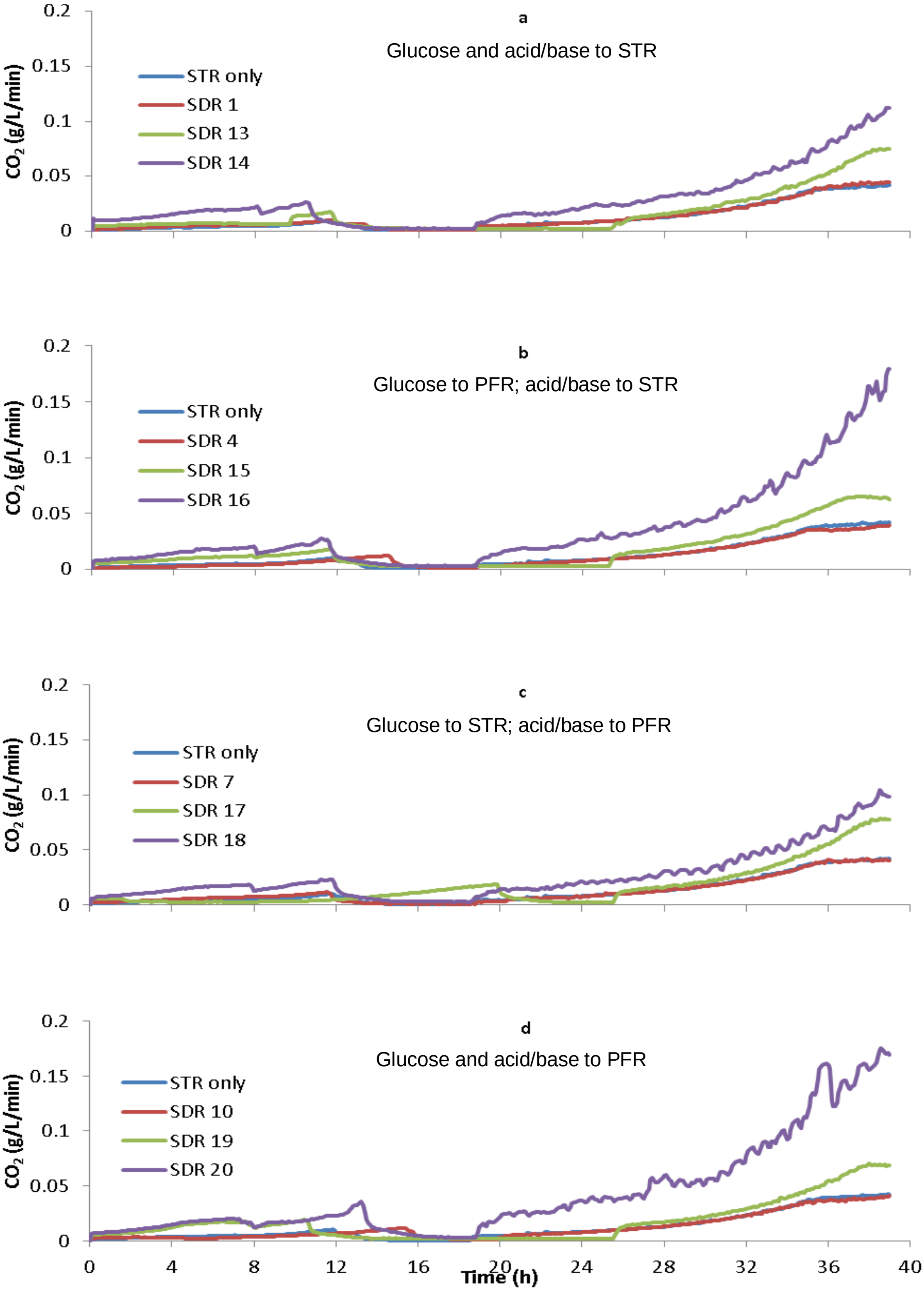

Figure 6.17 a – d CO_2 productivity profiles of various simulations compared to STR only. Legend STR only signifies the control fed-batch fermentation in a well-mixed stirred tank reactor.

In all cases, the maximum CO_2 productivity occurred at the end of the fermentation at 39 h. However, the simulations with the τ_{PFR} of 5 min exhibited the highest CO_2 productivity in comparison to the shorter τ_{PFR}. For example, in Figure 6.17 a, the CO_2 productivity at 39 h for SDR 14 (τ_{PFR} = 5 min) was 2.8-fold and 1.6-fold that of SDR 1 (τ_{PFR} = 1 min) and SDR 13 (τ_{PFR} = 2 min) respectively. This same trend was seen in other graphs of Figure 6.17, from which it can be inferred that the CO_2 productivity increased as the τ_{PFR} increased. SDR 16 and 20 produced the most CO_2 because they both had the longest τ_{PFR} in the oxygen limited PFR. The addition of the concentrated glucose feed into the poorly mixed PFR led to a localised high glucose concentration at its injection port. This resulted in a high metabolic rate within the limited oxygen environment of the PFR; the fermentative pathway was most likely used to produce ATP and CO_2 being the main side product also increased. The CO_2 productivity of SDR 16 and 20 and SDR 15 and 19 were relatively similar, suggesting that the localised high pH value at the point of addition in SDR 15 and 20 had a negligible effect on the production of CO_2.

6.4 Cadaverine production

The production of cadaverine depends on its central precursor L-aspartate, which is derived from one TCA cycle intermediate - oxaloacetate (Kind *et al.* 2011). The greatest concentration of cadaverine produced was in the latter stages (24 h – 39 h) of the fermentation in all cases (Figure 6.18 a – b). SDR 16 and 20 (τ_{PFR} = 5 min and glucose feed to PFR) showed the least specific metabolic quotient for cadaverine (q_{CAD}) (Table 6.3); this amounted to a 70 % loss in (q_{CAD}) when compared to the control fermentation, STR only. The estimation of q_{CAD} was based on the slope of the hourly change in cadaverine concentration per DCW concentration after 14 h in all simulations. There was a progressive decrease in cadaverine productivity as the τ_{PFR} increased and the f_m was kept constant. This trend was contrary to the results of Chapter 5, where after a τ_{PFR} > 2 min no further loss in cadaverine productivity was observed. The exception here was SDR 14, which showed a similar production profile to SDR 13 (Figure 6.18 a).

	Final cadaverine titre (gL^{-1})	Specific metabolic quotient for cadaverine (q_{CAD}) (gh^{-1} g-^{1})
STR only	20	0.057
SDR 1	16	0.045
SDR 13	9.6	0.039
SDR 14	11	0.045
SDR 4	15	0.043
SDR 15	9.8	0.040
SDR 16	5.6	0.017
SDR 7	14	0.042
SDR 17	11	0.038
SDR 18	8.0	0.029
SDR 10	14	0.041
SDR 19	9.9	0.037
SDR 20	5.3	0.017

Table 6.3 A summary of the final cadaverine concentrations and their specific metabolic quotients

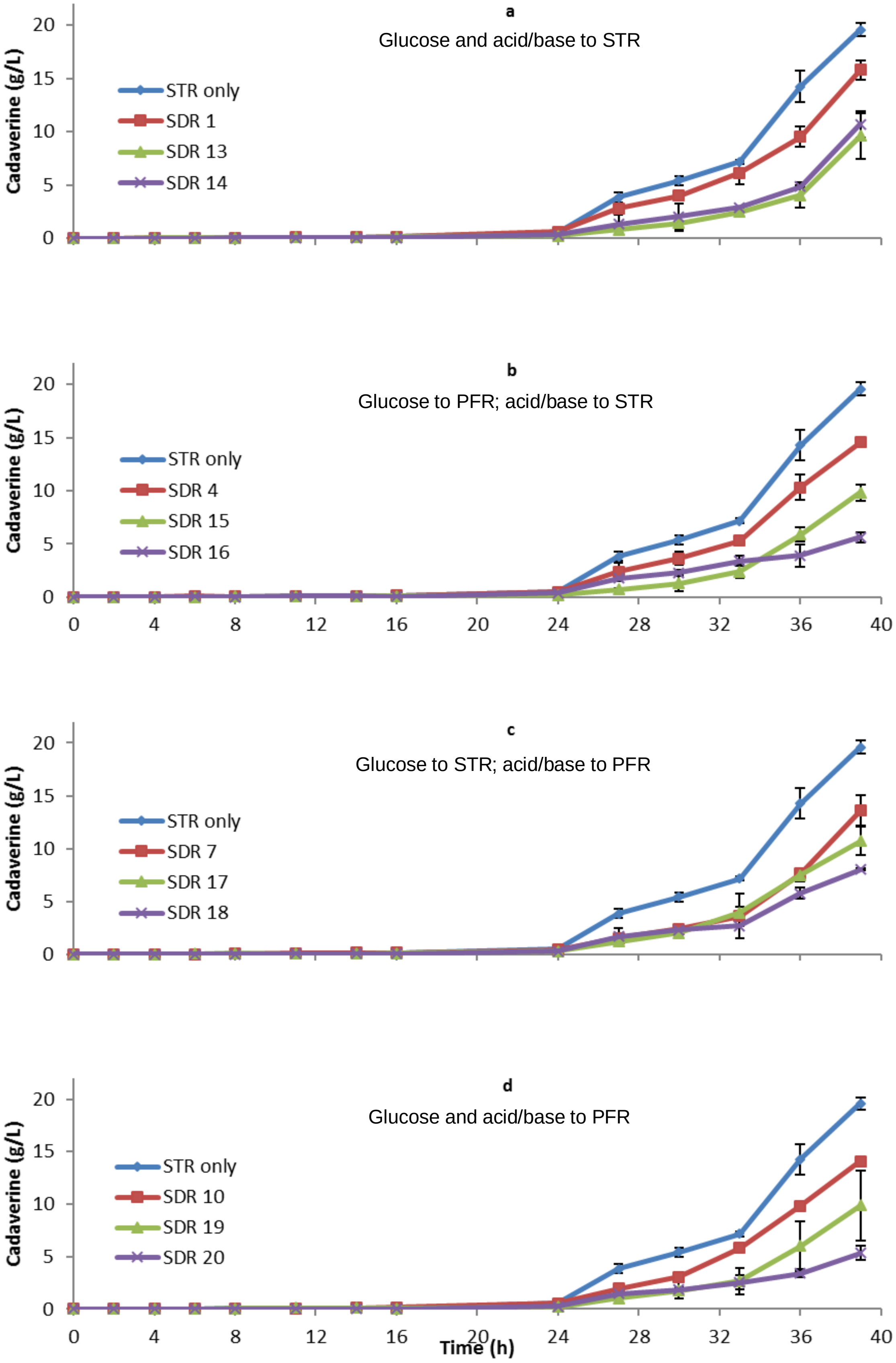

Figure 6.18 a – d Cadaverine production profiles of various simulations compared to STR only. Legend STR only signifies the control fed-batch fermentation in a well-mixed stirred tank reactor, each data point represents the mean of biological replicates and the error bars equivalent to their standard deviations.

The above results show that the rate of cadaverine production was dependent on the magnitude of the fermentation gradients. The bacterial cells which use alternative metabolic pathways in response to the harsh environment of the SDRs are most likely to lead to a decrease in cadaverine productivity (Figure 6.18 a – b). The biggest loss ($\approx$ 72 %) in the final cadaverine concentration was recorded for SDR 16 and 20 (Figure 6.18 b & d). However, for the τ_{PFR} of 1 and 2 min, the SDR setup (such as where base or glucose was introduced in the SDR) did not matter. For example, the q_{CAD} for SDR 13, 15 17 and 19 were similar, approximately 0.04 g $\cdot L^{-1} \cdot h^{-1} \cdot g^{-1}$ for the τ_{PFR} of 2 min. The final cadaverine decrease in concentration when the τ_{PFR} was 1 min and 2 min compared to the control fermentation were on average 24 % and 50 % respectively (Table 6.3). The glucose addition point only became an important factor for cadaverine productivity when the τ_{PFR} was increased to 5 min. This was observed in SDR 16 and 20, where the glucose feed was introduced to the oxygen limited PFR environment, causing the bacterial cells to mainly generate ATP via the fermentative pathway (Pirt, 1975; Stanbury *et al.,* 1999). However, doing so diverts the carbon flux typically available to the TCA cycle under aerobic conditions, where oxaloacetate is produced. The formation of oxaloacetate is regulated by the activities of the malate: quinone oxidoreductase, malate dehydrogenase, phosphoenolpyruvate carboxylase, phosphoenolpyruvate carboxykinase, pyruvate carboxylase and oxaloacetate decarboxylase enzymes (Wieschalka *et al.,* 2013). Thus, fermentation conditions that alter these enzymes and consequently reduce oxaloacetate production will result in the decline of L-aspartate available for generating cadaverine. Thus, the losses observed suggest that the harsh conditions imposed by the SDRs may have resulted in the adverse interaction of these relevant enzymes.

C. glutamicum being a facultative anaerobe adapts to a limited oxygen environment by upregulating its malate dehydrogenase enzyme activity within the TCA cycle (Inui *et al.,* 2007), an enzyme known to reduce oxaloacetate to succinic acid. This competitive reaction reduces the pool of oxaloacetate available for cadaverine formation. A second significant energy sink for *C. glutamicum* growing under a limited oxygen environment is its metabolic shift to the fermentative pathway. This shift increases the conversion of pyruvate to lactic and acetic acid by the action of the lactate dehydrogenase, pyruvate: quinone oxidoreductase and the CoA transferase A enzymes (Wieschalka *et al.,* 2013). This consequently reduces the carbon flux to the TCA cycle. Lastly, a localised high glucose environment as induced in SDR 16 and 20 may have activated the overflow metabolic pathway. If the increased carbon flux from glycolysis had led to the saturation of the glyceraldehyde-3-phosphate dehydrogenase and the pyruvate dehydrogenase enzymes, it would increase the production of dihydroxyacetone and lactate (Dominguez et al., 1998), thus, also divert the carbon flux from the TCA cycle.

A carbon balance analysis was performed to quantify how much the SDRs conditions affected the growing *C. glutamicum* cells. The same calculation as highlighted in Chapter 5 has been used here. The theoretical proportion of the unmeasured carbon-containing compounds helped quantify the magnitude of the bacterial cell's response to the SDRs investigated (Table 6.4).

Simulation	% of unquantified C – products	Deficit-degree of reduction
STR only	10.54	6.8
SDR 1	13	7.3
SDR 13	21	7.2
SDR 14	15	14
SDR 4	16	6.7
SDR 15	21	7.3
SDR 16	15	15
SDR 7	16	6.9
SDR 17	19	7.4
SDR 18	22	9.8
SDR 10	11	8.2
SDR 19	20	7.5
SDR 20	12	20

Table 6.4 A summary of the percentage composition of unmeasured carbon-based products derived from C. glutamicum DM1945x3 consumption of 1 mole of glucose

Table 6.4 identified three broad categories loosely based on the τ_{PFR}. The first set of simulations, SDR 1, 4, 7 & 10 (τ_{PFR} = 1 min) show 10 – 13 % unquantified carbon containing compounds and a low degree of reduction (6 – 8). These indicate the abundance of short-chained carbon containing compounds. In the second set, SDR 13, 15, 17 and 19 (τ_{PFR} = 2 min) had a higher percentage of carbon containing compounds with a low degree of reduction. These calculations highlight the presence of even more short-chained carbon containing compounds in these simulations. The last set, SDR 14, 16, 18 and 20 (τ_{PFR} = 5 min), showed a low percent of unquantified carbon containing compounds, but a high degree of reduction, indicating that in these simulations, the unquantified carbon containing compounds were long-chained. Overall, comparing the control STR only fermentation to any SDR show that the percentage of unquantified C – products and the deficit degree of reduction increases. Thus, indicating that the loss in cadaverine seen in Figure 6.18 was due to the diversion of more carbon flux to competing products as the magnitude of fermentation gradients increased.

In summary, the activation of the TCA cycle reductive path, overflow metabolic pathway and the metabolic shift to the fermentative pathway, as the cells responded to the oxygen limitation and/or high PFR environment, are some of the factors which contributed to the cadaverine loss in the SDRs experiments. Also, the carbon balance analyses indicate that the bacterial cell metabolic response was dependent on the time spent in the PFR and type of fermentation gradient (pH, DO and glucose) simulated. For example, when SDR 10 and 20 are compared, the varied cell response was easily seen (the difference between both simulations was the τ_{PFR}), as although both simulations had a similar percentage of unmeasured carbon containing compounds, SDR 20 deficit-degree of reduction suggests the abundance of unquantified long-chained carbon-containing compounds.

6.5 Lactate formation

Lactate is one of the primary metabolites in *C. glutamicum* fermentation (Dominguez *et al.,* 1998; Käß *et al.,* 2014). The final lactate concentrations (at 39 h) in all cases investigated indicate that gradients were formed when values were compared across the SDR (Figure 6.19).

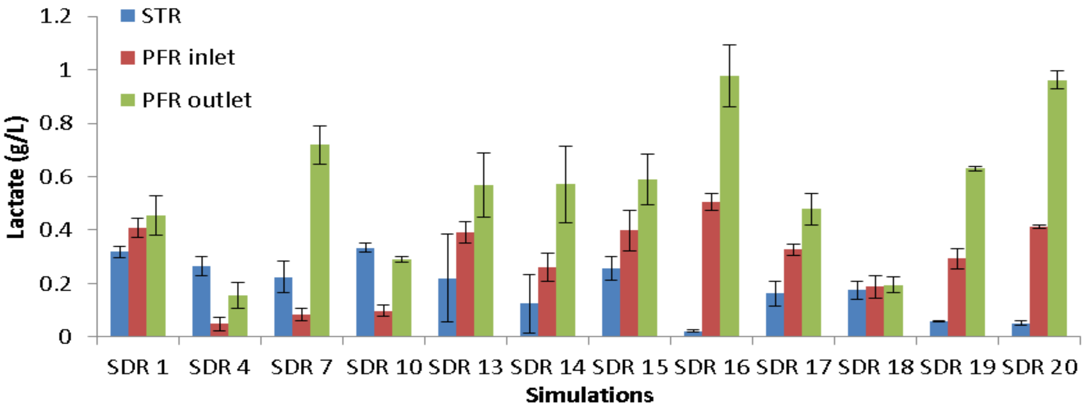

Figure 6.19 Lactate gradient across SDRs sampled at the end of fermentation (39 h), each data point represents the mean of biological replicates and the error bars equivalent to their standard deviations.

The highest concentration of lactate was consistently recorded at the PFR outlet, with SDR 16 and 20 (τ_{PFR} = 5 min) showing the most prominent gradient (Figure 6.19). This result is consistent with trends already seen in other assays above. Since the PFR was oxygen limited, the simulations where the concentrated glucose feed was added in this section encouraged energy production via the fermentative pathway. The fermentative pathway diverts the carbon flux from the TCA cycle, but also supports the conversion of pyruvate to lactate, acetate and formate downstream from glycolysis. Hence, the longer the cells spent in this environment, the more lactate is produced. However, the proportions produced of these metabolites depend on the bacterial cell strain, for example, in *C. glutamicum* fermentation lactate is one of the predominant metabolites (Figure 6.20), while in *E. coli* it is acetate (Dominguez *et al.,* 1998; Xu *et al.,* 1999).

This effect of the metabolic shift from the fermentative pathway was confirmed by the low values of lactate concentration recorded in the well oxygenated STR. However, in the STR some increase in lactate accumulation was seen during the cells exponential growth phase (8 h – 12 h) (Figure 6.21 a - d). This rise in lactate can be attributed to an increased rate of glycolysis (the breakdown of glucose into pyruvate). If the rate of the carbon flux from pyruvate into the TCA cycle is slower than that of glycolysis, the excess carbon is diverted into dihydroxyacetone and lactate upstream of glycolysis (a phenomenon known as the overflow metabolism) (Dominguez *et al.,* 1998).

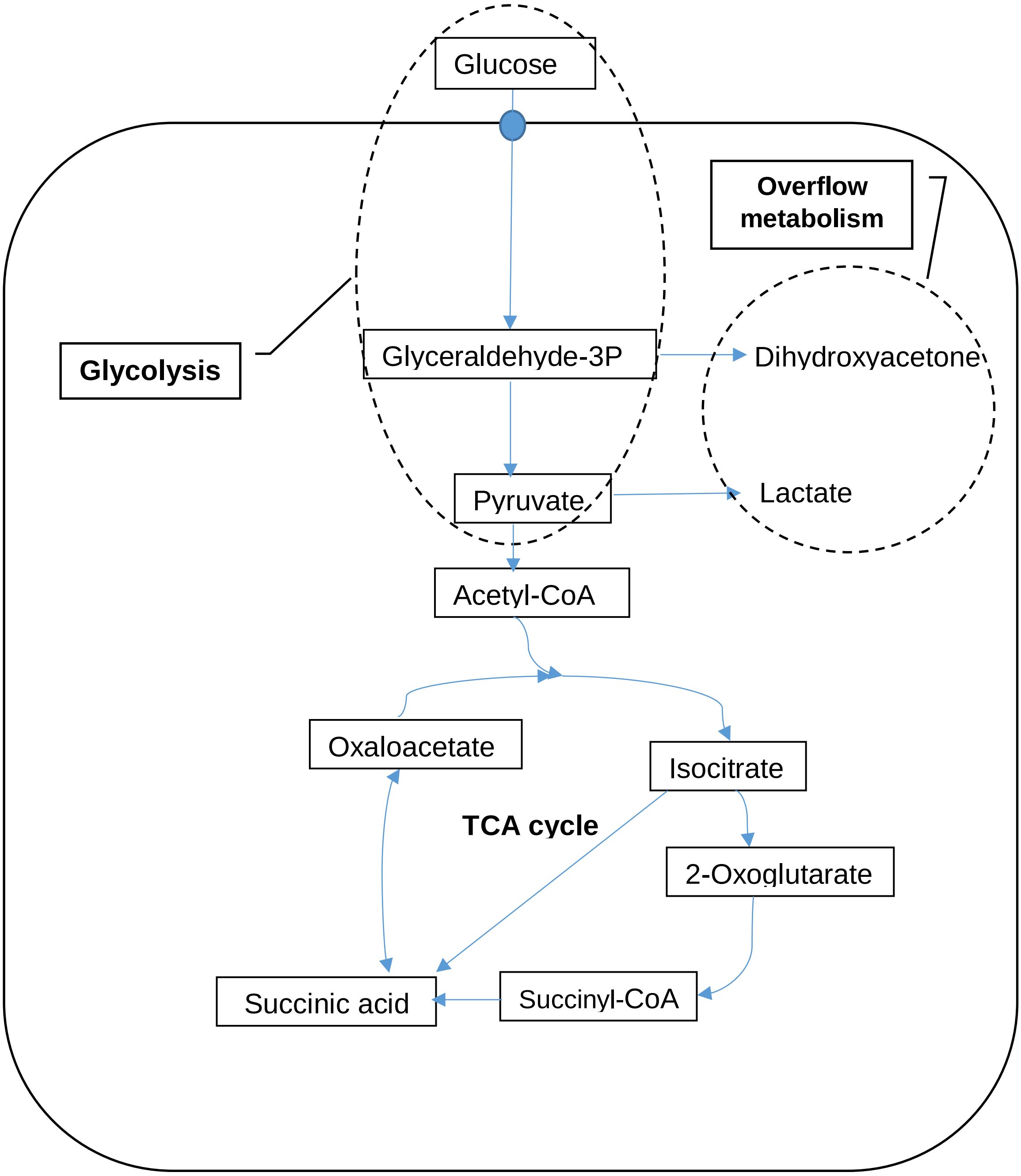

Figure 6.20 A simplified overview of C. glutamicum carbon metabolism highlighting its glycolysis, overflow and TCA cycle pathways adapted from Dominguez *et al.*, (1998).

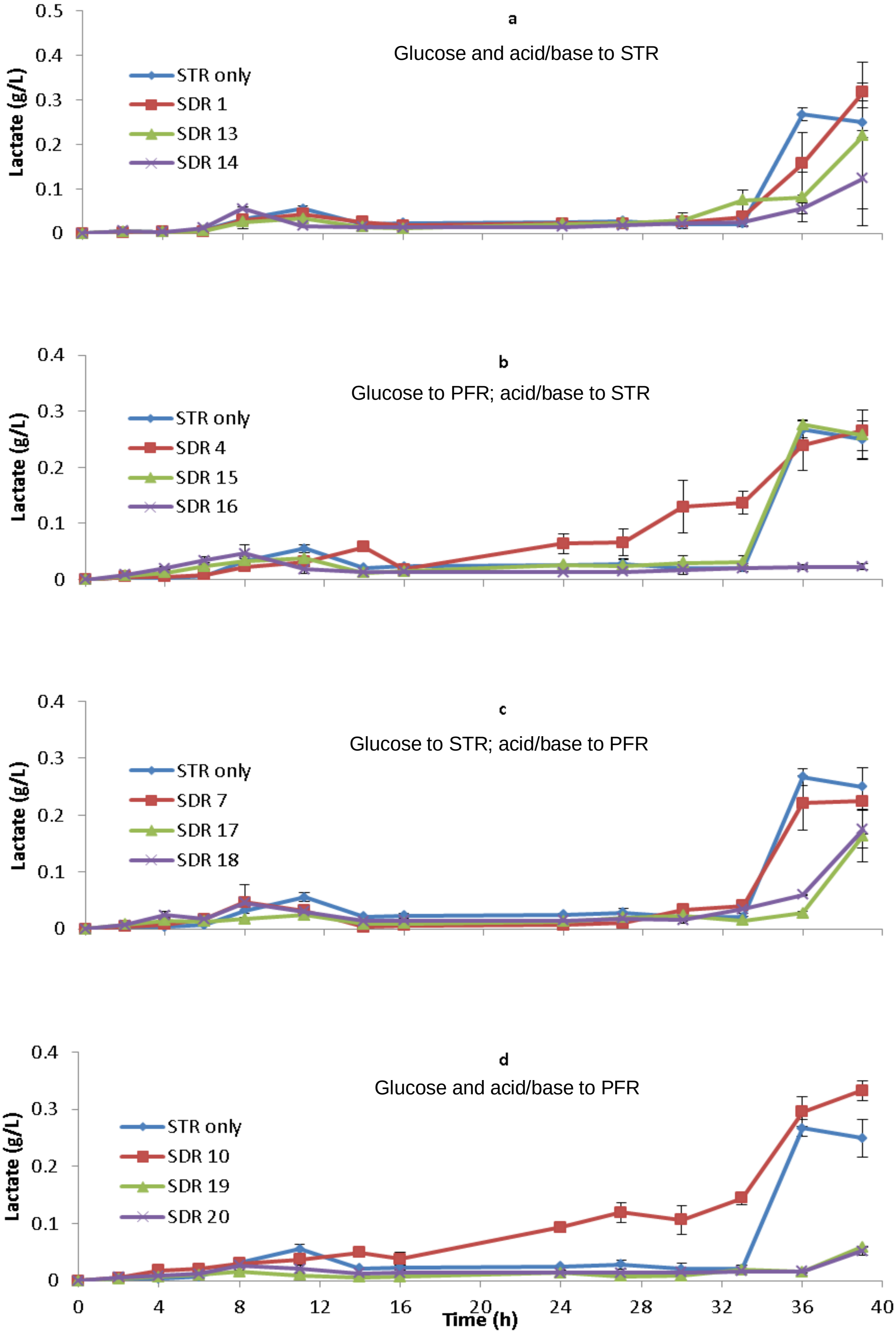

Figure 6.21 a – d Lactate accumulation profiles, each data points represent the mean values from biological duplicates and the error bars equivalent to their standard deviations.

Figure 6.21 a – d show that as soon as the cells entered the pseudo-stationary phase between 12 h and 24 h, the lactate concentration was reduced as the cells growth rate plummeted. In most of the simulations, the lactate production rate was later seen to increase at around 32 h during the exponential phase of the feeding profile. This ensuing increased metabolic rate would have instigated an unbalanced glycolysis reaction rate (the rate of pyruvate to acetyl CoA being slower than the rate of glucose to pyruvate). However, for simulations such as SDR 16 and 20 where the glucose was added at the PFR, the amount of lactate produced in the STR was lower. This was attributed to the lower amount of glucose available in the STR, as in these simulations, the glucose supplied was from that of the incoming PFR broth. Hence, since there were no localised high glucose concentrations within the STR for these simulations, the rate of glycolysis was slower, resulting in the low rates of lactate production seen. This also meant that bacterial cells in these simulations produced most of their lactate in the PFR section of the SDR, due to the high localised glucose concentration there.

The lactate profiles of Figures 6.19 and 6.21 a – d confirm that the point at which the concentrated glucose feed is added and DO of the localised environment is important. These factors determined the bacterial cell response and ultimately affected the fermentation productivity.

6.6 Glucose consumption

After the batch phase (0 – 14 h), glucose was the main growth-limiting substrate up until about 36 h (Figure 6.22 a - d). The glucose profiles showed a similar trend irrespective of the simulation. However, the rates of glucose consumption were slightly different, especially in the batch phase. The variations in the number of viable cells on start-up and those that survived the lag phase may have contributed to these differences.

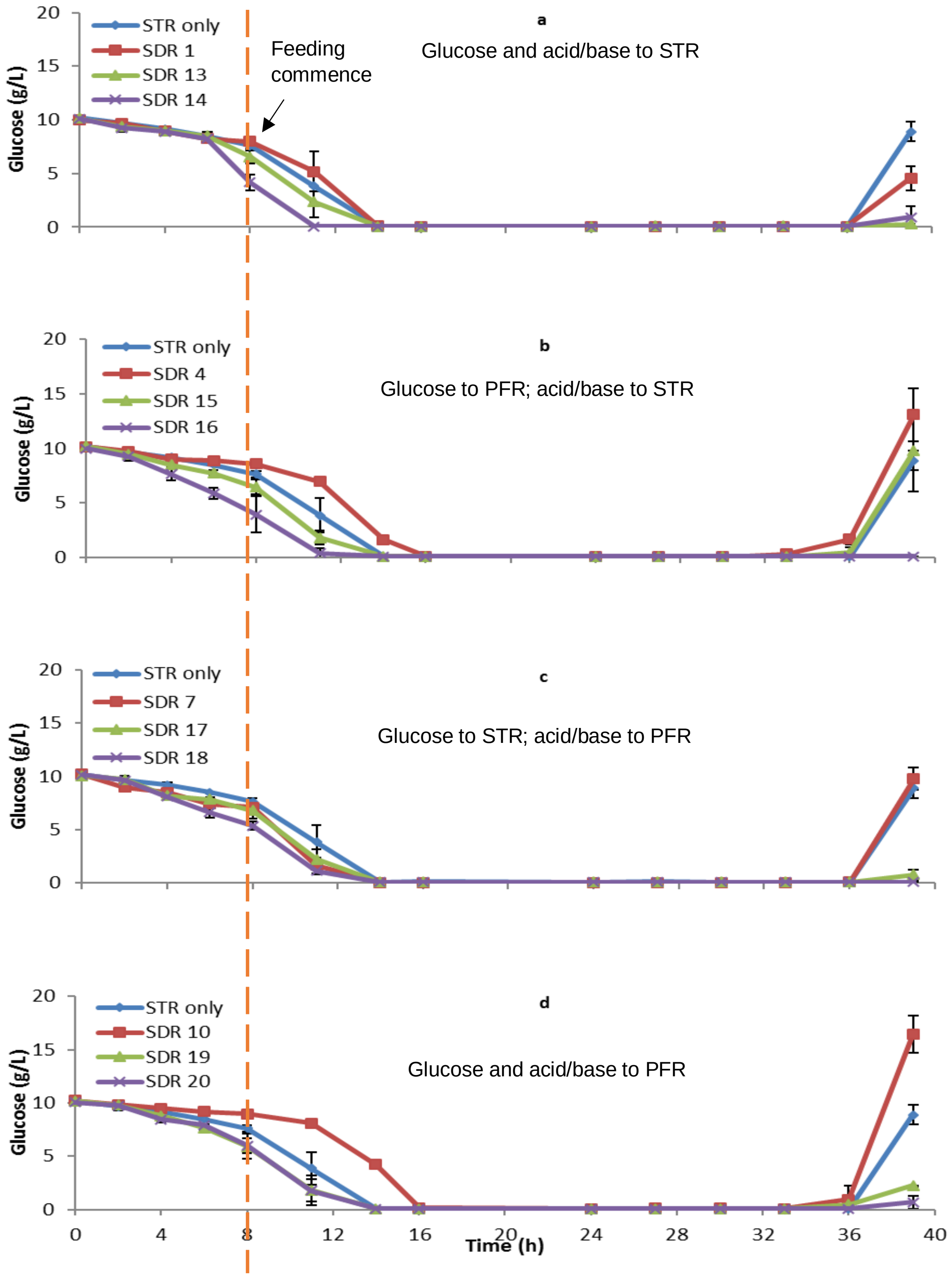

Figure 6.22 a – d Glucose consumption profiles, each data point represents the mean value from biological duplicates and the error bars equivalent to their standard deviations. The dashed line represents the start of feeding.

It is axiomatic that during the batch process, a steady state is never achieved and these variations seen in glucose consumption rates might be within the normal fluctuation of this biological system. The glucose substrate became limited from 16 h up till 36 h for all cases investigated. However, the subsequent accumulation after 36 h was most likely due to the feed pumping mismatch with the glucose consumption rate during this period.

6.7 Flow cytometric analyses

The metabolic measurement from the flow cytometer identified three different cell states, as illustrated in Section 5.7 of Chapter 5; the quadrants of Figure 6.23 also have the same meaning. Each of the quadrants grouped cells that had similar membrane integrity/potential. The following analysis will be divided into similar categories as highlighted Section 6.2.

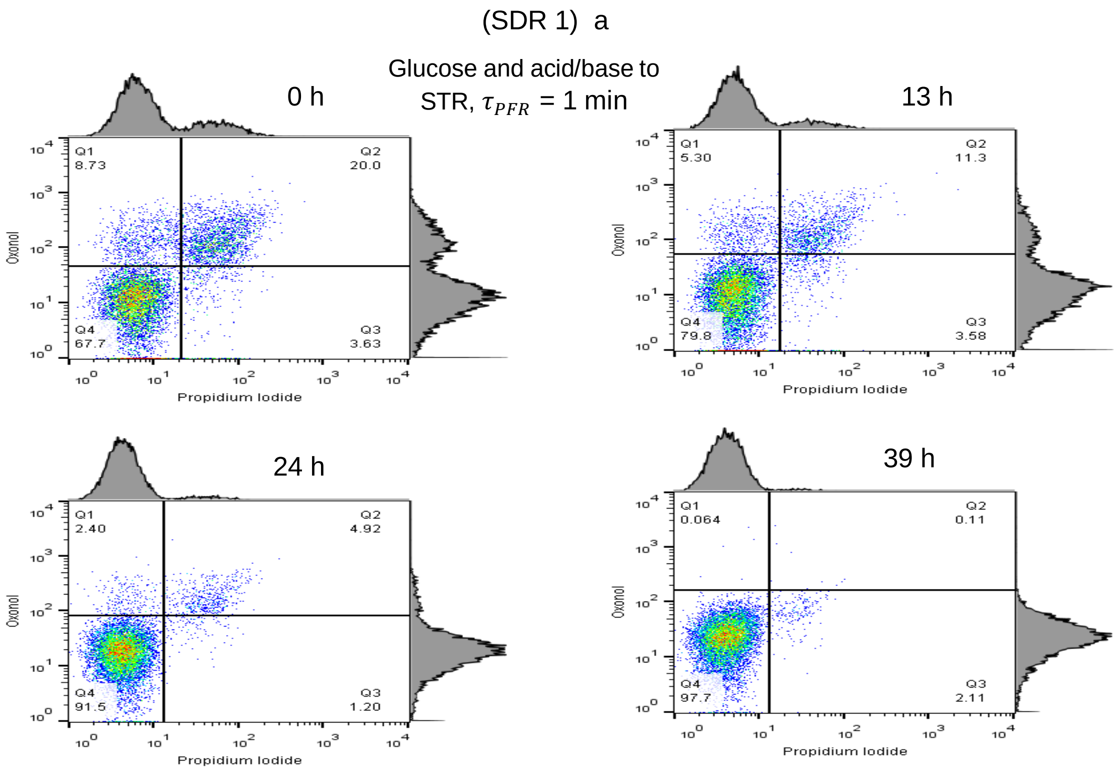

(SDR 13) b

Glucose and acid/base to STR, τ_{PFR} = 2 min

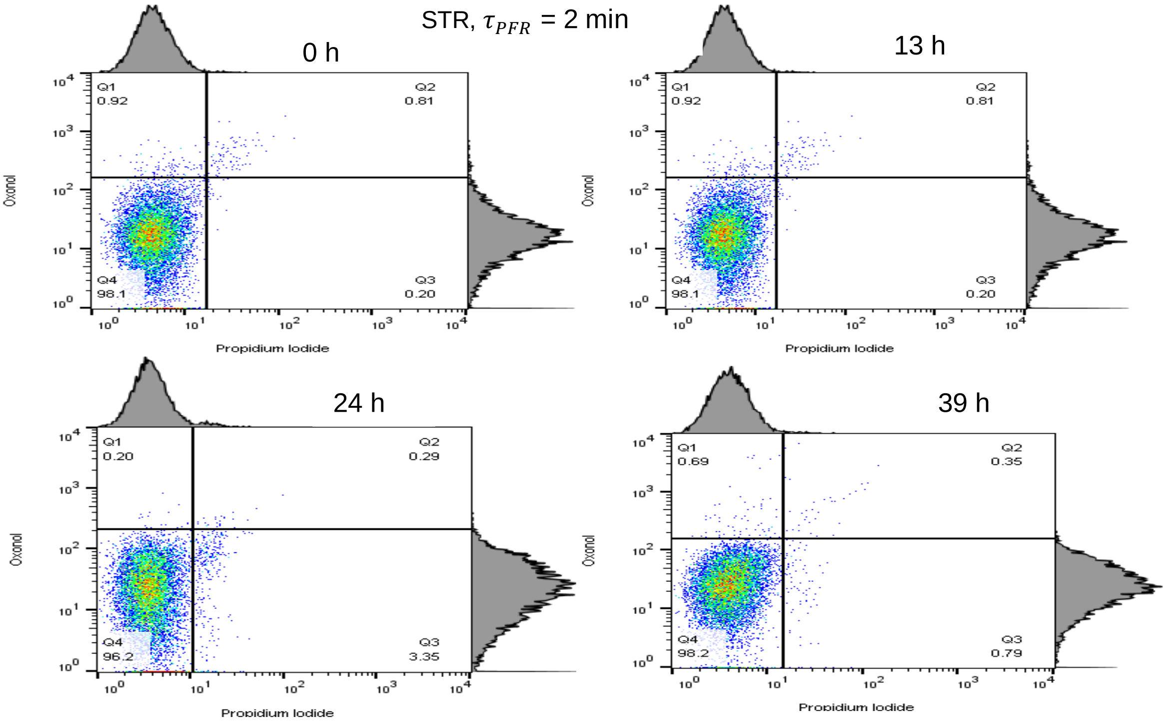

(SDR 14) c

Glucose and acid/base to STR, τ_{PFR} = 5 min

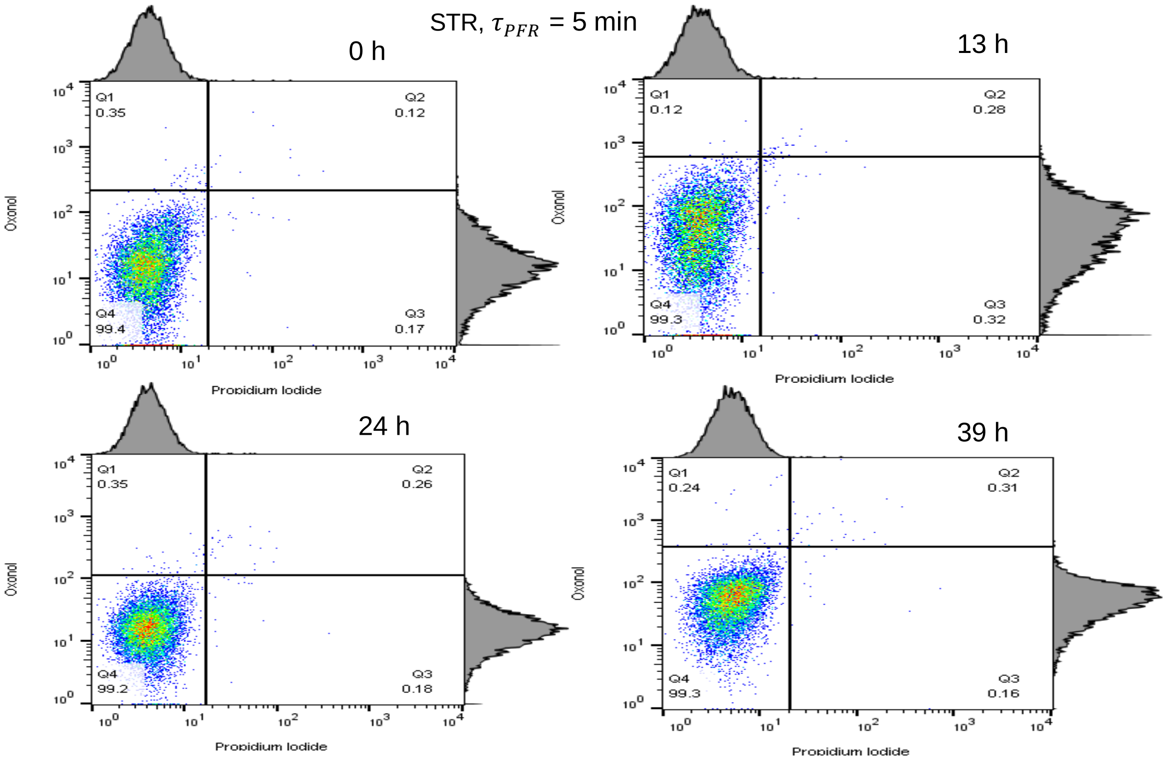

Figure 6.23 a – c Flow cytometer dot plots for SDR 1, 13 and 14 indicating the condition of the cell membrane at different time points during fermentation using the above fluorochromes. Each dot on the plot represents a cell of the 10000 cells interrogated.

SDR 1 (Figure 6.23 a) indicate a considerable subpopulation of dead and depolarised cells (Q2 and Q1 quadrants) from the start of the fermentation. This highlighted that the quality of inoculum on start-up was responsible. However, by 13 h the population from both Q1 and Q2 quadrants had reduced by 50 %, indicating the healthy cells of Q4 had outgrown the others. This trend continued until termination (39 h), where the predominant cell population was in the Q4 quadrant (healthy cells). At 39 h, there was also a significant population in the Q3 quadrant (≈ 2 %), which had remained relatively unchanged throughout the fermentation. It most likely indicated the presence of cell clusters (healthy and dead cells) (Nebe-Von-Caron *et al.,* 2000; Want *et al.,* 2011). This indicates a situation were one of two attached cells is stained by the PI and oxonol fluorochromes (a dead cell) and the other unstained (because it is healthy), which resulted in a false negative for oxonol. SDR 13 (Figure 6.23 b) on start-up was different from SDR 1 (inoculum variability), most of the cell population were in the Q4 quadrant (healthy cells), which remained relatively unchanged during the course of the fermentation. SDR 14 (Figure 6.23 c) showed a similar profile to SDR 13 at 0 h, the predominant cell population had intact membranes, and were hence deemed healthy. The population remained in the Q3 quadrant from start to finish. Hence, increasing the magnitude of fermentation gradients from Figure 6.23 a - c had an insignificant effect on *C. glutamicum* DM1945x3 membrane integrity.

(SDR 4) a

Glucose to PFR; acid/base to STR, τ_{PFR} = 1 min

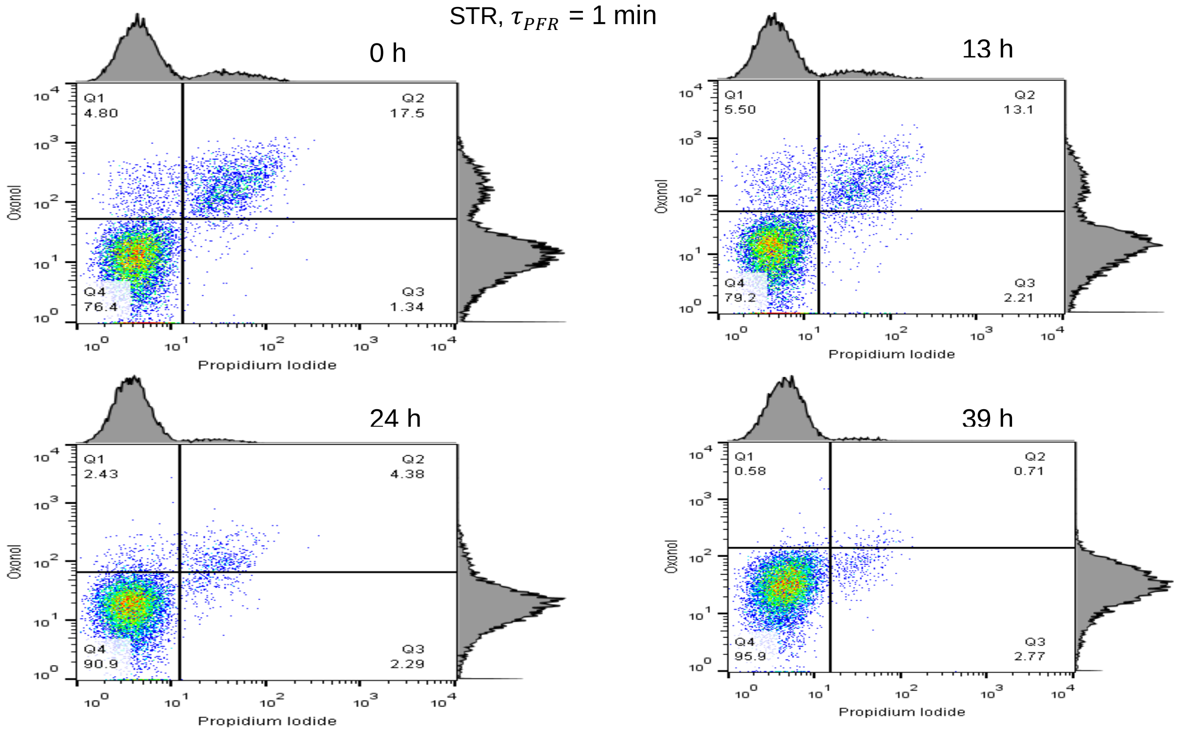

(SDR 15) b

Glucose to PFR; acid/base to STR, τ_{PFR} = 2 min

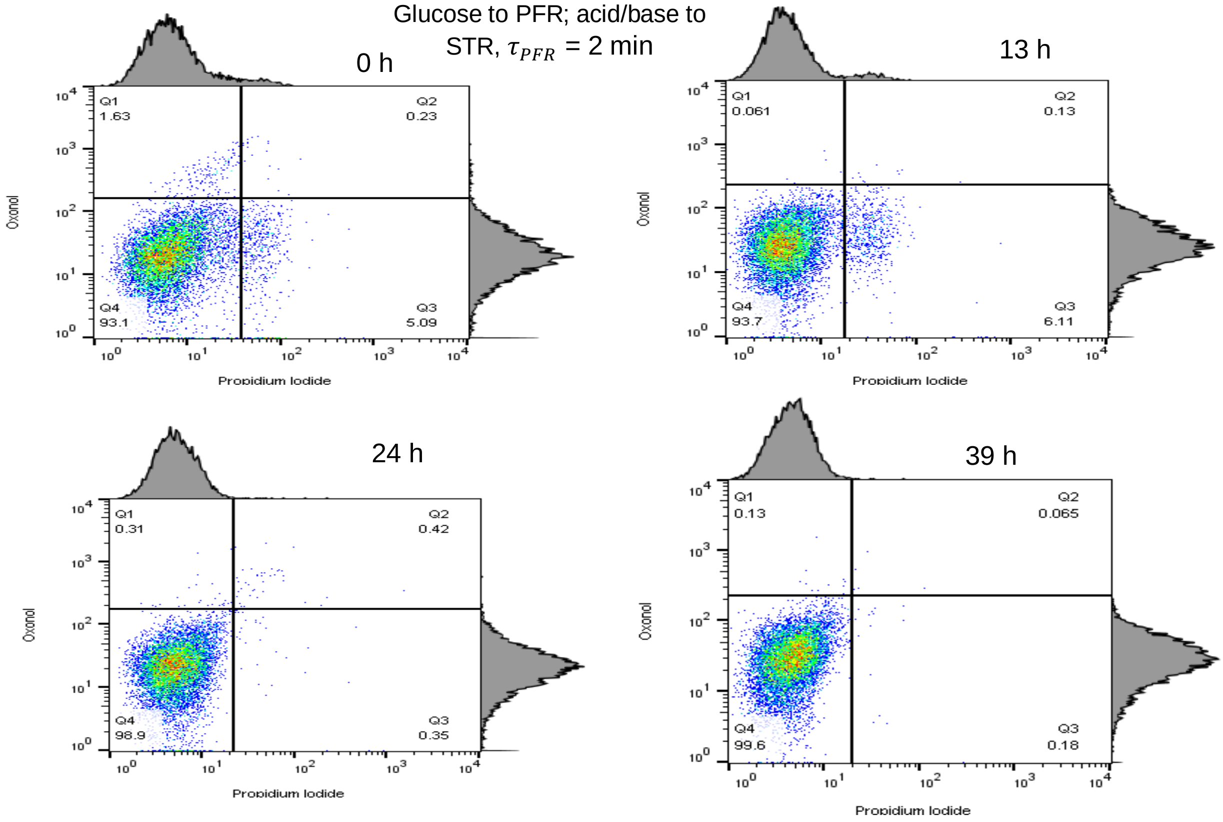

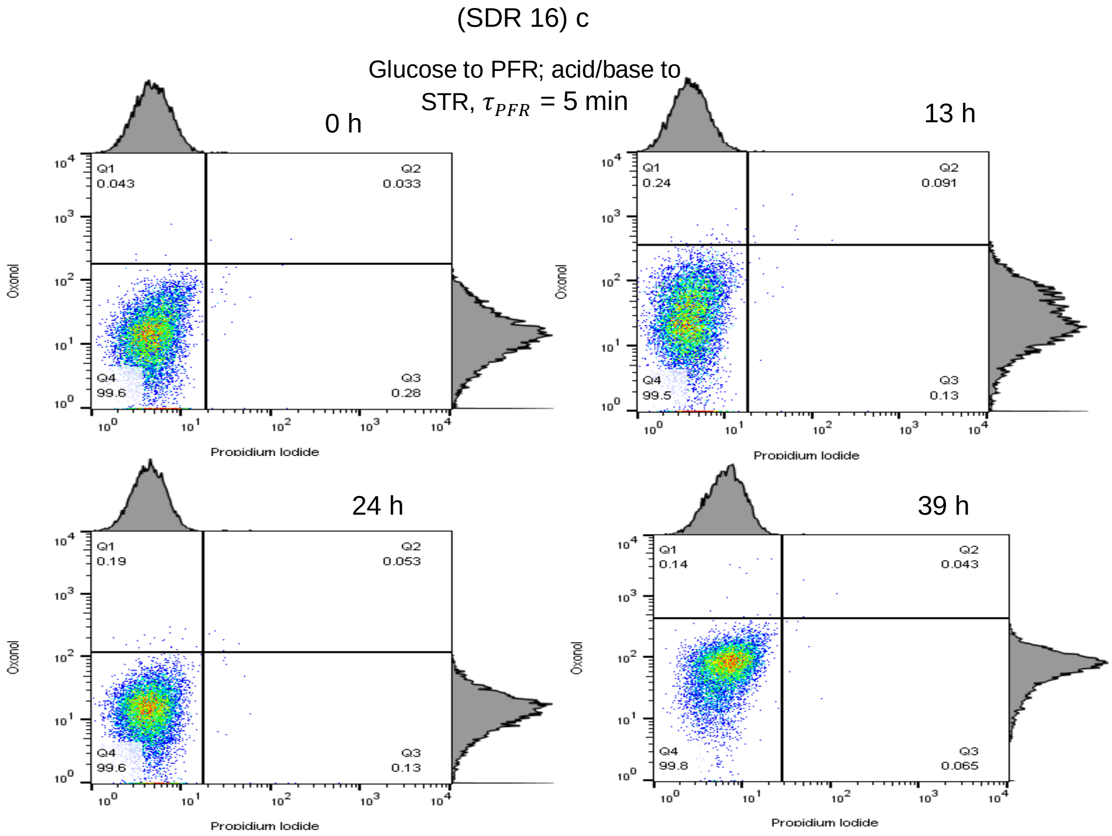

Figure 6.24 a – c Flow cytometer dot plots for SDR 4, 15 and 16 indicating the condition of the cell membrane at different time points during fermentation using the above fluorochromes. Each dot on the plot represents a cell of the 10000 cells interrogated.

SDR 4 (Figure 6.24 a) highlighted the quality of the inoculum, which resulted in the significant population of dead and depolarised cells along with the healthy cells at the start of the fermentation. This profile remained unchanged in the transition from batch to the fed-batch stage (13 h). However, by the 24 h, the healthy cell population had outgrown the others, increasing from 76 % to 91 % from 0 h to 24 h. By completion (39 h), the healthy cells population was at 96 %. The Q3 quadrant also saw an increase from 1 % on start to 3 % at the end, hence indicating an increase in a cluster of live and dead cells. SDR 15 (Figure 6.24 b) started up with a subpopulation of the depolarised cell cluster and healthy cells. However, between 0 h and 24 h most of the cells were in the Q4 quadrant (healthy cells) and on completion almost 100 % of the cells were healthy. For SDR 16 (Figure 6.24 c) from start to finish, almost 100 % of the cells were healthy. Figure 6.24 a – c findings indicated that the percentage of the cells in each subpopulation on start was a function of the inoculum quality, which subsequently affected the the final proportion.

(SDR 7) a

Glucose to STR; acid/base to PFR, τ_{PFR} = 1 min

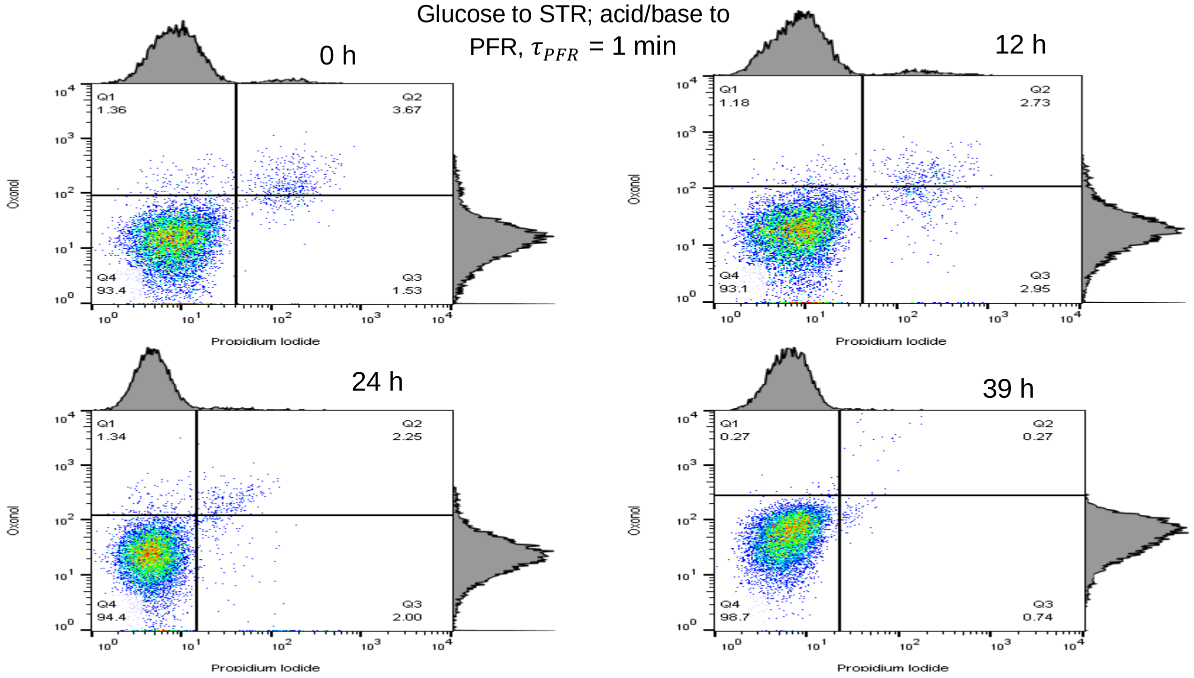

(SDR 17) b

Glucose to STR; acid/base to PFR, τ_{PFR} = 2 min

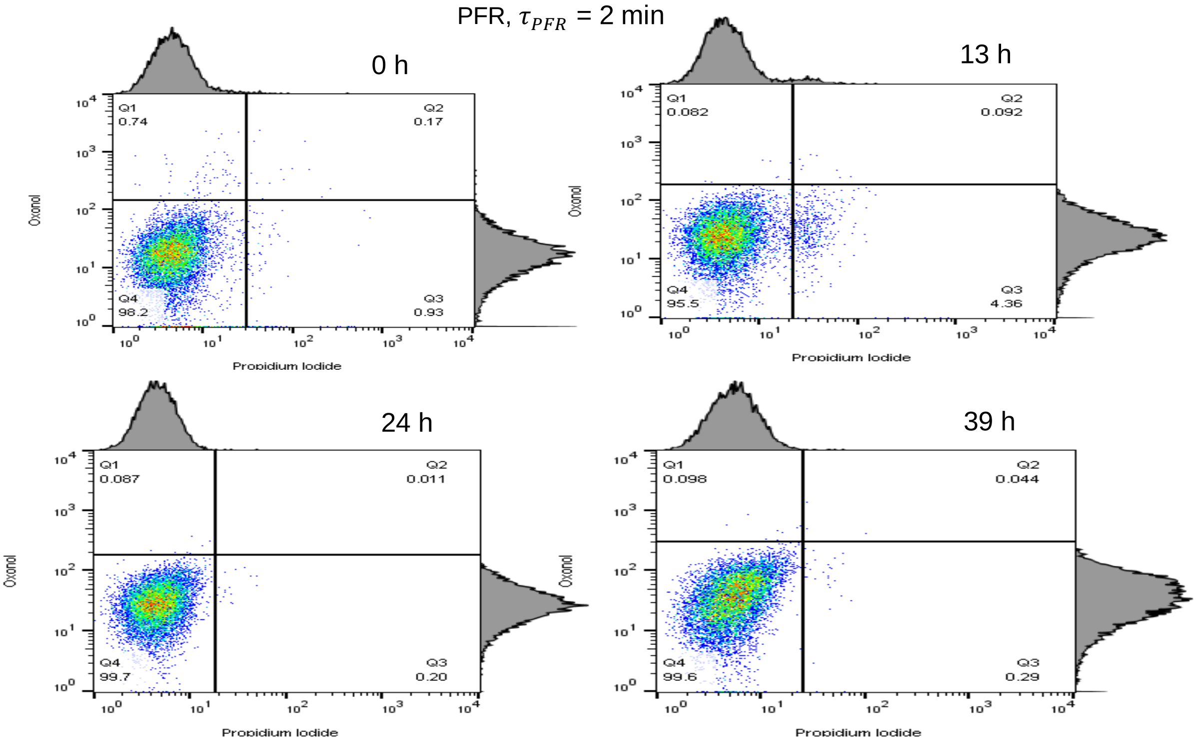

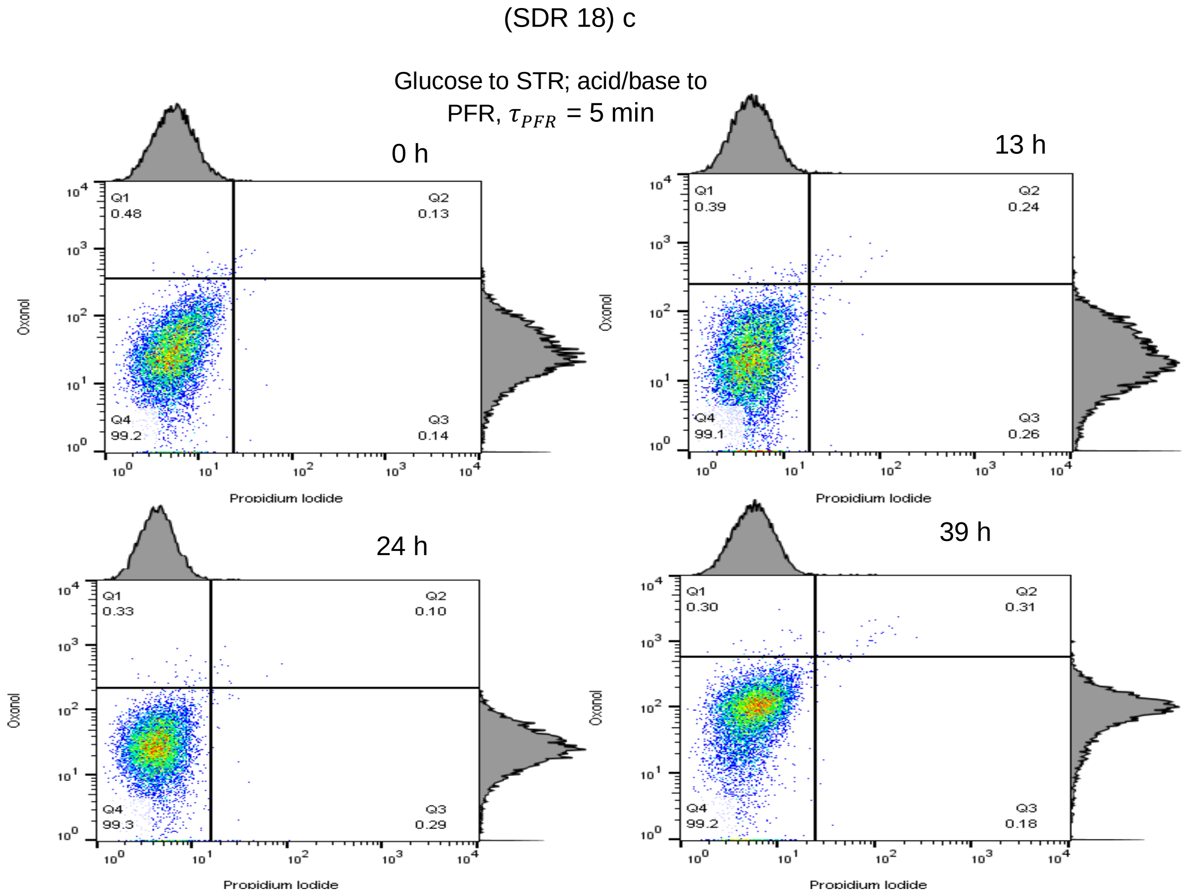

Figure 6.25 a – c Flow cytometer dot plots for SDR 7, 17 and 18 indicating the condition of the cell membrane at different time points during fermentation using the above fluorochromes. Each dot on the plot represents a cell of the 10000 cells interrogated.

SDR 7 (Figure 6.25 a) starts up with a relatively significant depolarised, dead and cell clusters (doublets of the live and dead cell) subpopulation, while the majority of the cells were healthy (93 %). These other subpopulations apart from the Q4 quadrant (healthy cells) persisted up till 24 h. At 39 h, the healthy cell population had increased to 99 %. SDR 17 (Figure 6.25 b) indicated a healthy inoculum; most of the cells were in the Q4 quadrant (98 %). However, by 13 h there was an increase in cells clustering (1 % to 4 %), which decreased from 24 h onwards, and at 39 h the population of healthy cells was almost at 100 %. SDR 18 (Figure 6.25 c) showed a consistently healthy cell population throughout, above 99 % in all timeframes.

(SDR 10) a

Glucose and acid/base to PFR

τ_{PFR} = 1 min

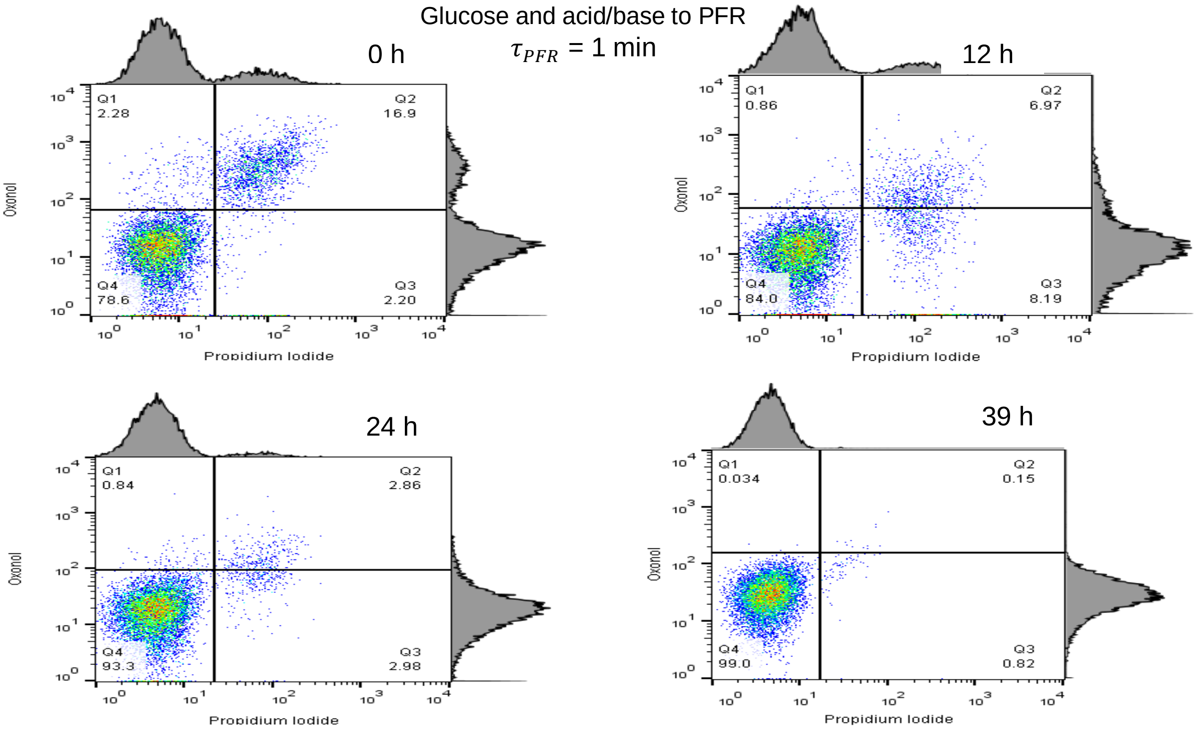

(SDR 19) b

Glucose and acid/base to PFR

τ_{PFR} = 2 min

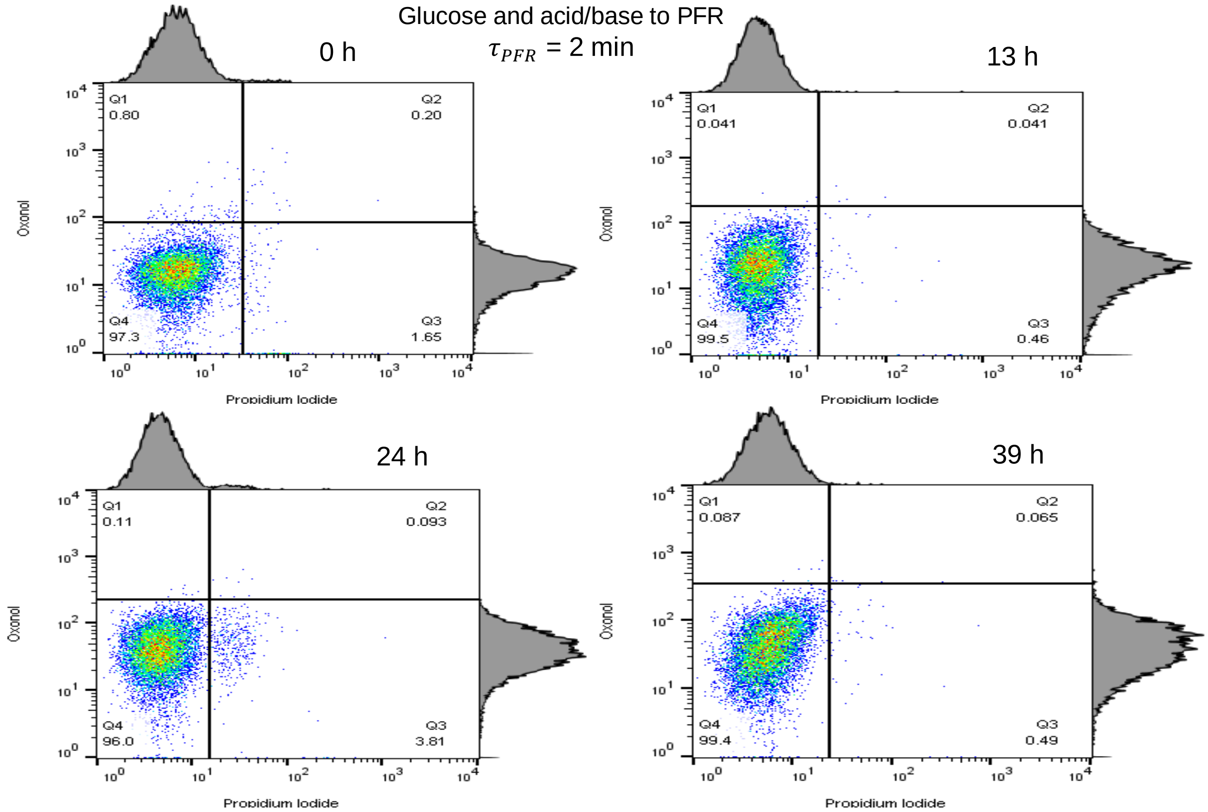

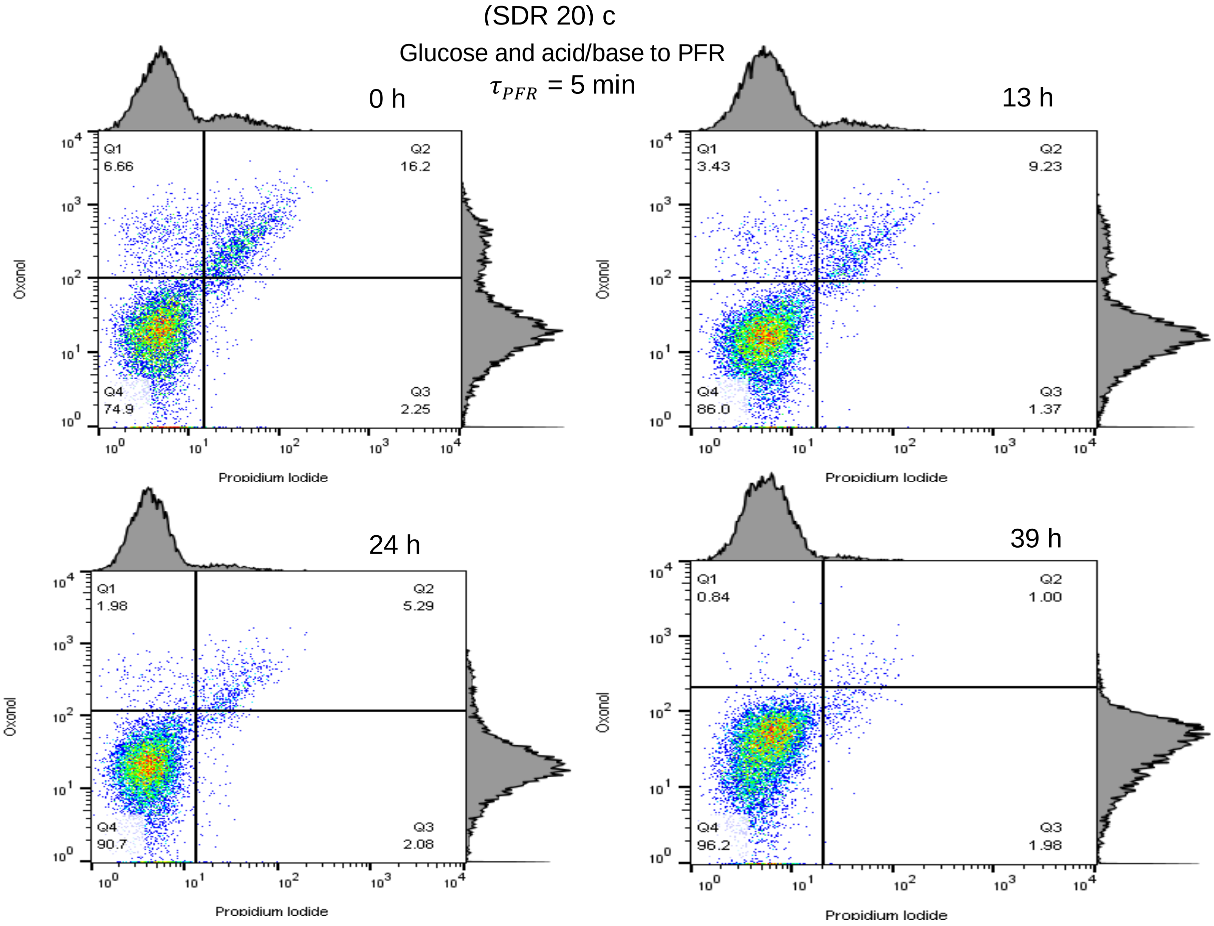

Figure 6.26 a – c Flow cytometer dot plots for SDR 10, 19 and 20 indicating the condition of the cell membrane at different time points during fermentation using the above fluorochromes. Each dot on the plot represents a cell of the 10000 cells interrogated.

SDR 10 (Figure 6.26 a) significant subpopulations at 0 h were in the Q2 (17 %) and Q4 (79 %) quadrants. By 13 h, the number of cells in Q3 quadrants had increased significantly (8 %) as cell clustering increased. However, at 39 h, these subpopulations had resolved into the Q4 (99 %) as the healthy cells outgrew the others. SDR 19 (Figure 6.26 b) started with most of the cells being healthy (97 %), although at 24 h cell clusters were highlighted at 4 %, but by 39 h 99 % of the cell population was healthy. SDR 20 (Figure 6.26 c) inoculum was diverse, reflected in the substantial varied subpopulation seen at 0 h (Q1 = 7 %, Q2 = 16 % and Q4 = 75 %). However, the profile by 39 h also showed an increase to 96 % in the Q4 quadrant (healthy cells) in tandem with other SDRs discussed above.

The general trend from Figure 6.23 to 6.26 showed an increase in healthy cells from start to end of these fermentations regardless of the simulation. The healthy cells at 39 h in all situations reached at least 95 % of the total. In all cases, the cell population heterogeneity was most at the start of the process when the healthy cells ranged from 70 % to 97 %. The inoculum quality has already been highlighted as a significant factor to this variability on start-up. This is especially seen in the flow cytometric analyses of SDR 1, 4, 7, 10, 15 and 20, where there was a substantial dead cell population (Q2 quadrant) at the beginning of these fermentations. The occupation of Q3 signified the presence of cell clusters, which was most likely due to the tendency of *C. glutamicum's* cells to form a V-shaped morphology on attaching to a sister cell (Neumeyer *et al.,* 2013). Thus, a healthy cell attached to a dead sister cell would most likely be segregated to the subpopulation in Q3. However, from these results here, there was no correlation between the prominence of Q3 and the fermentation gradients simulated.

6.8 Cell viability determination by plating

The limitations of this assay have already been highlighted in Chapter 5 and its tendency to underestimate the actual number of viable cells is well documented (Nebe-Von-Caron *et al.,* 2000). Here, this assay was used to evaluate if the cells ability to form colonies on an agar plate were affected by the different SDR environments investigated. An increasing fermentation gradient (for example, localised high glucose concentration) will elicit an increased cell response. Such a cell survives non-ideal conditions by synthesising stabilising compounds to maintain homeostasis, but at a high energy cost. A process which may affect the physiology of the cell. The CFU profiles indicate that the bacterial cells ability to form colonies on solid agar plates declined especially when τ_{PFR} = 5 min (Figure 6.27 a – d). This suggests that highest level of fermentation gradients, which occurred at the τ_{PFR} of 5 min affected the cells most. SDR 14, 16, 18 and 20 all showed the lowest cell count in their group and compared to the control STR only, the losses were 43 %, 51 %, 47 % and 30 % respectively. These differences confirm the decline in CFU as a response to the increased process heterogeneity. Figure 6.27 a – d, captures this trend of decrease in the CFU as the τ_{PFR} increased.

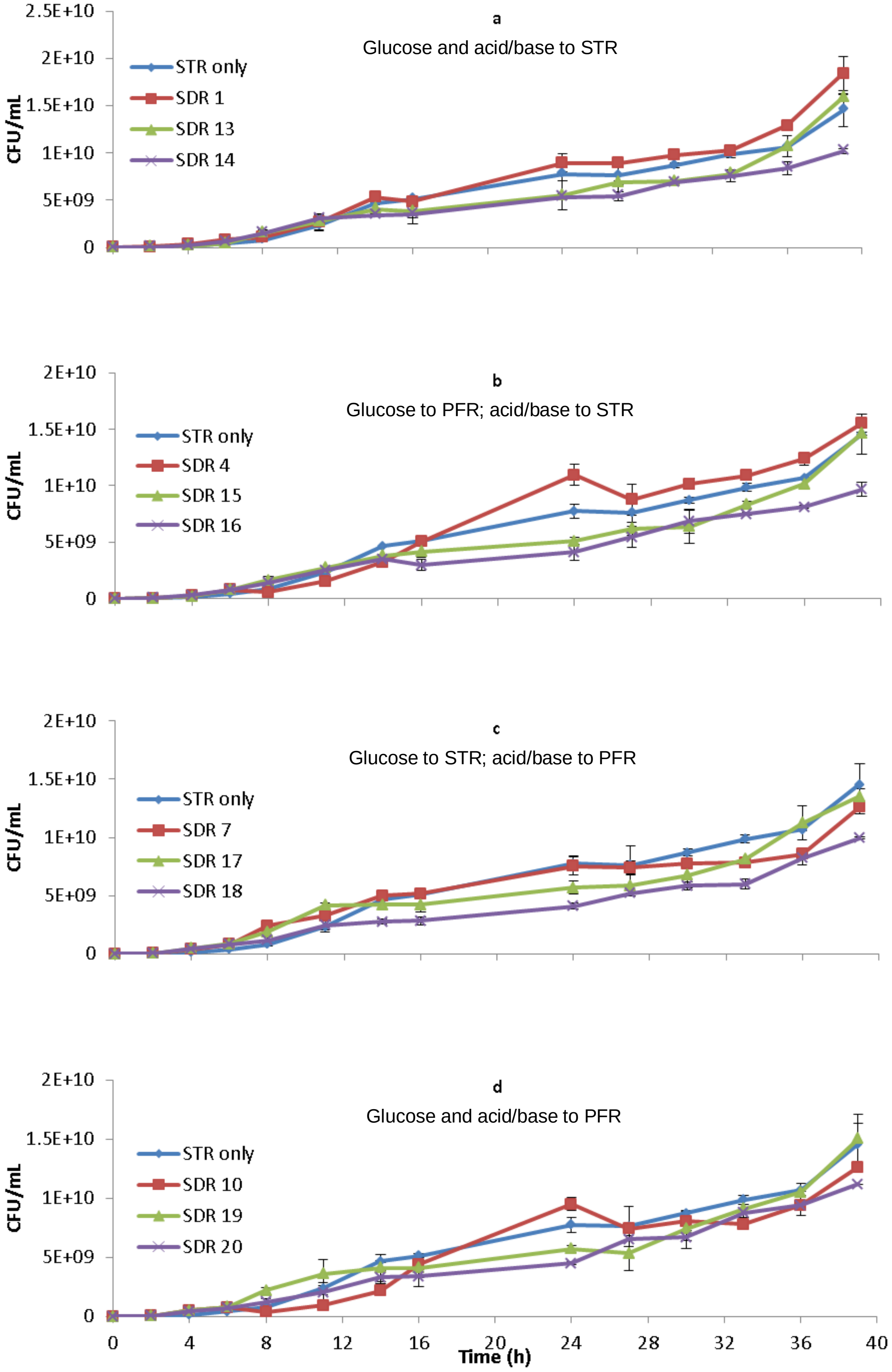

Figure 6.27 a – d CFU profiles, each data point represents the mean values from biological duplicates and the error bars equivalent to their standard deviations.

If the results here are considered with that of the flow cytometric analyses, it can be inferred that the number of viable but non-culturable cells increased as the magnitude of fermentation gradients increased. This is because the flow cytometer indicated that in all cases the broth was predominated by healthy cells at the end, but this did not result in more cells with the ability to form colonies on an agar plate (when τ_{PFR} > 5 min).

The process data logs for sections 6.2 to 6.8 for *C. glutamicum* DM1945x3 fed-batch fermentations can be seen in Appendix 26 to 33.

6.9 Conclusion

In summary, the strategy of keeping f_m constant was achieved by reducing the volume in the STR as the τ_{PFR} was increased. This made the fermentation gradients (DO, pH and glucose concentrations) in the PFR more pronounced and it also reduced the amount of time the cells spent in the well-mixed STR, in contrast to the strategy of Chapter 5. The resulting bacterial cell physiological response saw a 12.5 % decrease in µ when the τ_{PFR} was increased to 5 min. The increase in CO_2 productivity was closely linked to a localised high glucose, τ_{PFR} and limited oxygen environment. The combinations of these factors were highlighted as the major contributors to the decrease in cadaverine productivity observed, as the τ_{PFR} was increased. These results here suggest an inverse relationship between CO_2 productivity and cadaverine production. The carbon balance analyses confirmed this, as it implied that the bacterial cells responded to increasing fermentation gradients by producing more stabilising compounds to maintain internal homoeostasis (with CO_2 as the major side product from these stabilising reactions). The increased production of lactate was also linked to a limited oxygen and high glucose environment, while the flow cytometer and CFU analyses suggested the predominance of viable but non-culturable bacterial cells as the fermentation gradients increased. All these measurements confirm that *C. glutamicum* DM1945x3 did respond to changes in its surroundings and the level of response was a function of the simulated gradient investigated.

CHAPTER 7

7 Conclusion

Understanding how the large-scale environment differs from the bench-scale process development reactor is crucial for a successful bioprocess scale-up. Thus, creating an SDR (to be used within a laboratory) with an environment that successfully mimics the large-scale reactor negates the need for an expensive pilot scale platform. Although the large-scale fed-batch environment is difficult to replicate, with the correct SDR in place, the cost and risk of scaling up would be significantly reduced. Of the current SDR strategies for mimicking the large-scale environment such as the one-compartment, two-compartment and three-compartment reactors have been discussed; the two-compartment SDR achieves the right balance of functionality and relevance hence, its widespread use as a scale-down tool in bioprocess development.

In many commercial bioprocesses, genetic engineering is used to create high performing recombinants to increase productivity, which reduce cost. During the batch fermentation studies reported here, the effect of modifying the lysine producing *C. glutamicum* DM1945 to a cadaverine-producing strain (*C. glutamicum* DM1945x3) highlighted some physiological differences. This was mainly seen by the fact that *C. glutamicum* DM1945x3 had a reduced ability to form colonies on an agar plate, which suggests it is less resilient compared to its parent strain. Also, its level of cadaverine productivity was not commercially viable, indicating a suboptimal product transport system and metabolic pathway.

The feeding profile of all fed-batch process here was set for *C. glutamicum* DM1945x3, such that the specific growth rate was maintained at $\mu \approx 0.1$ h^{-1}. This low µ was selected to ensure that the switch to overflow metabolic pathway, and resulting side product(s) were minimised (Dominguez *et al.,* 1998; Xu *et al.,* 1999). There were two main scale-down strategies employed here in the systematic study of large-scale bioprocess inhomogeneities. The first only increased the τ_{PFR} to increase the magnitude of pH, glucose and dissolved gradients, while the other strategy increased both the τ_{PFR} and reduced the STR volume, to keep f_m constant.

Both strategies used the two-compartment reactor described in Chapter 3 subsection 3.5. Fermentation gradients such as (pH, glucose and dissolved oxygen) were introduced to the two-compartment reactor by varying the feed, pH controlling agent point of entry and the $\tau_{PFR.}$ Thus, the resulting SDR 1 – 12 simulations were used to study the *C. glutamicum* DM1945x3 physiological response to inhomogeneities that are known to occur in large-scale bioreactors. The initial scale-down strategy followed a similar fashion as George, Larsson, and Enfors, (1993); Onyeaka, Nienow, and Hewitt, (2003), where the magnitude of fermentation gradients was increased by only increasing the τ_{PFR}, which also increases the τ_{STR}. It was assumed that by increasing the $\tau_{PFR,}$ (the PFR being the poorly mixed zone) the bacterial cells spending more time in this zone would elicit a stronger physiological response to the simulated fermentation gradients. However, results here were mixed. There was no loss in the DCW productivity for SDR 1 – 12 simulations, which was in agreement with Käß et al., (2014) and Lemoine et al., (2015) where *C. glutamicum*'s DCW resilience to fermentation gradients was also highlighted. The cadaverine productivity differed in this regard, as it was dependent on the simulation conditions, and losses in production were recorded as the τ_{PFR} was increased up to 2 min, after which no further loss was observed, even when the τ_{PFR} was increased to 5 min. The bacterial cells most likely responded to the non-ideal SDR environment, by diverting some energy for cadaverine production to other competitive metabolic pathways to produce stabilising compounds for homeostasis, hence the losses observed (Bylund *et al.,* 1998). The CO_2 productivity increased as the τ_{PFR} increased, confirming the possible switch in metabolic pathways, but for the SDRs with the τ_{PFR} of 2 min and 5 min, the CO_2 productivity remained fairly constant. The carbon balance analyses also implied that the simulations which had a τ_{PFR} of 2 min and 5 min had similar product(s) profile. However, the lactate production profiles were relatively unchanged, regardless of the simulation conditions. The increased in lactate production correlated with the increase in the cell metabolic activity. Thus, the initial rise in lactate accumulation was seen during the exponential growth phase of the batch stage before feeding started and the final accumulation increased when the system reached high cell densities (> 20 gL^{-1} DCW after 33 h). The single-cell analyses (flow cytometry and CFU count) were used to assess how the bacterial cell viability changed throughout a process. One of the key finds highlighted by the flow cytometer was that the subpopulations (depolarised and dead cells) seen at the start of most of the fermentations was due to the inoculum condition at time of harvest. The quality of inoculum could be improved by cultivating the cells in a more controlled environment to ensure that there are no nutrient limitations at time of harvest. Alternatively, the inoculum could be harvested at an earlier time, before nutrient limitations set in the shake flasks. The flow cytometer did not indicate any significant difference when SDRs were compared, but it showed that in all cases investigated the bacterial cells progressively got healthier during fermentation, despite the different fermentation gradients simulated. This indicated that after *C. glutamicum* DM1945x3 adapted to the bioreactor's environment, the population of healthy cells outgrew that of other subpopulations. The CFU count, which measures a cell's ability to form a colony on an agar plate did not vary significantly when the different simulated fermentation gradients were compared. It however showed two different rates of increase in all SDRs:

(1) The start of fermentation to the end of the transition phase (batch to fed-batch phase 0 to 14 h), there was an approximately 1300-fold increase in the CFU count.

(2) The end of the transition phase (14 h) to the end of fermentation only a 3-fold increase was recorded.

These observations indicate that as the fermentation reached high cell densities and the system became limited in glucose, the bacterial cells ability to form colonies declined considerably. If *C. glutamicum* responds to the fed-batch environment by forming clusters as suggested by Käß *et al.*, (2014), then the CFU count towards the end of the process will most likely be underestimated. However, when the analyses of the flow cytometer and CFU are combined, it suggests that the number of healthy but nonculturable cells increased during fermentation. Thus, the decrease in C. glutamicum DM1945x3 CFU counts may be due to the interaction of the predominance of cell clusters and nonculturable, but metabolically active cells.

As already highlighted, changing the magnitude of the fermentation gradients by varying only the τ_{PFR} also affects the τ_{STR}. Hence, an increase in τ_{PFR} will lead to an increase in τ_{STR}, which meant that when the τ_{PFR} was increased from 2 min to 5 min the τ_{STR} also rose 2.5-fold. At the τ_{PFR} of 5 min, the cells were spending 50 min in the well-mixed relative ideal environment of the STR, which might have balanced out the effect of the other ≈ 10 % of cells spending more time in the non-ideal conditions of the PFR section. Thus, increasing the τ_{PFR} alone to increase the magnitude of fermentation gradients in a two-compartment reactor only works up to a point. The new SDR strategy developed here considered the increase in τ_{PFR} concurrently with a decrease in the STR volume to increase the magnitude of gradient experienced by the cells. This ensured that the mean frequency at the which the cells entered the PFR was kept constant, as the τ_{PFR} was varied. The results from this strategy (SDR 1, 4, 7, 10, SDR 13 – 20) indicated a slight reduction in DCW productivity as the τ_{PFR} increased; the μ only showed a decrease from 0.1 h^{-1} to 0.08 h^{-1}. The ease with which *C. glutamicum* switches between the metabolic pathways for biomass formation may be key to its DCW productivity robustness in the face of non-ideal fermentation conditions. The CO_2 production rate increased as the τ_{PFR} was increased. However, the highest amount of CO_2 produced occurred in SDR 16 and 20, i.e. the simulations where the concentrated glucose feed was introduced to the limited oxygen PFR environment. This hinted that to adapt, *C. glutamicum* DM1945x3 may have changed its metabolic pathway to generate ATP as the τ_{PFR} was varied. The calculations from the carbon mole balance estimated that the *C. glutamicum* DM1945x3 product profile changed with the different τ_{PFR} and SDR investigated. It showed that as the τ_{PFR} increased the unidentified carbon containing compounds became longer-chained. This suggests the increase of complex proteins formed to maintain homeostasis, as a response to the non-ideal conditions of the SDRs with the τ_{PFR} of 5 min. Cadaverine productivity was much more affected using this SDR strategy; its value generally decreased as the τ_{PFR} was increased and the greatest loss was seen in simulations where the glucose feed was added in the oxygen limited PFR section. These physiological responses suggest that the longer the τ_{PFR} in a high glucose, limited oxygen environment encourages *C. glutamicum* DM1945x3 to mainly produce ATP via the fermentative pathway, hence reducing the pool of oxaloacetate and consequently decreasing cadaverine production (Kind *et al.,* 2011). The trend of the lactate concentration profile was similar in the STR for all cases. However, in the PFR, lactate gradients were observed, its concentration increased from inlet to exit and the greater the τ_{PFR}, the larger the difference recorded between the inlet and exit concentrations. This confirms that *C. glutamicum* activates its fermentative pathway when exposed to an oxygen limited environment or an oxygen limitation induced by increased metabolic activity due to localised high glucose concentration. Hence, there was an increased production of lactate as the cells travelled along the PFR (Käß *et al.,* 2014). The cell viability showed the same trend in all cases and the flow cytometer analyses indicated that the cell population became healthier as fermentation progressed. However, the CFU count recorded a decline of the cells ability to form colonies on an agar plate; especially in the 5 min τ_{PFR} SDRs where the feed was introduced to the limited oxygen PFR section (SDR 14, 16, 18 and 20). This is a situation, which points to an increase in healthy but nonculturable cells. Also, the formation of cell clusters (which may be one of *C. glutamicum*'s stress response to the glucose limited fed-batch environment) could have contributed to this decrease in the CFU count.

Finally, the answers to some of the questions raised in the first chapter are as follows.

- How does genetic modification affect a bacterial cell? The effect of genetic modification on *C. glutamicum* DM1945 was subtle, most likely due to the direct gene integration modification method used to develop *C. glutamicum* DM1945x3. However, the resulting daughter strain was less resilient compared to its parent. This was observed in its reduced ability to form colonies on an agar plate.

- Do fermentation gradients lead to losses of productivity? If they do, how do changes in the cell result in these losses? The predominance of fermentation gradients due to poor mixing (mimicked by the two-compartment SDR) reduced the bioprocess performance here. A decrease in cadaverine formation by *C. glutamicum* DM1945x3 was observed as environment heterogeneity was increased by the SDR. *C. glutamicum* DM1945x3 adapted to the non-ideal SDR environment by changing its metabolic pathway to produce stabilising compounds. Hence, diverting some of the carbon flux from cadaverine production, resulting in the decline in observed yields.
- Is the magnitude of the cells physiological response related to the type of fermentation gradient(s) simulated? The type of fermentation gradients simulated, and the magnitude had an impact on *C. glutamicum* DM1945x3 growth and product profile. This was seen when the SDRs were compared, for example, glucose gradients had more effect than pH gradients. Also, the longer the cells spent in the oxygen-limited poorly mixed PFR, the larger the loss in cadaverine production.

- How does poor mixing affect the cell population homogeneity and viability? Long mixing times (mimicked by increasing the τ_{PFR}) resulting in the formation of fermentation gradients increased *C. glutamicum* DM1945x3 population of non-culturable, but metabolically active cells.

7.1 Further work

As already highlighted the *C. glutamicum* DM1945x3 strain used in most part of this study was a low cadaverine producer. Other investigators who have transferred the cadaverine-lysine antiporter (*CadB)* from *E.* coli to a lysine decarboxylase carrying *C. glutamicum* strain showed that it improved extracellular cadaverine yields by 73 % (Li *et al.,* 2014a). These studies suggest there may be other undiscovered cadaverine antiporters and competitive pathways, if found and modified, would result in a high cadaverine-producing bacteria strain. This would make cadaverine production from *C. glutamicum* industrially, viable. The new CRISPR technique should be explored to develop a commercially viable *C. glutamicum* cadaverine strain. The intracellular cadaverine concentrations were not measured here, but it is worth exploring to find out if the difference between the internal and external cadaverine concentration is substantial. If it is, it would confirm that more work should be done to improve the cadaverine transport system across the *C. glutamicum* cell membrane or perhaps improve yields by lysing the cells on harvest.

The magnitude of fermentation gradients simulated is a function of the SDR strategy adopted. This was highlighted here as the two different strategies led to a varied *C. glutamicum* physiological response. The ideal SDR would take the strategy of Chapter 6 further by randomly varying the broth recirculation cycle between the PFR and STR, hence varying the τ_{PFR} throughout the course of fermentation. This could be done by using a Monte Carlo function to change the τ_{PFR} in time. Such a strategy would create an SDR closer to the inherently stochastic environment of the large-scale fermenter.

The tracking of a cell lifeline around a reactor is now possible using the cell cycle model, single-cell analytical techniques (flow cytometry, Raman microscopy) and CFD (Fernandes *et al.,* 2011). Kuschel *et al.,* (2017) simulated 120,000 cells of *Pseudomonas putida* KT2440 travel paths, tracked for ≈ 260 s in a 54,000 L STR. Their results indicated that the presence of cell population heterogeneity was a function of the cell path travelled. These types of studies are set to improve, as computational power increases the ability to track more cells for longer times. Thus, more studies need to be undertaken to integrate scale-down fermentation studies to computational modelling work in other to improve the understanding of how the cell population distribution and productivity is affected by the inhomogeneous environment of the large-scale vessel.

The top feed addition fed-batch process was only considered, future work could develop SDR strategies to study large-scale subsurface fed-batch fermentations and the effect on bacterial cells. Also, the investigations here were restricted to studying the effect of chemical gradients on *C. glutamicum* cells; this could be extended to include physical variables, such as temperature and pressure gradients that occur during large-scale high cell density fermentations.

Recently, continuous fermentation has started gaining more prominence in the industry. Although, reduced cost and increased quality are some of the advantages mentioned by some big pharm representatives as reason for its increasing popularity. The tightening rules from regulatory bodies such the US Food and Drug administration agency is more likely the biggest contributor to this change. The current trend indicates that more emphasis is being placed on the QBD approach to bioprocess manufacture. Thus, developing SDR models to mimic the large-scale chemostat is worth pursing and could be an essential tool for studying the continuous fermentation environment.

One powerful analytical tool used here was the flow cytometer, which helped segregate the bacterial cells to three distinct sub-populations (live, depolarised and dead cells). This can be further exploited by using different fluorochromes to differentiate these *C. glutamicum* cells based on the energy levels of their mitochondria during fermentation. Other fluorochromes may also measure the cells ion pumping efficiency to differentiate otherwise unidentified sub-populations. These cell sub-populations could subsequently be sorted based on their distinct properties for microscopic analyses to increase understanding.

References

Adachi, N., Takahashi, C., Ono-Murota, N., Yamaguchi, R., Tanaka, T., & Kondo, A. (2013). Direct L-lysine production from cellobiose by Corynebacterium glutamicum displaying beta-glucosidase on its cell surface. *Applied Microbiology and Biotechnology*, **97**(16), 7165–7172.

Alex, C. (2017). Hydrodynamic Focusing in Flow Cytometry. Retrieved September 29, 2017, from https://bitesizebio.com/32361/hydrodynamic-focusing-flow-cytometry/

Amanullah, A., McFarlane, C. M., Emery, A. N., & Nienow, A. W. (2001). Scale-down model to simulate spatial pH variations in large-scale bioreactors. *Biotechnology and Bioengineering*, **73**(5), 390–9.

Ascanio, G., Castro, B., & Galindo, E. (2004). Measurement of Power Consumption in Stirred Vessels—A Review. *Chemical Engineering Research and Design*, **82**(9), 1282–1290.

Becker, J., & Wittmann, C. (2012). Bio-based production of chemicals, materials and fuels -Corynebacterium glutamicum as versatile cell factory. *Current Opinion in Biotechnology*, **23**(4), 631–40.

Becker, J., Zelder, O., Häfner, S., Schröder, H., & Wittmann, C. (2011). From zero to hero-Design-based systems metabolic engineering of Corynebacterium glutamicum for l-lysine production. *Metabolic Engineering*, **13**(2), 159–168.

Blombach, B., Hans, S., Bathe, B., & Eikmanns, B. J. (2009). Acetohydroxyacid synthase, a novel target for improvement of L-lysine production by Corynebacterium glutamicum. *Applied and Environmental Microbiology*, **75**(2), 419–427.

Boswell, C. D., Nienow, a W., Gill, N. K., Kocharunchitt, S., & Hewitt, C. J. (2003). The impact of fluid mechanical stress on saccharomyces cerevisiae cells during continuous cultivation in an agitated, aerated bioreactor; its implication for mixing in the brewing process and aerobic fermentations, **81**(March).

Bothun, G. D., Knutson, B. L., Berberich, J. a, Strobel, H. J., & Nokes, S. E. (2004). Metabolic selectivity and growth of Clostridium thermocellum in continuous culture under elevated hydrostatic pressure. *Applied Microbiology and Biotechnology*, **65**(2), 149–157.

Buchholz, J., Graf, M., Freund, A., … Takors, R. (2014). CO2/HCO3 perturbations of simulated large scale gradients in a scale-down device cause fast transcriptional responses in Corynebacterium glutamicum. *Applied Microbiology and Biotechnology*, **98**(20), 8563–8572.

Büchs, J. (2001). Introduction to advantages and problems of shaken cultures. *Biochemical Engineering Journal*, **7**(2), 91–98.

Bylund, F., Castan, a., Mikkola, R., Veide, a., & Larsson, G. (2000). Influence of scale-up on the quality of recombinant human growth hormone. *Biotechnology and Bioengineering*, **69**(2), 119–128.

Bylund, F., Collet, E., Enfors, S.-O., & Larsson, G. (1998). Substrate gradient formation in the large-scale bioreactor lowers cell yield and increases by-product formation. *Bioprocess Engineering*, **18**(3), 171.

Calik, P., Yilgor, P., Ayhan, P., & Demir, A. S. (2004). Oxygen transfer effects on recombinant benzaldehyde lyase production. *Chemical Engineering Science*,

59(22-23), 5075–5083.

Chamsartra, S., Hewitt, C., & Nienow, A. (2005). The impact of fluid mechanical stress on Corynebacterium glutamicum during continuous cultivation in an agitated bioreactor. *Biotechnology Letters*, **27**(10), 693–700.

Chavan, V. ., Ford, D. E., & Arumugam, M. (1975). Influence of Fluid Rheology on Circulation,Mixing and Blending. *The Canadian Iournal of Chemical Engineering*, **53**, 628 – 635.

Corran, H. S. (1975). *History of Brewing*, 1st Editio, David & Charles.

Cortés, G., Trujillo-Roldán, M. a., Ramírez, O. T., & Galindo, E. (2005). Production of β-galactosidase by Kluyveromyces marxianus under oscillating dissolved oxygen tension. *Process Biochemistry*, **40**(2), 773–778.

Davey, H. M., & Kell, D. B. (1996). Flow cytometry and cell sorting of heterogeneous microbial populations: the importance of single-cell analyses. *Microbiological Reviews*, **60**(4), 641–96.

Delaunay, S., Gourdon, P., Lapujade, P., … Goergen, J. L. (1999). An improved temperature-triggered process for glutamate production with Corynebacterium glutamicum. *Enzyme and Microbial Technology*, **25**(8-9), 762–768.

Dominguez, H., Rollin, C., Guyonvarch, A., Guerquin-Kern, J. L., Cocaign-Bousquet, M., & Lindley, N. D. (1998). Carbon-flux distribution in the central metabolic pathways of Corynebacterium glutamicum during growth on fructose. *European Journal of Biochemistry*, **254**(1), 96–102.

Eggeling, L., Oberle, S., & Sahm, H. (1998). Improved L-lysine yield with Corynebacterium glutamicum: Use of dapA resulting in increased flux combined with growth limitation. *Applied Microbiology and Biotechnology*, **49**(1), 24–30.

Enfors, S. (2011). Fermentation Process Engineering, 99.

Enfors, S. O., Jahic, M., Rozkov, a, … Manelius, a. (2001). Physiological responses to mixing in large scale bioreactors. *Journal of Biotechnology*, **85**(2), 175–85.

Fernandes, R. L., Nierychlo, M., Lundin, L., … Gernaey, K. V. (2011). Experimental methods and modeling techniques for description of cell population heterogeneity. *Biotechnology Advances*, **29**(6), 575–99.

Follmann, M., Becker, M., Ochrombel, I., Ott, V., Krämer, R., & Marin, K. (2009a). Potassium transport in corynebacterium glutamicum is facilitated by the putative channel protein CglK, which is essential for pH homeostasis and growth at acidic pH. *Journal of Bacteriology*, **191**(9), 2944–2952.

Follmann, M., Ochrombel, I., Krämer, R., … Marin, K. (2009b). Functional genomics of pH homeostasis in Corynebacterium glutamicum revealed novel links between pH response, oxidative stress, iron homeostasis and methionine synthesis. *BMC Genomics*, **10**, 621.

Friehs, K. (2004). Plasmid Copy Number and Plasmid Stability, 47–82.

García, F., Castro, E. G., & Santos, V. E. (2000). Oxygen transfer and uptake rates during xanthan gum production. *Enzyme and Microbial Technology*, **27**(9), 680–690.

Garcia, F., & Gomez, E. (2009). Bioreactor scale-up and oxygen transfer rate in microbial processes: An overview. *Biotechnology Advances*, **27**(2), 153–176.

Garcia, F., Gomez, E., Santos, V. E., & Merchuk, J. C. (2010a). Oxygen uptake rate in microbial processes: An overview. *Biochemical Engineering Journal*, **49**(3), 289–307.

Garcia, F., Gomez, E., Santos, V. E., & Merchuk, J. C. (2010b). Oxygen uptake rate in microbial processes: An overview. *Biochemical Engineering Journal*, **49**(3), 289–307.

George, S., Larsson, G., & Enfors, S.-O. (1993). A scale-down two-compartment reactor with controlled substrate oscillations: Metabolic response of Saccharomyces cerevisiae. *Bioprocess Engineering*, **9**(6), 249–257.

George, S., Larsson, G., Olsson, K., & Enfors, S.-O. (1998). Comparison of the Baker's yeast process performance in laboratory and production scale. *Bioprocess Engineering*, **18**(2), 135–142.

Georgi, T., Rittmann, D., & Wendisch, V. F. (2005). Lysine and glutamate production by Corynebacterium glutamicum on glucose, fructose and sucrose: Roles of malic enzyme and fructose-1,6-bisphosphatase. *Metabolic Engineering*, **7**(4), 291–301.

Gogate, P., Beenackers, A., & Pandit, A. (2000). Multiple-impeller systems with a special emphasis on bioreactors: a critical review. *Biochemical Engineering Journal*, **6**(2), 109–144.

Gray, D. R., Chen, S., Howarth, W., Inlow, D., & Maiorella, B. L. (1996). CO2 in large-scale and high-density CHO cell perfusion culture. *Cytotechnology*, **22**(1-3), 65–78.

Green, E. R., & Mecsas, J. (2016). Bacterial Secretion Systems: An Overview. *Microbiology Spectrum*, **4**(1), 215–239.

Gu, P., Yang, F., Su, T., Wang, Q., Liang, Q., & Qi, Q. (2015). A rapid and reliable strategy for chromosomal integration of gene(s) with multiple copies. *Scientific Reports*, **5**. doi:10.1038/srep09684

Hewitt, C., Boon, L., McFarlane, C., & Nienow, A. (1998). The Use of Flow Cytometry to Study the Impact of Fluid Mechanical Stress on Escherichia coli W3110 During Continuous Cultivation in an Agitated Bioreactor. *Biotechnology Letters*, **27**(10), 612–700.

Hewitt, C. J., & Nienow, A. W. (2007). The scale-up of microbial batch and fed-batch fermentation processes. *Advances in Applied Microbiology*, **62**(07), 105–35.

Hewitt, C., Onyeaka, H., Lewis, G., Taylor, I., & Nienow, A. (2007). A Comparison of High Cell Density Fed-Batch Fermentations Involving Both Induced and Non-Induced Recombinant Escherichia coli Under Well-Mixed Small-Scale and Simulated Poorly Mixed Large-Scale Conditions, **96**(3), 495–505.

Hewitt, C., Von Caron, N., Axelsson, B., McFarlane, C., & Nienow, A. (2000). Studies related to the scale-up of high-cell-density E. coli fed-batch fermentations using multiparameter flow cytometry: effect of a changing microenvironment with respect to glucose and dissolved oxygen concentration. *Biotechnology and Bioengineering*, **70**(4), 381–90.

Hewitt, C., Von Caron, N., Nienow, A., & McFarlane, C. (1999). The use of multi-parameter flow cytometry to compare the physiological response of Escherichia coli W 3110 to glucose limitation during batch, fed-batch and continuous culture cultivations. *Journal of Biotechnology*, **75**(2-3), 251–264.

Hoischen, C., & Kramer, R. (1990). Membrane alteration is necessary but not sufficient for effective glutamate secretion in Corynebacterium glutamicum. *Journal of Bacteriology*, **172**(6), 3409–3416.

Ikeda, M. (2006). Towards bacterial strains overproducing L-tryptophan and other aromatics by metabolic engineering. *Applied Microbiology and Biotechnology*, **69**(6), 615–626.

Inui, M., Suda, M., Okino, S., … Yukawa, H. (2007). Transcriptional profiling of Corynebacterium glutamicum metabolism during organic acid production under oxygen deprivation conditions. *Microbiology*, **153**(8), 2491–2504.

Junne, S., Klingner, A., Kabisch, J., Schweder, T., & Neubauer, P. (2011). A two-compartment bioreactor system made of commercial parts for bioprocess scale-down studies: impact of oscillations on Bacillus subtilis fed-batch cultivations. *Biotechnology Journal*, **6**(8), 1009–17.

Käß, F., Junne, S., Neubauer, P., Wiechert, W., & Oldiges, M. (2014). Process inhomogeneity leads to rapid side product turnover in cultivation of Corynebacterium glutamicum. *Microbial Cell Factories*, **13**(1), 6.

Kawaguchi, H., Verte, A. a, Okino, S., … Mol, J. (2006). Engineering of a xylose metabolic pathway in *Corynebacterium glutamicum*. *Applied and Environmental Microbiology*, **72**(5), 3418–3428.

Kind, S., Jeong, W. K., Schröder, H., Zelder, O., & Wittmann, C. (2010). Identification and elimination of the competing N-acetyldiaminopentane pathway for improved production of diaminopentane by Corynebacterium glutamicum. *Applied and Environmental Microbiology*, **76**(15), 5175–5180.

Kind, S., Kreye, S., & Wittmann, C. (2011). Metabolic engineering of cellular transport for overproduction of the platform chemical 1,5-diaminopentane in Corynebacterium glutamicum. *Metabolic Engineering*, **13**(5), 617–27.

Kind, S., & Wittmann, C. (2011). Bio-based production of the platform chemical 1,5-diaminopentane. *Applied Microbiology and Biotechnology*, **91**(5), 1287–96.

Kinoshita, S., Udaka, S., & Shimono, M. (1957). Studies on the Amino Acid Fermentation. *The Journal of General and Applied Microbiology*, **3**(3), 193–205.

Kuschel, M., Siebler, F., & Takors, R. (2017). Lagrangian Trajectories to Predict the Formation of Population Heterogeneity in Large-Scale Bioreactors. doi:10.3390/bioengineering4020027

Lapin, A., Mu, D., & Reuss, M. (2004). Dynamic Behavior of Microbial Populations in Stirred Bioreactors Simulated with Euler - Lagrange Methods : Traveling along the Lifelines of Single Cells †, (43), 4647–4656.

Lara, A. R., Galindo, E., Ramírez, O. T., & Palomares, L. A. (2006a). Living with heterogeneities in bioreactors: understanding the effects of environmental gradients on cells. *Molecular Biotechnology*, **34**(3), 355–381.

Lara, A. R., Leal, L., Flores, N., Gosset, G., Bolívar, F., & Ramírez, O. T. (2006b). Transcriptional and metabolic response of recombinant Escherichia coli to spatial dissolved oxygen tension gradients simulated in a scale-down system. *Biotechnology and Bioengineering*, **93**(2), 372–385.

Lara Márquez, A., Nguyen, C., Poncin, S., Wild, G., & Midoux, N. (1994). A novel hydrazine oxidation technique for the determination of kLa in gas-liquid and gas-liquid-solid reactors. *Chemical Engineering Science*, **49**(24), 5667–5679.

Larsson, G., & Törnkvist, M. (1996). Rapid sampling, cell inactivation and evaluation of low extracellular glucose concentrations during fed-batch cultivation. *Journal of Biotechnology*, **49**(1-3), 69–82.

Laura, W. (2014a). Glutamic Acid and Monosodium Glutamate (MSG) Market Size, Potential, Industry Outlook, Regional Analysis, Application Development, Competitive Landscape & Forecast, 2016 - 2023. Retrieved September 7, 2016, from https://www.gminsights.com/industry-analysis/glutamic-acid-and-monosodium-glutamate-msg-market-

Laura, W. (2014b). Lysine, Methionine Market Size For Animal Nutrition, Potential, Industry Outlook, Regional Analysis, Application Development, Competitive Landscape & Forecast, 2016 - 2023. Retrieved September 7, 2016, from https://www.gminsights.com/industry-analysis/lysine-methionine-market

Lee, J. W., Kim, H. U., Choi, S., Yi, J., & Lee, S. Y. (2011). Microbial production of building block chemicals and polymers. *Current Opinion in Biotechnology*, **22**(6), 758–767.

Lemoine, A., Maya Martnez-Iturralde, N., Spann, R., Neubauer, P., & Junne, S. (2015a). Response of Corynebacterium glutamicum exposed to oscillating cultivation conditions in a two- and a novel three-compartment scale-down bioreactor. *Biotechnology and Bioengineering*, **112**(6), 1220–1231.

Lemoine, A., Maya Martínez-Iturralde, N., Spann, R., Neubauer, P., & Junne, S. (2015b). Response of Corynebacterium glutamicum exposed to oscillating cultivation conditions in a two- and a novel three-compartment scale-down bioreactor. *Biotechnology and Bioengineering*, **9999**, 1–12.

Li, M., Li, D., Huang, Y., … Lu, F. (2014a). Improving the secretion of cadaverine in Corynebacterium glutamicum by cadaverine-lysine antiporter. *Journal of Industrial Microbiology and Biotechnology*, **41**(4), 701–709.

Li, Z., Nimtz, M., & Rinas, U. (2014b). The metabolic potential of Escherichia coli

BL21 in defined and rich medium, 1–17.

Limberg, M. H., Pooth, V., Wiechert, W., & Oldiges, M. (2016a). Plug flow vs. stirred tank reactor flow characteristics in two compartment scale down bioreactor: Setup specific influence on the metabolic phenotype and bioprocess performance of *Corynebacterium glutamicum*. *Engineering in Life Sciences*, **35**(19), 1–10.

Limberg, M. H., Schulte, J., Aryani, T., … Oldiges, M. (2016b). Metabolic profile of 1,5-diaminopentane producing Corynebacterium glutamicum under scale-down conditions: Blueprint for robustness to bioreactor inhomogeneities. *Biotechnology and Bioengineering*, **114**(3), 560–575.

Lin, H. Y., & Neubauer, P. (2000). Influence of controlled glucose oscillations on a fed-batch process of recombinant Escherichia coli. *Journal of Biotechnology*, **79**(1), 27–37.

Litsanov, B., Brocker, M., & Bott, M. (2012a). Efficient aerobic succinate production from glucose in minimal medium with Corynebacterium glutamicum. *Microbial Biotechnology*, **5**(1), 116–128.

Litsanov, B., Brocker, M., & Bott, M. (2012b). Toward homosuccinate fermentation: Metabolic engineering of Corynebacterium glutamicum for anaerobic production of succinate from glucose and formate. *Applied and Environmental Microbiology*, **78**(9), 3325–3337.

Lorantfy, B., Jazini, M., & Herwig, C. (2013). Investigation of the physiological response to oxygen limited process conditions of Pichia pastoris Mut(+) strain using a two-compartment scale-down system. *Journal of Bioscience and Bioengineering*, **116**(3), 371–9.

Marques, M. P. C., Cabral, J. M. S., & Fernandes, P. (2010). Bioprocess scale-up: Quest for the parameters to be used as criterion to move from microreactors to lab-scale. *Journal of Chemical Technology and Biotechnology*, **85**(9), 1184–1198.

Marquet, M., Uribelarrea, J. L., Huchenq, A., Laneelle, G., & Goma, G. (1986). Glutamate excretion by Corynebacterium ylutamicum: a study of glutamate accumulation during a fermentation course, 220–223.

Michel, B. J., & Miller, S. a. (1962). Power requirements of gas-liquid agitated systems. *AIChE Journal*, **8**(2), 262–266.

Mimitsuka, T., Sawai, H., Hatsu, M., & Yamada, K. (2007). Metabolic engineering of Corynebacterium glutamicum for cadaverine fermentation. *Bioscience, Biotechnology, and Biochemistry*, **71**(9), 2130–2135.

Nakamura, J., Hirano, S., Ito, H., & Wachi, M. (2007). Mutations of the Corynebacterium glutamicum NCgl1221 gene, encoding a mechanosensitive channel homolog, induce L-glutamic acid production. *Applied and Environmental Microbiology*, **73**(14), 4491–4498.

Namdev, P. K., Irwin, N., Thompson, B. G., & Gray, M. R. (1993). Effect of Oxygen Fluctuations on Recombinant Escherichia coli Fermentation, **41**, 666–670.

Namdev, P. K., P, Y., Murray, G., & B, T. (1991). Experimental simulation of large-scale bioreactor environments using Monte Carlo method. *Canadian Journal of Chemical Engineering*, **69**(2), 513–519.

Nebe-Von-Caron, G., Stephens, P. J., Hewitt, C. J., Powell, J. R., & Badley, R. a. (2000). Analysis of bacterial function by multi-colour fluorescence flow cytometry and single cell sorting. *Journal of Microbiological Methods*, **42**(1), 97–114.

Neubauer, P., Åhman, M., Törnkvist, M., Larsson, G., & Enfors, S. O. (1995a). Response of guanosine tetraphosphate to glucose fluctuations in fed-batch cultivations of Escherichia coli. *Journal of Biotechnology*, **43**(3), 195–204.

Neubauer, P., Haggstrom, L., & Enfors, S. . (1995b). Influence of substrate oscillations on acetate formation and growth yield in Escherichia coli glucose limited fed -batch cultivations. *Biotechnology and Bioengineering*, **47**(2), 139–146.

Neumeyer, A., Hübschmann, T., Müller, S., & Frunzke, J. (2013). Monitoring of population dynamics of Corynebacterium glutamicum by multiparameter flow cytometry. *Microbial Biotechnology*, **6**(2), 157–167.

Niimi, S., Suzuki, N., Inui, M., & Yukawa, H. (2011). Metabolic engineering of 1,2-propanediol pathways in Corynebacterium glutamicum. *Applied Microbiology and Biotechnology*, **90**(5), 1721–1729.

Noorman, H. (2011). An industrial perspective on bioreactor scale-down: what we can learn from combined large-scale bioprocess and model fluid studies. *Biotechnology Journal*, **6**(8), 934–43.

Nunheimer, T. D., Birnbaum, J., Ihnen, E. D., & Demain, A. L. (1970). Product inhibition of the fermentative formation of glutamic acid. *Applied Microbiology*, **20**(2), 215–217.

Oh, S. K. W., Nienow, a. W., Al-Rubeai, M., & Emery, a. N. (1989). The effects of agitation intensity with and without continuous sparging on the growth and antibody production of hybridoma cells. *Journal of Biotechnology*, **12**(1), 45–62.

Okino, S., Noburyu, R., Suda, M., Jojima, T., Inui, M., & Yukawa, H. (2008). An efficient succinic acid production process in a metabolically engineered Corynebacterium glutamicum strain. *Applied Microbiology and Biotechnology*, **81**(3), 459–64.

Oktyabrskii, O. N., & Smirnova, G. V. (2012). Redox potential changes in bacterial cultures under stress conditions. *Microbiology*, **81**(2), 131–142.

Oldshue, J. Y. (1966). Fermentation mixing scale-up techniques. *Biotechnology and Bioengineering*, **8**(1), 3–24.

Oliver, J. D. (1993). Formation of Viable but Nonculturable Cells. In *Starvation in Bacteria*, Boston, MA: Springer US, pp. 239–272.

Onyeaka, H., Nienow, A., & Hewitt, C. (2003). Further studies related to the scale-up of high cell density Escherichia coli fed-batch fermentations: the additional effect of a changing microenvironment when using aqueous ammonia to control pH. *Biotechnology and Bioengineering*, **84**(4), 474–84.

Oosterhuis, N. M., Kossen, N. W., Olivier, A. P., & Schenk, E. S. (1984). Scale-down and optimization studies of the gluconic acid fermentation by Gluconobacter oxydans. *Biotechnology and Bioengineering*, **27**(5), 711–720.

Palomares, L. A., & Ramirez, O. T. (2009). Bioreactor scale-up. *Encyclopedia of Industrial Biotechnology: Bioprocess, Bioseparation, and Cell Technology*, 1–17.

Pedersen, A. G., Andersen, H., Nielsen, J., & Villadsen, J. (1994). A novel technique based on 85Kr for quantification of gas-liquid mass transfer in bioreactors. *Chemical Engineering Science*, **49**(6), 803–810.

Pirt, S. (1975). *Principles of microbe and cell cultivation*, Blackwell Scientific.

Puech, V., Chami, M., Lemassu, A., … Daffé, M. (2001). Structure of the cell envelope of corynebacteria: Importance of the non-covalently bound lipids in the formation of the cell wall permeability barrier and fracture plane. *Microbiology*, **147**(5), 1365–1382.

Reisman, H. B. (1993). Problems in scale-up of biotechnology production processes. *Critical Reviews in Biotechnology*, **13**(3), 195–253.

Restek. (2016). Amino Acids (9-Fluorenylmethyl-Chloroformate Derivatives) on Raptor^{TM} ARC-18. Retrieved September 20, 2016, from http://www.restek.com/chromatogram/view/LC_FF0539/56-87-1

Rittmann, D., Lindner, S. N., & Wendisch, V. F. (2008). Engineering of a glycerol utilization pathway for amino acid production by Corynebacterium glutamicum. *Applied and Environmental Microbiology*, **74**(20), 6216–6222.

Sandoval, E. a, Gosset, G., Bolívar, F., & Ramírez, O. T. (2005). Culture of Escherichia coli under dissolved oxygen gradients simulated in a two-compartment scale-down system: metabolic response and production of recombinant protein. *Biotechnology and Bioengineering*, **89**(4), 453–63.

Saxena, R. K., Anand, P., Saran, S., Isar, J., & Agarwal, L. (2010). Microbial production and applications of 1,2-propanediol. *Indian Journal of Microbiology*, **50**(1), 2–11.

Schilling, B., Pfefferle, W., Bachmann, B., Leuchtenberger, W., & Deckwer, W. (1999). A special reactor design for investigations of mixing time effects in a scaled-down industrial L-lysine fed-batch fermentation process. *Biotechnology and Bioengineering*, **64**(5), 599–606.

Schmidt, F. R. (2005). Optimization and scale up of industrial fermentation processes. *Applied Microbiology and Biotechnology*, **68**(4), 425–35.

Schweder, T., Krüger, E., Xu, B., … Hecker, M. (1999). Monitoring of genes that respond to process-related stress in large- scale bioprocesses. *Biotechnology and Bioengineering*, **65**(2), 151–159.

Serpaggi, V., Remize, F., Recorbet, G., Gaudot-Dumas, E., Sequeira-Le Grand, A., & Alexandre, H. (2012). Characterization of the viable but nonculturable (VBNC) state in the wine spoilage yeast Brettanomyces. *Food Microbiology*, **30**, 438–447.

Siebert, D., & Wendisch, V. F. (2015). Metabolic pathway engineering for production of 1,2-propanediol and 1-propanol by Corynebacterium glutamicum. *Biotechnology for Biofuels*, **8**, 91.

SpecialChem. (2014). Global Demand for Bio-succinic Acid to Reach 593,400 Tons by 2020: Grand View Research. Retrieved October 13, 2016, from http://coatings.specialchem.com/news/industry-news/global-demand-for-bio-succinic-acid-to-reach-593-400-tons-by-2020-grand-view-research

Stanbury, P. F., Whitaker, A., & Hall, S. J. (1999). *Principles of Fermentation Technology*.

Suarez-Mendez, C., Sousa, A., Heijnen, J., & Wahl, A. (2014). Fast "Feast/Famine" Cycles for Studying Microbial Physiology Under Dynamic Conditions: A Case Study with Saccharomyces cerevisiae. *Metabolites*, **4**(2), 347–372.

Sweere, A. P. J., Janse, L., & Kossen, N. W. F. (1988). Experimental Simulation of Oxygen Profiles and Their Influence on Baker's Yeast Production: II. Two-

Fermentor System. *Biotechnology and Bioengineering*, **586**, 579–586.

Takors, R. (2012). Scale-up of microbial processes: impacts, tools and open questions. *Journal of Biotechnology*, **160**(1-2), 3–9.

Thielen, M. (2010, May). Bio-polyamides for automotive applications. *Bioplastics, MAGAZINE*, 10–11.

Toma, M. K., Ruklisha, M. P., Vanags, J. J., … Tengerdy, R. P. (1991). Inhibition of microbial growth and metabolism by excess turbulence. *Biotechnology and Bioengineering*, **38**(5), 552–556.

Trevors, J. T. (2011). Viable but non-culturable (VBNC) bacteria: Gene expression in planktonic and biofilm cells. *Journal of Microbiological Methods*, **86**(2), 266–273.

Vallino, J. J., & Stephanopoulos, G. (1992). Metabolic flux distributions in Corynebacterium glutamicum during growth and lysine overproduction. *Biotechnology and Bioengineering*, **41**(6), 633–646.

Van Ooyen, J., Noack, S., Bott, M., & Eggeling, L. (2013). Proline addition increases the efficiency of l-lysine production by Corynebacterium glutamicum. *Engineering in Life Sciences*, **13**(4), 393–398.

Van't Riet, K. (1979). Review of Measuring Methods and Results in Nonviscous Gas-Liquid Mass Transfer in Stirred Vessels. *Industrial & Engineering Chemistry Process Design and Development*, **18**(3), 357–364.

Vrabel, P., Van Der Lans, R. G. J. M., Luyben, K. C. A. M., Boon, L., & Nienow, A. W. (2000). Mixing in large-scale vessels stirred with multiple radial or radial and axial up-pumping impellers: Modelling and measurements. *Chemical Engineering Science*, **55**(23), 5881–5896.

Want, A., Hancocks, H., Thomas, C. R., Stocks, S. M., Nebe-von-Caron, G., & Hewitt, C. J. (2011). Multi-parameter flow cytometry and cell sorting reveal extensive physiological heterogeneity in Bacillus cereus batch cultures. *Biotechnology Letters*, **33**(7), 1395–1405.

Wieschalka, S., Blombach, B., Bott, M., & Eikmanns, B. J. (2013). Bio-based production of organic acids with Corynebacterium glutamicum. *Microbial Biotechnology*, **6**(2), 87–102.

Xu, B., Jahic, M., & Blomsten, G. (1999). Glucose overflow metabolism and mixed-acid fermentation in aerobic large-scale fed-batch processes with Escherichia coli, 564–571.

Yu, L. X. (2008). Pharmaceutical Quality by Design: Product and Process Development, Understanding, and Control. *Pharmaceutical Research*, **4**(2), 781–791.

Zhu, N., Xia, H., Wang, Z., Zhao, X., & Chen, T. (2013). Engineering of Acetate Recycling and Citrate Synthase to Improve Aerobic Succinate Production in Corynebacterium glutamicum. *PLoS ONE*, **8**(4). doi:10.1371/journal.pone.0060659

Appendices

Appendix 1

An overview of the Sartorius Biostat B plus design and dimensions

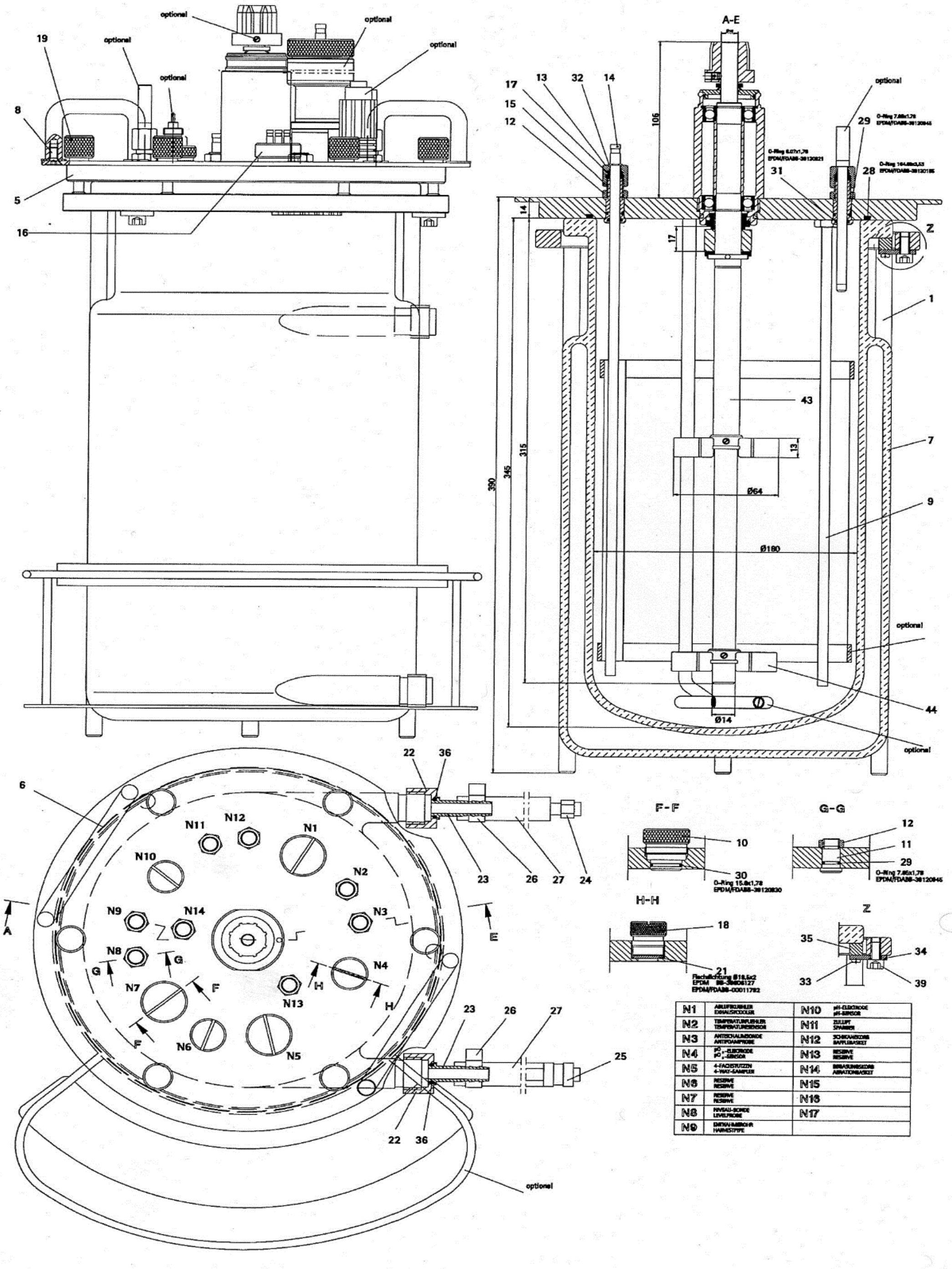

Figure 1, Biostat B plus double jacketed vessel and head plate dimensions

Ref.	Pcs.	Item	Description	Cat.-no
41	-	Coupling magnetic	1 Nm, 200 W, option	8847339
42	-	Coupling magnetic	1 Nm, 400 W, option	8847231
43	-	Stirrer shaft, kit 5 L	5 L, Ø 14- L = 315	8847355
44	-	6-blade disk impeller	Ø 64/14 H7	8847371
45	-	3 blade segment stirrer, adjustable	Ø 70/14 H7	8847401
46	-	Baffle basket, 5 L vessel		8846820
47	-	Sparger, kit, 5 L vessel		8846855
48	-	Sparger, 5 L vessel		38807779
49	-	Aeration basket, 5 L vessel		8848017
51	-	Exhaust cooler	B 5	38846880
52	-	Support exhaust cooler		8844593
53	-	Sterile filter	Midisart 2000	8810079
54	-	Exhaust fitting, kit	M10 x 1- Ø10.95/6-4	8807809
55	-	Exhaust fitting, kit	M10 x 1- Ø10.95/8.5	8807817
56	-	Inoculation port, kit	M10 x 1	8844631
57	-	Inoculation port	Ø 19- M26 x 1	8840601
58	-	1-Channel inoculation set	19/6, MD/B	8840610
59	-	Manual sampler		8844623
60	-	Bypass sampler	M26 x 1-Ø4	8844348
61	-	Harvest pipe 5 L	5 L	38807892
62	-	Sampling pipe 5 L	5 L	38807868
63	-	Spinfilter, 5 L vessel	L = 180; mesh 20 µm, Ø58/14	8847452
64	-	Spinfilter, 5 L vessel	L = 180; mesh 40 µm, Ø58/14	8847460
65	-	Spinfilter, 5 L vessel	L = 180; mesh 75 µm, Ø58/14	8847487
66	-	Draft tube, kit, for spinfilter	for 5 L vessel	38808279
67	-	Sampling pipe for spinfilter	for 5 L vessel	38840660
69	-	Storage bottle	500 ml	38823618
74	-	Redox-electrode, kit	MD/B 5,	8844194
75	-	Antifoam-electrode, kit	L 80/M 10	38844461
76	-	Level probe, kit	L 150/M10x1	8844488
77	-	Turbidity sensor, gap 1.5	10/1,5	8845638
78	-	Turbidity sensor, gap 3.0	10/3,0	8845646
79	-	Pt 100 pocket, kit	Ø 8/6.5- M10x1-310 lg	8848165
80	-	pH-electrode, kit, Hamilton*)	EF-Set 12/325/2 K8-HM	8837243
82	-	p02-electrode, kit, Hamilton*)	Set-12/325/2-L-HM	8837233

*) Electrodes manufactured by Mettler-Toledo are optionally available, on request

Appendix 2

An overview of the plug flow reactor design and dimensions

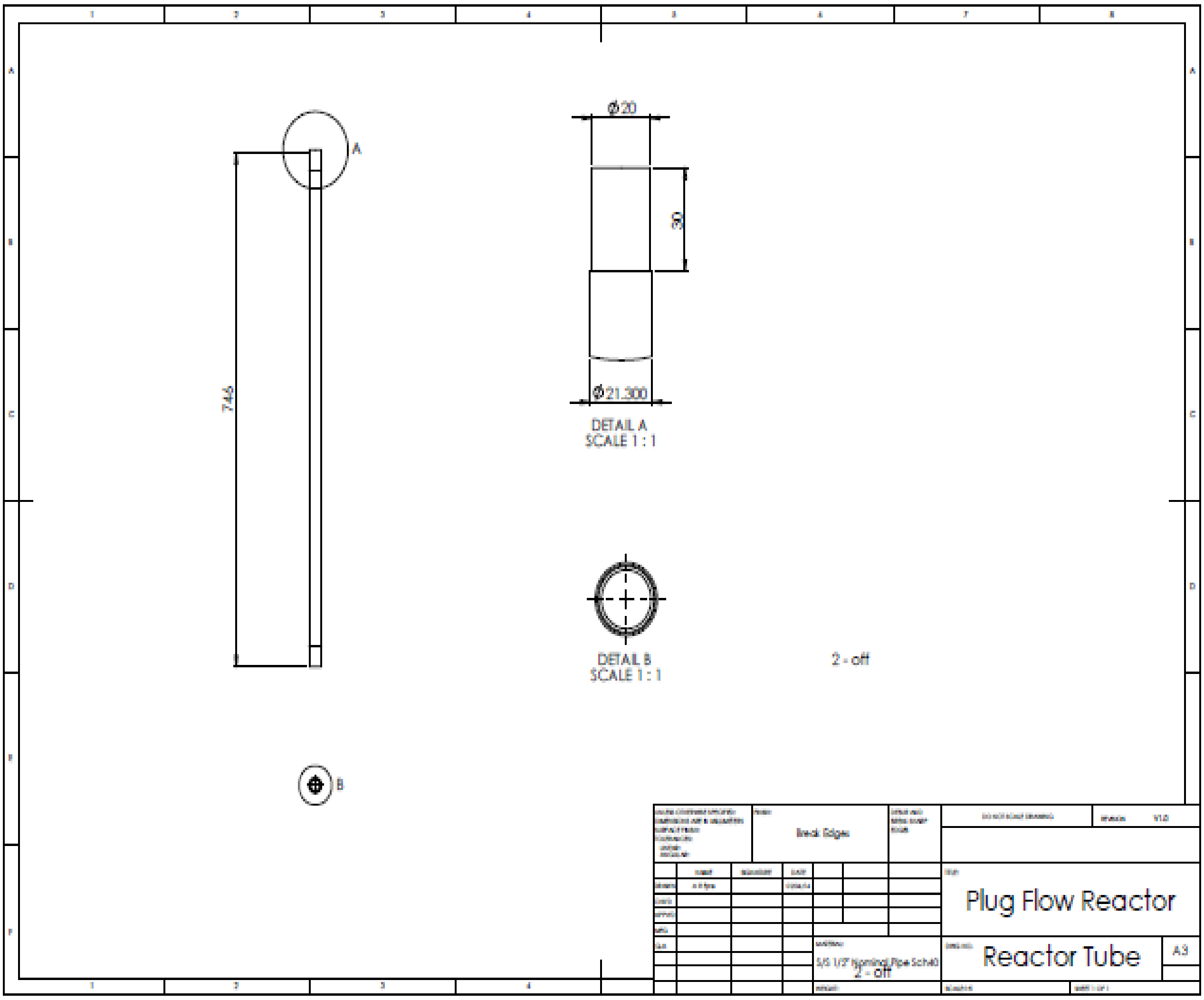

Figure 2, PFR tubular section dimensions

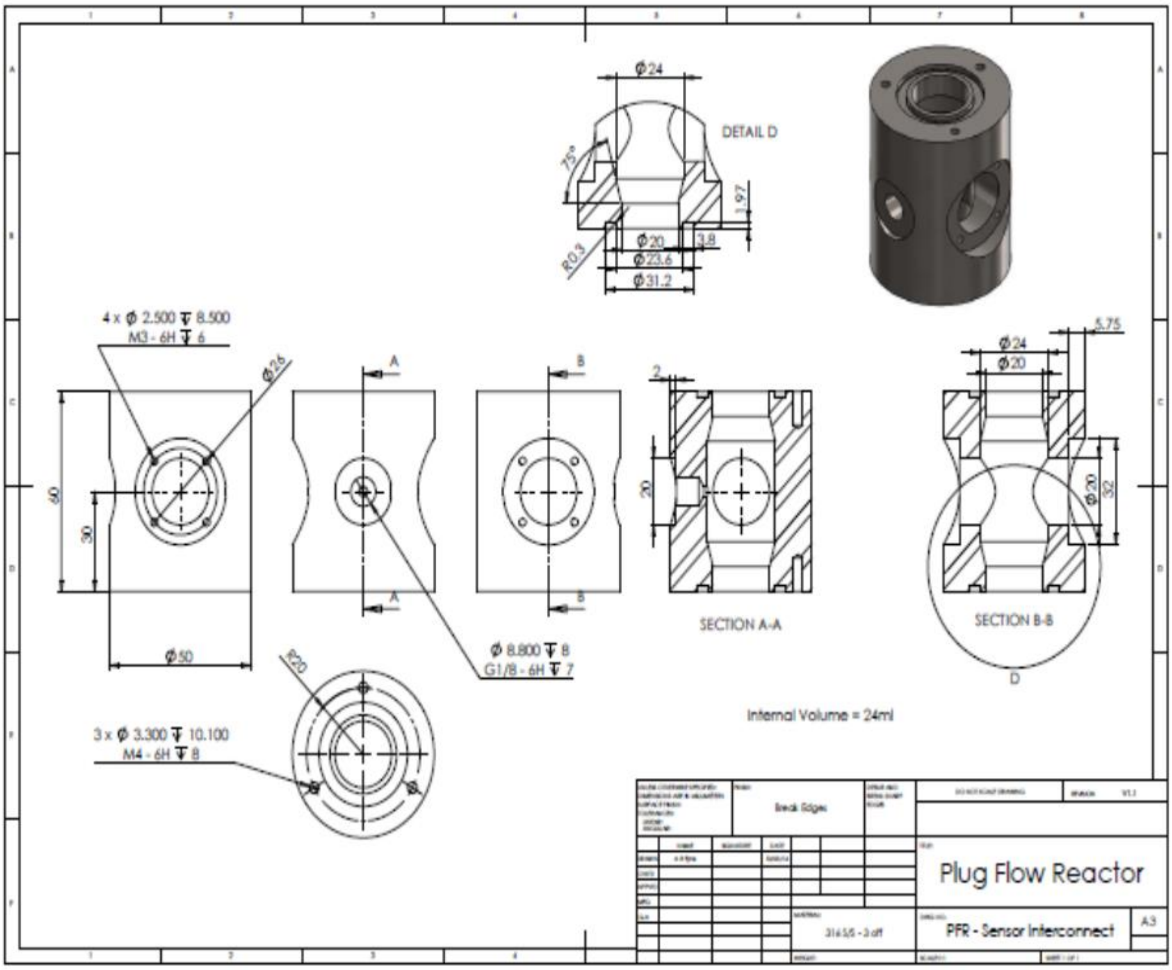

Figure 3, PFR interconnector dimensions

Appendix 2 describes the dimensions of the plug flow reactor, which was designed inhouse. Figure 2 shows the design of the tubular section; they were two in total connected by three interconnectors. Figure 3 shows the internal dimensions of the interconnectors, which connected the tubular sections and housed the pH and DOT sensors.

Appendix 3

Process log for *C. glutamicum* DM1945 batch fermentation

Time (h)	Lysine (g/L)	Glucose (g/L)	CFU/ml	DCW (g/L)	Lactate (g/L)
0	0.00	10	6.0E+08	0.02	0.00
2	0.012	9.4	1.2E+08	0.08	0.0060
4	0.0016	8.5	3.0E+08	0.56	0.0050
6	0.062	7.2	8.8E+08	0.82	0.0080
8	0.11	3.8	2.0E+09	2.0	0.0012
11	0.87	0.040	4.0E+09	4.4	0.011
14	0.88	0.070	4.5E+09	4.6	0.0090
16	0.90	0.040	5.0E+09	4.6	0.0070
24	0.90	0.020	4.9E+09	4.4	0.0066

Table 1 C. glutamicum DM1945 offline measurements in run 1

Time (h)	Lysine (g/L)	Glucose (g/L)	CFU/ml	DCW (g/L)	Lactate (g/L)
0	0.00	10	2.0E+07	0.02	0.00
2	0.011	9.2	7.8E+07	0.15	0.011
4	0.017	7.9	1.2E+08	0.38	0.017
6	0.077	6.5	8.7E+08	0.84	0.077
8	0.15	3.6	2.3E+09	2.4	0.15
11	0.80	0.59	4.7E+09	4.3	0.80
14	0.90	0.050	4.9E+09	4.9	0.90
16	0.90	0.060	5.2E+09	4.6	0.90
24	0.95	0.060	5.3E+09	4.8	0.95

Table 2 C. glutamicum DM1945 Offline measurements in run 2

Time (h)	Lysine (g/L)	Glucose (g/L)	CFU/ml	DCW (g/L)	Lactate (g/L)
0	0.00	10	5.6E+07	0.05	0.00
2	0.011	9.3	1.1E+08	0.29	0.029
4	0.013	8.0	3.4E+08	0.34	0.027
6	0.057	6.9	9.2E+08	0.50	0.038
8	0.094	3.8	2.2E+09	2.6	0.080
11	0.75	0.020	4.1E+09	4.2	0.079
14	0.80	0.010	4.6E+09	4.6	0.078
16	0.83	0.020	4.4E+09	4.7	0.077
24	0.85	0.020	4.7E+09	4.6	0.055

Table 3 C. glutamicum DM1945 offline measurements in run 3

Appendix 3 highlights the offline data measurements of samples taken during triplicate batch fermentations of the lysine producing *C. glutamicum* DM1945 strain (Table 1 – 3).

Appendix 4

Process log for *C. glutamicum* DM1945x3 batch fermentation

Time (h)	Cadaverine (g/L)	Glucose (g/L)	CFU/ml	DCW (g/L)	Lactate (g/L)
0	0.00	10	3.9E+06	0.04	0.00
2	0.024	9.4	7.8E+07	0.13	0.026
4	0.028	9.0	1.8E+08	0.46	0.027
6	0.037	8.5	3.8E+08	0.79	0.036
8	0.061	6.9	1.0E+09	1.3	0.035
11	0.31	2.2	1.9E+09	3.2	0.061
14	0.42	0.040	3.5E+09	4.5	0.020
16	0.44	0.020	3.6E+09	4.3	0.020
24	0.48	0.020	3.9E+09	4.1	0.023

Table 4 C. glutamicum DM1945x3 Offline measurements in run 1

Time (h)	Cadaverine (g/L)	Glucose (g/L)	CFU/ml	DCW (g/L)	Lactate (g/L)
0	0.00	10	1.0E+07	0.03	0.00
2	0.00050	9.8	6.1E+07	0.16	0.027
4	0.013	9.3	1.8E+08	0.52	0.024
6	0.027	8.5	2.4E+08	0.90	0.021
8	0.059	6.8	4.2E+08	1.9	0.029
11	0.24	2.4	2.5E+09	3.7	0.051
14	0.44	0.080	4.1E+09	4.1	0.023
16	0.41	0.050	4.5E+09	4.3	0.026
24	0.50	0.040	4.5E+09	4.3	0.027

Table 5 C. glutamicum DM1945x3 Offline measurements in run 2

Time (h)	Cadaverine (g/L)	Glucose (g/L)	CFU/ml	DCW (g/L)	Lactate (g/L)
0	0.0088	10	1.5E+07	0.02	0.00
2	0.021	9.5	6.8E+07	0.08	0.016
4	0.032	8.7	2.2E+08	0.21	0.024
6	0.051	7.5	5.3E+08	0.77	0.021
8	0.059	6.2	9.3E+08	1.9	0.034
11	0.29	2.0	3.3E+09	3.8	0.043
14	0.39	0.080	4.5E+09	4.2	0.019
16	0.36	0.090	4.8E+09	4.4	0.016
24	0.43	0.070	4.3E+09	4.4	0.015

Table 6 C. glutamicum DM1945x3 Offline measurements in run 3

Appendix 4 highlights the offline data measurements of samples taken during triplicate batch fermentations of the cadaverine producing *C. glutamicum* DM1945x3 strain (Table 4 – 6).

Appendix 5

Process concentration profiles for SDR 2 during *C. glutamicum* DM1945x3 fed-batch fermentation

In SDR 2, the cell broth mixtures were recirculated between the STR and PFR. The addition of feed (mainly containing glucose and trace elements), air and the pH controlling agent (NH_4OH) were introduced in the STR, while the τ_{PFR} was 2 min.

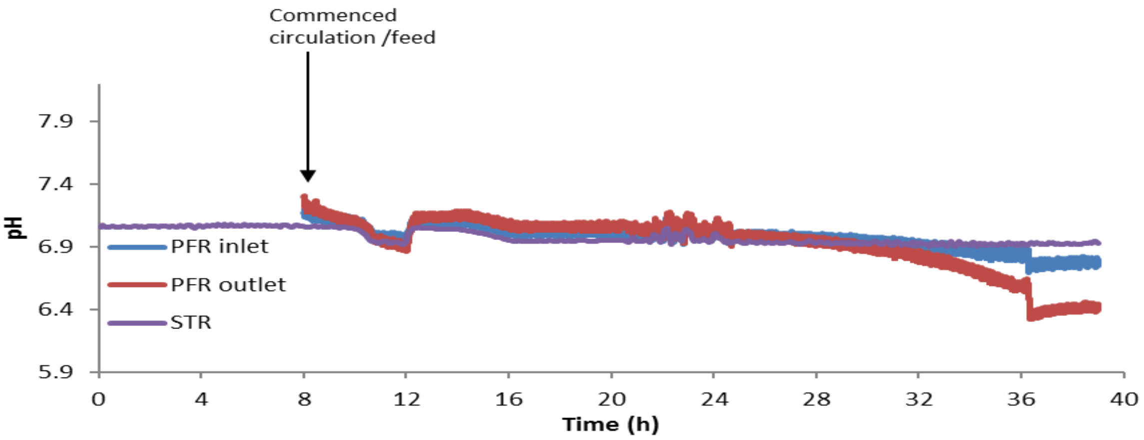

Figure 4 pH profiles at the PFR inlet/outlet and the STR for SDR 2

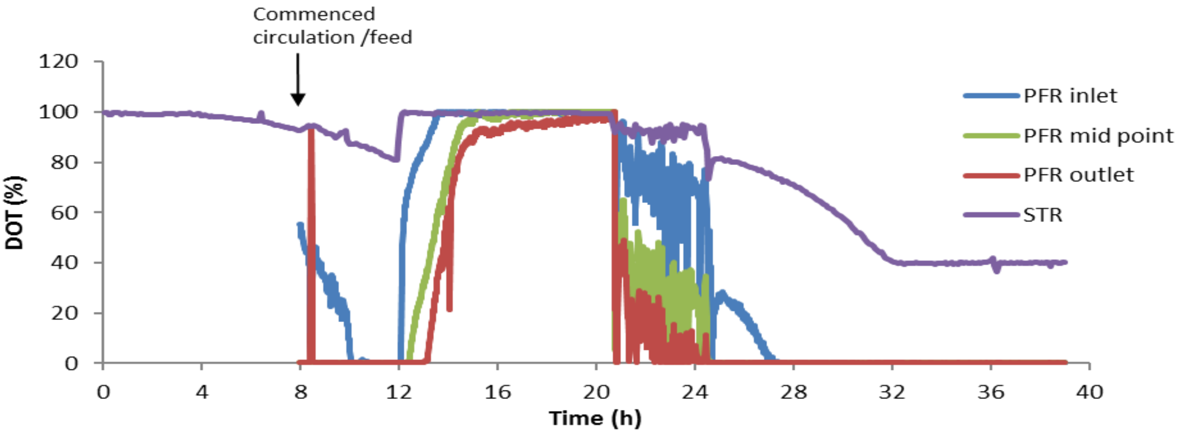

Figure 5 Dissolved oxygen tension profiles across SDR 2

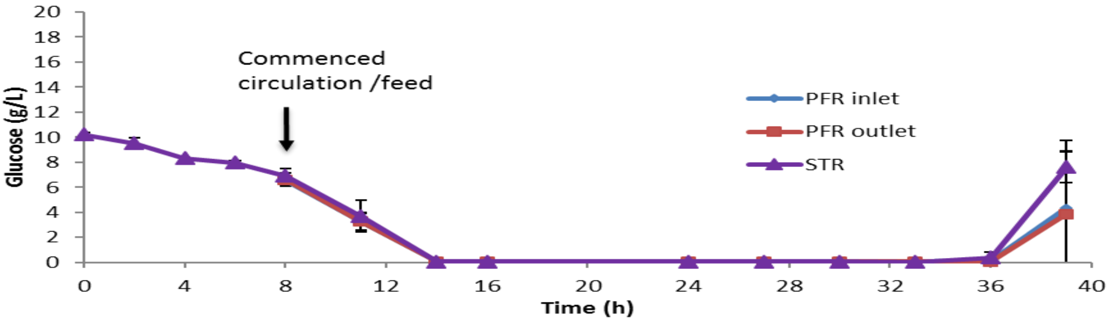

Figure 6 Glucose profiles across SDR 2, data points represent the mean values from biological replicates, and the error bars are equivalent to their standard deviations. The error bars between 14 h and 36 h are too small to be seen on this graph due to the high glucose concentrations at the start and end of fermentation.

Appendix 6

Process concentration profiles for SDR 3 during *C. glutamicum* DM1945x3 fed-batch fermentation

In SDR 3, the cell broth mixtures were recirculated between the STR and PFR. The addition of feed (mainly containing glucose and trace elements), air and the pH controlling agent (NH_4OH) were introduced in the STR, while the τ_{PFR} was 5 min.

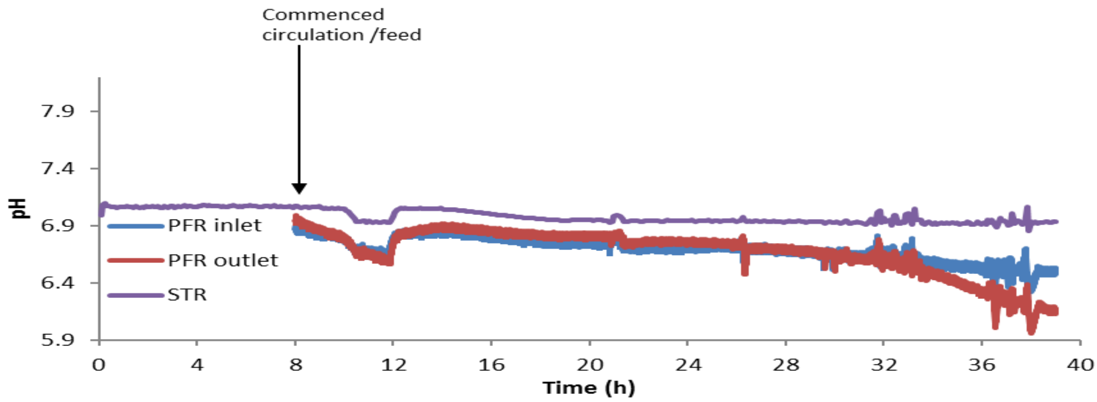

Figure 7 pH profiles at the PFR inlet/outlet and the STR for SDR 3

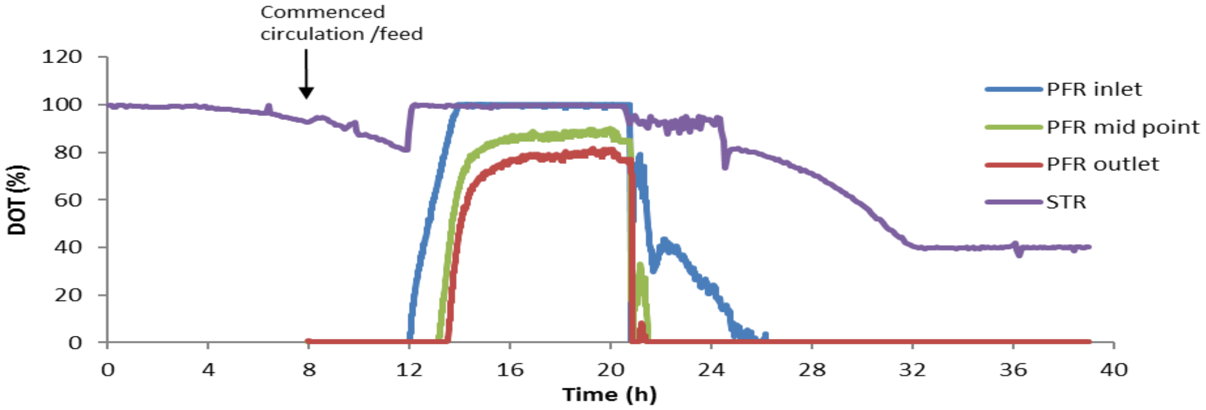

Figure 8 Dissolved oxygen tension profiles across SDR 3

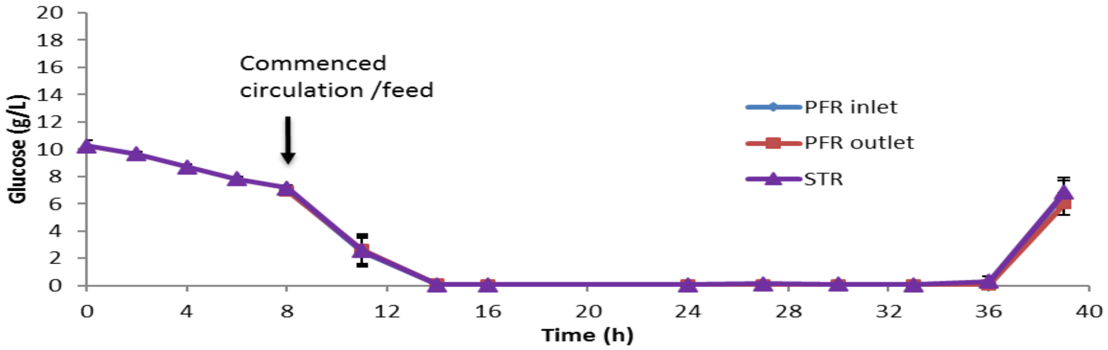

Figure 9 Glucose profiles across SDR 3, data points represent the mean values from biological replicates, and the error bars are equivalent to their standard deviations. The error bars between 14 h and 36 h are too small to be seen on this graph due to the high glucose concentrations at the start and end of fermentation

Appendix 7

Process concentration profiles for SDR 5 during *C. glutamicum* DM1945x3 fed-batch fermentation

In SDR 5, the pH controlling agent and air were introduced to the well-mixed STR section, while the substrate feed was added at the inlet of the poorly-mixed unaerated PFR with a τ_{PFR} of 2 min.

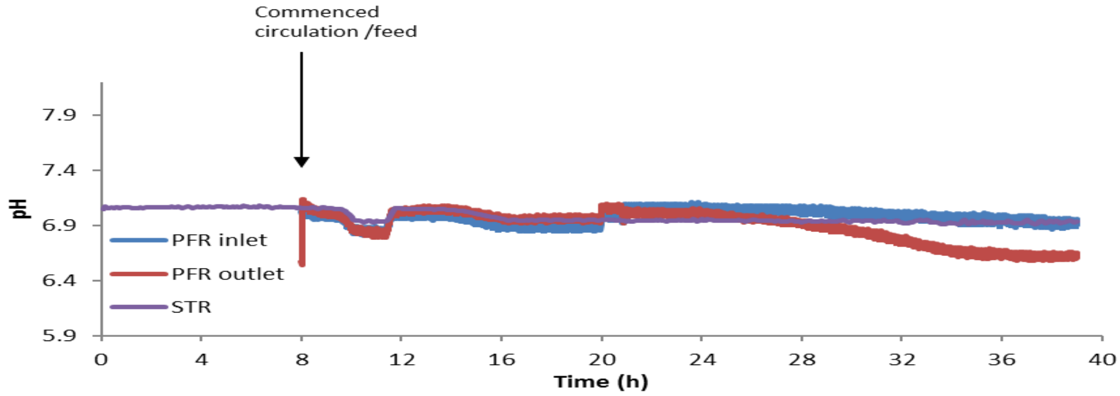

Figure 10 pH profiles at the PFR inlet/outlet and the STR for SDR 5

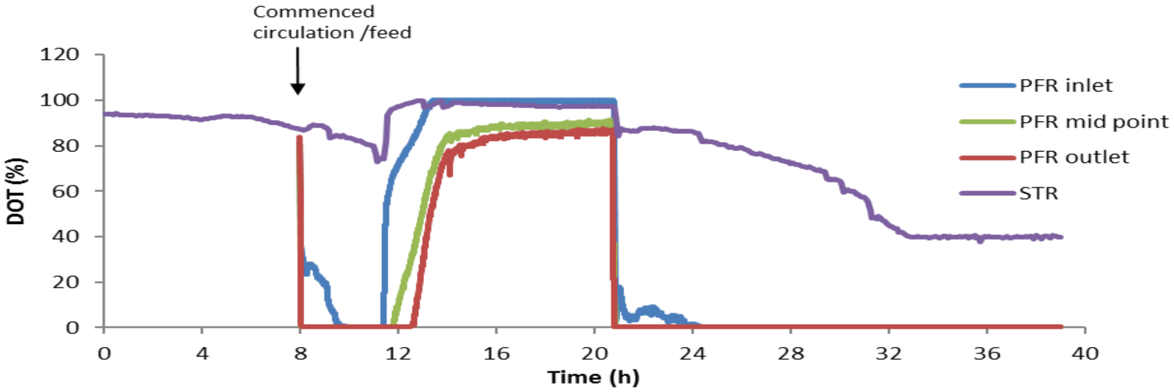

Figure 11 Dissolved oxygen tension profiles across SDR 5

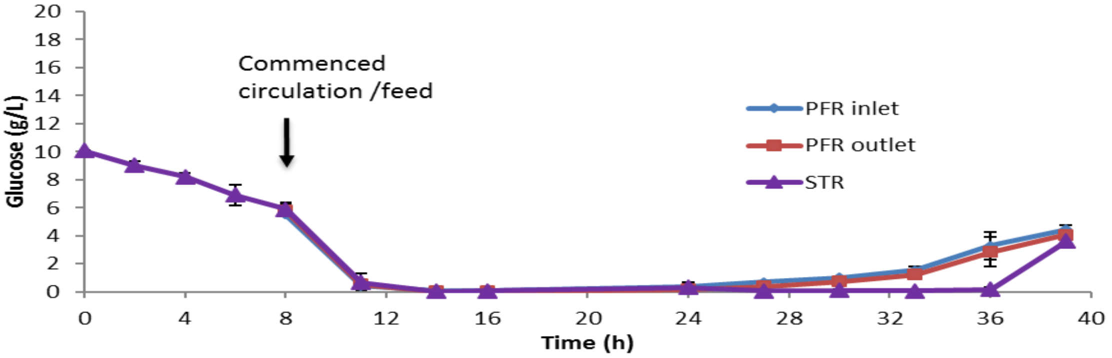

Figure 12 Glucose profiles across SDR 5, data points represent the mean values from biological replicates, and the error bars are equivalent to their standard deviations. The error bars between 14 h and 36 h are too small to be seen on this graph due to the high glucose concentrations at the start and end of fermentation

Appendix 8

Process concentration profiles for SDR 6 during *C. glutamicum* DM1945x3 fed-batch fermentation

In SDR 6, the pH controlling agent and air were introduced to the well-mixed STR section, while the substrate feed was added at the inlet of the poorly-mixed unaerated PFR with a τ_{PFR} of 5 min.

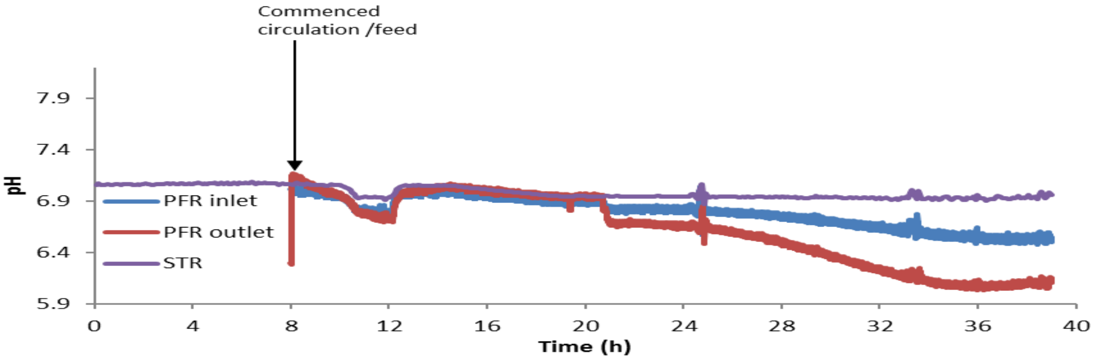

Figure 13 pH profiles at the PFR inlet/outlet and the STR for SDR 6

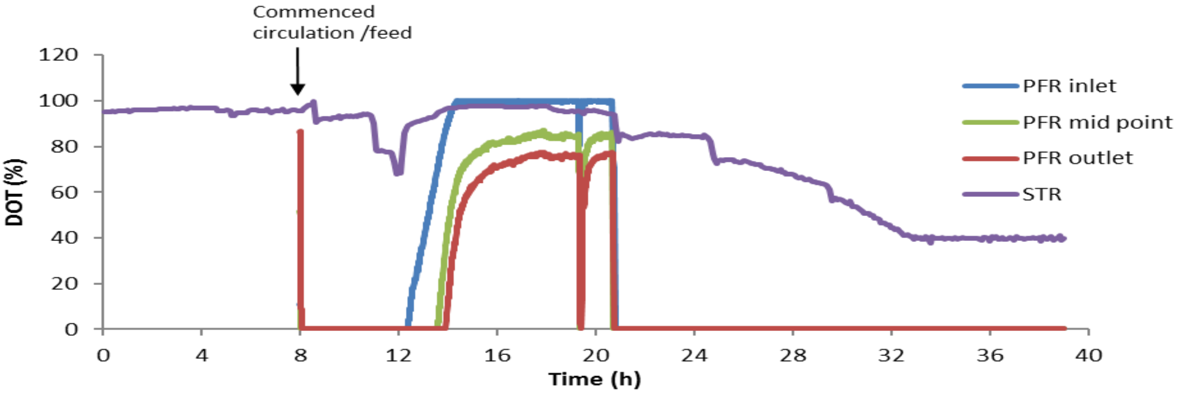

Figure 14 Dissolved oxygen tension profiles across SDR 6

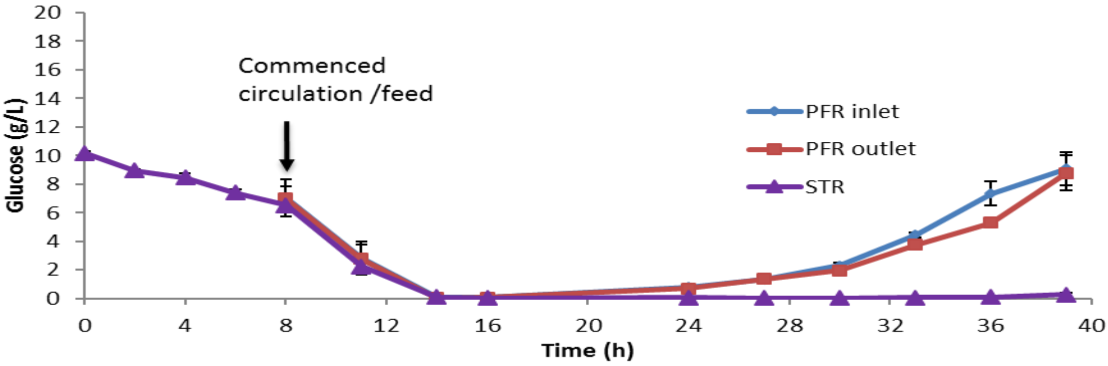

Figure 15 Glucose profiles across SDR 6, data points represent the mean values from biological replicates, and the error bars are equivalent to their standard deviations. The error bars between 14 h and 36 h are too small to be seen on this graph due to the high glucose concentrations at the start and end of fermentation

Appendix 9

Process concentration profiles for SDR 8 during *C. glutamicum* DM1945x3 fed-batch fermentation

In SDR 8, the glucose feed and air were introduced to the STR, while the pH controlling agent was introduced to the PFR with a τ_{PFR} of 2 min.

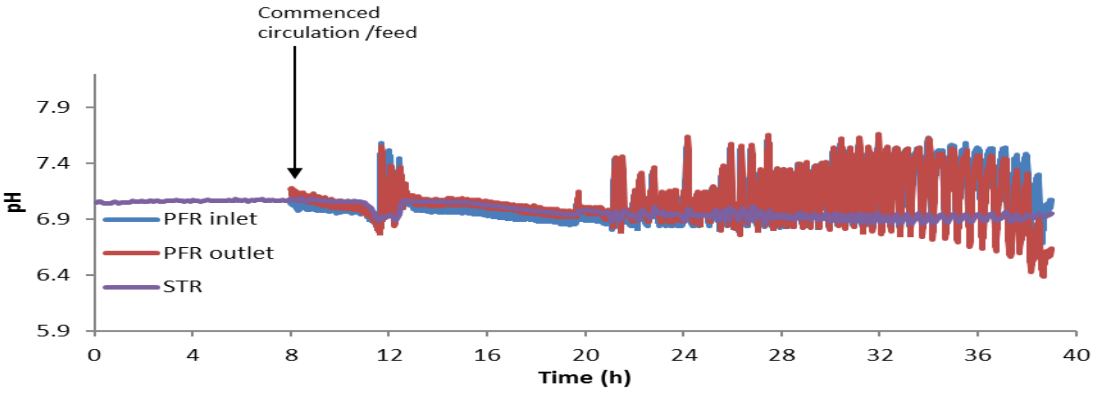

Figure 16 pH profiles at the PFR inlet/outlet and the STR for SDR 8

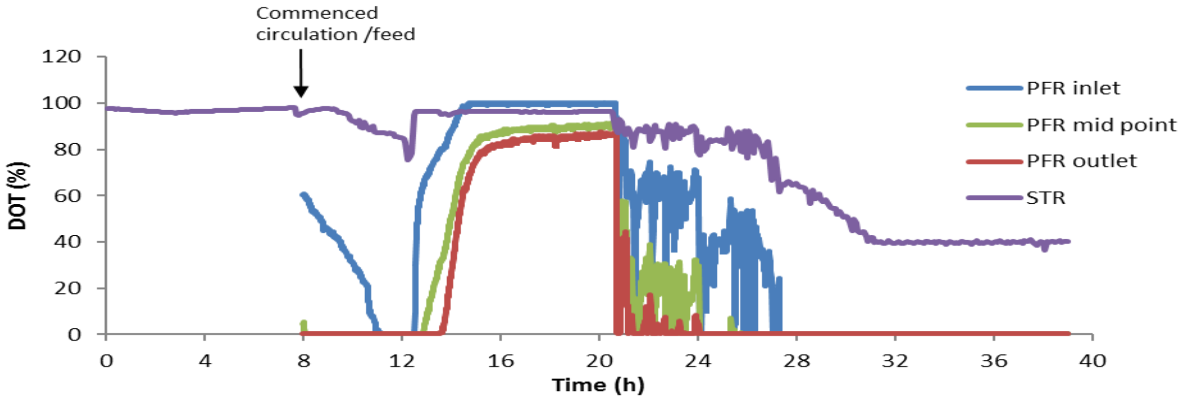

Figure 17 Dissolved oxygen tension profiles across SDR 8

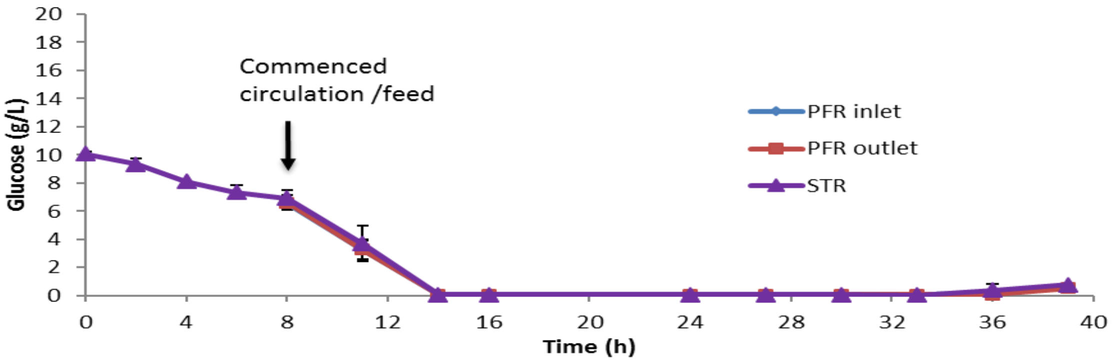

Figure 18 Glucose profiles across SDR 8, data points represent the mean values from biological replicates, and the error bars are equivalent to their standard deviations. The error bars between 14 h and 39 h are too small to be seen on this graph due to the high glucose concentrations at the start of fermentation

<u>Appendix 10</u>

Process concentration profiles for SDR 9 during *C. glutamicum* DM1945x3 fed-batch fermentation

In SDR 9, the glucose feed and air were introduced to the STR, while the pH controlling agent was introduced to the PFR with a τ_{PFR} of 5 min.

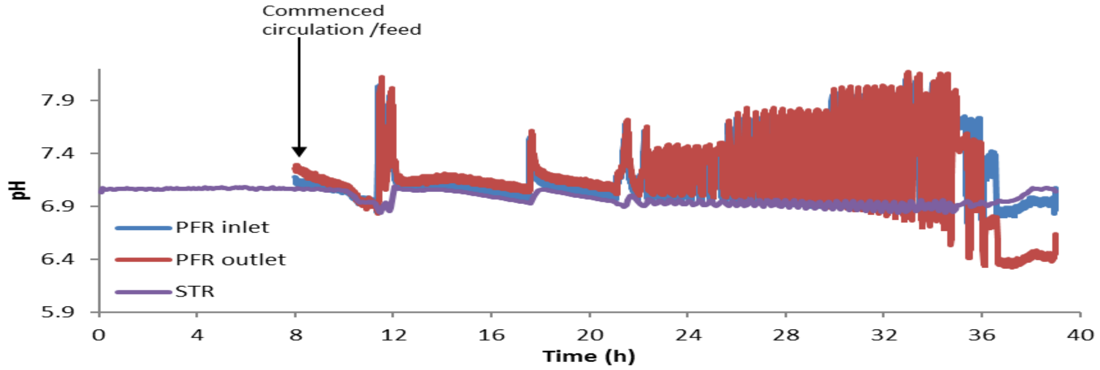

Figure 19 pH profiles at the PFR inlet/outlet and the STR for SDR 9

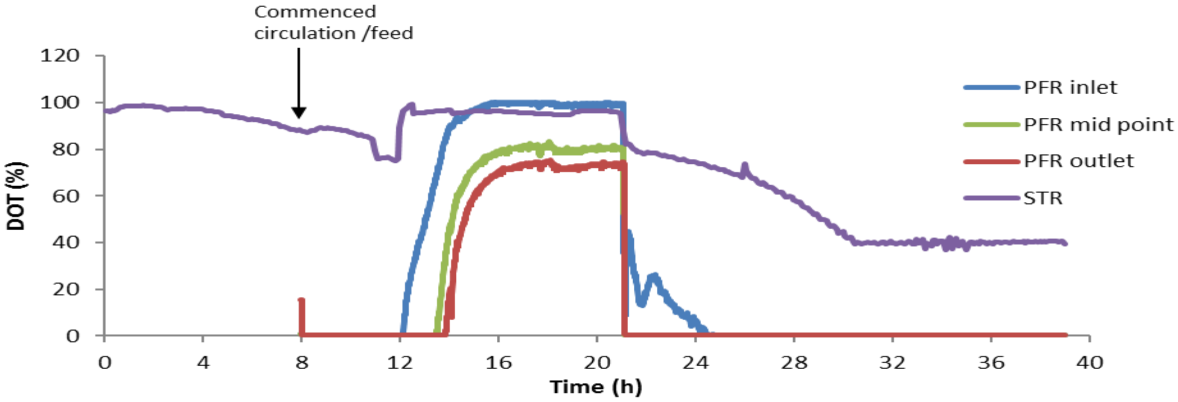

Figure 20 Dissolved oxygen tension profiles across SDR 9

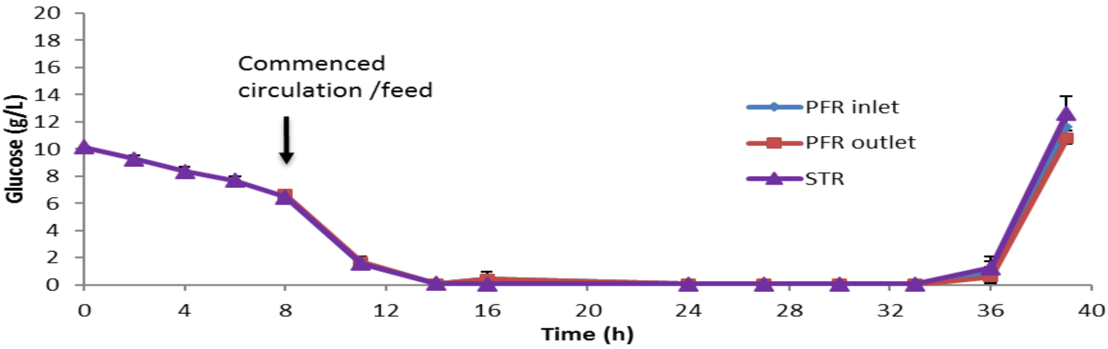

Figure 21 Glucose profiles across SDR 9, data points represent the mean values from biological replicates, and the error bars are equivalent to their standard deviations. The error bars between 14 h and 36 h are too small to be seen on this graph due to the high glucose concentrations at the start and end of fermentation

Appendix 11

Process concentration profiles for SDR 11 during *C. glutamicum* DM1945x3 fed-batch fermentation

In SDR 11, both glucose feed and base were injected into PFR section with a τ_{PFR} of 2 min, while air was sparged at the STR.

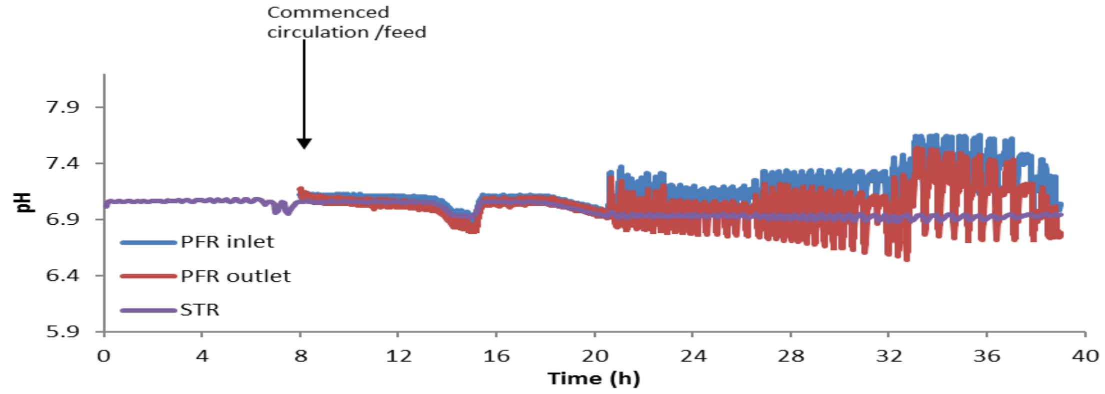

Figure 22 pH profiles at the PFR inlet/outlet and the STR for SDR 11

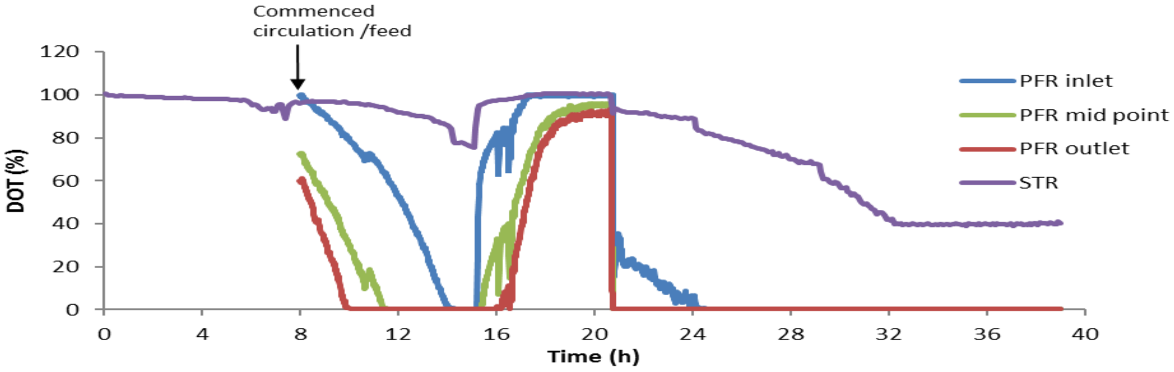

Figure 23 Dissolved oxygen tension profiles across SDR 11

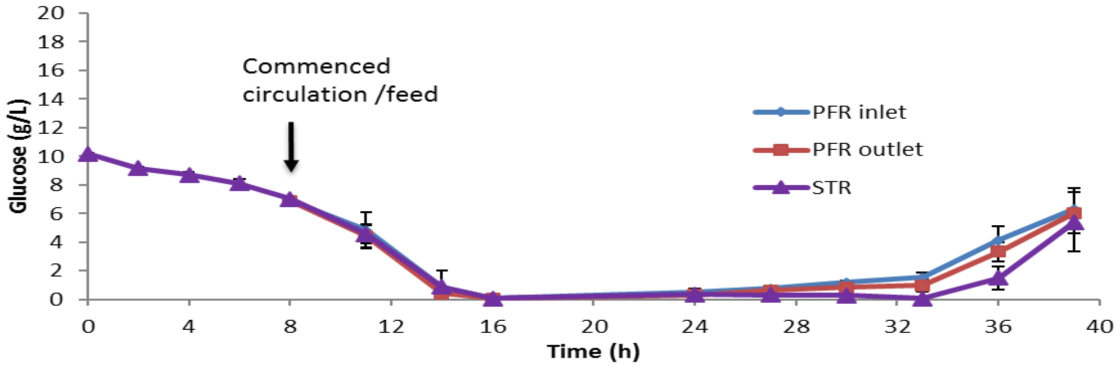

Figure 24 Glucose profiles across SDR 11, data points represent the mean values from biological replicates, and the error bars are equivalent to their standard deviations. The error bars between 14 h and 33 h are too small to be seen on this graph due to the high glucose concentrations at the start and end of fermentation

Appendix 12

Process concentration profiles for SDR 12 during *C. glutamicum* DM1945x3 fed-batch fermentation

In SDR 12, both glucose feed and base were injected into PFR section with a τ_{PFR} of 5 min, while air was sparged at the STR.

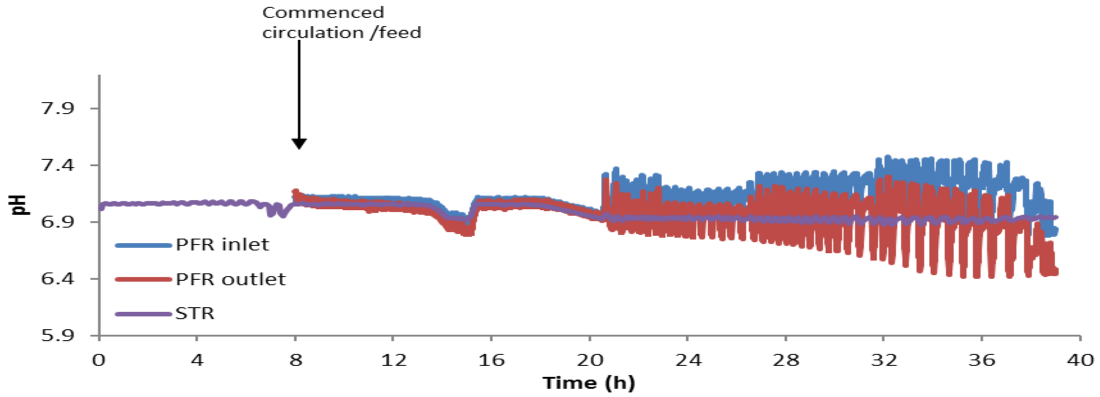

Figure 25 pH profiles at the PFR inlet/outlet and the STR for SDR 12

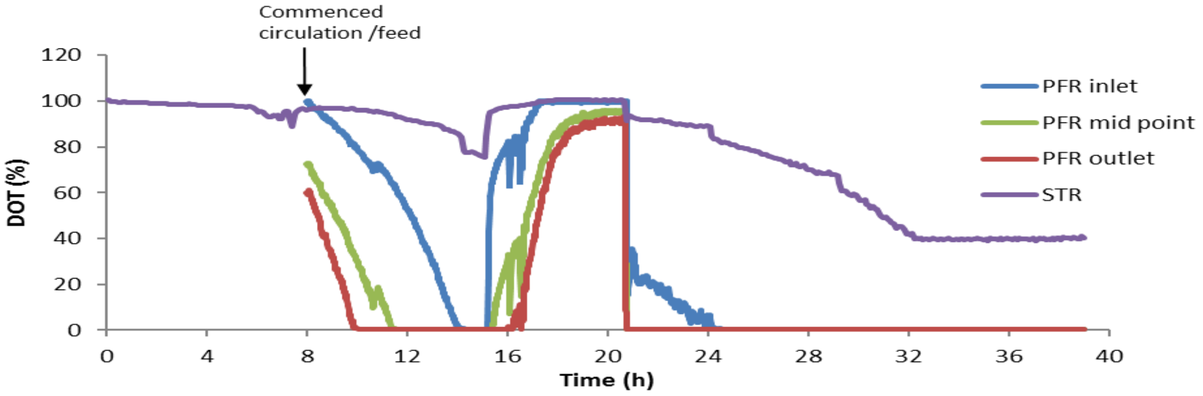

Figure 26 Dissolved oxygen tension profiles across SDR 12

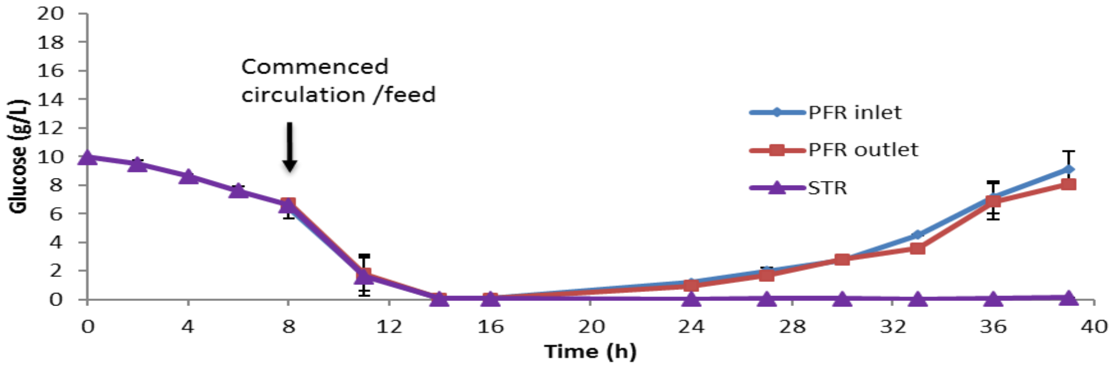

Figure 27 Glucose profiles across SDR 12, data points represent the mean values from biological replicates, and the error bars are equivalent to their standard deviations.

Appendix 13

Process log for *C. glutamicum* DM1945x3 fed-batch fermentation (STR only)

Time (h)	Cadaverine (g/L)	Glucose (g/L)	CFU/mL	DCW (g/L)	Lactate(g/L)
0	0.00	10	4.0E+06	0.04	0.00
2	0.0080	9.4	2.4E+07	0.13	0.0050
4	0.020	9.0	1.6E+08	0.43	0.0039
6	0.035	8.5	4.5E+08	0.86	0.0079
8	0.049	7.4	8.8E+08	1.3	0.036
11	0.084	2.7	2.7E+09	2.9	0.061
14	0.098	0.05	4.7E+09	3.6	0.020
16	0.13	0.11	5.3E+09	4.1	0.020
24	0.51	0.00	8.2E+09	6.3	0.023
27	3.5	0.12	8.8E+09	8.4	0.023
30	5.7	0.00	8.9E+09	12	0.013
33	7.0	0.00	9.6E+09	17	0.016
36	13	0.00	1.1E+10	25	0.28
39	20	8.2	1.3E+10	29	0.23

Table 7 C. glutamicum DM1945x3 offline measurements in run 1 (SDR only)

Time (h)	Cadaverine (g/L)	Glucose (g/L)	CFU/mL	DCW (g/L)	Lactate(g/L)
0	0.00	10	2.0E+06	0.03	0.00
2	0.0040	9.9	1.5E+07	0.12	0.0034
4	0.013	9.4	1.1E+08	0.42	0.0024
6	0.025	8.5	3.7E+08	0.88	0.0052
8	0.041	7.8	7.3E+08	1.2	0.029
11	0.063	4.9	2.0E+09	3.7	0.051
14	0.11	0.10	4.6E+09	4.1	0.023
16	0.12	0.10	5.0E+09	4.3	0.026
24	0.60	0.03	7.3E+09	6.8	0.027
27	4.2	0.07	6.4E+09	11	0.033
30	5.1	0.10	8.5E+09	14	0.028
33	7.3	0.00	1.0E+10	21	0.026
36	15	0.07	1.1E+10	26	0.26
39	19	9.5	1.6E+10	30	0.27

Table 8 C. glutamicum DM1945x3 offline measurements in run 2 (SDR only)

Appendix 13 highlights the offline data measurements of samples taken during replicate fed-batch fermentations of *C. glutamicum* DM1945x3 in the STR only control simulation (Table 7 & 8).

Appendix 14

Process log for *C. glutamicum* DM1945x3 fed-batch fermentation (SDR 1)

Time (h)	Cadaverine (g/L)	Glucose (g/L)	CFU/mL	DCW (g/L)	Lactate(g/L)
0	0.00	10	2.0E+07	0.06	0.00
2	0.018	9.4	8.7E+07	0.07	0.0013
4	0.034	8.8	3.8E+08	0.31	0.0040
6	0.049	8.0	8.9E+08	0.73	0.0037
8	0.060	7.6	1.2E+09	1.0	0.034
11	0.095	2.3	3.3E+09	4.1	0.043
14	0.11	0.08	5.5E+09	4.7	0.019
16	0.11	0.10	4.7E+09	4.3	0.016
24	0.58	0.07	8.3E+09	6.5	0.024
27	2.9	0.04	8.6E+09	8.5	0.024
30	4.2	0.03	1.0E+10	13	0.025
33	5.4	0.03	1.0E+10	19	0.037
36	10	0.07	1.3E+10	27	0.11
39	15	7.9	2.0E+10	33	0.33

Table 9 C. glutamicum DM1945x3 offline measurements in run 1(SDR 1)

Time (h)	Cadaverine (g/L)	Glucose (g/L)	CFU/mL	DCW (g/L)	Lactate(g/L)
0	0.00	10	1.8E+07	0.05	0.00
2	0.012	9.7	9.2E+07	0.09	0.0029
4	0.016	9.0	3.0E+08	0.22	0.0023
6	0.032	8.3	8.2E+08	0.64	0.0043
8	0.047	8.0	1.0E+09	1.3	0.026
11	0.077	5.2	2.1E+09	2.7	0.044
14	0.12	0.09	5.2E+09	5.4	0.032
16	0.16	0.07	5.0E+09	4.7	0.020
24	0.62	0.03	9.6E+09	6.7	0.021
27	2.8	0.01	9.3E+09	9.3	0.021
30	3.9	0.01	9.6E+09	14	0.026
33	6.9	0.07	1.0E+10	18	0.036
36	8.8	0.06	1.3E+10	27	0.21
39	16	4.6	1.7E+10	32	0.30

Table 10 C. glutamicum DM1945x3 offline measurements in run 2 (SDR 1)

Appendix 14 highlights the offline data measurements of samples taken during replicate fed-batch fermentations of *C. glutamicum* DM1945x3 in the SDR 1 simulation (Table 9 & 10).

Appendix 15

Process log for *C. glutamicum* DM1945x3 fed-batch fermentation (SDR 2)

Time (h)	Cadaverine (g/L)	Glucose (g/L)	CFU/mL	DCW (g/L)	Lactate(g/L)
0	0.00	10	3.1E+06	0.040	0.00
2	0.0060	9.8	4.9E+07	0.070	0.0032
4	0.019	8.4	1.6E+08	0.59	0.0059
6	0.023	7.8	6.6E+08	0.72	0.0092
8	0.011	6.5	9.9E+08	0.90	0.014
11	0.0042	2.8	1.9E+09	2.4	0.016
14	0.0088	0.060	3.4E+09	3.9	0.0083
16	0.020	0.060	3.9E+09	3.3	0.0088
24	0.14	0.070	6.0E+09	4.7	0.0080
27	1.3	0.060	7.1E+09	7.3	0.013
30	1.9	0.060	7.4E+09	11	0.0098
33	3.2	0.060	7.2E+09	17	0.013
36	5.8	0.060	1.1E+10	25	0.028
39	9.9	6.8	1.3E+10	32	0.21

Table 11 C. glutamicum DM1945x3 offline measurements in run 1(SDR 2)

Time (h)	Cadaverine (g/L)	Glucose (g/L)	CFU/mL	DCW (g/L)	Lactate(g/L)
0	0.00	10	4.0E+06	0.060	0.00
2	0.0072	9.2	3.9E+07	0.12	0.0060
4	0.0085	8.2	1.9E+08	0.23	0.0045
6	0.010	8.1	5.9E+08	0.90	0.0080
8	0.0028	7.3	8.5E+08	1.6	0.016
11	0.015	4.6	2.1E+09	3.0	0.021
14	0.030	0.070	3.7E+09	5.2	0.013
16	0.026	0.070	3.6E+09	4.5	0.012
24	0.16	0.070	5.8E+09	5.6	0.013
27	0.87	0.070	5.0E+09	7.8	0.018
30	1.9	0.060	6.1E+09	11	0.016
33	3.0	0.050	7.2E+09	18	0.014
36	6.5	0.68	8.5E+09	25	0.038
39	8.7	8.5	1.2E+10	32	0.12

Table 12 C. glutamicum DM1945x3 offline measurements in run 2 (SDR 2)

Appendix 15 highlights the offline data measurements of samples taken during replicate fed-batch fermentations of *C. glutamicum* DM1945x3 in the SDR 2 simulation (Table 11 & 12).

Appendix 16

Process log for *C. glutamicum* DM1945x3 fed-batch fermentation (SDR 3)

Time (h)	Cadaverine (g/L)	Glucose (g/L)	CFU/mL	DCW (g/L)	Lactate(g/L)
0	0.00	11	4.1E+06	0.060	0.00
2	0.0046	9.8	3.9E+07	0.19	0.0032
4	0.0071	8.6	2.0E+08	0.49	0.0059
6	0.0093	7.7	7.6E+08	0.86	0.0092
8	0.014	7.3	1.0E+09	1.4	0.0064
11	0.019	3.2	1.9E+09	2.1	0.017
14	0.033	0.060	3.2E+09	4.0	0.013
16	0.023	0.090	4.1E+09	3.8	0.015
24	0.21	0.070	6.9E+09	5.5	0.024
27	0.82	0.24	5.5E+09	6.7	0.018
30	2.0	0.16	6.8E+09	11	0.0033
33	3.0	0.06	7.5E+09	15	0.052
36	3.6	0.58	8.1E+09	24	0.15
39	8.0	7.6	9.1E+09	29	0.22

Table 13 C. glutamicum DM1945x3 offline measurements in run 1(SDR 3)

Time (h)	Cadaverine (g/L)	Glucose (g/L)	CFU/mL	DCW (g/L)	Lactate(g/L)
0	0.00	10	4.9E+06	0.04	0.00
2	0.0083	9.5	4.9E+07	0.12	0.0064
4	0.0095	8.8	2.9E+08	0.34	0.0045
6	0.018	8.0	8.9E+08	0.76	0.0083
8	0.025	7.0	1.2E+09	1.1	0.043
11	0.052	1.9	2.0E+09	2.7	0.042
14	0.047	0.090	4.1E+09	3.9	0.026
16	0.046	0.090	3.0E+09	3.5	0.030
24	0.24	0.080	6.2E+09	4.2	0.035
27	1.5	0.050	5.2E+09	5.9	0.039
30	2.4	0.060	6.0E+09	9.8	0.048
33	2.6	0.080	6.5E+09	14	0.054
36	3.9	0.060	7.8E+09	22	0.10
39	9.2	6.1	1.0E+10	31	0.22

Table 14 C. glutamicum DM1945x3 offline measurements in run 2 (SDR 3)

Appendix 16 highlights the offline data measurements of samples taken during replicate fed-batch fermentations of *C. glutamicum* DM1945x3 in the SDR 3 simulation (Table 13 & 14).

Appendix 17

Process log for *C. glutamicum* DM1945x3 fed-batch fermentation (SDR 4)

Time (h)	Cadaverine (g/L)	Glucose (g/L)	CFU/mL	DCW (g/L)	Lactate(g/L)
0	0.00	10	4.6E+06	0.060	0.00
2	0.0036	9.9	5.8E+07	0.16	0.0032
4	0.0081	9.0	3.0E+08	0.32	0.0059
6	0.013	8.6	6.6E+08	0.35	0.0092
8	0.044	8.5	7.0E+08	0.64	0.021
11	0.068	6.7	1.5E+09	1.0	0.026
14	0.093	1.6	3.2E+09	3.7	0.059
16	0.12	0.060	5.2E+09	4.6	0.016
24	0.47	0.060	1.0E+10	6.3	0.077
27	3.0	0.070	7.8E+09	9.2	0.050
30	4.1	0.080	1.1E+10	13	0.16
33	5.5	0.060	1.1E+10	18	0.15
36	9.5	1.3	1.3E+10	25	0.21
39	14	11	1.6E+10	29	0.29

Table 15 C. glutamicum DM1945x3 offline measurements in run 1(SDR 4)

Time (h)	Cadaverine (g/L)	Glucose (g/L)	CFU/mL	DCW (g/L)	Lactate(g/L)
0	0.00	10	5.0E+06	0.05	0.00
2	0.0083	9.5	4.1E+07	0.09	0.0064
4	0.020	9.0	1.9E+08	0.28	0.0045
6	0.22	9.1	9.0E+08	0.39	0.0083
8	0.057	8.7	4.6E+08	0.90	0.025
11	0.084	7.1	1.6E+09	1.4	0.038
14	0.16	1.6	3.2E+09	3.9	0.058
16	0.17	0.10	4.9E+09	4.0	0.020
24	0.52	0.00	1.2E+10	5.3	0.051
27	1.8	0.00	9.7E+09	7.2	0.083
30	3.2	0.00	9.8E+09	12	0.096
33	5.2	0.54	1.1E+10	17	0.12
36	11	2.0	1.2E+10	25	0.27
39	15	15	1.6E+10	30	0.24

Table 16 C. glutamicum DM1945x3 offline measurements in run 2 (SDR 4)

Appendix 17 highlights the offline data measurements of samples taken during replicate fed-batch fermentations of *C. glutamicum* DM1945x3 in the SDR 4 simulation (Table 15 & 16).

Appendix 18

Process log for *C. glutamicum* DM1945x3 fed-batch fermentation (SDR 5)

Time (h)	Cadaverine (g/L)	Glucose (g/L)	CFU/mL	DCW (g/L)	Lactate(g/L)
0	0.00	10	3.7E+06	0.050	0.00
2	0.0072	8.8	4.3E+07	0.10	0.0053
4	0.010	8.0	3.0E+08	0.21	0.0098
6	0.019	7.4	9.4E+08	0.49	0.019
8	0.038	6.2	9.5E+08	1.1	0.026
11	0.061	1.1	2.4E+09	5.0	0.092
14	0.070	0.040	3.3E+09	4.3	0.015
16	0.063	0.070	3.8E+09	4.4	0.015
24	0.18	0.57	5.2E+09	5.2	0.024
27	1.1	0.080	4.6E+09	8.6	0.018
30	2.0	0.17	5.3E+09	12	0.025
33	2.3	0.11	8.5E+09	17	0.051
36	6.5	0.27	9.8E+09	25	0.036
39	12	4.0	1.2E+10	31	0.033

Table 17 C. glutamicum DM1945x3 offline measurements in run 1(SDR 5)

Time (h)	Cadaverine (g/L)	Glucose (g/L)	CFU/mL	DCW (g/L)	Lactate(g/L)
0	0.00	10	4.9E+06	0.060	0.00
2	0.0062	9.2	5.7E+07	0.090	0.0064
4	0.020	8.4	2.9E+08	0.16	0.0037
6	0.029	6.4	8.7E+08	0.20	0.024
8	0.034	5.6	1.4E+09	0.64	0.030
11	0.048	0.24	2.9E+09	2.6	0.029
14	0.050	0.060	3.4E+09	3.0	0.017
16	0.050	0.060	3.6E+09	3.4	0.016
24	0.16	0.060	5.1E+09	4.0	0.018
27	1.1	0.060	6.9E+09	6.6	0.018
30	1.4	0.060	7.1E+09	9.2	0.020
33	2.0	0.060	8.0E+09	14	0.024
36	4.7	0.060	1.1E+10	20	0.028
39	11	3.3	1.3E+10	31	0.069

Table 18 C. glutamicum DM1945x3 offline measurements in run 2 (SDR 5)

Appendix 18 highlights the offline data measurements of samples taken during replicate fed-batch fermentations of *C. glutamicum* DM1945x3 in the SDR 5 simulation (Table 17 & 18).

Appendix 19

Process log for *C. glutamicum* DM1945x3 fed-batch fermentation (SDR 6)

Time (h)	Cadaverine (g/L)	Glucose (g/L)	CFU/mL	DCW (g/L)	Lactate(g/L)
0	0.00	11	3.9E+06	0.050	0.00
2	0.0098	8.9	4.9E+07	0.10	0.0053
4	0.020	8.2	2.7E+08	0.21	0.0098
6	0.024	7.6	8.4E+08	0.49	0.019
8	0.044	6.8	1.2E+09	1.5	0.027
11	0.078	2.5	2.0E+09	2.5	0.047
14	0.10	0.12	4.1E+09	3.5	0.035
16	0.094	0.040	3.4E+09	4.1	0.018
24	0.36	0.080	5.7E+09	5.1	0.041
27	0.66	0.010	5.5E+09	7.0	0.038
30	2.8	0.020	6.2E+09	11	0.032
33	3.2	0.060	7.8E+09	16	0.023
36	8.0	0.010	8.7E+09	24	0.021
39	9.4	0.38	1.1E+10	28	0.081

Table 19 C. glutamicum DM1945x3 offline measurements in run 1 (SDR 6)

Time (h)	Cadaverine (g/L)	Glucose (g/L)	CFU/mL	DCW (g/L)	Lactate(g/L)
0	0.00	10	5.1E+06	0.060	0.00
2	0.0040	9.0	4.7E+07	0.090	0.0064
4	0.0063	8.7	3.3E+08	0.16	0.0037
6	0.014	7.2	9.7E+08	0.20	0.024
8	0.018	6.3	1.9E+09	1.4	0.039
11	0.046	2.0	2.4E+09	1.9	0.050
14	0.065	0.070	3.9E+09	3.2	0.025
16	0.060	0.060	4.4E+09	3.1	0.030
24	0.27	0.070	5.8E+09	4.2	0.040
27	2.4	0.070	5.6E+09	5.8	0.032
30	3.5	0.060	6.8E+09	9.5	0.030
33	3.9	0.070	8.3E+09	15	0.033
36	7.8	0.15	9.8E+09	22	0.024
39	12	0.15	1.5E+10	33	0.095

Table 20 C. glutamicum DM1945x3 offline measurements in run 2 (SDR 6)

Appendix 19 highlights the offline data measurements of samples taken during replicate fed-batch fermentations of *C. glutamicum* DM1945x3 in the SDR 6 simulation (Table 19 & 20).

Appendix 20

Process log for *C. glutamicum* DM1945x3 fed-batch fermentation (SDR 7)

Time (h)	Cadaverine (g/L)	Glucose (g/L)	CFU/mL	DCW (g/L)	Lactate(g/L)
0	0.00	10	2.8E+06	0.050	0.00
2	0.0078	8.9	5.1E+07	0.19	0.0043
4	0.018	8.2	3.9E+08	0.31	0.0085
6	0.033	7.6	7.8E+08	0.82	0.019
8	0.078	7.0	2.5E+09	1.8	0.068
11	0.16	1.1	3.3E+09	4.5	0.031
14	0.20	0.040	4.9E+09	4.2	0.0054
16	0.22	0.00	5.2E+09	4.1	0.011
24	0.49	0.030	8.1E+09	5.5	0.0077
27	1.8	0.040	7.0E+09	7.3	0.014
30	2.7	0.060	8.0E+09	13	0.030
33	5.1	0.040	7.5E+09	17	0.041
36	7.7	0.00	8.3E+09	25	0.19
39	15	9.0	1.3E+10	31	0.27

Table 21 C. glutamicum DM1945x3 offline measurements in run 1(SDR 7)

Time (h)	Cadaverine (g/L)	Glucose (g/L)	CFU/mL	DCW (g/L)	Lactate(g/L)
0	0.00	10	4.6E+06	0.050	0.00
2	0.0023	9.0	3.9E+07	0.010	0.0031
4	0.0093	8.7	4.3E+08	0.27	0.0069
6	0.012	7.2	8.4E+08	0.44	0.014
8	0.030	7.2	2.4E+09	0.98	0.025
11	0.058	2.2	3.3E+09	4.4	0.033
14	0.062	0.030	5.1E+09	4.9	0.00
16	0.065	0.00	5.1E+09	5.1	0.00
24	0.35	0.020	7.0E+09	7.1	0.0052
27	1.3	0.00	7.8E+09	9.6	0.0056
30	2.2	0.010	7.5E+09	15	0.037
33	2.2	0.040	8.2E+09	19	0.040
36	7.6	0.13	8.8E+09	28	0.26
39	13	10	1.2E+10	33	0.18

Table 22 C. glutamicum DM1945x3 offline measurements in run 2 (SDR 7)

Appendix 20 highlights the offline data measurements of samples taken during replicate fed-batch fermentations of *C. glutamicum* DM1945x3 in the SDR 7 simulation (Table 21 & 22).

Appendix 21

Process log for *C. glutamicum* DM1945x3 fed-batch fermentation (SDR 8)

Time (h)	Cadaverine (g/L)	Glucose (g/L)	CFU/mL	DCW (g/L)	Lactate(g/L)
0	0.00	10	3.2E+06	0.050	0.00
2	0.0068	9.1	4.6E+07	0.090	0.0090
4	0.019	8.1	3.2E+08	0.22	0.020
6	0.020	7.7	6.2E+08	0.32	0.013
8	0.042	6.5	9.9E+08	0.90	0.014
11	0.064	2.8	1.9E+09	2.4	0.016
14	0.060	0.060	3.4E+09	3.9	0.0083
16	0.069	0.060	3.9E+09	3.3	0.0088
24	0.23	0.070	6.0E+09	4.7	0.0080
27	0.95	0.060	7.1E+09	7.3	0.013
30	1.6	0.060	7.4E+09	11	0.0098
33	2.9	0.060	7.2E+09	17	0.013
36	5.8	0.060	1.1E+10	25	0.028
39	11	0.68	1.3E+10	32	0.21

Table 23 C. glutamicum DM1945x3 offline measurements in run 1(SDR 8)

Time (h)	Cadaverine (g/L)	Glucose (g/L)	CFU/mL	DCW (g/L)	Lactate(g/L)
0	0.00	10	2.9E+06	0.060	0.00
2	0.00	9.6	4.0E+07	0.10	0.014
4	0.0052	8.1	4.7E+08	0.21	0.020
6	0.0076	7.0	9.4E+08	0.42	0.013
8	0.016	7.3	8.5E+08	1.6	0.016
11	0.023	4.6	2.1E+09	3.0	0.021
14	0.044	0.070	3.7E+09	5.2	0.013
16	0.037	0.070	3.6E+09	4.5	0.012
24	0.16	0.070	5.8E+09	5.6	0.013
27	0.76	0.070	5.0E+09	7.9	0.018
30	1.3	0.060	6.1E+09	11	0.016
33	2.9	0.050	7.2E+09	18	0.014
36	6.0	0.68	8.5E+09	25	0.038
39	9.0	0.85	1.2E+10	32	0.12

Table 24 C. glutamicum DM1945x3 offline measurements in run 2 (SDR 8)

Appendix 21 highlights the offline data measurements of samples taken during replicate fed-batch fermentations of *C. glutamicum* DM1945x3 in the SDR 8 simulation (Table 23 & 24).

Appendix 22

Process log for *C. glutamicum* DM1945x3 fed-batch fermentation (SDR 9)

Time (h)	Cadaverine (g/L)	Glucose (g/L)	CFU/mL	DCW (g/L)	Lactate(g/L)
0	0.00	10	4.4E+06	0.040	0.00
2	0.0040	9.1	3.6E+07	0.12	0.0034
4	0.0029	8.6	5.2E+08	0.42	0.020
6	0.091	7.9	7.8E+08	0.66	0.018
8	0.017	6.6	1.2E+09	1.9	0.025
11	0.028	1.9	2.3E+09	2.9	0.024
14	0.038	0.070	4.5E+09	3.5	0.012
16	0.036	0.080	4.8E+09	4.2	0.015
24	0.19	0.060	6.4E+09	4.7	0.012
27	1.2	0.060	5.9E+09	7.0	0.015
30	2.1	0.080	6.5E+09	11	0.020
33	3.4	0.050	6.9E+09	19	0.020
36	5.0	1.8	9.1E+09	26	0.072
39	11	11	1.2E+10	30	0.14

Table 25 C. glutamicum DM1945x3 offline measurements in run 1(SDR 9)

Time (h)	Cadaverine (g/L)	Glucose (g/L)	CFU/mL	DCW (g/L)	Lactate(g/L)
0	0.00	10	3.0E+06	0.030	0.00
2	0.0056	9.5	4.1E+07	0.15	0.0066
4	0.0052	8.1	4.5E+08	0.34	0.017
6	0.0036	7.5	6.2E+08	0.53	0.023
8	0.0083	6.3	1.2E+09	0.98	0.044
11	0.019	1.3	2.7E+09	3.3	0.067
14	0.027	0.14	4.9E+09	3.3	0.025
16	0.037	0.070	5.1E+09	3.6	0.023
24	0.28	0.11	6.7E+09	4.5	0.036
27	1.9	0.10	6.3E+09	6.0	0.030
30	2.9	0.090	6.9E+09	10	0.041
33	3.6	0.090	8.5E+09	16	0.042
36	4.9	0.70	1.0E+10	24	0.094
39	9.4	13	1.3E+10	31	0.13

Table 26 C. glutamicum DM1945x3 offline measurements in run 2 (SDR 9)

Appendix 22 highlights the offline data measurements of samples taken during replicate fed-batch fermentations of *C. glutamicum* DM1945x3 in the SDR 9 simulation (Table 25 & 26).

Appendix 23

Process log for *C. glutamicum* DM1945x3 fed-batch fermentation (SDR 10)

Time (h)	Cadaverine (g/L)	Glucose (g/L)	CFU/mL	DCW (g/L)	Lactate(g/L)
0	0.00	10	4.0E+06	0.040	0.00
2	0.0095	9.9	4.9E+07	0.23	0.0034
4	0.015	9.6	4.9E+08	0.35	0.020
6	0.021	9.1	8.0E+08	0.85	0.018
8	0.036	8.9	3.3E+08	1.0	0.029
11	0.071	8.0	8.8E+08	3.3	0.037
14	0.12	3.9	2.4E+09	3.6	0.045
16	0.16	0.17	4.1E+09	4.3	0.046
24	0.53	0.080	9.1E+09	6.5	0.10
27	2.1	0.070	7.5E+09	7.7	0.11
30	3.2	0.090	7.5E+09	13	0.090
33	6.0	0.070	7.7E+09	18	0.14
36	10	0.050	8.8E+09	25	0.28
39	14	15	1.3E+10	31	0.32

Table 27 C. glutamicum DM1945x3 offline measurements in run 1(SDR 10)

Time (h)	Cadaverine (g/L)	Glucose (g/L)	CFU/mL	DCW (g/L)	Lactate(g/L)
0	0.00	10	3.6E+06	0.050	0.00
2	0.0085	9.7	3.2E+07	0.19	0.0066
4	0.013	9.4	5.2E+08	0.49	0.017
6	0.030	9.2	6.8E+08	0.74	0.023
8	0.040	9.0	4.2E+08	1.1	0.032
11	0.072	8.3	9.9E+08	3.4	0.039
14	0.13	4.5	1.9E+09	3.9	0.053
16	0.19	0.12	4.7E+09	3.9	0.030
24	0.52	0.09	9.9E+09	5.9	0.087
27	1.8	0.13	7.3E+09	8.6	0.13
30	2.9	0.11	8.6E+09	13	0.12
33	5.7	0.10	7.9E+09	20	0.15
36	9.5	1.8	1.0E+10	27	0.31
39	14	18	1.2E+10	30	0.35

Table 28 C. glutamicum DM1945x3 offline measurements in run 2 (SDR 10)

Appendix 23 highlights the offline data measurements of samples taken during replicate fed-batch fermentations of *C. glutamicum* DM1945x3 in the SDR 10 simulation (Table 27 & 28).

Appendix 24

Process log for *C. glutamicum* DM1945x3 fed-batch fermentation (SDR 11)

Time (h)	Cadaverine (g/L)	Glucose (g/L)	CFU/mL	DCW (g/L)	Lactate(g/L)
0	0.00	10	3.6E+06	0.040	0.00
2	0.0083	9.1	4.1E+07	0.20	0.0073
4	0.014	8.8	4.3E+08	0.39	0.0075
6	0.024	8.3	6.2E+08	0.88	0.012
8	0.058	7.2	1.6E+09	1.8	0.025
11	0.10	4.1	2.6E+09	3.2	0.028
14	0.13	0.070	3.0E+09	4.9	0.025
16	0.077	0.090	3.4E+09	4.4	0.013
24	0.24	0.62	6.6E+09	5.5	0.023
27	1.1	0.58	6.4E+09	8.6	0.024
30	2.0	0.54	5.6E+09	11	0.026
33	3.6	0.070	7.6E+09	18	0.021
36	7.7	2.1	8.6E+09	25	0.078
39	12	6.9	1.1E+10	32	0.096

Table 29 C. glutamicum DM1945x3 offline measurements in run 1(SDR 11)

Time (h)	Cadaverine (g/L)	Glucose (g/L)	CFU/mL	DCW (g/L)	Lactate(g/L)
0	0.00	10	3.3E+06	0.030	0.00
2	0.0013	9.3	4.8E+07	0.15	0.0046
4	0.084	8.6	3.9E+08	0.43	0.0092
6	0.015	7.9	7.7E+08	0.96	0.011
8	0.028	6.9	1.1E+09	1.1	0.013
11	0.035	5.0	1.8E+09	2.7	0.013
14	0.068	1.7	3.1E+09	3.3	0.019
16	0.079	0.056	3.9E+09	4.0	0.0069
24	0.31	0.054	5.5E+09	6.2	0.0074
27	2.2	0.056	7.9E+09	6.9	0.0080
30	2.6	0.054	7.0E+09	11	0.0074
33	2.6	0.053	6.9E+09	15	0.0084
36	6.5	0.95	8.1E+09	26	0.067
39	11	4.0	1.2E+10	32	0.082

Table 30 C. glutamicum DM1945x3 offline measurements in run 2 (SDR 11)

Appendix 24 highlights the offline data measurements of samples taken during replicate fed-batch fermentations of *C. glutamicum* DM1945x3 in the SDR 11 simulation (Table 29 & 30).

Appendix 25

Process log for *C. glutamicum* DM1945x3 fed-batch fermentation (SDR 12)

Time (h)	Cadaverine (g/L)	Glucose (g/L)	CFU/mL	DCW (g/L)	Lactate(g/L)
0	0.00	10	3.2E+06	0.030	0.00
2	0.00	9.3	3.2E+07	0.34	0.0073
4	0.0097	8.5	4.8E+08	0.54	0.0075
6	0.010	7.8	8.2E+08	0.92	0.012
8	0.011	6.5	1.2E+09	1.9	0.018
11	0.040	0.68	2.5E+09	3.4	0.028
14	0.052	0.070	3.8E+09	3.6	0.013
16	0.045	0.070	3.8E+09	4.0	0.012
24	0.21	0.030	6.6E+09	6.9	0.029
27	2.1	0.080	5.8E+09	7.5	0.030
30	2.7	0.060	6.6E+09	12	0.032
33	4.5	0.030	7.2E+09	19	0.026
36	6.8	0.050	8.1E+09	25	0.091
39	8.6	0.15	9.6E+09	33	0.063

Table 31 C. glutamicum DM1945x3 offline measurements in run 1(SDR 12)

Time (h)	Cadaverine (g/L)	Glucose (g/L)	CFU/mL	DCW (g/L)	Lactate(g/L)
0	0.00	10.02	4.3E+06	0.030	0.00
2	0.00	9.7	3.6E+07	0.200	0.0046
4	0.0075	8.7	3.6E+08	0.36	0.0092
6	0.021	7.4	7.9E+08	0.84	0.011
8	0.036	6.7	1.1E+09	1.4	0.045
11	0.048	2.5	2.3E+09	3.0	0.053
14	0.052	0.090	3.5E+09	3.2	0.042
16	0.056	0.090	4.5E+09	3.1	0.033
24	0.21	0.070	6.8E+09	4.7	0.029
27	1.5	0.060	6.0E+09	7.1	0.038
30	1.9	0.060	7.4E+09	11	0.038
33	3.7	0.070	7.8E+09	16	0.065
36	5.4	0.080	9.3E+09	25	0.11
39	11	0.12	1.2E+10	30	0.13

Table 32 C. glutamicum DM1945x3 offline measurements in run 2 (SDR 12)

Appendix 25 highlights the offline data measurements of samples taken during replicate fed-batch fermentations of *C. glutamicum* DM1945x3 in the SDR 12 simulation (Table 31 & 32).

Appendix 26

Process log for *C. glutamicum* DM1945x3 fed-batch fermentation (SDR 13)

Time (h)	Cadaverine (g/L)	Glucose (g/L)	CFU/mL	DCW (g/L)	Lactate(g/L)
0	0.00	10	3.7E+06	0.050	0.00
2	0.0070	9.1	3.4E+07	0.090	0.0042
4	0.029	8.8	1.7E+08	0.39	0.0030
6	0.031	8.3	4.6E+08	0.76	0.0082
8	0.041	7.0	1.8E+09	1.4	0.016
11	0.13	3.4	2.6E+09	3.8	0.039
14	0.17	0.055	3.7E+09	4.5	0.013
16	0.19	0.085	4.3E+09	4.7	0.0073
24	0.28	0.042	6.6E+09	5.3	0.016
27	0.89	0.12	7E+09	6.2	0.028
30	1.9	0.074	7.1E+09	12	0.042
33	2.4	0.10	7.7E+09	17	0.058
36	4.9	0.075	9.9E+09	28	0.12
39	11	0.31	1.6E+10	32	0.34

Table 33 C. glutamicum DM1945x3 offline measurements in run 1(SDR 13)

Time (h)	Cadaverine (g/L)	Glucose (g/L)	CFU/mL	DCW (g/L)	Lactate(g/L)
0	0.00	10	3.0E+06	0.060	0.00
2	0.0060	9.7	1.5E+07	0.12	0.0054
4	0.019	9.2	1.3E+08	0.56	0.0030
6	0.029	8.8	3.9E+08	0.98	0.0032
8	0.033	6.1	1.3E+09	1.4	0.036
11	0.056	1.32	2.9E+09	3.7	0.027
14	0.056	0.064	4.4E+09	4.4	0.015
16	0.057	0.061	3.3E+09	4.5	0.016
24	0.18	0.064	4.4E+09	5.0	0.025
27	0.70	0.060	6.7E+09	6.0	0.019
30	0.93	0.058	6.9E+09	10	0.019
33	2.6	0.062	7.8E+09	16	0.091
36	3.2	0.054	1.2E+10	22	0.042
39	8.1	0.26	1.6E+10	30	0.10

Table 34 C. glutamicum DM1945x3 offline measurements in run 2 (SDR 13)

Appendix 26 highlights the offline data measurements of samples taken during replicate fed-batch fermentations of *C. glutamicum* DM1945x3 in the SDR 13 simulation (Table 33 & 34).

Appendix 27

Process log for *C. glutamicum* DM1945x3 fed-batch fermentation (SDR 14)

Time (h)	Cadaverine (g/L)	Glucose (g/L)	CFU/mL	DCW (g/L)	Lactate(g/L)
0	0.00	10	3.2E+06	0.052	0.00
2	0.0040	9.0	3.9E+07	0.077	0.0022
4	0.0099	8.8	2.0E+08	0.49	0.0043
6	0.014	8.1	5.6E+08	0.96	0.012
8	0.028	4.7	1.4E+09	1.9	0.053
11	0.051	0.080	2.8E+09	3.6	0.017
14	0.062	0.077	3.4E+09	4.4	0.014
16	0.058	0.071	2.8E+09	4.2	0.014
24	0.38	0.077	5.6E+09	7.1	0.015
27	0.71	0.076	5.1E+09	8.7	0.015
30	1.17	0.075	6.9E+09	12	0.023
33	2.9	0.074	7.1E+09	16	0.019
36	4.8	0.072	7.9E+09	20	0.065
39	9.9	1.6	1.0E+10	27	0.048

Table 35 C. glutamicum DM1945x3 offline measurements in run 1(SDR 14)

Time (h)	Cadaverine (g/L)	Glucose (g/L)	CFU/mL	DCW (g/L)	Lactate(g/L)
0	0.00	10	3.0E+06	0.060	0.00
2	0.0082	9.5	2.9E+07	0.092	0.0094
4	0.019	9.0	1.8E+08	0.33	0.0035
6	0.030	8.4	6.9E+08	0.86	0.013
8	0.035	3.6	1.7E+09	1.7	0.059
11	0.066	0.0092	3.3E+09	4.8	0.016
14	0.059	0.011	3.5E+09	3.4	0.015
16	0.080	0.014	4.3E+09	4.4	0.014
24	0.27	0.013	5.1E+09	5.6	0.015
27	2.0	0.013	5.8E+09	8.1	0.020
30	2.9	0.015	6.8E+09	12	0.022
33	2.9	0.017	8.0E+09	15	0.029
36	5.0	0.018	8.9E+09	20	0.047
39	12	0.20	1.0E+10	30	0.20

Table 36 C. glutamicum DM1945x3 offline measurements in run 2 (SDR 14)

Appendix 27 highlights the offline data measurements of samples taken during replicate fed-batch fermentations of *C. glutamicum* DM1945x3 in the SDR 14 simulation (Table 35 & 36).

Appendix 28

Process log for *C. glutamicum* DM1945x3 fed-batch fermentation (SDR 15)

Time (h)	Cadaverine (g/L)	Glucose (g/L)	CFU/mL	DCW (g/L)	Lactate(g/L)
0	0.00	10	3.6E+06	0.059	0.00
2	0.0026	9.7	4.8E+07	0.070	0.0042
4	0.036	8.6	1.7E+08	0.28	0.0089
6	0.061	7.6	7.7E+08	0.89	0.019
8	0.11	6.9	1.9E+09	1.5	0.028
11	0.16	2.2	2.8E+09	3.5	0.048
14	0.20	0.063	3.7E+09	4.6	0.0071
16	0.22	0.055	3.8E+09	3.8	0.013
24	0.29	0.055	5.3E+09	3.9	0.025
27	0.81	0.045	5.8E+09	5.0	0.034
30	1.8	0.054	5.3E+09	8.9	0.038
33	2.9	0.033	8.5E+09	15	0.039
36	5.4	0.75	1.1E+10	24	0.27
39	10	12	1.5E+10	31	0.23

Table 37 C. glutamicum DM1945x3 offline measurements in run 1(SDR 15)

Time (h)	Cadaverine (g/L)	Glucose (g/L)	CFU/mL	DCW (g/L)	Lactate(g/L)
0	0.00	10	4.2E+06	0.051	0.00
2	0.0020	9.2	4.6E+07	0.083	0.0094
4	0.0045	8.3	2.1E+08	0.19	0.015
6	0.012	7.9	8.2E+08	0.46	0.028
8	0.024	6.0	1.4E+09	0.92	0.038
11	0.046	1.3	2.7E+09	3.0	0.028
14	0.040	0.063	3.9E+09	3.5	0.018
16	0.044	0.061	4.5E+09	4.6	0.017
24	0.12	0.059	4.9E+09	4.7	0.028
27	0.62	0.054	6.6E+09	4.8	0.016
30	0.79	0.062	7.4E+09	7.3	0.021
33	2.0	0.058	8.1E+09	14	0.022
36	6.3	0.058	9.8E+09	22	0.28
39	9.3	7.1	1.5E+10	31	0.29

Table 38 C. glutamicum DM1945x3 offline measurements in run 2 (SDR 15)

Appendix 28 highlights the offline data measurements of samples taken during replicate fed-batch fermentations of *C. glutamicum* DM1945x3 in the SDR 15 simulation (Table 37 & 38).

Appendix 29

Process log for *C. glutamicum* DM1945x3 fed-batch fermentation (SDR 16)

Time (h)	Cadaverine (g/L)	Glucose (g/L)	CFU/mL	DCW (g/L)	Lactate(g/L)
0	0.00	9.9	4.3E+06	0.066	0.00
2	0.0032	9.0	5.8E+07	0.19	0.0082
4	0.0069	7.2	3.0E+08	0.45	0.019
6	0.11	5.5	6.7E+08	0.79	0.029
8	0.021	2.8	1.5E+09	1.3	0.058
11	0.11	0.035	2.6E+09	3.7	0.013
14	0.11	0.037	3.3E+09	4.5	0.012
16	0.10	0.032	2.6E+09	4.5	0.015
24	0.52	0.029	3.6E+09	6.2	0.013
27	1.6	0.030	4.8E+09	7.4	0.014
30	2.2	0.034	6.1E+09	13	0.018
33	3.1	0.037	7.4E+09	15	0.024
36	3.2	0.038	8.2E+09	23	0.025
39	5.3	0.034	1.0E+10	29	0.026

Table 39 C. glutamicum DM1945x3 offline measurements in run 1(SDR 16)

Time (h)	Cadaverine (g/L)	Glucose (g/L)	CFU/mL	DCW (g/L)	Lactate(g/L)
0	0.00	10	3.0E+06	0.059	0.00
2	0.0020	9.5	6.4E+07	0.33	0.0094
4	0.0045	8.0	2.6E+08	0.52	0.022
6	0.012	6.3	9.0E+08	0.96	0.039
8	0.024	5.1	1.3E+09	1.6	0.035
11	0.046	0.70	2.5E+09	3.7	0.025
14	0.040	0.090	3.7E+09	3.8	0.014
16	0.044	0.074	3.3E+09	3.9	0.013
24	0.12	0.084	4.6E+09	4.4	0.014
27	0.62	0.073	6.1E+09	7.4	0.014
30	0.79	0.078	7.6E+09	11	0.016
33	2.0	0.075	7.6E+09	17	0.017
36	6.3	0.074	8.0E+09	23	0.019
39	9.3	0.074	9.2E+09	30	0.019

Table 40 C. glutamicum DM1945x3 offline measurements in run 2 (SDR 16)

Appendix 29 highlights the offline data measurements of samples taken during replicate fed-batch fermentations of *C. glutamicum* DM1945x3 in the SDR 16 simulation (Table 39 & 40).

Appendix 30

Process log for *C. glutamicum* DM1945x3 fed-batch fermentation (SDR 17)

Time (h)	Cadaverine (g/L)	Glucose (g/L)	CFU/mL	DCW (g/L)	Lactate(g/L)
0	0.00	10	2.2E+06	0.046	0.00
2	0.0088	9.8	4.3E+07	0.098	0.0093
4	0.020	8.0	5.6E+08	0.21	0.019
6	0.043	7.7	9.8E+08	0.68	0.010
8	0.060	7.3	2.2E+09	1.4	0.014
11	0.087	2.9	4.3E+09	3.9	0.030
14	0.13	0.043	4.5E+09	5.6	0.00
16	0.14	0.080	3.8E+09	3.7	0.00050
24	0.32	0.053	6.1E+09	3.8	0.012
27	1.0	0.049	5.2E+09	5.6	0.018
30	1.7	0.083	6.0E+09	10	0.032
33	4.3	0.056	8.1E+09	15	0.010
36	7.9	0.042	1.0E+10	25	0.025
39	12	1.07	1.3E+10	32	0.20

Table 41 C. glutamicum DM1945x3 offline measurements in run 1(SDR 17)

Time (h)	Cadaverine (g/L)	Glucose (g/L)	CFU/mL	DCW (g/L)	Lactate(g/L)
0	0.00	10.0	3.9E+06	0.067	0.00
2	0.0020	9.6	3.3E+07	0.019	0.0053
4	0.0045	8.3	4.0E+08	0.36	0.0097
6	0.012	7.9	7.9E+08	0.86	0.016
8	0.024	6.2	1.7E+09	1.8	0.019
11	0.046	1.6	4.1E+09	3.1	0.018
14	0.040	0.063	3.9E+09	4.8	0.017
16	0.044	0.070	4.6E+09	4.1	0.018
24	0.12	0.071	5.3E+09	5.2	0.014
27	0.62	0.065	6.5E+09	6.2	0.022
30	0.79	0.074	7.5E+09	9.5	0.014
33	2.0	0.075	8.2E+09	16	0.019
36	6.3	0.069	1.2E+10	23	0.030
39	9.3	0.42	1.4E+10	31	0.13

Table 42 C. glutamicum DM1945x3 offline measurements in run 2 (SDR 17)

Appendix 30 highlights the offline data measurements of samples taken during replicate fed-batch fermentations of *C. glutamicum* DM1945x3 in the SDR 17 simulation (Table 41 & 42).

Appendix 31

Process log for *C. glutamicum* DM1945x3 fed-batch fermentation (SDR 18)

Time (h)	Cadaverine (g/L)	Glucose (g/L)	CFU/mL	DCW (g/L)	Lactate(g/L)
0	0.00	10	3.5E+06	0.049	0.00
2	0.0028	9.5	3.9E+07	0.28	0.010
4	0.0023	8.1	4.9E+08	0.62	0.029
6	0.0093	7.0	7.9E+08	0.98	0.011
8	0.015	5.1	9.9E+08	1.9	0.049
11	0.050	0.88	2.1E+09	3.7	0.031
14	0.048	0.072	2.6E+09	4.4	0.014
16	0.048	0.069	2.6E+09	4.3	0.015
24	0.28	0.072	3.9E+09	7.9	0.016
27	2.2	0.066	5.2E+09	7.9	0.016
30	2.6	0.071	5.6E+09	13	0.017
33	2.7	0.070	6.3E+09	17	0.033
36	5.4	0.073	8.6E+09	21	0.059
39	8.1	0.068	1.0E+10	29	0.15

Table 43 C. glutamicum DM1945x3 offline measurements in run 1(SDR 18)

Time (h)	Cadaverine (g/L)	Glucose (g/L)	CFU/mL	DCW (g/L)	Lactate(g/L)
0	0.00	10	4.0E+06	0.043	0.00
2	0.012	9.8	4.8E+07	0.19	0.0033
4	0.010	8.1	3.4E+08	0.56	0.020
6	0.020	6.2	8.8E+08	0.77	0.023
8	0.038	5.6	1.4E+09	1.0	0.043
11	0.058	1.3	2.8E+09	3.0	0.029
14	0.060	0.082	2.9E+09	3.3	0.014
16	0.052	0.074	3.1E+09	3.4	0.014
24	0.28	0.080	4.3E+09	5.6	0.013
27	1.2	0.076	5.2E+09	7.5	0.020
30	2.0	0.069	6.1E+09	12	0.014
33	2.7	0.082	5.7E+09	15	0.037
36	6.2	0.068	7.8E+09	21	0.060
39	8.0	0.069	9.9E+09	28	0.20

Table 44 C. glutamicum DM1945x3 offline measurements in run 2 (SDR 18)

Appendix 31 highlights the offline data measurements of samples taken during replicate fed-batch fermentations of *C. glutamicum* DM1945x3 in the SDR 18 simulation (Table 43 & 44).

Appendix 32

Process log for *C. glutamicum* DM1945x3 fed-batch fermentation (SDR 19)

Time (h)	Cadaverine (g/L)	Glucose (g/L)	CFU/mL	DCW (g/L)	Lactate(g/L)
0	0.00	10	3.9E+06	0.042	0.00
2	0.0088	9.9	3.6E+07	0.11	0.0029
4	0.010	9.0	5.1E+08	0.29	0.0070
6	0.023	7.8	7.1E+08	0.66	0.0084
8	0.058	6.7	2.0E+09	1.3	0.012
11	0.10	2.6	2.8E+09	3.3	0.011
14	0.13	0.084	3.3E+09	4.2	0.0056
16	0.077	0.10	3.5E+09	3.5	0.0056
24	0.24	0.059	5.5E+09	3.9	0.017
27	1.1	0.055	4.3E+09	5.6	0.0064
30	2.0	0.054	6.7E+09	10	0.0084
33	3.6	0.050	8.6E+09	16	0.020
36	7.7	0.88	1.0E+10	26	0.014
39	12	2.3	1.4E+10	32	0.059

Table 45 C. glutamicum DM1945x3 offline measurements in run 1(SDR 19)

Time (h)	Cadaverine (g/L)	Glucose (g/L)	CFU/mL	DCW (g/L)	Lactate(g/L)
0	0.00	10	4.4E+06	0.036	0.00
2	0.0063	9.7	4.0E+07	0.21	0.0036
4	0.020	8.6	4.6E+08	0.33	0.0068
6	0.044	7.5	8.8E+08	0.84	0.013
8	0.082	5.1	2.4E+09	1.3	0.018
11	0.12	1.1	4.4E+09	4.2	0.0076
14	0.13	0.066	4.9E+09	4.4	0.0066
16	0.097	0.063	4.7E+09	3.7	0.0088
24	0.22	0.063	5.9E+09	4.2	0.011
27	0.93	0.062	6.4E+09	5.7	0.0086
30	1.5	0.065	8.1E+09	10	0.0094
33	1.7	0.068	9.6E+09	17	0.018
36	4.4	0.065	1.1E+10	26	0.018
39	7.5	2.2	1.7E+10	31	0.058

Table 46 C. glutamicum DM1945x3 offline measurements in run 2 (SDR 19)

Appendix 32 highlights the offline data measurements of samples taken during replicate fed-batch fermentations of *C. glutamicum* DM1945x3 in the SDR 19 simulation (Table 45 & 46).

<u>Appendix 33</u>

Process log for *C. glutamicum* DM1945x3 fed-batch fermentation (SDR 20)

Time (h)	Cadaverine (g/L)	Glucose (g/L)	CFU/mL	DCW (g/L)	Lactate(g/L)
0	0.00	10	3.6E+06	0.039	0.00
2	0.00	9.7	4.1E+07	0.13	0.0073
4	0.0045	8.7	4.3E+08	0.32	0.0075
6	0.0075	8.0	6.2E+08	0.78	0.012
8	0.014	6.5	1.0E+09	1.3	0.036
11	0.019	2.8	1.6E+09	2.0	0.016
14	0.035	0.059	2.9E+09	4.1	0.012
16	0.031	0.059	2.8E+09	4.8	0.013
24	0.24	0.055	4.6E+09	7.8	0.014
27	1.2	0.054	6.9E+09	9.9	0.014
30	2.5	0.059	7.4E+09	13	0.015
33	3.0	0.062	8.7E+09	16	0.016
36	3.1	0.061	9.2E+09	23	0.016
39	4.8	1.1	1.1E+10	29	0.057

Table 47 C. glutamicum DM1945x3 offline measurements in run 1(SDR 20)

Time (h)	Cadaverine (g/L)	Glucose (g/L)	CFU/mL	DCW (g/L)	Lactate(g/L)
0	0.00	10	3.3E+06	0.044	0.00
2	0.00	9.8	4.8E+07	0.52	0.0046
4	0.0034	8.2	3.9E+08	0.86	0.0092
6	0.0094	7.9	7.7E+08	1.1	0.011
8	0.013	5.5	1.4E+09	2.4	0.018
11	0.016	0.78	2.5E+09	3.9	0.026
14	0.020	0.085	3.7E+09	4.4	0.014
16	0.033	0.074	4.0E+09	5.8	0.014
24	0.29	0.051	4.4E+09	7.0	0.014
27	1.7	0.048	6.1E+09	7.8	0.014
30	1.2	0.053	6.0E+09	14	0.015
33	2.0	0.055	8.8E+09	17	0.017
36	3.7	0.053	9.6E+09	22	0.017
39	5.8	0.25	1.1E+10	30	0.047

Table 48 C. glutamicum DM1945x3 offline measurements in run 2 (SDR 20)

Appendix 33 highlights the offline data measurements of samples taken during replicate fed-batch fermentations of *C. glutamicum* DM1945x3 in the SDR 20 simulation (Table 47 & 48).